Republic of Iraq
Ministry of Higher Education and Scientific Research
University of Babylon
College of Materials Engineering
Department of Polymer and Petrochemical Industries

Synthesis of wound dressings from Nanofiber Textile by electrospinning Technique

A Thesis Submitted to the College of Materials Engineering / University of Babylon in a Partial Fulfillment of the Requirements for the Degree of Doctor of Philosophy in Materials Engineering/ Polymer

Submitted By
Dalal Abbass Kadham Salman

Supervised by:
Prof. Auda Jabbar Braihi (Ph.D)
Prof. Hanaa Jawad Kadham (Ph.D)

2023AD 1444AH

بسم الله الرحمن الرحيم

وَيَرَى الَّذِينَ أُوتُوا
الْعِلْمَ الَّذِي أُنْزِلَ إِلَيْكَ
مِنْ رَبِّكَ هُوَ الْحَقَّ
وَيَهْدِي إِلَى صِرَاطِ
الْعَزِيزِ الْحَمِيدِ

٦ سبأ

Supervisors' Certification

We certify that this thesis entitled **" Synthesis of wound dressings from Nanofiber Textile by electrospinning Technique "was** prepared by **" Dalal Abbass Kadham "** under our supervision at Babylon University/College of Material Engineering/Department of Polymer and Petrochemical Industries**,** in Partial Fulfillment of the Requirements for the Degree of the Doctor of Philosophy in Materials Engineering / Polymer.

Supervisor Signature **Supervisor Signature**

Prof. Dr. Auda J. Braihi **Prof. Dr. Hanaa J. Kadham**

Date / /2023 **Date / /2023**

Examination Committee Certification

We certify that we have read this thesis entitled "**Synthesis of wound dressings from Nanofiber Textile by electrospinning Technique**" and as an Examination Committee examined the student (**Dalal Abbass Kadham Salman**) on its contents and that, in our opinion, it meets the standard of a thesis and is adequate for the award of the Doctor Degree of Philosophy in Materials Engineering/ Polymer Engineering.

Signature:
Prof. Dr. Zuhair Jabbar Abdul Ameer
Karbala University/College of Engineering
Date: / /2023
(Chairman)

Signature:
Prof. Dr. Auda Jabbar Braihi
University of Babylon /College of Materials Engineering
Polymer and Petrochemical Industries Department
Date: / /2023
(Member)

Signature:
Prof. Dr. Hanaa Jawad Kadhim
University of Babylon /College of Education forPure Sciences/ Physics Department
Date: / /2023
(Member)

Signature:
Assist. Prof. Dr. Asra Ali Hussien
University of Babylon/ College of Materials Engineering
Polymer and Petrochemical Industries Department
Date: / /2023
(Member)

Signature:
Assist. Prof. Dr. Salih Abbas Habeeb
University of Babylon/ College of Materials Engineering
Polymer and Petrochemical Industries Department
Date: / /2023
(Member)

Signature:
Prof. Dr. Massar Najim Obaid
University of Technology/ College of Engineering
Materials Engineering Department
Date: / /2023
(Member)

Signature:
Assist. Prof. Dr. Qahtan Adnan Hamad
University of Technology/ College of Engineering
Materials Engineering Department
Date: / /2023
(Member)

Approval of Polymer and Petrochemical Industries
(Head of the Department)

Signature:
Prof. Dr. Zoalfokkar Kareem Mezaal
Date: / /2023

Approval of Materials Engineering College
(Dean of the College)

Signature:
Prof. Dr. Imad Ali Disher
Date: / /2023

Acknowledgement

First of all I thank **Allah who** gave me the ability and desire to complete this work.

I would like to express my deep appreciation and sincere thanks ***Prof. Dr. Auda Jabbar Braih and Prof. Dr. Hanaa Jawad Kadham*** *whom I genuinely like, admire, and respect as academicians. I have learned a great deal from their approach to the solution of problems, from their profound insights into relevant points of issues and from their philosophical views. Their advice and guidance have been of a great value to me while conducting this research for this I will be indebted to them.*

I would like to thank the Materials engineering collage in University of Babylon for giving me the opportunity to get the PhD-degree in materials science.

Sincere thanks are also expressed to the staff of the material engineering college especially in polymers and petrochemical industries laboratories for the encouragement during this work.

Finally, I would like to thank my family; my friends and everyone help me to accomplish the present work.

Dalal

2023

Dedication

To

My Father and Mother

My Sister and My Brothers

My Husband

My children

Mahdi & Fatima

Dalal

2023

Abstract

Traditional wound dressings lack moisture retention, water absorption, hydrophilicity, bacteriostasis, and some of their components penetrate the epidermis and injure the body. Thus, novel dressings are needed to address these issues. Electrospinning was used to make PVA-based polymeric wound dressings.

Nano polymeric fiber textiles were made using PVA, HAc, collagen, and their binary and tertiary blends. Essential oils (EOs) and solids were mixed in various amounts to make the best dressings. Ocimum basilicum, Rosemary, and L. nobilis are EOs; G. lucidum, Capsicum annuum, and Iodine are solid additions (I_2). "Final textile" contained all these ingredients. Many tests were needed to finish the work. Some of these tests are for solutions (viscosity-shear rate, surface tension, and electrical conductivity), while others are for electrospun nanofiber textiles (wettability, Fourier Transform Infrared Spectroscopy (FTIR), Field Emission Scanning Electron Microscopy (FESEM) images, Energy dispersive x-ray (EDX) analysis, Atomic Force Microscopy (AFM), texture directionality, thermal transitions, UV-Visible absorbance, XRD, nanoindentation, and texture directionality). The final dressing cloth and TEBADERM dressing were used to track damaged mice's healing. The PVA solution and all its blends are non-Newtonian with a shear-thinning phenomenon and adding collagen or HAc to PVA reduces viscosity and increases surface tension, especially HAc. Electrical conductivity increases. FTIR showed the tertiary blend contains PVA, HAc, and Collagen without chemical reaction. Additives cause shear thickening at lower shear rates. Except for L. nobilis EO, most additives improved surface tension and electrical conductivity differently. FTIR showed all components in the textile.

Based on the wettability results, three formulations were chosen as the best for wound dressings and subsequently examined. Their contact angles fell from 70^o for pure PVA to 46.505^o, 51.37^o, and 41^o for 55:45 (10 wt.% PVA:

7wt.% Coll), 55:45:5.5% HAc, and 55:22.5:22.5 (10wt.% PVA, 7wt.% Coll, 5.5wt. % HAc). These dressings collect excess exudates and limit water evaporation to keep the wound moist. Capsicum annuum, Iodine, and L.nobilis EO accelerate medication release and dressing degradation. The final textile had reduced wettability, thus working parameters were altered to improve wettability. The average diameter of these selected textiles decreased (compared with 298.1992 nm for pure PVA) and the percentage of carbon rose at the expense of hydrogen, according to FESEM pictures and EDX data. All additions increase fiber diameter (20–76.81%), form honeycomb, branched, fused, and twisted fibers, beads, and varied porosities. The resulting textile's average diameter rose by 118.5%, its distribution shifted over a larger range, its morphology is crosslinked, fused nanofibers with some beads, and its porosity is medium. The textile is sticky, made of fused, branching, and thick fibers with poor porosity, and its average diameter decreased by 23% after 3 hours at 70°C. AFM showed all roughness parameters decreasing. Texture directionality studies indicated nanofibers on the collector without a preferred direction, except for the textile with 5.5 wt.% HAc, where 70% of the fibers aligned in one direction (0.63^{o}). According to DSC studies, these three fabrics had higher Tg and enthalpy than pure PVA, indicating improved mechanical characteristics and thermal stabilities. Additives increased roughness and fiber directionality. These additions induced phase separation (two Tg's instead of one for the neat blend), immiscibility, altered enthalpies, and drug release from uncompacted dressings to damaged skin. Collagen, HAc, and their combined absorption from MUV to NUV and visible regions, especially HAc addition, meaning fabrics absorb more radiation and release it as heat. Thus, these textiles do not inhibit vitamin D production, and the heat created within skin tissue kills germs, speeding wound healing and improving antibacterial effectiveness.

All additions induced π to π* and n to n* transitions, thus current textiles absorb light at two wavelengths (two absorbent beaks appeared).

The antioxidant test demonstrated that the final textile had stronger DPPH free radical scavenging activity than the neat blend, which speeds tissue repair. Rosemary oil excelled iodine against S. aureus, but iodine outperformed E. coli.

The final textile has the highest Candida-fighting activity, followed by Rosemary oil and Iodine. After five days, the nanofiber textile-treated mice were entirely healed, while the other wounds remained moist, red, and coagulated. XRD showed that additives change lattice properties and nucleate crystalline structures. Nanoindentation hardness studies showed that for the final textile, hardness and reduced elastic modulus dropped with contact depth increased.

List of Contents

List of Figures

List of Tables:

List of Abbreviations

Abbreviate	Meaning
AFM	Atomic Force Microscopy
Ag NPs	Silver nanoparticles
AMR	Antimicrobial-resistant
ASTM	American Society for Testing and Materials
bFGF	basic fibroblast growth factor
BDO	1,4-butandiol
Cin	Cinnamon
DSC	Differential scanning calorimeter
DL	Drug loading
DW	Distilled water
DMF	N, N-Dimethylformamide
DMSO	Dimethylsulfoxide
DPPH	2,2-diphenyl-1-picrylhydrazyl
CA	Contact Angle
DSC	Differential scanning calorimetry
Coll.	Collagen
CSNM	curcumin-loaded sandwich-like nanofibrous membrane
CuONPs	Copper II oxide nanoparticles
cur	curcumin
CSA	Capsicum annuum
ECM	Extracellular Matrix
E-coli	Escherichia coli

EDS	Electron dispersive spectroscopy
EGF	Epidermal growth factor
ES	Electrospinning
EE	Entrapment efficiency
EPU	Ethanol-soluble polyurethane
FD	Freeze drying
FESEM	Field emission scanning electron microscopy
FGF	Fibroblast growth factor
FPU	Fluorinated polyurethane
FTIR	Fourier transform infrared spectroscopy
GC-MS	Gas chromatography-mass spectroscopy
GL	Ganoderma lucidum
GLSP	Ganoderma lucidum spore powder
GLP	Ganoderma lucidum polysaccharide
HaCaT	Human keratinocyte cells
HDI	Hexamethylene diisocyanate
IE	Inhibition efficiency
IZ	Inhibition zone
KGF	Keratinocyte growth factor
LNO	Laurus nobilis oil
MH	Muller–Hinton
NFM	Nanofibrous membranes
OBO	Ocimum basilicum oil
P	Water vapor permeability
PDGF	Platelet-derived growth factor

PCL	Polycaprolactone
PEP	Peppermint essential oil
Pm	Permeance
PLA	Polylactide
PLGA	Poly (L-lactide-co-glycolide)
PHBV	Poly (3- hydroxybutyrate-co-3-hydroxy valerate)
PLLA	Poly-L-lactide acid
POE	Polyorthoester
PU	Polyurethane
PVA	Poly (vinyl alcohol)
RH	Relative humidity
RNS	Reactive nitrogen species
RO	Rosemary oil
ROS	Reactive Oxygen Species
SF	Silk fibroin
STEP	Spinneret-Based Tunable Engineered Parameters
TGF-β	Transforming growth factor β
TOLCENs	Tea tree oil liposomes
TSE	Traditional solvent extraction
VEGF	Vascular endothelial growth factor

List English Symbols

Symbol	Meaning	Units
Er	Modulus of elasticity	Gpa
M_w	Molecular weight	g/mol
T	Absolute temperature	K
T_c	Crystallisation temperature	^oC
T_g	Glass transition temperature	^oC
ΔH‡	activation enthalpy	J/g
Sa	Average Roughness	nm
Sq	Root Mean Square	nm
Sy	Peak-to-peak	nm
Sz	Ten-point height	nm
ΔS_m	Change of entropy	J/K

List of Greek Symbols

Symbol	Meaning	Units
$\dot{\gamma}$	Shear rate	S^{-1}
η	Viscosity	cp
Θ	Contact angle	degree
λ	x-ray wavelength	A°
β	Half-width of peak	rad
Σ	electrical conductivity	mS/cm
ρ	Density	kg/m^3

Chapter One
Introduction

1.1 Introduction

Electrospun fibers have been widely studied for use in several applications due to the process simple, the ability to control fiber characteristics, and the wide range of materials that are spinnable by this technique Biomedical applications, in particular, take advantage of electrospun nanofibers for use such as tissue scaffold, wound dressing, and drug delivery [1]. For these applications, control of the surface wettability, biocompatibility, and biodegradation are significant factors [2]. Cell adhesion and growth on extracellular matrix (ECM) are greatly influenced by their properties including surface wettability, roughness, topography, and chemical composition. Surface wettability has been recognized as an important factor in controlling the dynamic interaction between an implanted surface and cells in vitro or in vivo. These surfaces with different wettability are usually achieved by introducing functional groups, incorporating amphiphilic moieties, creating charged materials, oxidization, and so on. Despite the achievements, most of these modifications still suffer from complex synthesis routes or long-term instability, which are not suitable for studying cell behaviors [3].

Skin, as the largest and outermost organ of the human body, provides the barrier between the internal organism and external environment for protecting the body from invasion of pathogens and preventing water loss. It is estimated that approximately 312.9 million people throughout the world suffer from surgically induced wounds annually, and 76 million people undergo the wounds caused by complications of diabetes, obesity, cardiovascular disease, and so on [4]. Over the past decades, wound care has progressively become a major worldwide public health concern. Because inefficient and defective treatment of skin damages can even be fatal. Hence, intensive research has been performed in this area focusing on developing efficient therapeutic approaches and designing new dressing materials that

can improve the wound healing procedure. For the restoration of the injured tissue, the wound healing process consists of a cascade of events, including hemostasis, inflammation, and proliferation as well as remodeling of the tissue [5].

Wound curing is the net interactions by the whole of cytokines production factors, consanguinity, and the extracellular grid [6]. Antimicrobial polymeric materials can be applied in drug delivery, wound healing or dressing, sutures, and dental application [7].

There are a number of problems with conventional skin dressings, including a lack of moisture retention, poor water absorption, and ineffective bacteriostasis.

For example, a gauze dressing can offer some protection for skin traumatic wounds, but it has poor hydrophilicity.

The downside of hydrogel dressings is that the exudate will lead to maceration and bacterial proliferation of the hydrogel dressings, despite their high hydrophilicity and ability to give a soothing and cooling effect to reduce the temperature of cutaneous wounds.

Good biodegradability and hydrophilicity (which can activate macrophages to launch an inflammatory response and speed wound Healing) characterize alginate dressings, however, they had a weak bacteriostatic effect.

Collagen dressings, which function similarly to the extracellular matrix by forming a physiological contact between the wound surface and its environment, may speed up the healing process, although allogeneic or heterogeneous collagen may be rejected by the immune system.

Nanosilver dressings are very effective in killing bacteria, but they can enter the body through the skin and mucous membranes and do harm if they build up.

Therefore, it is essential for wound dressings to not only keep the wound site wet but also to provide antibacterial actions to prevent infection and expedite the healing process. And picking the right manufacturing method to make these perfect wound dressings is crucial.

Electrospun nanofiber dressings have been shown to be highly effective in encouraging skin regeneration in wound therapy, making them a prime choice for use in wound healing applications for the following reasons:

1- The nano fiber's structural and morphological similarities to the proteins of the extracellular matrix explain why they can speed up the healing process when applied to injured tissues (skin regeneration).
2- Could promote both cell growth, proliferation, migration, and antibacterial activity.
3- This method can be used to create a reinforced fiber (containing nanoparticles, for instance) that improves the surface environment of the fiber, allowing for better cellular proliferation and enhanced mechanical capabilities.
4- The operating conditions of this technique can be controlled, so the required property (such as the desired wettability) can be obtained.

Electrospun polymeric nanofibers are suitable for delivering bioactive molecules to the wound sites [8]

Synthetic polymers, especially those with biocompatible and biodegradable characteristics, may offer effective alternatives for the treatment of severe wounds and burn injuries. Ideally, the scaffold material should induce as little pain as possible, enable quick healing, and direct the growth of defect-free epidermal cells. The best material with this multifunctionality, such as self-healing dressings, should be hydrophilic and have uninterrupted and direct contact with the damaged tissue. In addition, the ideal biomaterial should have some antibacterial properties [9].

Electrospinning (ES) is a simple and effective technique method for preparing nanofibers with diameters ranging from 5 to 500 nm; 10^2 to 10^4 times smaller than those prepared by the traditional methods of solution or melt spinning. Wound dressing from electrospun nanofibrous membranes (NFM), potentially offers many advantages over conventional processes. With its huge surface area and microporous structure, the NFM could quickly start signaling pathways and attract fibroblasts to the derma layer, which can excrete important extracellular matrix components, such as collagen and several cytokines (e.g., growth factors and angiogenic factors), to repair damaged tissue as in treating the scarred skin (figure 1.1) [10].

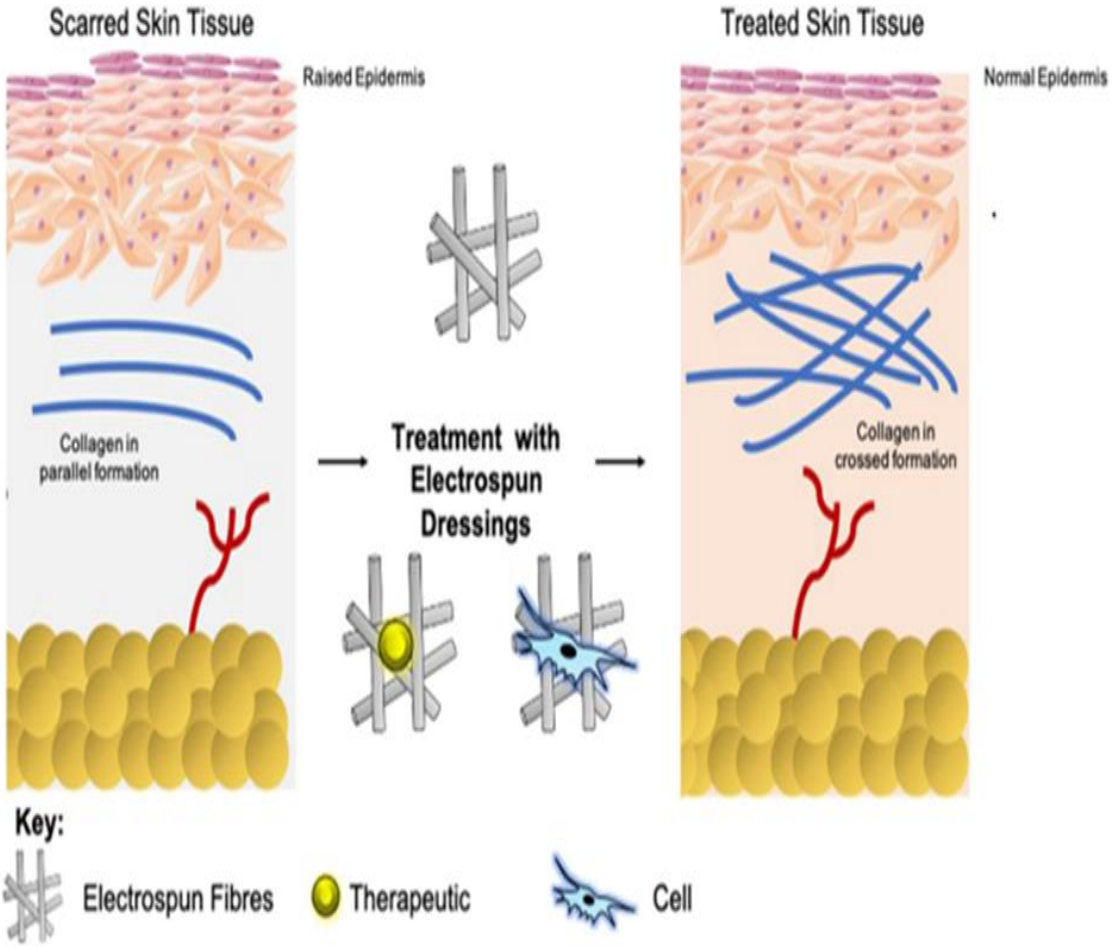

Fig.1.1: Treatment of scarred skin with electrospun polymeric nanofibers [11].

The electrospun membrane is also important for cell attachment and proliferation in wound healing. In the electrospinning process, a polymeric solution placed inside a syringe is driven out from a metal capillary that is

connected to a high voltage power supply. Nanofibers are collected in the form of a nonwoven matrix on a grounded collector after solvent evaporation. By adopting appropriate process parameters, such as solvent, polymer concentration, and flow rate, electrospun nanofibers with various diameters can be obtained [12].

Wound healing is a complex tissue regeneration process that the body undergoes as a response to wounding openings or missing cellular structures because of various types of traumatic injury.

In adult humans, optimal wound healing involves:

(1) rapid hemostasis.

(2) appropriate inflammation

(3) mesenchymal cell differentiation, proliferation, and migration to the wound site

(4) suitable angiogenesis

(5) prompt reepithelialization (re-growth of epithelial tissue over the wound surface)

(6) proper synthesis, crosslinking, and alignment of collagen to provide strength to the healing tissue. To facilitate effective wound healing, a wound site is typically covered with a sterile dressing material to avoid infection and to promote the healing process [13].

1.2 Aim of thesis

Manufacture of biocompatible tissues with the human body, as the prepared tissues are characterized:

- They absorb and store the necessary moisture to keep the skin from drying out and damaging.
- It is also used to treat and heal wounds more quickly than without using these tissues.

- Prepare and characterize an active polymeric wound dressings using many of the additives to overcome some shortcomings of the traditional dressings.

1.3 Thesis layout

This thesis consists of the following chapters:

Chapter one: Is an introduction about nanofibers used in wound dressing and the aim of this study.

Chapter two: Focus on the biomaterial types, nanofibers manufacturing methods, especially electrospinning (ES) technique, the used materials and historical perspective.

Chapter three: Introduces the experimental work, which describes the used materials, procedure of sample processing according to ASTM standards and test equipment selected.

Chapter four: covers the results and discussion of the experimental work.

Chapter five: Summarizes the work conclusions and gives some suggestions for future work. Additionally, references as well as Arabic abstract are included.

.

Chapter Two
Theoretical Background and Literature Survey

2.1 Introduction

There are various types of techniques employed to prepare nanofibers and nanofibrous scaffolds. Those techniques include melt-blowing, phase separation, template synthesis, self-assembly, etc. However, the most useful and commonly employed technique is electrospinning [14]. This electrospinning method has been utilized since the 1890s [15]. The technique uses electrostatic force to pull the fibers from the droplet produced at the tip of a spinneret.

Different experiments have been performed to evaluate suitable parameters for electrospinning nanofibers with good physicochemical properties for biomedical applications. The development of nanofibrous scaffolds during electrospinning is influenced by the following three parameters main categories: solution parameters (e.g., solution viscosity, conductivity, and surface tension), process parameters (e.g., flow rate, applied voltage, the distance between collector and tip, and electric field stimulated by the collector), ambient parameters (e.g., humidity and temperature).

The electrospinning technique can produce continuous fibers utilizing a broad range of materials such as polymers and their composites. This method can produce nanofibers/nanofibrous scaffolds with average diameters ranging from micron to nanosized diameter [16]. Some examples of nanofibrous scaffolds include nanofibrous mats, nanofibrous membranes, nanofibrous webs, nanofibrous patches, etc.

There are several biomedical applications of electrospun nanofibers and nanofibrous scaffolds, such as wound dressings, drug delivery systems, tissue regeneration, etc. The nanofibrous scaffolds that are based on polymers play a vital role in wound healing applications. It is very important to select appropriate polymers for the preparation of

nanofibrous scaffolds that would be appropriate with the required features for wound dressing. Natural polymers, such as chitosan, silk, cellulose, hyaluronic acid (HA), and collagen have been electrospun for applications in drug delivery [17]. Recent studies of the biological and physical properties of natural polymers have demonstrated that biopolymers possess good biocompatibility and are very useful in the development of nanofibrous scaffolds for wound healing [18]. Electrospun nanofibrous materials made from synthetic polymers have demonstrated excellent mechanical properties compared to biopolymers. Furthermore, synthetic polymers are very soluble in a wide range of solvents, which promote their use in the electrospinning method. Biopolymers are combined with synthetic polymers to control the degradation rate, improve the morphology and mechanical properties of the nanofibrous scaffolds. The electrospun nanofibrous materials have been used to accelerate the wound healing process. The advantages of nanofibres network over the traditional dressing materials come from its large surface/volume ratio. This helps to promote permeation of water molecules through the dressing to regulate the moisture level at the wound surface, an important factor to promote cell growth and reduce inflammation. The large surface/volume ratio system also allows drugs, for example, antibacterial drugs or cell growth promoters, to be retained within the structure to control infections and facilitate new growths. In addition, materials of proven biocompatibility and biodecomposability such as Poly-L-lactide acid (PLLA), Polyorthoester (POE), and Poly (L-lactide-co-glycolide) (PLGA) can be selected for fabricating fibres encapsulated with drugs and controlling the release of the drugs. These advantages would lead to less frequency in dressing replacement and a better environment for wound healing. The parameters used in

electrospinning influence the generation of bead-free and smooth electrospun fibers. To better understand the fabrication and electrospinning technique of polymeric nanofibers, it is crucial to understand the effects of the regulated parameters [19].

2.2 Biomaterials

Biomaterial is a nonviable (able to function successfully after implantation) substance intended to interact with biological systems. Their usage within a physiological medium is possible with the efficient and reliable characteristics of the biomaterials. These characteristic features are provided with a suitable combination of chemical, mechanical, physical, and biological properties, to design well-established biomaterials [20]. Biomaterials are specifically designed by utilizing bimetals, biopolymers, and biocomposites (Figure 2.1)

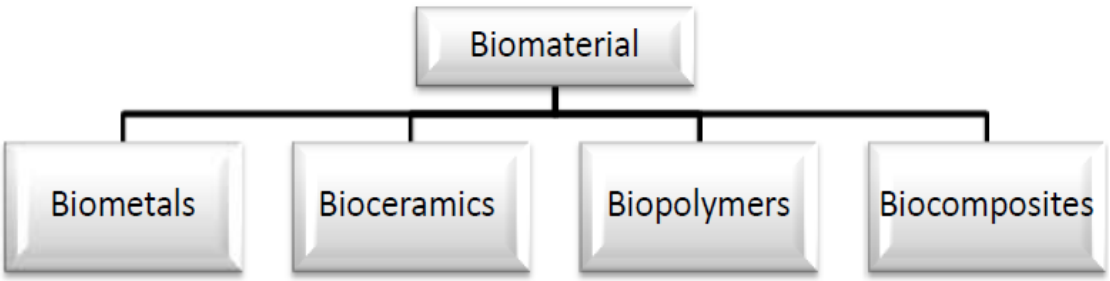

Fig.2.1: General classification of biomaterials.

Biometals: Metallic implant materials have gained immense clinical importance in the medical field for a long time. Many of metal and metal alloys which were used for medical requirements include stainless steel (316L), titanium and its alloys (Cp-Ti, Ti6Al4V), cobalt-chromium alloys (Co Cr), aluminum alloys, zirconium niobium, and tungsten heavy alloys. The rapid growth and development in biomaterial field has created scope to develop many medical products made of metal, such as dental implants, craniofacial plates and screws parts of artificial hearts, pacemakers, clips, valves, balloon catheters, medical devices, and

equipments; and bone fixation devices, dental materials, medical radiation shielding products, prosthetic and orthodontic devices for biomedical applications. Though there are other classes of materials from which biomaterials can be prepared, engineers prefer metals as a crucial one to design the required biomaterial. The main criteria in selection of metal based materials for biomedical applications are their excellent biocompatibility, convenient mechanical properties, good corrosion resistance, and low cost [21].

Biopolymers: Polymers are the convenient materials for biomedical applications and are used as cardiovascular devices for replacement and proliferation of various soft tissues. Many polymeric materials have been used as implants. Their current applications of them include cardiac valves, artificial hearts, vascular grafts, breast prosthesis, dental materials, contact, and intraocular lenses, fixtures of extracorporeal oxygenators, dialysis and plasmapheresis systems, coating materials for medical products, surgical materials, tissue adhesives, etc. [22].

The composition, structure, and organization of constituent macromolecules specify the properties of polymers. Further, the versatility in diverse applications requires the production of polymers that are prepared in different structures and compositions with appropriate physicochemical, interfacial, and biomimetic properties to meet specific purposes. The advantages of the polymeric biomaterials over other classes of materials are (i) easy to manufacture, (ii) ease of secondary processability, (iii) availability with desired mechanical and physical properties, and (iv) reasonable cost.

Polymers for biomedical applications can be classified into two categories namely; synthetic and natural. The synthetic polymeric systems include acrylics, polyamides, polyesters, polyethylene,

polysiloxanes, polyurethane, etc. Though the processability is easy in case of polymers, the main disadvantage of these synthetic polymers is the general lack of biocompatibility in the majority of cases and hence their utility is often associated with inflammatory reactions [18]. This problem can be overcome by the usage of natural polymers. For example, the natural polymers, such as chitosan, carrageenan, and alginate are used in biomedical applications, such as tissue regeneration and drug delivery systems [18].

Bioceramics: The use of ceramics was motivated by their inertness in the body, their assay formability into a variety of shapes and porosities, high compressive strength, and excellent wear characteristics. Ceramics are used as parts of the musculoskeletal system, hip prostheses, artificial knees, bone grafts, dental and orthopedic implants, orbital and middle ear implants, cardiac valves, and coatings to improve the biocompatibility of metallic implants. Though ceramics are utilized for designing biomaterials, they have been preferred less commonly than either metals or polymers. Applications of ceramics in some cases are severely restricted due to brittleness and poor tensile strength. However, bioceramics of phosphates are widely used to manufacture ideal biomaterials due to their high biocompatibility and bone integration, as well as being the materials that are most similar to the mineral component of the bones [23].

Biocomposites: Composite materials have a continuous bulk phase called matrix and one or more discontinuous dispersed phases called reinforcement, which usually has superior properties than the matrix. Separately, there is a third phase named as interphase between matrix and reinforced phases [21]. Composites have unique properties and are usually stronger than any of the single materials from which they are

made, hence are applied to some difficult problems where tissue in-growth is necessary. In recent years, scientific research has been focused to develop variety of biomedical composite materials because they are new alternative solutions for loadbearing tissue components. Composite scaffolds with porous structures tailored from combinations of bioglass particles and biodegradable polymers with mechanical properties that are close to cancellous bone are potentially in use. Hard-tissue applications, such as skull reconstruction, bone fracture repair, total knee, ankle, dental, hip, and other joint replacement applications are possible with fiber-reinforced composite materials [22]. The main advantage of the composite biomaterials is though the individual metals or ceramic materials suffer from disadvantages like exhibition of low biocompatibility and corrosion by metals, brittleness, and low fracture strength by ceramic materials, the composite materials provide alternative route to improve many undesirable properties of homogenous materials (metals or ceramics). The properties of the constituent materials have significant influence on composite biomaterials. One of the factors "linear expansion" plays a crucial role in designing composite biomaterial. Often composites are made from constituents that have similar linear expansion constants. If the constituent materials possess distinct linear expansion constants, contact area (interface) between reinforcement and matrix materials can generate large voids through the contact surface, which blots the purpose of the implant. Therefore, more care is required in selection of individual constituents while processing the composite biomaterial by bone tissue engineers [20].

2.3 Nanofibers Techniques.

2.3.1 Drawing

Drawing is another method utilized to produce fibers. It is similar to dry spinning. This method requires only a sharp tip or a micropipette

which is considered as the main advantage of this technique. In this method, a sharp tip is used to draw a droplet of a previously deposited polymer solution as liquid fibers. After that solvent is evaporated due to the high surface area which causes the solidifying of the liquid fibers. Hollow glass micropipettes can be used instead of the sharp tip with a continuous dosage of the polymer to avoid the volume shrinking problem which limits the continuous drawing of the fibers and affects its diameter (Fig 2.2).

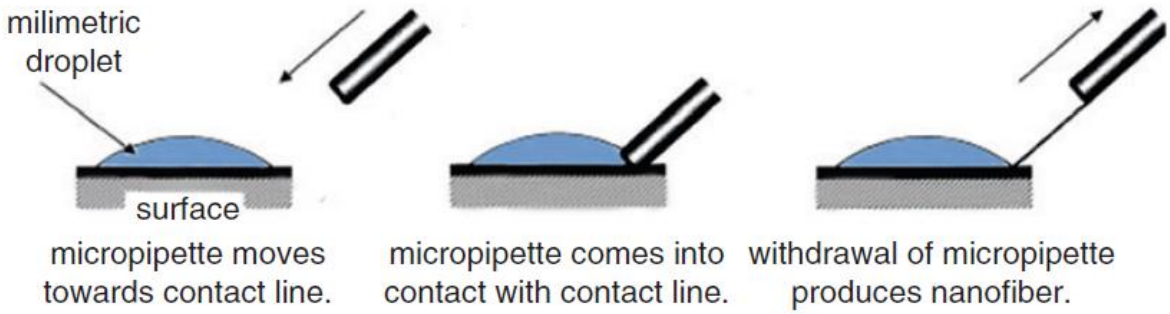

Fig.2.2: Drawing technique which produces nanofibers [23].

After dipping the micropipette into the droplet using a micromanipulator, the micropipette is pulled gently from the liquid and moved at a low speed (about 10^{-4} m/s); as a result, nanofibers will be pulled and deposited on the surface by touching it with the end of the micropipette. This process was repeated several times on every droplet to form nanofiber [24]. Continuous nanofibers in any arrangement can be produced using this method. Beside that precise control of drawing's key parameters, such as drawing speed and viscosity can be achieved which enable repeatability and control on the dimensions of the fabricated fibers [23]. Although this process is simple but limited to laboratory scale as nanofibers are formed one by one, it is a discontinuous process with small productivity (one-by-one single nanofibers can be produced), and it is also possible to control the dimensions of the fibers by this method. Only

viscoelastic material can be used in this method to withstand the stress produced by the pulling, and only fibers with diameters larger than 100 nm can be produced depending on the orifice size [23].

2.3.2 Spinneret-Based Tunable Engineered Parameters (STEP)

STEP technique allows the formation of 3D structures. Using this technique, fibers with diameters from nanometers to micrometers can be obtained. In addition, the absence of electrical instability due to the absence of electric source in the fabrication process allows collection of highly aligned fibers of uniform dimension on the substrate. This technique uses a micropipette spinneret and a rotating substrate mounted onto a three degree of freedom micro-positioning stage (Fig 2.3); thus, the substrate undergoes both, rotational and translational motions.

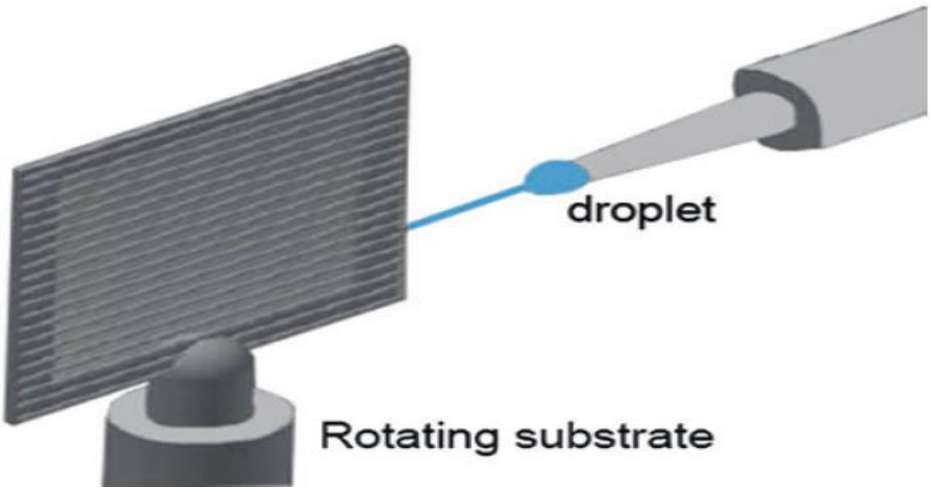

Fig 2.3 Spinneret-based tunable engineered parameter (STEP) setup [25].

The polymer solution extruded from the micropipette forms a droplet, which in contact with the movable substrate extends into filament. The polymeric filament is continuously extracted from the solution droplet and subsequently deposited on the substrate in parallel configurations. Several factors govern the fiber diameter, length, and defects including polymer solution content (polymer type and molecular weight, solvent properties) and concentration. Like other fiber manufacturing platforms, STEP technique

has challenges in the deposition of fragile nanofibers of substantial lengths at submicron spacing [26, 25].

2.3.3 Template Synthesis

In this method, polymeric, metallic, semiconductors, or ceramics nanofibers can be produced using nonporous membrane containing numerous cylindrical pores (5–50 mm thickness). It implies the use of a template or mold to obtain a desired material or structure and produce nanofibers. The template refers to a metal oxide membrane.

By this technique, nanofibers are created by passing polymer solution through the pores of nanoscale diameter under the application of water pressure on one side, which causes extrusion of the polymer, and giving fibers upon coming in contact with solidifying solution (Fig 2.4).

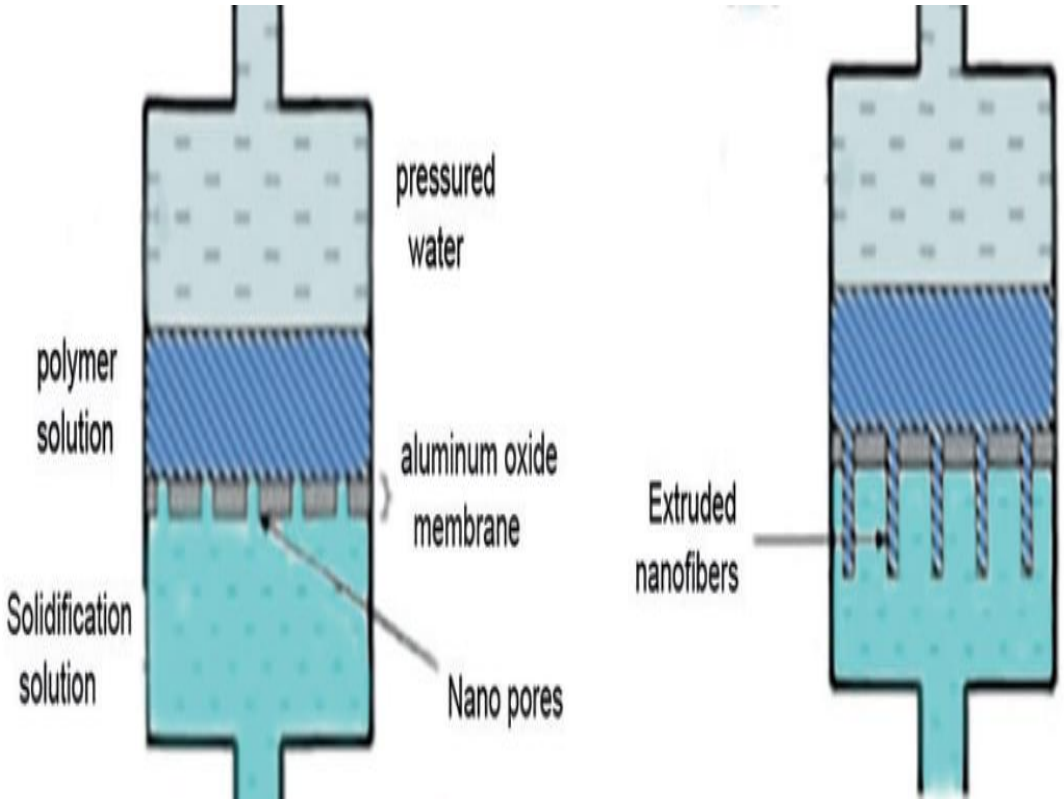

Fig. 2.4:Template synthesis technique [27].

This method cannot produce nanofibers with long fiber length, only a few micrometers long are obtained, and the diameter of these fibers is determined

by the pore size of the membrane [15,12]. The ability to fabricate nanofibers with different diameter, using different templates is one of the advantages of this method.

2.3.4 Self-Assembly

The self-assembly method (Figure 2.5) is one of the bottom-up nanomaterial fabrication methods by which molecules organize and arrange themselves into patterns or structures through non-covalent forces such as hydrogen bonding, hydrophobic forces, and electrostatic reactions [28]. It is a good technique for producing very small nanofibers (lower than 100 nm to few nm) with a length of several micrometers by forming supramolecular hydrogels through the self-assembly of small molecules via weak interactions such as hydrogen bonding and hydrophobic interactions.

The main mechanism is based on the intermolecular forces that bring small units (molecules) together; the shape of the smaller units of molecules determines the over shape of the macromolecular nanofiber. The main disadvantage of the method is that it is a complex, long, and extremely elaborate technique with low productivity and the lack of fine control of the fiber dimensions. In addition, this method is limited to prepare nanofibers from small active molecules that can self-assemble by themselves or under an external stimulus [29].

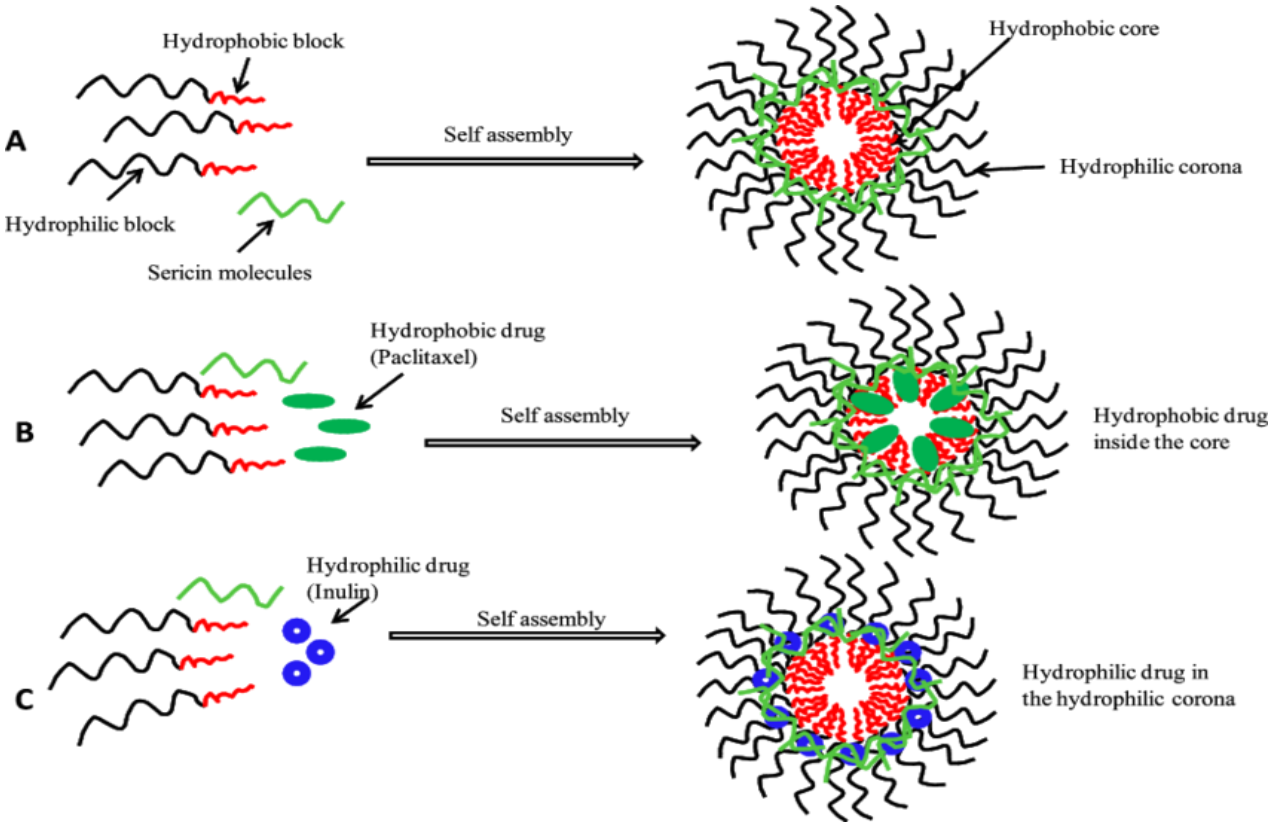

Fig.2.5: A schematic representation showing self-assembly of SS–P nanoparticles.

2.3.5 Freeze Drying (FD)

This fiber formation technique is also known as ice segregation-induced self-assembly or solid-liquid phase separation. It involves three major steps (Figure 2.6): first the solution is frozen at a low temperature (-70 to -80 ℃) allowing ice-crystal growth and nucleation, followed by primary drying process in which the ice of the frozen sample is removed through direct sublimation by putting the frozen sample in a chamber and reducing its pressure to a few millibars through a partial vacuum and the reduced pressure allows direct sublimation of the water without any chemical reaction or side products, and finally most of the unfrozen water in the material is removed by desorption in a secondary drying process.

Freeze drying (FD) has some important advantages over other techniques. Therefore, it has drawn increasing attention to the fabrication of nanofibers. It can fabricate porous structures with controllable sizes directly from polymers, such as chitin, without structure directing

additives or pretreatments needed, which cannot be achieved by other techniques, such as self-assembly and electrospinning. In addition, no high temperature and further leaching step are required for the freeze-drying process, and the use of water and ice crystals instead of an organic solvent in the scaffold fabrication process makes this process more suitable for biomedical applications. Although there are several advantages of the freeze-drying method, it is still a big challenge to engineer scaffolds with hierarchical structures (e.g., vascularized systems) using this approach. The nanofiber mats produced from this method can find application as drug delivery systems, as precursors for highly porous carbon nanofibers or as templates for synthesis of inorganic fibers [17,13].

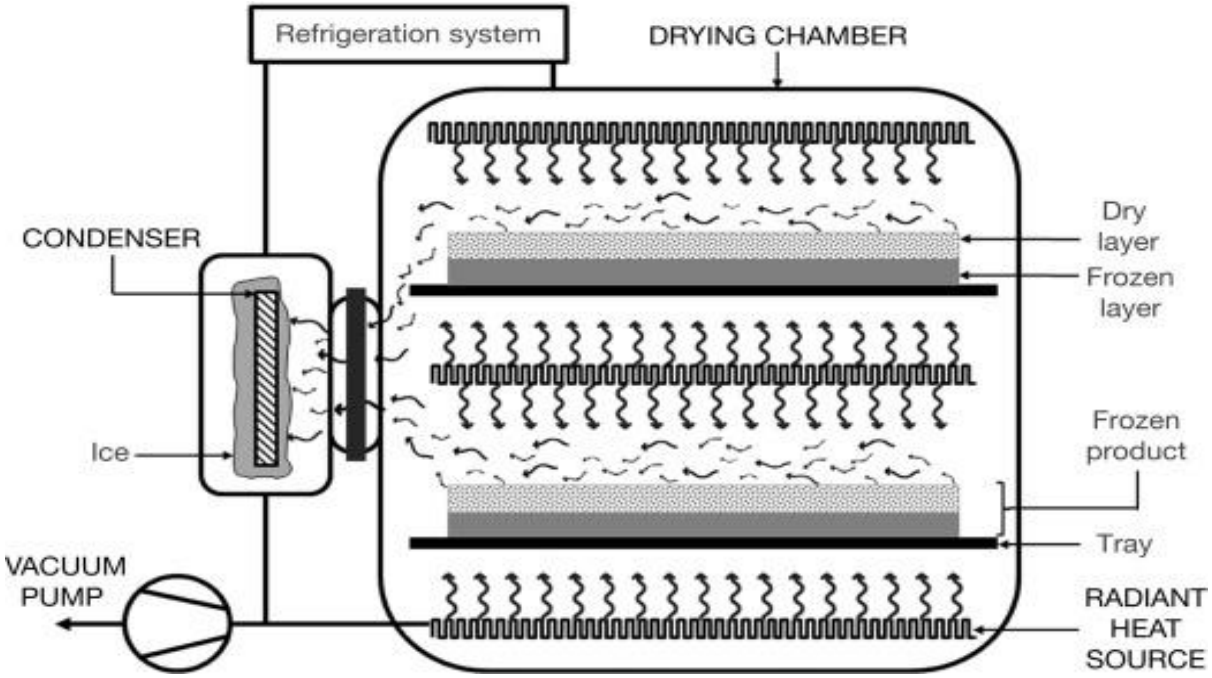

Fig.2.6: Basic components of a typical freeze-dryer system.

2.4 Electrospinning Technique

The electrospinning method includes utilizing a high voltage delivered to polymer solution in which charges will induce inside the solution. When critical limit is exceeded by the charge's addition, jet is generated first from drop that is in the needle tip leading to the construction the

"Taylor cone". The jets run to the region of lowest voltage which is the grounded collector. as shown in Figure 2.7 [31].

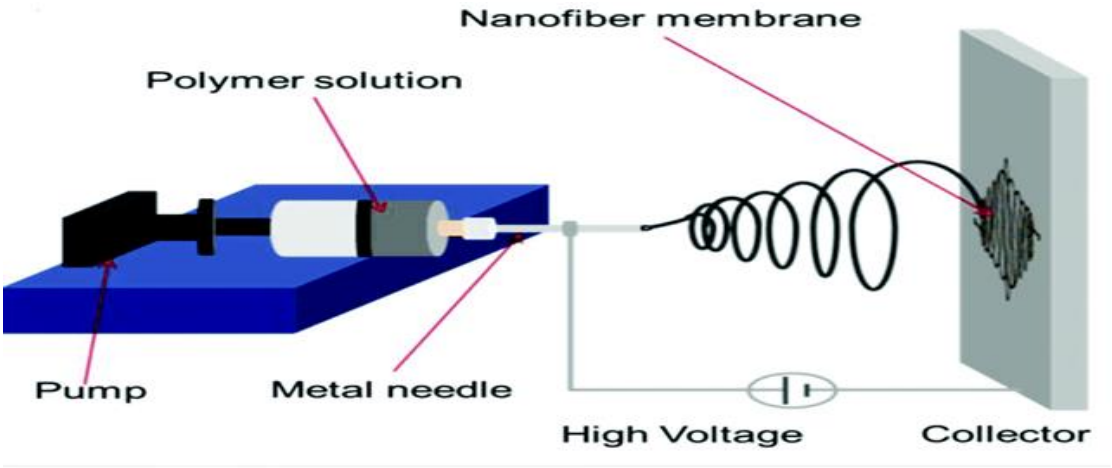

Fig.2.7: Electrospinning Setup [32].

2.4.1 Factors affecting electrospinning technique

To obtain fibers with high orientation and desirable properties, several parameters must be controlled, some of which belong to the prepared solution, some are specific to the process, and some are specific to ambient conditions

2.4.1.1 The Polymer Solution parameters

1. Concentration Effects:

Usually, increasing the concentration of solution, the fiber diameter will increase [33] .

2. Molecular weight and viscosity of solution

Basically, polymer solution often has appropriate molecular weight and adequate viscosity. Viscosity making the polymer solution to be stretched and molecular weight play an important role in entanglement and determines the chain length, therefore, when increased the chain length, the entanglement chance increase leading to make jet solution breakage not to be occur [34]. High viscosity is required to form jets without beads but not too high in which difficulties in pumping the solution occurs [35].

3. Conductivity:

The conductivity of solution is necessary property to get smoother fibers with small and high diameters so, charges increased in solution and on the transferred jets if the electrical conductivity of the solution improves. Improving conductivity of solution may be done by adding salts or ions, most of the protein and medicines create ions when dissolved in water.

Charges, also play an important role in stretching the solution so that increasing the charges has effect to increase the stretching of solution, also tends to form smoother fiber diameter [36].

4. Surface Tension:

The charges that are developed in the polymeric solution should be highly enough in electrospinning to overcome the solution's surface tension. The solution is stretched as the solution jet speeds from the source's tip to the collector, and the solution's surface tension may cause the solution to split up into droplets.

Surface tension regarded as a characteristic of a solution’s surface that makes this phenomenon. A homogeneous attractive force is produced on a liquid molecule immersed inside a solution by the surrounded liquid molecules. Molecules which to be found near the surface of liquid affected by the two forces one of them is the attractive forces come from the bulk molecules and the other is from the gas molecules and the later stronger than the former. As a result, the surface becomes in tension, causing the surface of the solution contracted, which is counterbalanced by repulsive forces arising the impacts of molecules that exist in the inner of the solution.

The total impact of all the surface liquid molecules pushing on each other leads the liquid surface to shrink, decreasing the surface area. As a

result, a spherical form has the lowest ratio of surface area to volume for a droplet of water [37].

5. Dielectric Constant

A higher dielectric constant gives lesser beads formation and smaller diameter of nanofibers [38]. N, N-Dimethylformamide (DMF) solvent usually is added to the solution to enhance fibers morphology due to its higher dielectric constant[39]. With a larger dielectric constant, the electrospinning jet's bending instability improves as well. This may also assist the decrease of the fiber diameter owing to the larger jet path [40].

6. Volatility

Invariably, it is the evaporation of solvent from the jet that yields a solid polymer nanofiber at the collector plate. Ideally, all traces of solvent must be removed by the time the nanofiber hits the collector. If not, the wet fibers may fuse together to form a melded or reticular mat. Sometimes, a flat ribbon-like nanofibers derived from the fluid –filled, incompletely dry nanofiber due to slow subsequent evaporation of solvent and collapse of the tube, are obtained. Using volatile solvents avoids this difficulty. However, when using highly volatile solvents the solution may dry on the capillary or needle, causing blockage to flow [41].

2.4.1.2 Environment of Parameters

1. Humidity

The electrospinning environment's humidity affects the solution of polymer during electrospinning. When electrospinning is done at normal atmosphere, water is likely to condense on the fiber's surface at high humidity. As a result, the fiber morphology, particularly polymer dissolved in volatile solvents, may be affected the creation of holes on the surface of the nanofibers was discovered to be caused by high humidity

[42]. Humidity has a direct effect on nanofiber porosity and in which increasing the humidity will increase the porosity [43].

2. Atmosphere type

The electrospinning process is influenced by the air composition in the electrospinning environment. Under a high electric field, different gases behave differently. Helium, for example, will decompose in a strong electric field, making electrospinning impossible. When Freon ®-12 gas is used instead of air, the fibers produced double the diameter of the nanofibers produced in air [44].

3. Temperature

The temperature of the solution increases the rate of evaporation, also increasing it will decrease the viscosity of the polymer solution. The fibers formed at a higher temperature when polyurethane is electrospun have a more uniform diameter [45]. This may be because the solution has a lower viscosity and the polymer is more soluble, permit the solution from being stretched equally. Columbic forces can generate a larger stretching force on the solution with a lower viscosity, resulting in smaller diameter fibers [46].

2.4.1.3 Processing Parameters

1. Applied Voltage (V)

Generally, one can summarize the increasing of applied voltage on the fiber diameter and morphology as follows:

a. Increasing of voltage leads to greater the stretching of the electro spinning jet due to the increase in columbic force exerted by the charges.
b. Increasing the voltage leads to increasing of the jet acceleration and hence decreasing the flight time of the electro spinning jet.
c. Increasing the voltage can reduce fiber diameters.
d. Crystallinity also increases with proper flight time [47].

2. Feed Rate

Feed rate will determine the amount of solution available for the ES process, generally:

a. Low flow rate is suitable to get enough time of polarization of solution
b. High flow rate leads to increase the beads of fibers with thick diameter.
c. Short drying time is prior to reach the collector and low stretching forces [48].

3. Capillary Tip Diameter

The using of smaller diameter led to:

a. Reduce the formation of beads, this is because of less volume of solution at the tip is collected which lead to reduce fiber diameter.
b. Also, smaller needle diameter produces the smaller droplet, this means higher the surface tension, for fixed voltage the time for stretch increases and fiber will elongate before it is reaching the collector [49].

4. Gap Distance

The distance between the needle tip to collector seems less important in the formation and morphology of resultant Nano fibers [50]. The using electrospinning distance is between (5-15 cm), (5-10 cm) range is very effected on nanofibers morphology and diameter, while over (10 cm) there is not their significance effect on the nanofiber's diameter and morphology. Generally low distance leads to:

a- Incomplete evaporation of the solvent and increases the speed of resulting fiber to access to the collector.

b- Possible lead to the formation of beads Nano fibers [51].

5. Collector Geometry

There are many types of collectors discovered for different application, such as: wire mesh, pin, grids, parallel or gridded bar,

rotating rods or wheel, liquid bath, where figure 2.8 shows the most widely used form of collectors.

A non-conducting material collector reducing the amount of fiber being deposited with lower packing density. Porous collector yields fibers with lower packing density as compared to non-porous collector plate. In porous collector plate, the surface area is increased so residual solvent molecules get evaporated fast as compared to non-porous. The cylinder rotate collector leads to alignment nanofibers while the flat plate collector leads to collect the nanofibers as a random shape [50].

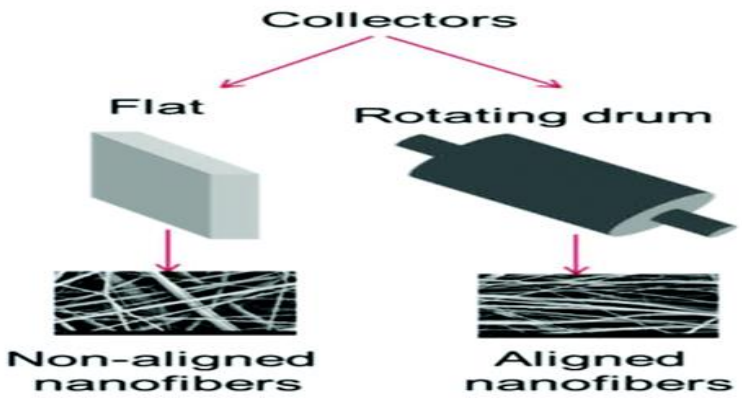

Fig.2.8: Types of collectors [50].

2.5 Phases of Wound Healing

Wound passes by different phases, as shown in figure 2.9:

1. Wound occurring distribution of the healthy tissues in the site.
2. Hemostasis stage: the creation of a clot to prevent any further bleeding.
3. Inflammation stage: penetration of neutrophils to the injured site.
4. Proliferation stage: infiltration of fibroblasts to the injured site and keratinocytes, and granulation tissue appears.
5. Maturation, the final phase which may last for years. During the final stage, fibroblasts disappear and the ECM matures [52].

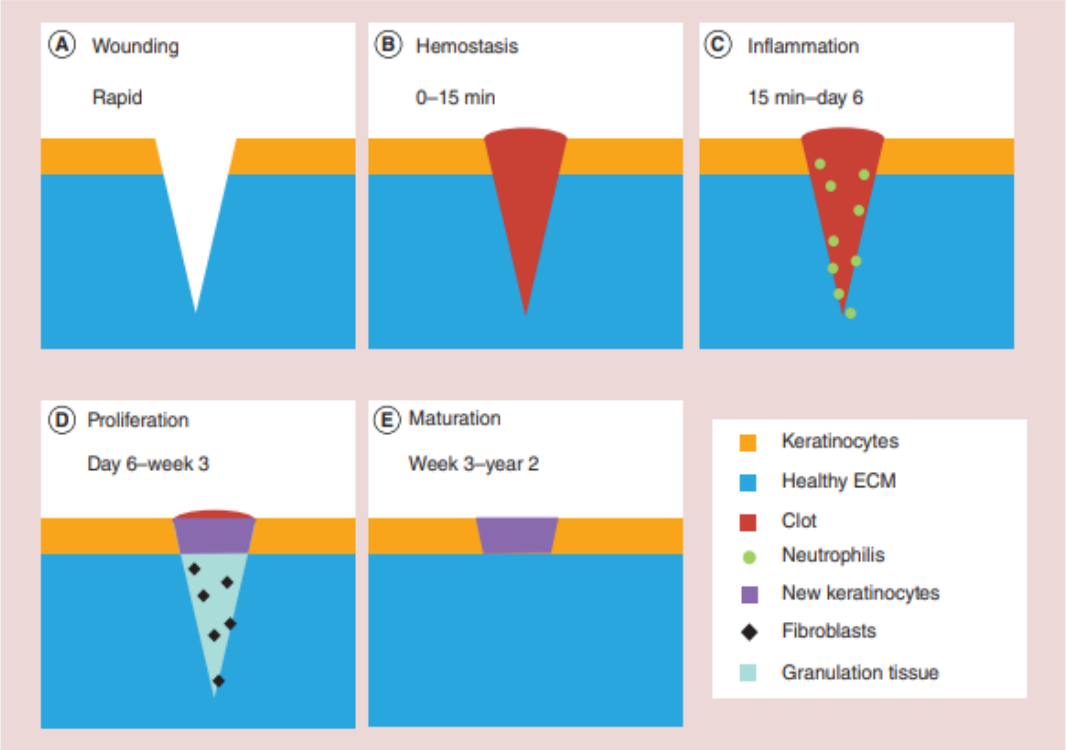

Fig.2.9: Schematic representation of the different phases of wound healing.

2.6 Wound healing Requirements:

An ideal wound dressing should absorb excessive exudates; control the moisture in the wound bed; possess good mechanical stability; have great gases transmission; protect from microorganism colonization and infections; be non-toxic, biocompatible, and biodegradable; ensure easy and non-painful removal after completed skin regeneration; and be available at an acceptable cost. The above-mentioned features are summarized in Figure 2.11[53].

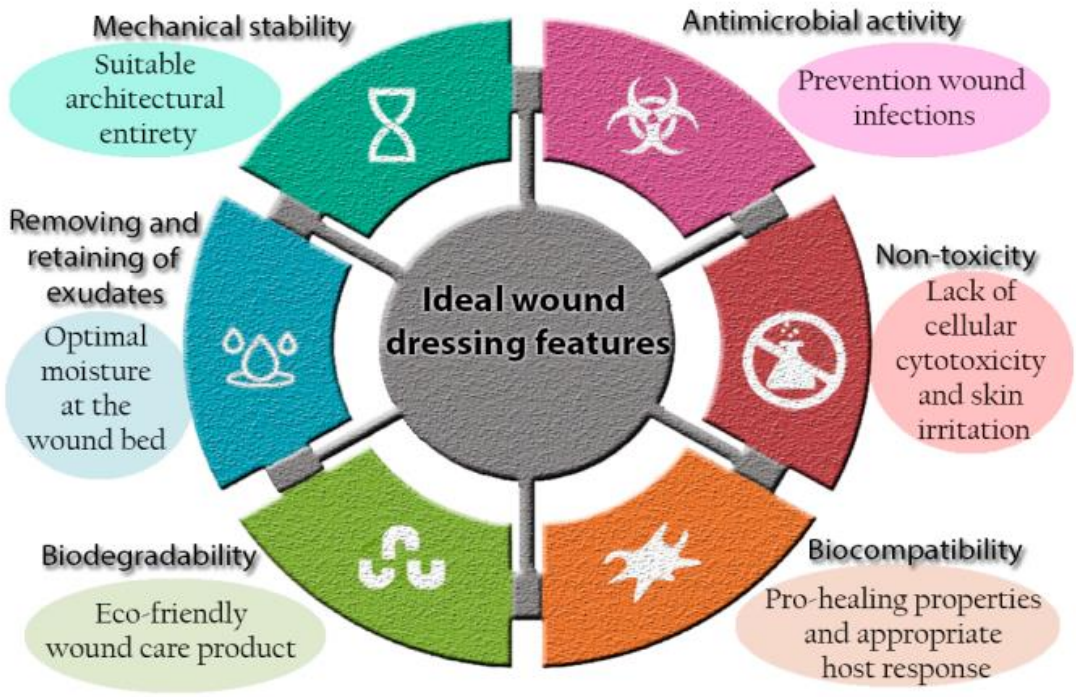

Fig.2.10: The features of the ideal wound dressing [53].

2.6.1 Moist

Wounds heal faster in a moist environment. In addition, the moist environment has other benefits that make the wounds heal with less scarring. Beside providing faster wound healing, the moist wound environment has other clinically relevant benefits. It facilitates autolytic debridement, reduces pain, reduces scarring, activates collagen synthesis, facilitates, and promotes keratinocyte migration over the wound surface, and supports the presence and function of nutrients, growth factors, and other soluble mediators in the wound microenvironment. The moist environment is also favorable for various topical treatments as well as for tissue and cell transplantation. Benefits of the Moist Wound Environment:

- Increases keratinocyte migration and reepithelialization
- Increases collagen synthesis
- Increases autolytic debridement
- Decreases necrosis
- Decreases pain

- Decreases inflammation
- Decreases scarring
- Allows cell–cell signaling and supports function of soluble mediators such as GFs
- Allows precise delivery of topical treatments
- Provides desirable environment for cell and tissue transplantation. Consequently, moist wound dressings play a vital role in the management of both acute and chronic wounds [54].

2.6.2Anti-inflammatory activity

Inflammation is involved in the first stage of wound healing process, which is characterized by the migration of leukocytes into the wound, and mainly starts by the aggregation of platelets followed by infiltration of leukocytes. Leukocytes are indispensable cellular components involved in the inflammatory response, which affect the pathogens, tissue degradation, and tissue formation, as well. The inflammatory response is crucial for the healing process, which orchestrates the cellular cascades associated with wound healing by supplying the growth factor as well as cytokine signals. On the other hand, in the physiological inflammatory response, inflammatory cells can cause preventive and inhibitory effects against bacterial invasion and debris degradation, as well [55].

2.6.3 Antibacterial activity

The antibacterial agents are antimicrobial drug used to treat or prevent the inflection caused by bacteria. These materials are inhibiting the bacterial reproduction. There are three essential mechanisms of antibacterial agents:

a) Inhibition of cell wall synthesis, such as Pencillins, Cephalosprins, Carbonnems and Glycopeptide drivitves.

b) Inhibition of protein synthesis, such as Aminogycosides, Macrolides, Tetracyclines, Lincomycins and Chlroamphenicol.

c) Inhibition of bacterial nucleic acid synthesis, such as Sulfonamides, Metronidazole, Quinolones, Rifampicin and Pyrimidine drivitives.

The microorganism (called also, microbes) is too small, microscopic organisms, some of microorganism are helpful, such as yeast, while the others are harmful by causing diseases, such as bacteria, fungi, viruses, archaea, protozoa and algae.

They are two types of bacteria:

a. Gram negative bacteria: They are more harmful and have a thinner layer (8-12nm) sandwiched between an inner and outer membrane. Examples are Escherichia coli (E-coli), Yersinia pestis and chlamydia trachomatis.

b. Gram positive bacteria: They have smooth and thicker cell wall (20-30nm), such as *staphylococcus* (staphella).

E-coli is a Gram negative, non-spore-forming, straight rod (1.1–1.5 m - 2.0–6.0 m) arranged in pairs or singly; is motile by means of peritrichous flagella or may be non-motile; and may have capsules or microcapsules. E-coli is a facultatively anaerobic, chemo-organotrophic microorganism [56]. It is oxidase negative, catalase positive, fermentative (glucose, lactose, D-mannitol, D-sorbitol, arabinose, maltose), reduces nitrate, and is -galactosidase positive. Approximately 95 % of E-coli strains are indole and methyl red positive but are Voges-Proskauer and citrate negative. Staphella is Gram-positive coccus- shaped microorganism (with diameter of between 0.7 m to1.2 m) that generally occurs in grapelike clusters but can also be found in singles and pairs [57].

Antibacterial agents are added to polymers to kill or inhibit the growth of microorganisms or to improve the mechanical properties of these polymers. Antibacterial agent activity is affected by: -

a) Concentration of antibacterial agent.
b) Environmental conditions.
c) Polymer type.
d) Microorganisms' sensitivity

The killing or inhibiting activity of addition agents, salt, or metal ions, have been increasing with increased the concentration of antibacterial agent. While at very lower concentrations they may be lose antimicrobial activity. The same result appears when studying the effect of environmental conditions. Temperature, pH, and moisture affect the efficiency of most antimicrobial agents. The studies showed that activity of antibacterial agent was higher in acidic conditions (pH 6) than in basic conditions (pH 8) [41 ,42].

2.6.4 Interrupted Growth Factor Activity

Growth factors are biological polypeptides that play a critical role almost in all phases of the wound healing process. These polypeptides stimulate the initial inflammation phase that occurs during the granulation phase of tissue development. Examples of growth factors that are significantly involved in the wound healing mechanism include transforming growth factor β (TGF-β), fibroblast growth factor (FGF), epidermal growth factor (EGF), basic fibroblast growth factor (bFGF), keratinocyte growth factor (KGF), vascular endothelial growth factor (VEGF), and platelet-derived growth factor (PDGF). These factors are prominently decreased in patients with diabetes and then result in a delayed wound healing process. The decreased levels of TGF-β1 increases the recruitment of activated

inflammatory cells leading to a delayed inflammatory phase to the proliferation phase in the diabetic wound healing process [60].

2.6.5 Antioxidation potential

Reactive Oxygen Species (ROS) are small oxygen-derived molecules mainly produced by the respiratory chain in mitochondria; some of them are hydrogen peroxide H_2O_2, superoxide anion O^{-2} or peroxide O_2^{-2}. They are oxidizing agents and mayor contributors to cell damage [61], but also have beneficial roles and, in particular, play a crucial role in the preparation of the normal wound healing response [62]. Therefore, a suitable balance between low or high levels of ROS is essential. Low levels of ROS are beneficial in protecting tissues against infection and stimulating effective wound healing by production of cell surviving signaling but, when present in excess, produce oxidative stress leading to cell damage and a pro-inflammatory status [63]. Redox imbalance occurs whether the levels of ROS exceed the capacity of endogenous antioxidants to scavenge them, which dysregulates the healing process. There are no a clear cut-off point for ROS level in tissues, but for the hydrogen peroxide (the most common ROS) the range 100–250 μM is considered for normal wounds [64]. In addition, some studies have reported that level of 10 μM of hydrogen peroxide act as chemo-attractant and stimulates the proliferation of fibroblasts and endothelial cells; at 100 μM stimulates angiogenesis via the production of vascular endothelial growth factor; but at 500 μM led to a pro-inflammatory status through the production of macrophage inflammatory protein 1-α. The antioxidants are chemical compounds that can donate their electrons to other molecules, such as ROS, thus preventing them from taking electrons from other biologically important molecules, such as proteins or DNA. Based on the mechanism of action, there are two types of antioxidant compounds: non-enzymatic and enzymatic. Non-enzymatic antioxidants are low molecular weight

compounds, such as vitamin E, vitamin C, glutathione and flavonoids. Enzymatic antioxidants include the superoxide dismutase, catalase, glutathione peroxidases and thioredoxin-1 and -2, among others [65]. Antioxidants catalyze a complex cascade of reactions to convert ROS into more stable molecules, such as H_2O and O_2, so they denominate as ROS scavengers. Regulation of redox balance, through the modulation of ROS and antioxidant levels, is a target for new therapies. Antioxidant substances that maintain non-toxic ROS levels in the wound tissues could improve healing. Thus, the interest in using antioxidant compounds for wound treatment is growing, and several biomaterials have been developed and tested [66].

2.6.6 Water vapor transmission rate

Wound healing is a complicated pathophysiological process that requires a desirable microenvironment, in which moisture is one of the most important factors. All cells of the human body live in their own fluid microenvironment. After injury, the evaporative water loss from the wound surface can be approximately twenty times greater than that of normal skin. When the wound is directly exposed to air, it dehydrates, and a scab is formed, which aims at protecting the wound from bacterial infection. However, a cell in a dry or low moisture microenvironment will lose its vitality and function and even die. It has also been reported that healing under wet conditions is faster than dry scab conditions [67]. Thus, a suitable wound dressing is essential in controlling water evaporation from a wound. The primary fundamental function and requirement for a wound dressing is to maintain the optimal moisture for wound healing. Great progress in wound dressings has been made in the past quarter century, but the current studies primarily focus on investigating the effects of different materials on wound healing, using specific cells for optimal regeneration, or trying to encapsulate chemical drugs or biomolecules to accelerate wound healing [68]. The basic

physical property of wound dressings that may influence the wound healing process has not yet been studied thoroughly, i.e., the water vapor transmission rate (WVTR), which directly regulates the moisture microenvironment of wound healing.

The ability of a dressing to control water loss can be determined by the WVTR. Therefore, the wound surface moisture can be regulated using various wound dressings with different WVTRs. An extremely high WVTR may lead to the dehydration of a wound, whereas an unacceptably low WVTR may cause the accumulation of wound exudates. Hence, a dressing with a suitable WVTR is required to provide a moist environment for establishing the best milieu for natural healing [67].

The WVTR of a material was calculated according to the following equation:

$$WVTR = mass / (area \times time) = (P/L)(Pw)(\Delta RH) \quad \text{(2.1)}$$

P is the water vapor permeability, L is the membrane thickness, (P/L) is the water vapor transmission (or permeance, Pm), Pw is the saturated water vapor pressure at the experimental temperature and the Δ (RH) is the difference of relative humidity between inside atmosphere and outside atmosphere of the membrane sealed cup. Permeance value and the water vapor permeability of the material were calculated using the following equations:

$$Permeance\ (Pm) = WVTR / Pw(\Delta RH) \quad \text{(2.2)}$$

$$Water\ vapor\ permeability\ (P) = permeance \times thickness \quad \text{(2.3) [69]}$$

2.6.7 Biocompatibility

The biocompatibility of materials is the most important factor for wound dressing application as wounds can be potentially exposed to cytotoxic environments that would exacerbate the healing process. Consequently, it is important to ensure that the wound dressing material itself is not inherently

toxic so in vitro and in vivo assessment must be utilized to properly screen the materials selection process for cytocompatibility. Fortunately, for polysaccharides they are biocompatible because of their origin in the extracellular matrix that plays a significant role during the wound healing process. Additionally, they are biodegradable and do not elicit an inflammatory immune response [70].

2.6.8 Bioactive Molecule Incorporation and Release

Advanced wound dressings developed more recently incorporate bioactive molecules to enhance patient comfort and to help accelerate the wound healing process. Antimicrobial dressings are one type of bioactive molecule important during the wound healing process that inhibits potential bacterial infections caused by acute tissue injury, post-operative surgery or from more chronic, pathological states such as diabetes. Many anti-microbial dressings are impregnated with silver, which broadly acts against infections caused by skin burns and wounds. Silver has been the traditional antimicrobial agent to treat bacterial colonies such as Staphylococcus aureus and P. aeruginosa. Its mechanism of action involves the influx of silver ions to the bacterial cytoplasm, where they shut down enzyme activity and as a result, potassium ions leak out the cell. The released ions cause the cytoplasm to burst and destroy the cell wall, leading to apoptosis. Silver can only be applied locally but has been effective inhibiting bacterial growth and its resistance. However, silver's spectrum of use should be limited because of its cytotoxicity. Therefore, the inherent antimicrobial activity of polysaccharides such as chitosan with less silver may be utilized as an alternative, less cytotoxic wound dressing. Polysaccharide materials are ideal for bioactive molecule incorporation because their biodegradability can be controlled in the body based on their polymer structural properties, tuning bioactive release. Also, they are inherently bioactive that may serve as

ligands, binding to receptors on the fibroblast's surface during wound healing to promote extracellular matrix production [71].

2.6.9 No toxic component

Free from toxic materials that can damage and lead to dire consequences.

2.6.10 adhesiveness

Providing an optimum amount of adhesive material to the wound site (excessive adhesive sustains an injury).

2.6.11 Thermal insulation

Maintaining the optimal temperature of wound site to reduce pain [72].

2.6.12 Flexibility

Flexibility is an important physical property of any dressing, affecting its ability to form an intimate contact with the wound. A recent study examining the conformability of wound dressings described several benefits for conformable dressings, including maintenance of a moist wound environment, and suggested that conformable dressings that form an intimate contact with the wound are likely to reduce dressing-related tissue trauma compared with dressings that are less flexible. Conformability of a dressing to give an intimate contact with the wound bed is becoming widely recognized as an important performance parameter; in this context, gauze is very poorly conformable. The elimination of 'dead space' has been identified as an important function for healing. Less flexible dressings are also prone to introduce mechanical stresses, leading to dressing-related tissue trauma. For an intimate contact with the wound, the dressing must be able to conform to the body shape. It has been argued that a dressing must also be able to conform to the surface of the wound bed; how well it conforms, or is flexible, is an important characteristic with significant implications for how effective it is at supporting healing [73].

2.6.13 Wettability and contact angle

Wetting is commonly characterized by the contact angle, which is defined as the angle between the tangent to the liquid–vapor interface and the solid surface at the three-phase contact line (Figure 2.11).

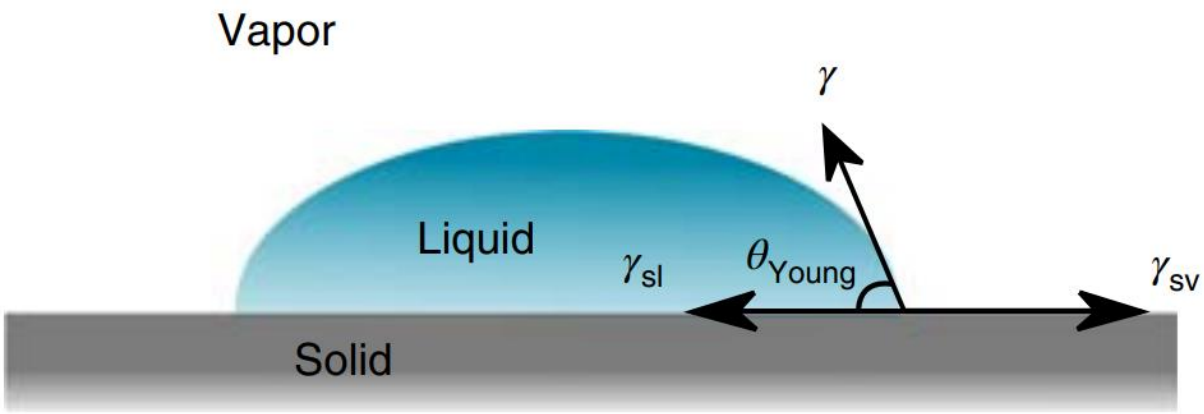

Fig.2.11: A drop of water on an ideal solid substrate.

Young contact angle (θ_{Young}) is determined by a balance of the horizontal projection of the surface tension of the water along the solid surface ($\gamma \cos\theta_{Young}$) and interfacial tensions γ_{sv} and γ_{sl}. an ideal solid surface (i.e., one that is atomically smooth, chemically homogeneous, nonreactive and nondeformable by the liquid) has traditionally been defined using the Young equation [74]:

$$cos\theta_{young} = \frac{\gamma_{sv} - \gamma_{sl}}{\gamma} \quad \text{..... (2.4)}$$

where θ_{Young} is the Young contact angle, $\boldsymbol{\gamma_{sv}}$ and $\boldsymbol{\gamma_{sl}}$ the solid–vapor and solid–liquid interfacial tensions, respectively, and γ the surface tension of the liquid. From the Young equation, it is known that a solid surface with high surface energy (i.e., high solid–vapor interfacial tension γ_{sv}) tends to show a low contact angle, whereas a low-energy surface would exhibit a high contact angle [75].

Surface wettability has an important role in many biological, chemical, and physical processes. In agriculture, the efficiency of pesticides is strongly

affected by the wettability of the plants, as well as the surface tension and viscosity of the liquid pesticide formulations. In medicine, decreasing the contact angle of titanium implants allows for better bone cell attachment, enabling better integration of the implant with the bone [76]. Antimicrobial properties of food packaging can be optimized by increasing the contact angle of the package materials, which allows for prolonged release of antimicrobial agents and leads to increased shelf life of, for example, meat products and poultry. Wetting also has an important role in many industrial processes: for painting and printing, both the liquid surface tension and the properties of the solid must be optimized to ensure suitable adhesion of the liquid to the solid [77]. Solid surface energy must be considered in many processes requiring, for example, heat transfer or lubrication. In oil recovery, the solid material must be designed to selectively absorb oil but not water, a quality also determined by its wetting properties [78]. Based on the water contact angle measurements, the materials can be classified as hydrophilic or hydrophobic. A water contact angle at 90° is used as a threshold value. Surfaces with water contact angle less than 90° is termed hydrophilic and above 90° hydrophobic. Hydrophilic surfaces are generally considered low fouling surfaces and be enough to limit cell adhesion or blood platelet activation which would then appear to enhance biocompatibility. Reduced protein fouling is likely to reduce both bacterial and mammalian cell adhesion [79]. This can be an advantage especially in short term implant surfaces but in applications where a cell adhesive surface is desired this presents a challenge. There are several proposed solutions to overcome these challenges but overall, the material properties are always balanced between the promotion of cell adhesion and infection and eventually biofilm formation prevention.

Surface roughness also influences the wettability and biocompatibility. At the cellular level, biological responses, such as the orientation and migration of cells as well as their ability to produce organized cytoskeletal arrangements are directly influenced by the surface topography. There are also evidences that suitable surface roughness, at the nano- and micrometer level, can lead to successful osseointegration of titanium implants, which is important for dental and other bone-connecting implants [80]. Due to this, porous titanium coatings have also gained a lot of interest, but increased surface roughness also enhances bacterial adhesion increasing the infection risks. In addition, surface roughness also affects wettability as the wettability of the surface is further enhanced by the surface roughness. Simply put, if the contact angle is below 90 °, adding roughness to the surface will decrease the contact angle even further. Then on the other hand, if the contact angle is above 90 °, adding roughness will increase the contact angle even more (Figure 2.12) [81]. As both surface roughness and wettability affect how proteins and cell interact with the material, it is important to separate the effect of the two from each other [82].

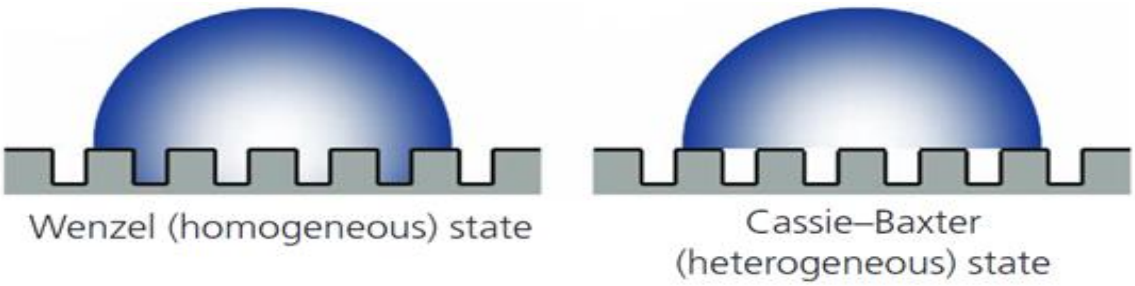

Fig.2.12: Illustration of homogeneous and heterogeneous states for a liquid drop sitting on a rough surface [81].

With the increasing attention to healthcare, the practical values of wettability materials in biomedical-related fields are receiving remarkable interests and research. Previous literatures have revealed that surface wettability, especially the superwettability like superhydrophobicity and

superhydrophilicity, have great influence on the biomolecular behaviors such as adhesion and proliferation [83]. To be specific, the superhydrophobic surfaces are capable of effectively resisting bacterial adhesion, protein adsorption, cell adhesion, and blood coagulation, while the superhydrophilic ones have the ability of antibacterial and facilitating cell attachment. These features make the superwetting biomaterials appropriate for biomedical engineering applications including cell culture, biosensing and serving as implant materials [84]. In particular, the emergence of super wettability patterned surfaces provides an effective platform to regulate the physiological process. Among them, the superhydrophobic–superhydrophilic patterned surfaces have demonstrated indispensable values on the micropatterning of the living cells for tissue engineering, cell-based microarrays, and cellular fundamental research [85]. In general, the superwetting biomaterials display great prospects in biomedical engineering field [86].

2.7 Characteristics of nanofibers required for wound healing:

The Extracellular matrix (ECM) is a ubiquitous non-cellular component of tissues and organs comprised by a heterogeneous febrile meshwork of mainly glycoproteins, proteoglycans and other small molecules that provide a support for cells. However, the role of the ECM is not merely structural but also functional. It generates a specific microenvironment in constant communication with cells, interacting with surface receptors and supplying assistance in an array of diverse fundamental processes such as cell adhesion, migration, differentiation, growth, apoptosis, etc. and is thus involved in wound healing [87]. Nanofibers usually show stochastic alignment, which makes them resemble the natural nanofibrous mesh of the ECM [88]. Moreover, the high surface area of nanofibers allows for chemical functionalisation of the surface, efficient fluid absorption and drug delivery

of encapsulated pharmaceuticals such as antimicrobials or growth factors, which can enhance wound healing [89]. Small interstices, together with the high effective surface area, can make nanofibres promote haemostasis.

Furthermore, the high surface porosity of nanofibres permits gaseous exchange across the wound, preventing desiccation and dehydration [90]. In addition, materials composed of ultrafine fibres can better adapt to the contour of the wound than sophisticated 3D materials, which is paramount in the design of medical dressings.

In healthy skin, collagen fibrils form a basket-weaved structure, and thus the special arrangement of electrospun nanofibres can affect the wound healing process. Figure 2.13 shows a schematic of the potential role of a nanofibrous scaffold in wound healing.

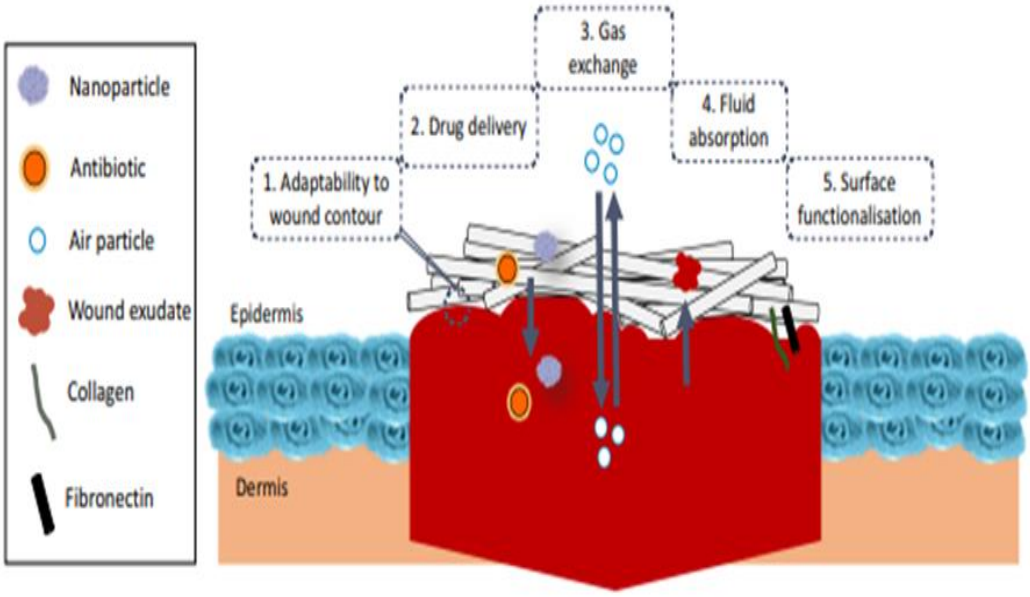

Fig.2.13: Nanofibers as dressing materials for wound healing.

Owing to dimensions in the nanometer range, porosity, and high surface area, nanofibrous scaffolds can display properties relevant for wound healing, such as: (1) adaptability to the irregular contour of the wound, thus enhancing suppleness and resilience of the scaffold; (2) encapsulation and delivery of different cargos such as antimicrobials and nanoparticles; (3) gas exchange to avoid dehydration; (4) fluid absorption, eliminating the excess

of wound exudate typical of chronic wounds and preventing growth of microorganisms and (5) surface functionalization with molecules such as collagen or fibronectin, which increases biocompatibility and further promotes wound healing [91].

2.8 The Effect of PH on Wound

Healthy, intact skin has a slightly acidic pH ranging from 4.0 to 6.0. This is an important aspect of the skin's barrier function since it regulates bacterial flora and prevents infection. When a wound occurs, the skins acidic milieu and pH is disrupted, exposing the more neutral pH (7.4) of the underlying tissue. With successful healing and re-epithelialization, the skin returns to be acidic. Acute wounds have a more neutral pH, and, during acute wound healing, there is a drop in pH caused by various factors, including hypoxia1 and increased production of lactic acid. An acidic pH environment is beneficial, by increasing fibroblast proliferation and migration and regulating bacterial colonization. If, however wound healing is delayed, then the pH will oscillate and become increasingly alkaline over time (Figure 2.14). At this stage, the wound is described as chronic and the synthesis of ECM molecules becomes impaired, thus arresting the healing process. Recordings of the chronic wound environment have been in the range of pH 7.15 to 8.9 [117].

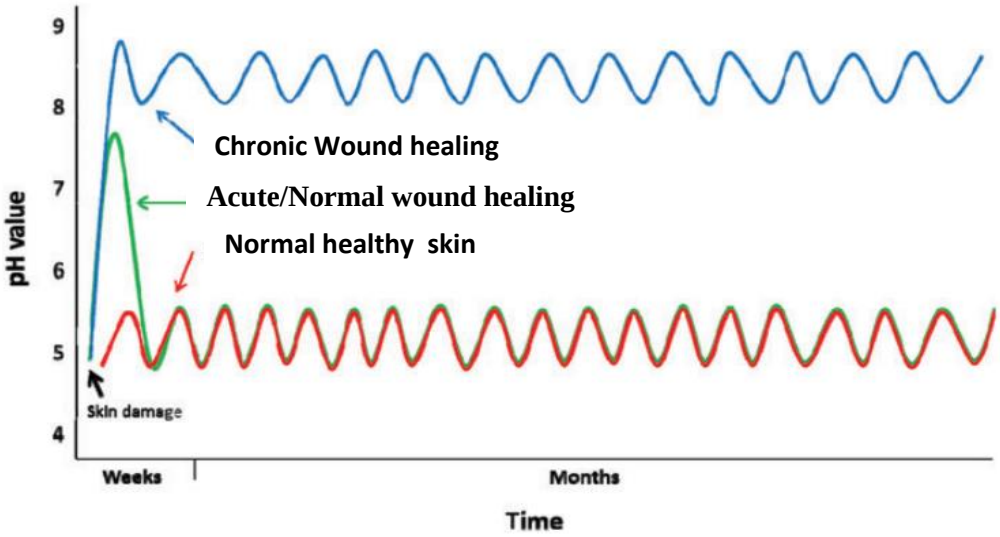

Fig.2.14: Time course of pH of healthy skin, acute wounds, and chronic wounds showing the main differences with time [117].

Various environmental factors affect the growth of bacteria, including temperature, pH, dissolved gases, osmotic pressure, and water availability. Most bacterial organisms grow best around pH values of 6.5–7.0; however, some thrive in very acidic (e.g., Acetobacter) or very alkaline conditions (e.g., Candida). Organisms grow at a range of pH defined as three cardinal points: (1) the minimum pH, below which the organism cannot grow; (2) the maximum pH, above which the organism cannot grow; and (3) the optimum pH, at which the organism grows best. Each microbial species has its own pH range in which it grows best (Table 2.1) [92].

Table 2.1: The optimum growth pH for the most prevalent microorganisms isolated from wounds.

Wound-associated microorganisms	Optimum PH for growth
Staphococcus aureus	7.0-7.5
Enterococcus faecelis	7.0-9.0
Pseudomonas aeruuginosa	6.6-7.0
Coagulase-negative staphylococci	7.0-7.5
Anaerobic bacteria	6.0-7.0

Escherichia coli	6.0-7.0
Klebsiella spp.	5.5-7.0
Candida spp.	7.0-8.0

2.9 Materials Used in Research

2.9.1 Poly (Vinyl alcohol); PVA

PVA is soluble in water, slightly soluble in ethanol and insoluble in other organic solvents [93]. It is tasteless and odorless. Other properties such as pH, viscosity, drying, melting point, refractive index, and residue on ignition are based on molecular weight and hydrolysis percentage [94].. For example, the partially hydrolyzed PVA (87–89%) is more soluble in water and it has more flexibility and adhesion to hydrophobic surfaces. On the other hand, highly hydrolyzed PVA (91–99%) is more stable in the presence of organic solvents and has more tensile strength and adhesion onto hydrophilic surfaces [95].

Hydroxyl groups of PVA (Figure 2.15), produce inter and intramolecular hydrogen bonding. They have an important effect on the rheological and mechanical properties of the polymer, which is determined by the density and spatial arrangement of hydroxyl groups [96]. These bonding are also responsible for phenomena such as phase separation and gelation, which means the solution properties are time-depending. Rheological and viscoelastic properties of the PVA solutions are affected by the effectiveness of the physical bonding and polymerization degree and the molecular orientation is developed easier by steady shear [97]. It is important that a polymeric drug delivery system overcomes all the limitations and disadvantages related to conventional therapeutic agents and must be biodegradable, biocompatible, and non-toxic. The most representative delivery systems are hydrogels, microparticles, and loaded polymeric nanoparticles. It has been proved that the individual properties of polymers

are key for their use for specific targets [98]. In this regard, PVA is one of the most used polymers in the biomedical filed based on its mechanical properties, high ability to form films, nontoxicity, water-solubility, no carcinogenicity, hydrophilicity, good compatibility and biodegradability in human tissues and fluids [99]. As well, PVA has three remarkable properties for a polymer to be used as a delivery system: high surface stabilization, chelation properties and low protein adsorption properties resulting in low cell adhesion compared with other hydrogels. All previous mentioned properties made that PVA would be extensively used in many biomedical applications, including wound dressings [100].

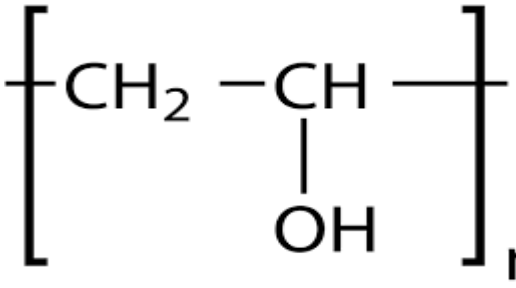

Fig.2.15: Chemical structure of polyvinyl alcohol.

2.9.2 Collagen

Collagen is the most abundant family of proteins in the body. It is found in large amounts in tissues (skin, tendons, cartilage, vessels, viscera, etc.), where it has a wide range of structural and mechanical functions, including:

- Providing a structural support framework for tissues and organs.
- Providing elasticity to skin and the tissues of the cardiovascular system.
- Playing major roles in organ development, wound healing and tissue repair through its involvement in cell differentiation and migration, entrapment, local storage and delivery of growth factors and cytokines [101].

It is a good candidate to be used in electrospinning for several reasons, such as:

- Collagen is the most abundant protein in the body where it acts as a structural building block of the ECM found in most native tissues.
- Collagen possesses natural binding sites for the adhesion of osteoblasts, which aid in bone formation.
- It has known chemical, mechanical, and biocompatible properties.
- There are many processing methods that can be used to isolate collagen in large quantities.
- It can increase cell adhesion and the differentiation of many cells. Unfortunately, collagen alone does not have the mechanical and structural support to perform well after implantation [102]. The chemical structure of collagen shown in figure 2.16.

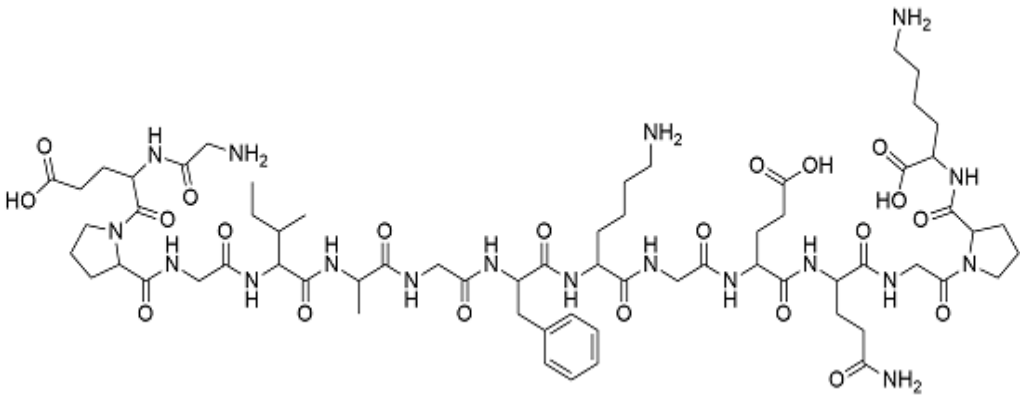

Fig.2.16: Chemical structure of collagen.

2.9.3 Hyaluronic acid (HA)

Hyaluronan is a naturally occurring biopolymer used in medical applications ranging from cataract surgery and post-surgical adhesion prevention to hydrophilic coatings. A unique biopolymer, hyaluronan is one of a number of polysaccharides that occurs in the body's mucous membranes and is known as mucopolysaccharides. It was first isolated from the vitreous body of the eye in 1934 by Karl Meyer, who called hyaluronic acid. The term

hyaluronan is attributed to Endre Balazs, who coined it to encompass the different forms the molecule can take—for example, the acid form, hyaluronic acid, and the salts, such as sodium hyaluronate, which form at physiological pH of 3 [103].

Over the years, quite a lot is known about the appearance of the hyaluronan molecule; its behavior; its occurrence in different tissues and body fluids; the manner in which it is synthesized by the cells, metabolized, and cleared from the body; and the nature of some of the functions it performs. Hyaluronan and related polysaccharides are called glycosaminoglycans [104]. These substances are made up largely of repeating disaccharide units containing a derivative of an amino sugar.

The most abundant glycosaminoglycans in the body are chondroitin sulfates; others are keratin sulfate, heparin and heparin sulfate, and dermatan sulfate. Figure 2.17 shows the disaccharide unit of hyaluronan, consisting of alternating glucuronic acid and N-acetylglucosamine units, which are repeated over and over to form long chains. Each repeating disaccharide unit has one carboxylate group, four hydroxyl groups, and an acetamido group. Hyaluronan differs from the other major glycosaminoglycans in that it does not have sulfate groups [105].

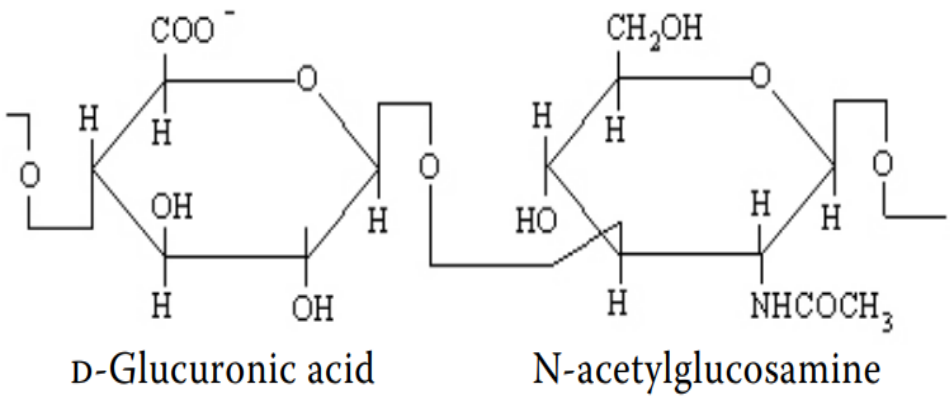

Fig.2.17. Chemical structure of Hyaluronic Acid [106].

In the body, hyaluronan is synthesized by many types of cells and extruded into the extracellular space where it interacts with the other constituents of the extracellular matrix to create the supportive and protective structure around the cells. It is present as a constituent in all body fluids and tissues and is found in higher concentrations in the vitreous humor of the eye and the synovial fluid in the joints. In mammals, the highest reported concentration is found in the umbilical cord [107]. Hyaluronan is also a major contributor to wound healing [108]. This polymer plays a significant role in the inflammation, granulation, and remodeling phases that the body undergoes, as seen in Table 2.2:

Table 2.2: Hyaluronic Acid and the Wound Healing Process [109].

Wound-Healing Phase	Contributing Role of HA
Inflammation	Activation of macrophages and neutrophils
	Moderation of inflammation
Granulation	Cellular differentiation
	Cellular Proliferation
	Cellular Migration
Remodeling	Reduced Scar Formation

Hyaluronan possesses a unique set of characteristics: its solutions manifest very unusual rheological properties and are exceedingly lubricious, and it is very hydrophilic.

- *Rheological Properties*. In solution, the hyaluronan polymer chain takes on the form of an expanded, random coil. These chains entangle with each other at very low concentrations, which may contribute to the unusual rheological properties. At higher concentrations, solutions have an extremely high but shear-dependent viscosity [110].
- *Lubricity.* The extraordinary rheological properties of hyaluronan solutions make them ideal as lubricants. There is evidence that hyaluronan separates most tissue surfaces that slide along each other. Solutions of hyaluronan are extremely lubricious and have been

shown to reduce postoperative adhesion formation following abdominal and orthopedic surgery [110].

- *Hydrophilicity.* As mentioned, the polymer in solution assumes a stiffened helical configuration, which can be attributed to hydrogen bonding between the hydroxyl groups along the chain. As a result, a coil structure is formed that traps approximately 1000 times its weight in water [111].

2.9.4 Ganoderma lucidum (Rishi Mushroom)

Genus Ganoderma is found in the genus Ganoderma of the kingdom Fungi, the phylum Basidiomycota, the subphylum Agaricomycotina, the order Polyporales, and the family Ganodermataceae [112]. Ganoderma lucidum is an edible woody-brown color saprotrophic fungus that lives on dead or dying trees and old stumps or logs. Also, known as Reishi or Lingzi mushroom is very typical for traditional Chinese medicine. Antitumor, immune modulation, liver protection, and other bioactivities can be found in G. lucidum spores [113].

This mushroom is commonly grown in Malaysia because of the country's year-round dampness and high temperatures. Polysaccharides and triterpenoids found in G. lucidum fruiting bodies may have therapeutic potential in the treatment or prevention of peripheral or central inflammatory disorders, according to a chemical study. Bioactive antioxidant metabolites can be found in a variety of Ganoderma species [114].

As a result of their minimal risk of side effects, mushrooms and other herbal medicines are increasingly being used as nutraceuticals, food supplements and cosmeceuticals.

Numerous G. lucidum triterpenes exhibit significant biological action (Figure 2.18) against a wide range of diseases Cancer [115], antioxidant [116], immunomodulator [117], anti-inflammatory, hypocholesterolemic

[118], hypoglycaemic, antimicrobial [119], cardioprotective, antiarthritic, anti-hyperpigmentation, proapoptotic, antiandrogenic, anti-allergicand antinociceptive

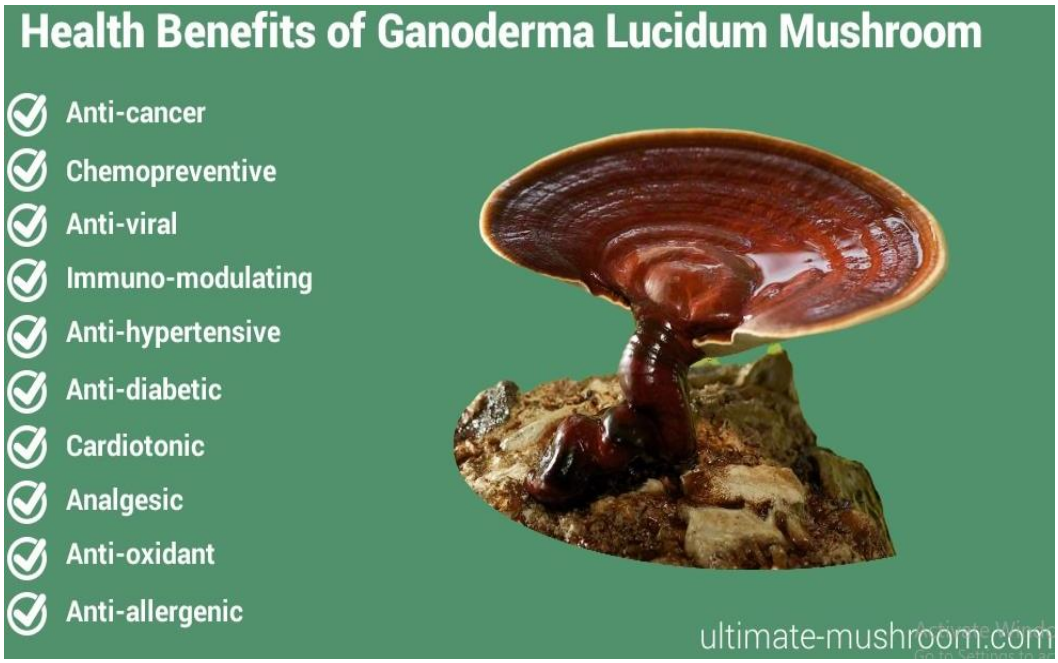

Fig.2.18. Benefits of Rishi mushroom.

Polysaccharides, triterpenoids, and proteins are three of GL's most important components since they are critical to the fungus's biological actions. GLSP (Ganoderma lucidum spore powder), which is shown in (Figure 2.19) has been used to improve the biological effects of these biomolecules compared to GL itself. As a result, more effort is being put into extracting Ganoderma lucidum polysaccharide (GLP), which is the most important component.

Extraction of GLP with standard solvents is the most often used approach traditional solvent extraction (TSE). Although TSE is simple and safe to use, high temperatures (70–80 °C) and extended extraction durations are necessary. Multiple runs are needed to optimize the product because the procedure is inefficient. Ultrasound-assisted extraction (UAE) was tested in GLP extraction to address these constraints. This method was shown to be

more effective and less expensive, all while requiring less solvent and less extraction time [120].

Fig.2.19: Ganoderma Lucid Powder.

Many of useful compounds can be isolated from the Ganoderma Lucid, such as triterpenes (figure 2.20), which have antidiabetic actions by normalizing plasma glucose and insulin levels.

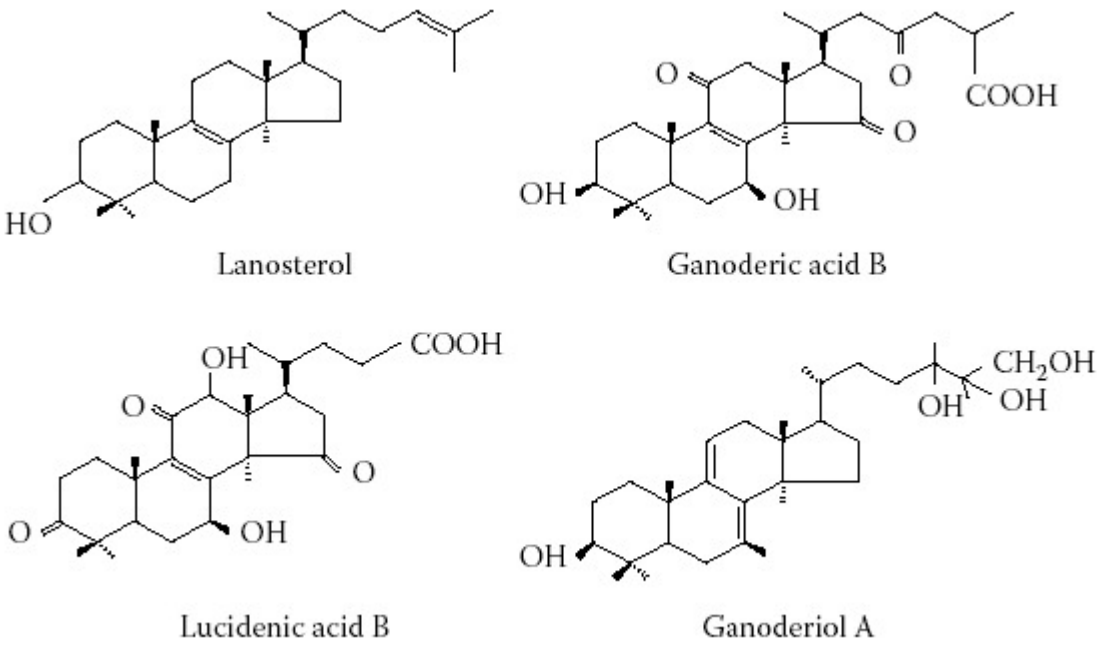

Fig.2.20:Chemical structure of lanosterol and three of the many triterpenes isolated from Ganoderma lucidum [121].

2.9.5 Pepper (Capsicum annuum L.)

Peppers belong to the genus Capsicum [122] and excellent sources of phytochemicals, such as anthocyanins, vitamins, phenolic acids, flavonoids, carotenoids, and capsaicinoids (Figure 2.21) [4]. Numerous studies have demonstrated the antibacterial activity of capsaicin and dihydrocapsaicin bioactive compounds isolated from Capsicum annuum. Capsicum species have been used for the treatment of arthritis, rheumatism, stomach aches, skin rashes, dog/snake bites, and flesh wounds [123]. These therapeutic applications are related to the capsaicin, phenolic compound, and carotenoid content of peppers [124]. Carotenoids are the pigments responsible for the yellow, orange, and red color of many types of peppers; however, they are more than mere pigments and play an important role as antioxidants as well. In their capacity as antioxidants, carotenoids protect cells and tissues from harmful radical oxygen species (ROS), acting as scavengers of singlet molecular oxygen , peroxyl radicals, and reactive nitrogen species (RNS) [125].

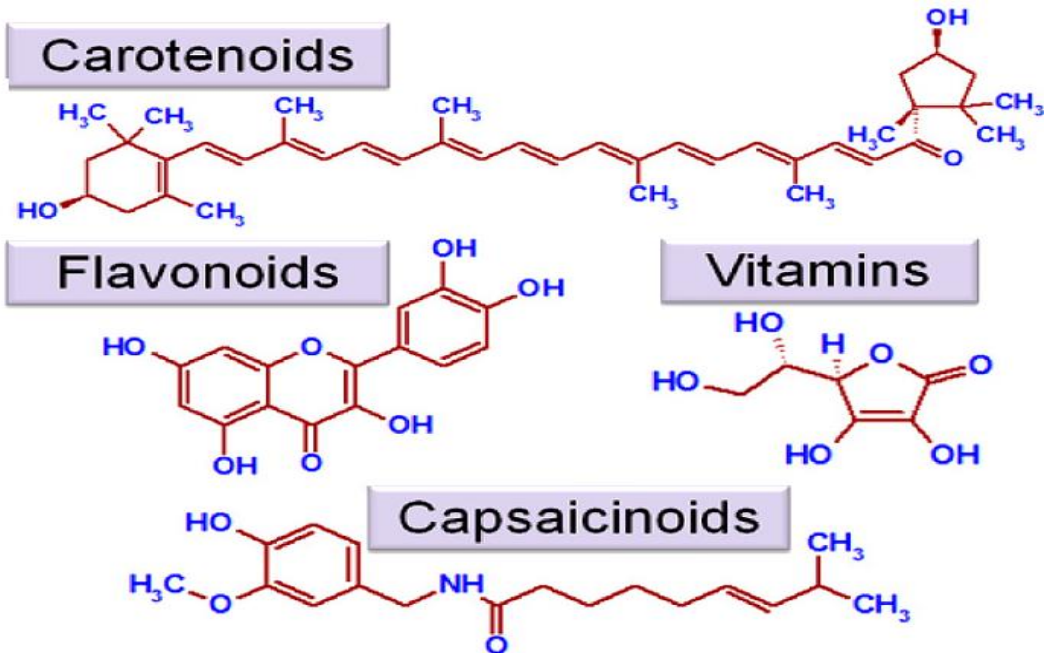

Fig.2.21:Structure of compounds present in Capsicum annuum L. [126].

2.9.6 Iodine (I_2)

Iodine (Figure 2.22) is a chemical element with the symbol I and atomic number 53. The heaviest of the stable halogens, it exists as a semi-lustrous, non-metallic solid at standard conditions that melts to form a deep violet liquid at 114 °C (237 °F), and boils to a violet gas at 184 °C (363 °F) . it is a natural dark violet, non-metallic element that plays a key role in human metabolism. It is essential to produce thyroid hormones and an iodine deficiency can result in hypothyroidism. Iodine occurs naturally in the form of iodide ions in sea water, fish, oysters, and certain seaweeds. It can also be found in vegetables grown in iodine rich soil and dairy products. It has been described as 'the most potent antiseptic available [127]. It is toxic if taken orally undiluted. The lethal dose for an adult human is 30 mg/kg, which is about 2.1–2.4 grams for a human weighing 70 to 80 kg. Excess iodine can be more cytotoxic in the presence of selenium deficiency. Iodine supplementation in selenium-deficient populations is, in theory, problematic, partly for this reason. The toxicity derives from its oxidizing properties, through which it denaturates proteins (including enzymes) [128].

Fig.2.22: Iodine (I_2) [128].

2.9.7 Rosmarinus officinalis L.

Rosmarinus officinalis L. is a medicinal plant that belongs to the Lamiaceae family and is commonly known as rosemary. Beside the culinary

uses due to the characteristic aroma, this plant is also widely employed by indigenous populations, where it grows wild [129].

Rosmarinus Officinalis has demonstrated potent antibacterial and antifungal activities in multiple studies. Like its antioxidant activity, the antimicrobial activity of rosemary depends on the chemical composition of its essential oil, which can vary greatly depending on location, climate, and time of harvest. The anti-microbial activity of oil is also determined by the interactions between its components [130]. Rosemary has been shown to inhibit the growth of bacteria such as Escherichia coli, Listeria monocytogenes, and Staphylococcus aureus. The significance of rosemary's antibacterial effect does not end there, however. According to one study, rosemary has the potential to inhibit the drug resistance of some bacteria by overcoming and reducing the impermeability of these bacteria's membranes [131]. This represents an innovative strategy for containing and eliminating resistant strains of bacteria. Rosemary essential oil can also increase the susceptibility of certain bacteria to standard antibiotics [132]. This impressive antibacterial activity makes R. officinalis a strong defense against common food pathogens and a promising new preservative that could replace artificial additives [133].

In addition to its antibacterial properties, Rosmarinus officinalis has several antifungal mechanisms. The plant's essential oil has been shown to inhibit the adhesion of Candida albicans by denaturing cellular structures and altering membrane permeability. According to one study, rosemary can even prevent the development of highly resistant fungal biofilms. By coating nano particles with rosemary essential oil, a nano bio system was produced that significantly inhibited the adherence and biofilm development of Candida fungal strains [134]. Both these new strategies are necessary alternatives to traditional medicine in the treatment against drug-resistant fungi. The ability

to inhibit the growth and aflatoxin production of many fungi contributes to rosemary's potential as an effective food preservative [135]. Rosemary contains many chemicals as shown in Figure 2.23.

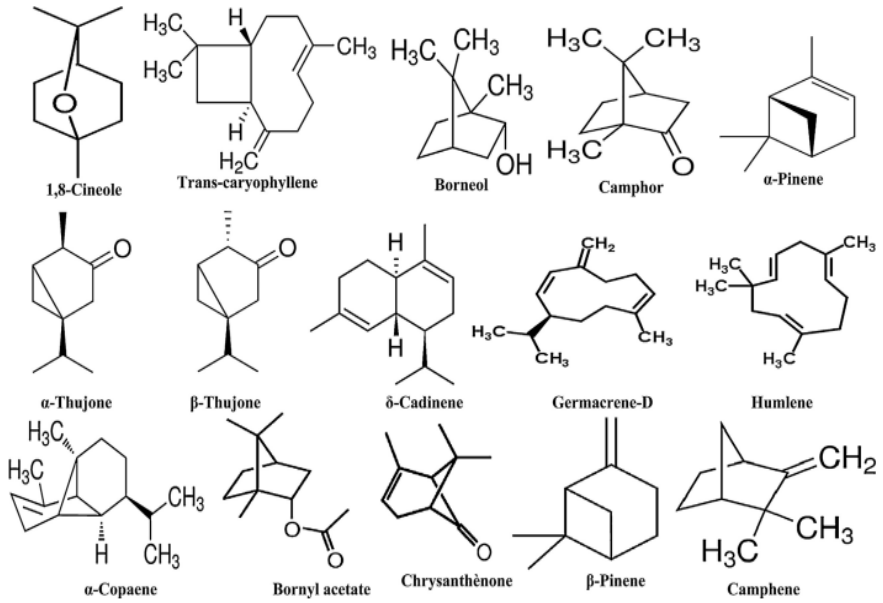

Fig.2.23: Structures of chemicals components of Rosemarinus officinalis essential oil (ROEO) [136].

2.9.8 Bay laurel (Laurus nobilis L., Lauracea)

Laurus nobilis L. is an aromatic herb used extensively to add a distinctive aroma and flavor to food. Their leaves can be used as a spice, to treat a variety of complaints, neuralgia, and intestinal cramps and for its beneficial effect upon the digestive system. Its antimicrobial activity against both gram-positive and gram-negative bacterial species has been also demonstrated. From the laurel leaves can be obtained a complex mixture of phytochemicals according to the extraction process that was used. The essential oil is the hydrophobic and volatile fraction recovered by distillation and their chemical composition commonly included mono- and sesquiterpenes; while by alcoholic or hydroalcoholic extraction, polar compounds such as flavonoids, saponins, alkaloids, and polyphenols are usually obtained [137].

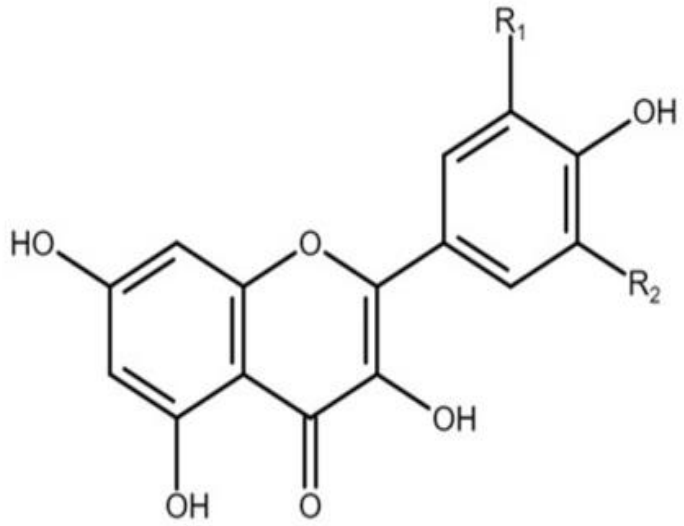

Flavonol	R1	R2
Kaempferol	H	H
Quercetin	OH	H
Isorhamnetin	OMe	H

Fig.2.24: Chemical structure of the main flavonols found in Laurus nobilis L.[138]

2.9.9 Ocimum Basilicum

Ocimum basilicum possess the potential of reducing the risks of certain microbial infections due to the presence of active antimicrobial compounds. Essential oils, alkaloids, tannins, steroids, flavonoids, phenols and resins might be included in these secondary metabolites [139]. Different basil extracts might be consisted of essential oils, vitamins and poly phenolic compounds and many other biologically active compounds which exhibit insecticidal, antipathogenic and stress-relieving properties and treats ailments related to respiratory tract, excretory organs, gastric illnesses, skin and eye problems [140]. Medicinal plant, specifically species of Ocimum plants are highly ranked due to possession of exhibiting varying properties of curing different diseases [141]. Considerable amount of naturally occuring antioxidants which is contained by Ocimum basilicum have protecting effects against numerous degenerative ailments [142]**.** In drug metabolism, Ocimum basilicum is found to have chemomodulatory effects. Therefore, using natural products of plants is highly beneficial against

oxidative damage caused by different degenerative and toxic agents and in preventing from side effects of various chemical products [143].

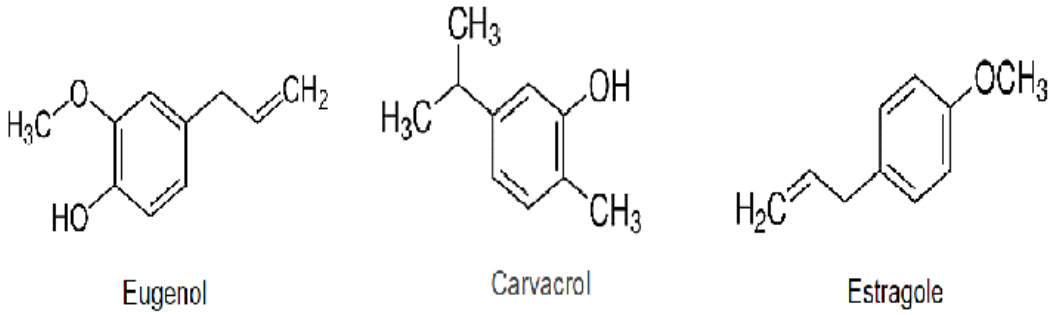

Fig.2.26: Chemical structure of active compound Ocimum [144].

2.10 Literature Survey

Minoo Sadri et al. (2015), investigated the effect of green tea extract as a natural and ecofriendly antibacterial additive on the healing effect of chitosan/ polyethylene oxide wound dressing nanofiber produced by electrospinning method. Results showed that the optimum conditions were Voltage; 20 kV, feed rate; 0.5 ml/h, nozzle-collector distance; 10 cm, and chitosan/polyethylene oxide weight ratio; 0.9%. The healing ability of the prepared nanofibers was studied on the rat's wound. Chitosan/polyethylene oxide/ green tea showed the best healing effects in comparison with the other prepared wound dressings. These results confirmed that green tea extract helps to keep wound surface moist, reduces inflammation and increases the speed of recovery and healing [145].

Hadi H. et al. (2015), studied the antibacterial and anti-inflammatory activities of sodium alginate-lavender essential oil nanofiber to promote burn healing. Authors demonstrated that nanofibrous dressings of sodium alginate and lavender essential oil not only possessed antibacterial activity against S. aureus, but they also effectively inhibited the production of pro-inflammatory cytokines both in-vitro and in-vivo. This resulted in a fast recovery of animals exposed to UVB irradiation, without the appearance of erythema on their injured skin. The strong anti-inflammatory action of

sodium alginate was evident in all the conducted investigations. On the other hand, lavender oil expressed a high antimicrobial effectiveness and also acted to control the induced inflammation [146].

Faegheh P. et al. (2017), prepared a biocompatible and non-toxic herbal wound dressing encapsulation of Hypericum perforatum alcoholic extract at different concentrations (10, 30 and 50 % v/v) into poly e-caprolactone electrospun nanofibers. The electrospinning processing parameters, such as needle tip to collector distance, applied voltage and flow rate of feed solution were changed until accumulated nano-scale fibers without bead structures were obtained.The antibacterial activity of the optimized bandages was investigated by the disc diffusion method against strains of S. aureus and E. coli.

The release content of the herbal drug was tested by the total immersion method in phosphate buffer saline and displayed a constant drug liberation with time. Water vapor transmission rate for the wound dressing was evaluated by pseudo-extra cellular fluid for optimal samples. The crystallinity and thermal behavior of the mats with and without H. perforatum alcoholic extract were studied by X-ray diffraction and differential scanning calorimetry (DSC). The results of antibacterial activity, cell culture and In vitro methyl thiazolyl tetrazolium assays demonstrated these unique structures as being very useful as burn and ulcer dressings [147].

Jung C. et al. (2017), prepared polycaprolactone (PCL) nanofibers containing Spirulina extract for dermal wound healing in a rat model. Alginate, with its hydrophilic structures capable of holding large amounts of water, to support the backbone of the nanofibers. The morphological characteristics, hydrophilicity, water absorbance, skin adhesiveness, toxicity to human keratinocyte cells (HaCaT), and Spirulina extract emission over

time were assessed. Alginate improved the efficacy of Spirulina PCL nanofibers in moisture maintenance and adhesion ability, which highly affected recovery in the rat skin wound model [148].

Shababdoust et al. (2017), studied two series of polyurethane (PU), based on polycaprolactone (PCL) as soft segments with two diferent molecular weights (2000 and 530 Da), and hexamethylene diisocyanate (HDI) and 1,4-butandiol (BDO) as hard segments were synthesized to fabricate curcumin-loaded electrospun nanofbrous PCL-based PU substrate. Chemical structures of the synthesized PUs were characterized by FTIR and NMR spectroscopy techniques. The thermal properties were analyzed by DSC, surface hydrophilicity was studied by static contact angle and bulk hydrophilicity was evaluated by water uptake test. Thereafter, bead-free PU nanofberous substrate containing curcumin was fabricated by electrospinning and morphology of the mats was observed by SEM. Mechanical properties of the electrospun mats in comparison with polymeric flms were assessed by a universal test machine. The in vitro release of curcumin was studied by UV–Vis spectroscopy. The optical density of the bacterial solutions was used to evaluate the antibacterial activity of the curcumin-loaded nanofbrous mats against Escherichia coli.

The results showed that curcumin-loaded PU synthesized by PCL with molecular weight of 2000 Da displayed better mechanical properties as well as better antibacterial properties in wound dressing application [149].

Rashid A. et al. (2018), prepared novel electrospun chitosan/polyvinyl alcohol/zinc oxide nanofibrous mats by electrospining technique with antibacterial and antioxidant properties for diabetic wound healing. Non-healing wound is a serious complication of diabetes, associated with extremely slow wound closure, and a high rate of infection, resulting in amputation or losses of limbs, high health care cost and poor quality of

patient's life. These nanofiber mats comprise of wound healing activities of chitosan-PVA nanofibers and antibacterial properties of ZnO.

The results revealed that chitosan/PVA/ZnO nanofibrous membranes possessed higher antibacterial potential against E. coli, P. aeruginosa, B. subtilis and S. aureus compared to chitosan/PVA nanofibrous membranes and higher antioxidant potential The in vivo wound healing studies showed that chitosan/PVA/ZnO nanofibrous membranes resulted in accelerated wound healing [150].

Min S. K. et al. (2018), developed a coaxial Alginate-PCL nanofibrous dressing for controlled release of spirulina extract. The bioactivity release pattern, water absorbance, and mechanical strength must be controllable. Spirulina extract was physically impregnated inside a nanofiber without significant chemical bonding to PCL or Alginate polymers. This led to an initial burst and continual release of bioactive molecules from the nanofiber. By altering the concentration of Spirulina extract, mechanical strength and water absorbance were controllable. In addition, the dressing patch showed no cytotoxicity towards human epithelial cells, not causing skin-irritation [151].

Robin A. et al. (2018) developed a PVA membrane with biosynthesized silver nanoparticles for wound dressing. Plant extract from a medicinal plant Mimosa pudica was utilized for the synthesis of bAg. Synthesized bAg were characterized by UV and FTIR. The morphology of bAg was obtained from Transmission Electron Microscopy (TEM) and found that they were spherical in morphology with average particle size 7.63 ± 1.2 nm. bAg nanoparticles incorporated PVA membranes were characterized using several physicochemical techniques such as SEM, Energy Dispersive X-Ray Spectroscopy (EDS) and XRD.

The results confirmed the successful incorporation of bAg in PVA fibers. PVA nanofiber membranes containing bAg had good mechanical strength, exudate absorption, antibacterial activity, blood compatibility, and cytocompatibility.

Qingchang C. et al. (2019), fabricated nanobioglass incorporated chitosan- PVA (polyvinyl alcohol) trilayer nanofibrous membrane (nBG-TFM) via sequential electrospinning. This membrane exhibited excellent biocompatibility, antibacterial activity and regeneration promotion effect. Furthermore, spatially designed structure optimized functions of each component and provided more suitable microenvironment as compared with uniform membrane. Rat full-thickness skin defects model and mice diabetic chronic wound model showed that nBG-TFM could achieve significantly accelerated and enhanced healing, in terms of complete re-epithelialization, improved collagen alignment and formation of skin appendages [152].

Ozlem E.et al. (2019), produced perforatum oil loaded electrospun polymeric wound dressing material to be used in wound therapy. Perforatum oil is known to have curative effect on wound-healing process. Wound dressing material was produced in two layers, the upper layer was made of electrospun PCL nanofibres to maintain membrane integrity and mechanical strength while the bottom layer that is designed to be in contact with the wound was formed by electrospraying while the electrospining of PEG/H. perforatum oil and PCL polymer solutions from opposite directions (concurrently).

FTIR, optical and electron microscopy, tensile and gas permeability, contact angle, swelling and in vitro release tests were utilized for material characterization. Encapsulation of H. perforatum oil in PEG capsules which were hold by PEG fibres among PCL fibres was confirmed. H. perforatum oil was released in controlled manner. Antimicrobial activity tests on S.

aureus and E. coli revealed that H. perforatum content exhibited antimicrobial activity on both. Material was found to be biocompatible and suitable for use as wound dressing according to the results of in vitro tests, in which L929 mouse fibroblast cell line incubated with materials for investigation of biocompatibility (WST-1) and cell–material interactions [153].

Yan G. et al. (2019), fabricated a notable chitosan/poly (ethylene oxide) nanofiber mats containing tea tree oil liposomes (TOLCENs) using electrospinning process. The microstructures and morphology were characterized by scanning electron microscopy. The porosity, fluid absorbability, water vapor permeability and mechanical properties of nanofiber mats were also estimated by ethanol density method, gravimetric method, dish method and tensile test, respectively. Compared to the chitosan/poly (ethylene oxide) composite freeze-dried sponges containing tea tree oil liposomes, TOL-CENs had greater porosity, water absorption, breathability, and better mechanical properties. In addition, the controlled-release properties and long-term bactericidal capability of the material were also assessed.

From the analysis of the release kinetics and mechanism, it was found that the significant decreased terpinen-4-ol concentration gradient from liposomal surface to the outside of material was the key to the sustained terpinen-4-ol release in virtue of liposomal encapsulation. TOL-CENs exhibited long-term and more excellent microbicidal effects against Staphylococcus aureus, Escherichia coli and Candida than chitosan/poly (ethylene oxide) nanofiber mats. The combination of tea tree oil liposomes and chitosan in nanofiber mats synergistically destroyed cell membrane, prevented cell adhesion and caused the irregular aggregation of cytoplasm,

resulting in cell disintegration observed by transmission electron microscope [154].

Hasham S. Sof et al. (2019), simultaneously loaded lavender oil and silver nanoparticles (Ag NPs) onto polyurethane nanofibers for wound-healing applications. An abundance of Ag NPs in the fibers decreased the diameter of the fibers while increased concentration of the lavender oil increased the diameter. The Ag NPs and lavender oil improved the hydrophobicity of the nanofibers and ensured the proliferation of chicken embryo fibroblasts cultured in-vitro on these fiber dressings. The anti-bacterial efficiency of the nanofiber dressings was investigated using E. coli and S. aureus, which yielded zones of inhibition of 5.9 ± 0.5 and 16.2 ± 0.8 mm, respectively, indicating excellent bactericidal properties of the dressings [9].

Irem U. et al. (2019), fabricated and characterized various concentrations of peppermint essential oil (PEP) loaded on poly(ε-caprolactone) (PCL) electrospun fiber mats for healing applications, where PEP was intended to impart antibacterial activity to the fibers. SEM images showed that the morphology of mats was smooth, uniform, and bead-free. The average fiber diameter was reduced by the addition of PEP from 1.6 ± 0.1 to 1.0 ± 0.2 μm. Functional groups of the fibers were determined by Raman spectroscopy.

Gas chromatography-mass spectroscopy (GC-MS) analysis demonstrated the actual PEP content in the samples. In vitro degradation was determined by measuring weight loss and their morphology change, showing that the electrospun fibers slightly degraded by the addition of PEP. The wettability of PCL and PEP loaded electrospun fiber mats was measured by determining contact angle and it was shown that wettability increased with the incorporation of PEP. The antimicrobial activity results revealed that PEP loaded PCL electrospun fiber mats exhibited inhibition

against S.aureus (gram-positive) and E.coli (gram-negative) bacteria. In addition, an in-vitro cell viability assay using normal human dermal fibroblast (NHDF) cells revealed improved cell viability on PCL/PCL electrospun fiber mats [155].

Majid S. et al. (2020), prepared porous electrospun poly(ε-caprolactone)/gelatin nanofbrous mat containing cinnamon for wound healing application: in vitro and Cinnamon (cin) was loaded into poly(ε-caprolactone)/gelatin (PCL/Gel) nanofbrous matrices to fabricate an appropriate mat to improve wound healing. Mats were fabricated from PCL/ Gel [1:1 (w/w)] solution with 1, 5 and 25% (w/v) of cinnamon. The fabricated mats with and without cinnamon were used to treat the full-thickness excisional wounds in Wistar rats. The results indicated that the amount of cinnamon had a direct effect on porosity, mechanical properties, water uptake capacity, water contact angle, water vapor transmission rate and cell proliferation. In addition, the results of in vivo study indicated that after 14 days, the wounds which were treated with PCL/Gel 5% cin had better wound closure (98%) among other groups. These results suggest that the cinnamon can be used as a suitable material for wound healing[156].

Petr S. et al. (2020), prepared curcumin/usnic acid-loaded electrospun nanofibers based on hyaluronic acid distilled water/Dimethylsulfoxide(DMSO) solvent systems at room temperature. The mean nanofibers diameter is 298 nm. The loading of the hydrophobic curcumin and usnic acid into hydrophilic hyaluronic acid matrix was performed without utilizing toxic chemical agents such as dicyclohexylcarbodiimide (DCC) and 4-dimethylaminopyridine (DMAP). It is supposed that the absence of the above-mentioned catalyst reagents can provide the biocompatibility of materials based on curcumin/usnic acid-loaded hyaluronic acid. The possible presence of DMSO in residual amounts

in the fibrous materials is expected to enhance the anti-inflammatory properties and local analgesic and antiseptic activity of the fibers.

During the electrospinning process, the effect of the electric voltage was demonstrated. It was found that the prepared solutions are easily electrospun despite the molecular ratio of hyaluronic acid and biologically active agents. This technology of curcumin/usnic-acid-loaded hyaluronic acid fibers obtainment significantly broadens the application of the electrospun fibers filled by pharmacological agents in modern biomedical systems, such as wound dressings, ambustial materials and drug delivery scaffolds [157].

Md. Abdus Shahid et al. (2020), manufactured multicomponent Nano fibrous mat by electro spinning technique from a blended solution of polyvinyl alcohol, honey, and Curcumin longa (turmeric) extract as the wound dressing material. Ethyl acetate extraction was followed to obtain a restorative component of turmeric. Nanofibers of fabricated mat show an average diameter of 340 nm with better moisture management properties compared to polyvinyl alcohol nanomat alone. The agar diffusion method has been used to evaluate the antibacterial activity against Staphylococcus [158].

Ismail A. I. et al. (2020), prepared innovative and bioactive wound dressings prepared by electrospinning mimicking the native structure of the extracellular matrix (ECM). Bilayer wound dressing material was produced by sequential electrospinning of quaternized poly (4-vinyl pyridine) (upper layer) on the Centella Asiatica (CA) extract containing electrospun poly (D, L-lactide-co-glycolide) (PLGA)/poly (3- hydroxybutyrate-co-3-hydroxy valerate) (PHBV) blend membrane (lower layer).

SEM was utilized to show a uniform and bead-free fiber structure of electrospun membranes. The average diameter of CA extract containing electrospun PLGA/PHBV blend membrane was calculated 0.471±0.11 µm.

Chemical, thermal, mechanical properties, and adsorption capacity of electro spun membranes, as well as the cumulative release of CA from the electro spun PLGA/PHBV membrane, were investigated. Viability, adhesion, and attachment of human fibroblast cells on the electrospun membranes on pre-set days were evaluated by the colorimetric Cell Titer 96 Aqueous One Solution Cell Proliferation Assay (MTS assay) and SEM.

Results revealed that CA loaded bilayered electrospun wound dressing showed promoted attachment and proliferation of fibroblasts. Hence, it can be concluded that CA extract containing bilayered electrospun wound dressing has a promising potential for wound healing applications [120].

Yunpeng Y. et al. (2021), manufactured thymol-loaded polyurethane fibrous membranes by a portable electrospinning device with multi-functions, including adjustable perfusion speed for a large range from 0.05 mL/h to 10 mL/h and high voltage up to 11 kV, was designed. The thymol-loaded ethanol-soluble polyurethane (EPU) skin-like W&B nanofibrous membranes with antibacterial activity were fabricated via the custom-designed device. Ultimately, the resultant nanofibrous membranes composed of EPU, fluorinated polyurethane (FPU), and thymol presented uniform structure, robust waterproofness with the hydrostatic pressure of 17.6 cm H2O, excellent breathability of 3.56 kg m^{-2} d^{-1}, the high tensile stress of 1.83 MPa and tensile strain of 453%, as well as high antibacterial activity. These results demonstrate that the new-type device has potential as a portable electrospinning apparatus for the fabrication of antibacterial membranes directly on the wound surface and puts a new way for the development of portable electrospinning devices [159].

Kai C. et al. (2021), prepared a novel curcumin-loaded sandwich-like nanofibrous membrane (CSNM) using sequential electrospinning for the hemostasis, antibacterial and accelerate wound healing. The morphology of

the nanofibrous membrane was analyzed by SEM. In addition, the water absorption capacity, water vapor transmission rate, water contact-angle, and in vitro drug release were all tested. Then in vitro and in vivo hemostatic experiments demonstrated that CSNM has a good hemostatic effect. Antioxidant effect was assessed by the DPPH radical scavenging method and CSNM presented a high antioxidant activity. Additionally, CSNM demonstrated excellent antibacterial activity by the disk diffusion method. Furthermore, the rat dorsal skin defects model revealed that the CSNM distinctly induced the granulation tissue grew, collagen deposition and epithelial tissue remodeling. Meanwhile, the results of the immunohistochemical staining showed that the CSNM can facilitate the expression of CD31 and TGF-β in the early stage of the wound, thereby accelerating wound healing. In general, this study proved that the multifunctional CSNM has great potential as wound dressing in wound healing [160].

Muhammad N. S. et al. (2022), studied antibacterial and cytocompatible tricomponent composite electrospun nanofibers made of PVA, CuONPs, and Momordica charantia (bitter gourd) extract as a wound dressing. Metallic nanoparticles have several biomedical applications due to their antibacterial qualities, yet they're also poisonous. Developing green nanoparticle production to avoid toxicity. Adding Momordica charantia extract reduced copper oxide nanoparticle toxicity and gave electrospun nanofibers antioxidant characteristics. Copper oxide content was tuned to achieve good antibacterial activities with low toxicity. Morphological features, chemical interactions, crystalline structures, elemental analyses, antibacterial activity, cell adhesion, and toxicity were characterized. All samples had consistent shape without bead formation, but CuO concentration increased nanofiber diameters. The sample containing 0.6% CuO has the most antibacterial

activity. Nanofibrous mats were also cytocompatible with NIH3T3 fibroblasts. Nanoparticles increased nanofibers' mechanical characteristics. Nanofibrous mats are recommended for wound dressing due to their good performance [161].

Marwah S. M. et al. (2022), By electrospinning Nicaraven-loaded collagen solution, a biopolymer wound dressing was made. After dissolving collagen in acetic acid, Nicaraven was added at 2 w/w%, 4 w/w%, and 6 w/w%. The result was electrospun. Several trials were done to characterize the wound dressings. Nicaraven-loaded scafolds were nontoxic to L929 fibroblast cells and protected them against oxidative stress. Different formulations of Nicaraven-loaded collagen wound dressings were tested in a rat model of excisional diabetic wound. In the study, collagen/4% Nicaraven and collagen/6% Nicaraven wound dressings had a higher percentage of wound closure, epithelium thickness, and collagen deposition than collagen/2% Nicaraven, collagen-only, and sterile gauze. Gene expression studies demonstrated that the wound dressings lowered glutathione peroxidase, NFK, and MMP9 gene expression levels. Wound healing using collagen/4% Nicaraven and collagen/6% Nicaraven scafolds was related with increased b-FGF, VEGF, and collagen type I gene expression. Wound healing activity of collagen/4% Nicaraven and collagen/6% Nicaraven was similar. This study suggests collagen wound dressings with 4% and 6% Nicaraven can heal diabetic wounds in the clinic [162].

Walaa S. A. et al. (2022), developed a skin patch using a biocompatible polymer to treat skin infections caused by AMR bacteria. Electrospinning was used to prepare and characterize bee venom melittin. Melittin-loaded fibers had smooth surfaces without beads or pores, indicating effective preparation. 1030 160 nm was the average fiber diameter. Melittin fibers had

49 3 g/mg drug loading and 84 5% entrapment efficiency. This system's high EE% indicates its preparation. In vitro release of melittin-loaded fibers showed 40% release after 5 min and full release after 120 min. Rapid disintegration and dissolution of PVP fibers caused this releasing behavior. In vitro cytotoxicity of melittin demonstrated a 24-h exposure to 10 g/mL is safe, but not 48 or 72 h. The antimicrobial MIC investigation showed a MIC of 5 g/mL against sensitive and resistant strains of S. aureus, A. baumannii, E. coli, and C. albicans yeast. The antimicrobial inhibition zone test of melittin fibers showed its antibacterial efficiency against all tested microorganisms, supporting its usage as a wound dressing patch for human skin infections. Before clinical use, the safety and activity of this fibrous system should be evaluated in vivo on an infected skin animal model [163].

2.10 Summary of Literature Review

The literature review covers several researchers who have studied nanofiber dressings for wound healing, studying antibacterial, antioxidants, and Antifungal behavior, effect of natural fillings and their types on them Behavior.

Most researchers have focused on the use of hydrophilic polymers nature and soluble in toxic organic solvents for production Hydrophilic nanofibers or the use of water-soluble polymers for Preparation of nanofibers for abrasion treatment.

During her current studies, she is interested in preparing nanofibers with Super hydrophilic properties based on lowest contact angle in wettability test.

In addition, he used essential oils (Ocimum basilicum oil, Laurus nobilis oil, Rosemary oil) and solids (I_2, Capsicum annuum, G. lucidum), where they were put together in the final sample on nanofibers that are more anti-bacterial, antioxidant and anti-fungal and improve the growth and fusion of

cells, thus accelerating the process of healing the wound, where the wound was treated within five days.

.

Chapter Three

Experimental Work

3.1 Introduction

This chapter includes:

1- Listing the used materials (PVA, HAc, Coll., Iodine (I_2), Ocimum basilicum oil, Laurus nobilis oil, Rosemary oil, Capsicum annuum, Ganoderma lucidum) and mention their properties.

2- Describe the procedures used to prepare nanofiber textile and the procedure to investigate the antibacterial action of nanofiber textile against Escherichia coli (E-coli) and Staphylococcus aureus (staphella) microorganisms.

3- Listing the required tests and the devices used.

3.2 Materials

3.2.1 Poly (vinyl alcohol); PVA

PVA was purchased from Verdean house, Daryaganj, New Delhi-110002 (India), CAS NO: 9002-89-5 with the properties listed in Table (3.1).

Table 3.1: Properties of the used polyvinyl alcohol.

Property	Data
Color	White crystalline powder- flakes – granules
Solubility	Cold water soluble (partially hydrolyzed)
Viscosity (cP)	27-33
Molecular weight (g/mol)	160,000
Degree of hydrolysis (%)	86.0 -89.0

3.2.2Collagen Powder (Coll.)

Coll. is a biodegradable polymeric material with a molecular weight (360,000), CAS NO: 9007-34-5 from CDH (India).

3.2.3 Hyaluronic Acid Sodium Salt (HAc)

Purchased from SRL Pvt. Ltd., India company, CAS NO: 9067-32-7 with the properties listed in Table (3.2).

Table 3.2: Properties of the used Hyaluronic Acid Sodium Salt.

Property	Data
Color	white powder
Purity (%)	99.31
Molecular weight(kDa)	10000-20000
PH	7
Glucuronic acid (%)	47.02
Chlorides (%)	0.3
Iron (ppm)	< 80
Heavy metal (ppm)	<10
Arsenic (ppm)	< 2
Protein (%)	0.03

3.2.4 G. lucidum

Purchased from DXN PHARMACEUTICAL SDN BHD, ingredients of reishi mushroom powder (G. lucidum): mycelium and fruit body with the properties listed in Table (3.3)

Table 3.3: Properties of the used Ganoderma lucidum

Property	Data
Product name	Ganoderma lucidum
CAS NO	9012-72-0
Active ingredient	Polysaccharides, Triterpenes
Molecular Formula (M.F)	C18H30O14
Particle size	100% pass-through 80 mesh
Appearance	Brown, yellow fine powder
Solubility	Good solubility in water

Elements	Copper, Zinc, Manganese, Magnesium, Phosphorus, Sulfur, Potassium, and Selenium

3.2.5 Capsicum annuum

Purchased from MB2B in China with the properties listed in Table (3.4)

Table 3.4: Properties of the used Capsicum annuum

Property	Data
Latin name	Capsicum annum Linn
Appearance	Brown fine powder
Shelf life	24 months
Purity	100% pure
Particle size	100% pass 80 mesh
Loss of drying	2.55%
Total heavy metal (ppm)	≤10.0
Lead (ppm)	≤2.0
Arsenic (ppm)	≤0.1
Cadmium (ppm)	≤1.0

3.2.6 Iodine (I_2)

Iodine was purchased from Flucku, a Swiss company, CAS ON: 7553-56-2 with the following properties listed in Table 3.5.

Table (3.5): Properties of the used Iodine.

Property	Data
Color	dark gray/purple black
Physical state	solid element
Density (g/cm^3)	4.93 at 20°C
Melting point (°C)	114
Boiling point (°C)	184

3.2.7 Ocimum basilicum oil

Ocimum basilicum oil was purchased from SNN Natural Products, New Delhi, CAS NO: 84775-71-3 with the properties listed in Table (3.6)

Table 3.6: Properties of the used Ocimum basilicum oil.

Property	Data
Appearance	transparent fluid
Colour	light yellow to yellow green
Odor	specific, of basil
Relative density, g/cm3	from 0.870 to 0.900
Refractive index (20 °C)	from 1.4650 to 1.4800
Optical rotation (25 °C), °C	from -8.5 to -17.5
Solubility in 80% ethanol (V/V)	01:01
Acid value, mg KOH/g	more than 4
Ester value, mg KOH/g	4 to 15
Linalool	50 to 70
Limonene	5 to 7
Methyl cinnamate	1.5 to 3
Methylhavicol	0.5 to 1.5

3.2.8 Rosemary oil

Rosmarinus officinalis was purchased from SNN Natural Products, New Delhi, CAS NO: 8000-25-7 with the properties listed in Table (3.7)

Table 3.7: Properties of the used Rosemary oil.

Property	Data
Appearance	transparent fluid
Colour	Pale yellow
Relative density, g/cm3	0.899
Refractive index (20 °C)	1.463
Optical Rotation	-18

Solubility	Solubility in alcohol

3.2.9 Laurus nobilis oil

Laurus nobilis oil was purchased from SNN Natural Products, New Delhi, CAS ON: 8007-48-5 with the properties listed in Table (3.8)

Table 3.8: Properties of the used Laurus nobilis oil.

Property	Data
Appearance	transparent fluid
Colour	Pale green to olive-green liquid
Relative density, g/cm3	0.917
Refractive index (20 °C)	1.3329
Optical Rotation	-18
Solubility in 80% ethanol (V/V)	01:01
Acid value	2,3
Ester value	21,74

3.3 Preparation Electrospinning Solutions

3.3.1 Preparation of (PVA: Coll: HAc) blend

PVA solution (10 wt.%) was prepared as the neat solution, and another Coll. and HAc solutions (with different concentrations) were also prepared. These polymeric solutions were mixed so that, 15 binary polymeric blends and three tertiary blends were obtained, in addition to the single PVA solution, as shown in table (3.10).

The neat solution was prepared by dissolving 10 gm PVA in DW by magnetic stirring at RT for 60 minutes. Coll. solutions (3, 5, and 7 wt.%) and HAc solutions (3.5 and 5.5 wt.%) were prepared by dissolving appropriate amounts of them separately in DW at RT with mixing for 30 and 60 min,

respectively. A duration of 60 min was adopted to prepare the tertiary blends to incorporate the three polymeric solutions shown in figures (3.1, 3.2).

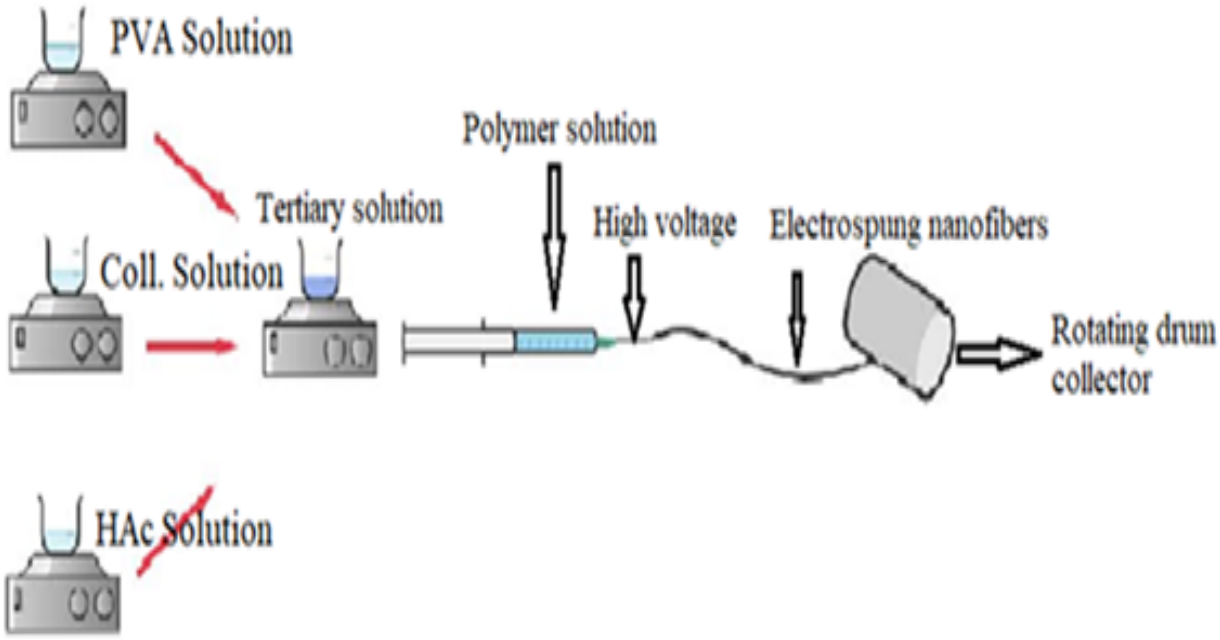

Fig.3.1: Scheme diagram of preparation tertiary solution and electrospinning process.

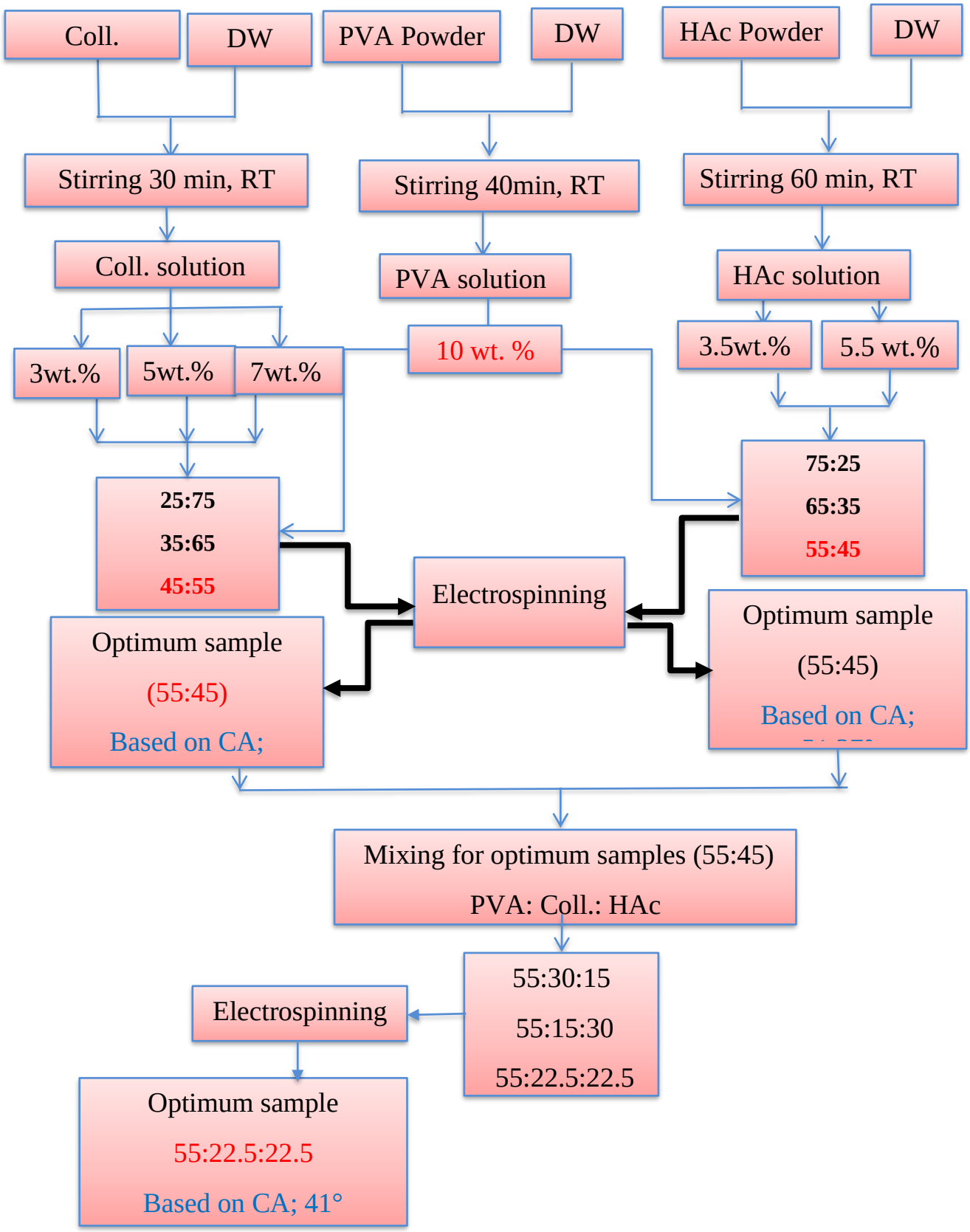

Fig.3.2: The general procedure for preparing (PVA: Coll: HAc) solution.

Table (3.9): Components of the prepared polymeric blends

Sample	Ratios (%)
10% PVA	100
10%PVA: 3%Coll.	75:25
	65:35
	55:45
10%PVA: 5%Coll.	75:25
	65:35
	55:45
10%PVA: 7%Coll.	75:25
	65:35
	55:45
10%PVA: 3.5%HAc	75:25
	65:35
	55:45
10%PVA: 5.5%HAc	75:25
	65:35
	55:45
10%PVA: 7%Coll.: 5.5%HAc	55:30:15
	55:15:30
	55:22.5:22.5

3.3.2 Preparation of (Tertiary polymeric: G. lucidum) Solution and (Tertiary polymeric: Capsicum annuum) Solution:

Solutions for both powders are prepared by adding the powder to the triple solution. They are added to the triple solution with different weights (1, 3, and 6) wt.% by using a magnetic mixer for 10 hours to obtain a homogeneous solution at room temperature. The G. lucidum solution and Capsicum annuum solution symbolize the A and B symbols. The general procedure for preparing samples is shown in figures (3.3, and 3.7).

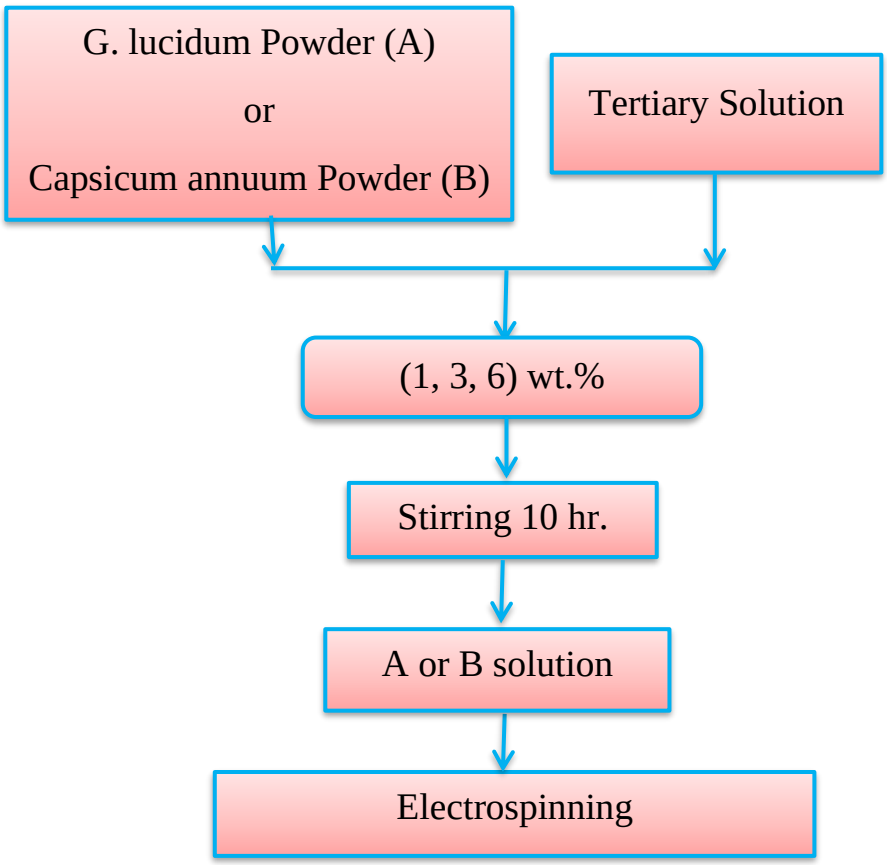

Fig.3.3: The general procedure for preparing (Tertiary polymeric: G. lucidum Solution and (Tertiary polymeric: Capsicum annuum) Solution.

3.3.3 Preparation of (Tertiary polymeric: I_2) Solution:

Preparation of (Tertiary polymeric: I_2) Solution by I_2 solution was carried out according to the following procedure: grinding the iodine molecules to powder, adding I_2 powder (0.1,0.2,0.3) wt.% to 0.1 M from acetic acid to obtain complete solubility for iodine. It is an addition to the triple solution at RT with mixing for 10 hr. to get a homogeneous solution at room temperature. The resulting solution after adding iodine is denoted by the symbol C. The general procedure for preparing solution (C) is shown in figures (3.4, and 3.7).

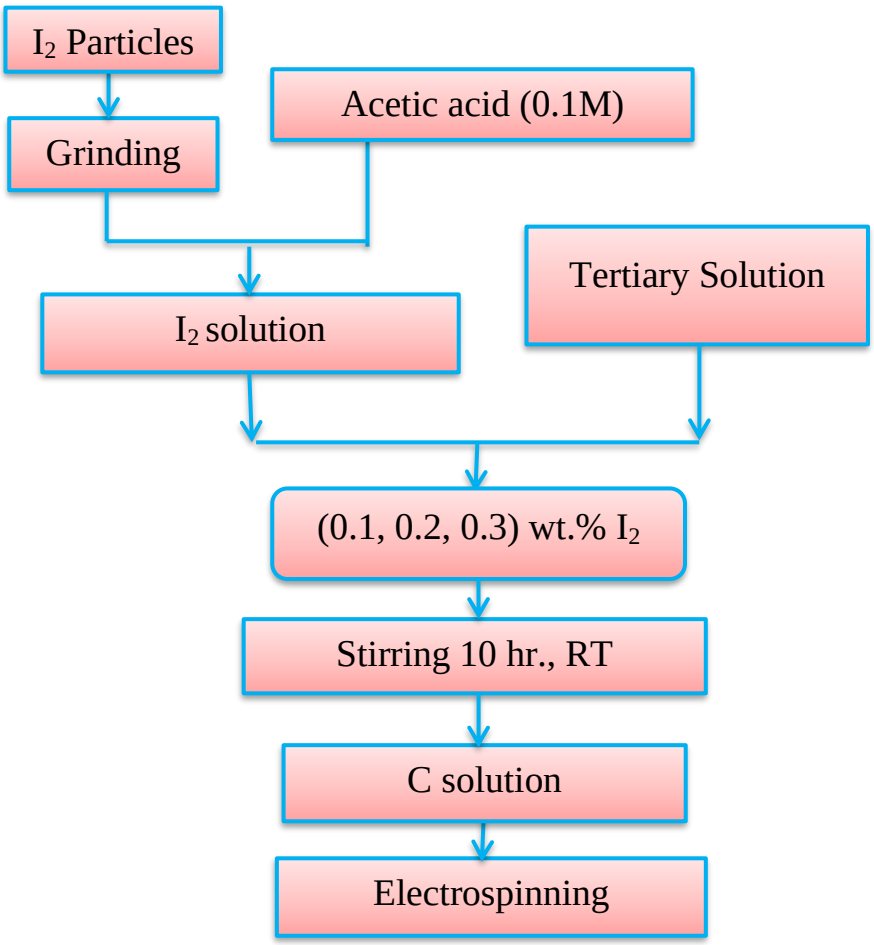

Fig.3.4: The general procedure for preparing (Tertiary polymeric: I_2) solution.

3.3.4 Preparation of Tertiary blend: Oil Solutions:

The solutions to which oils are added (Ocimum basilicum , Rosemary, and L.nobilis are prepared the same way. The oil is added directly to the triple solution. It is mixed well for 10 hours until the color of the solution turns from transparent to white in the case of adding basil oil and rosemary oil and turns green when adding laurel oil. The solutions obtained from the oils (Ocimum basilicum, Rosmary, and L.nobilis) are symbolized by D, E, and F. The general procedure for preparing (Tertiary polymeric: Oil) Solution is shown in figures (3.5, and 3.7).

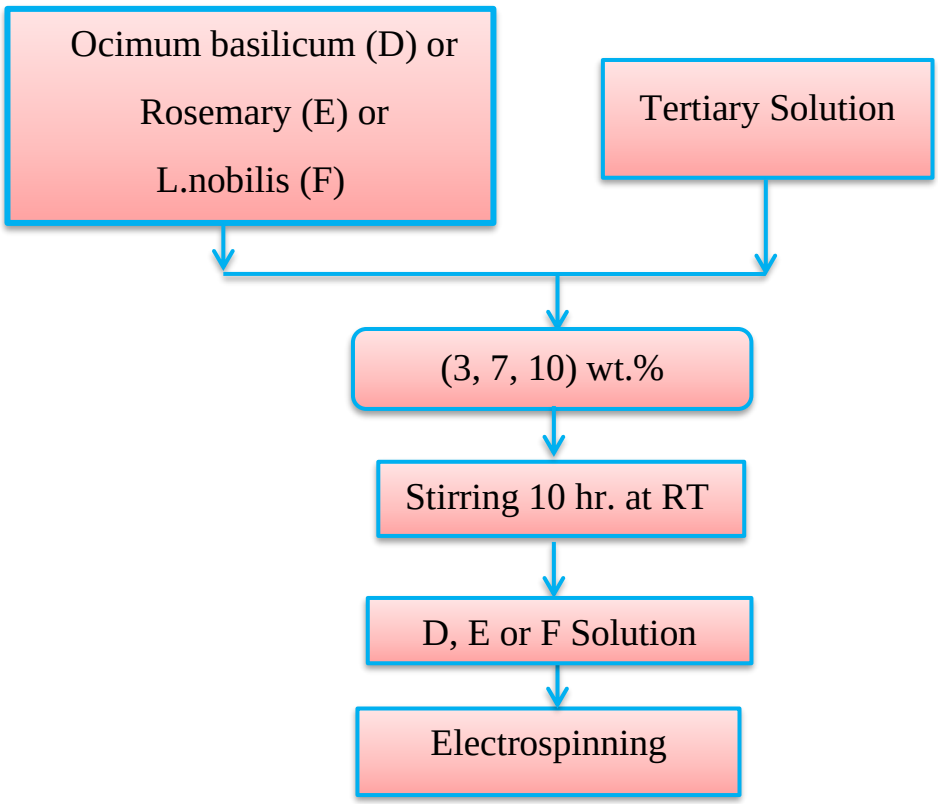

Fig.3.5: The general procedure for preparing Tertiary blend: Oil solutions.

3.3.5 Preparation of the final solution:

The final solution is prepared by combining the highest percentage of all the previously prepared solutions. Mixed for 24 hours at room temperature to obtain a homogeneous brown solution. After the mixing process, the pH is measured at 6, then NaOH is added to obtain a base solution suitable for the application. The general procedure for preparing the final solution is shown in figures (3.6 and 3.7)

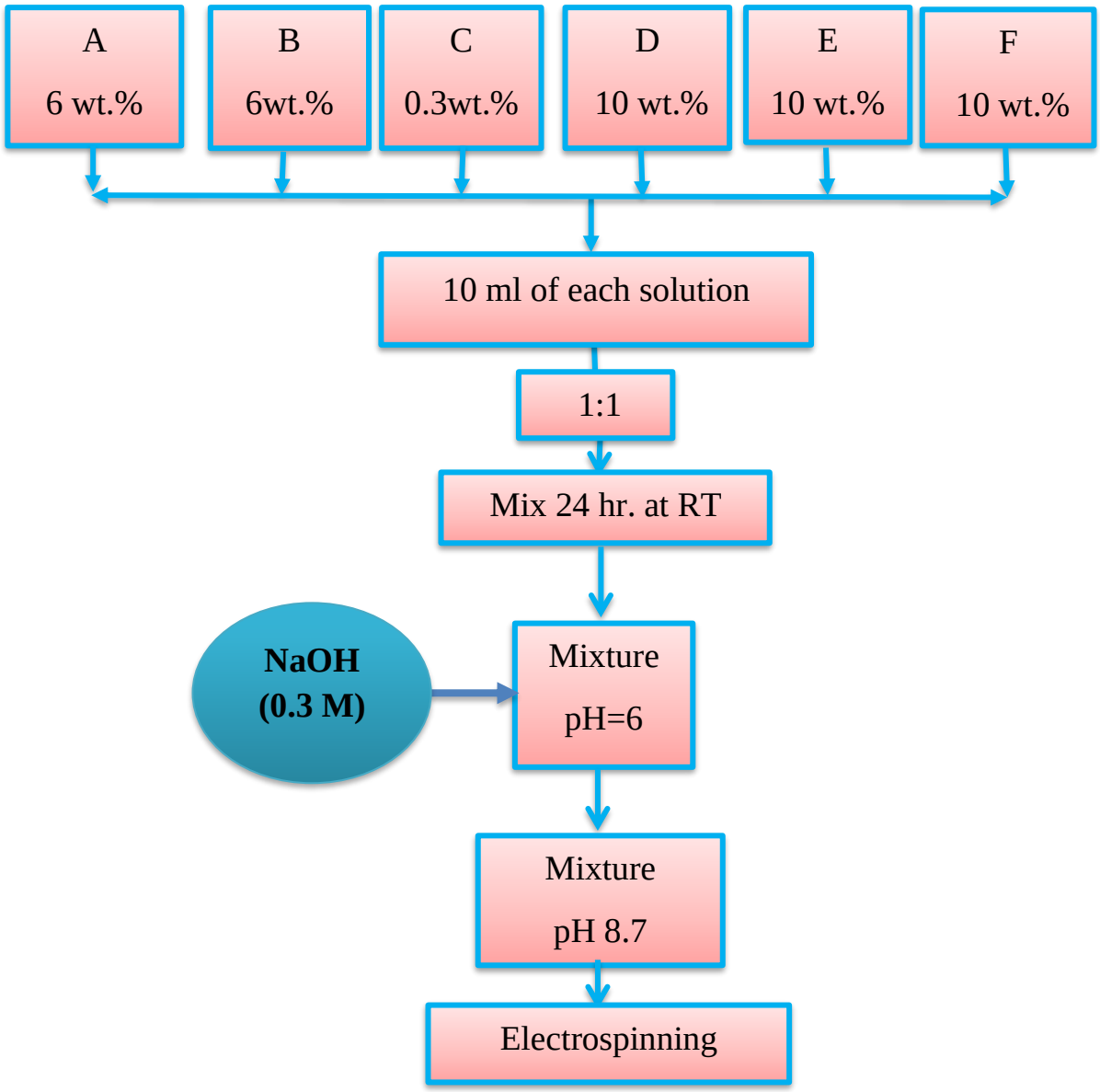

Fig.3.6: The general procedure for preparing the final solution.

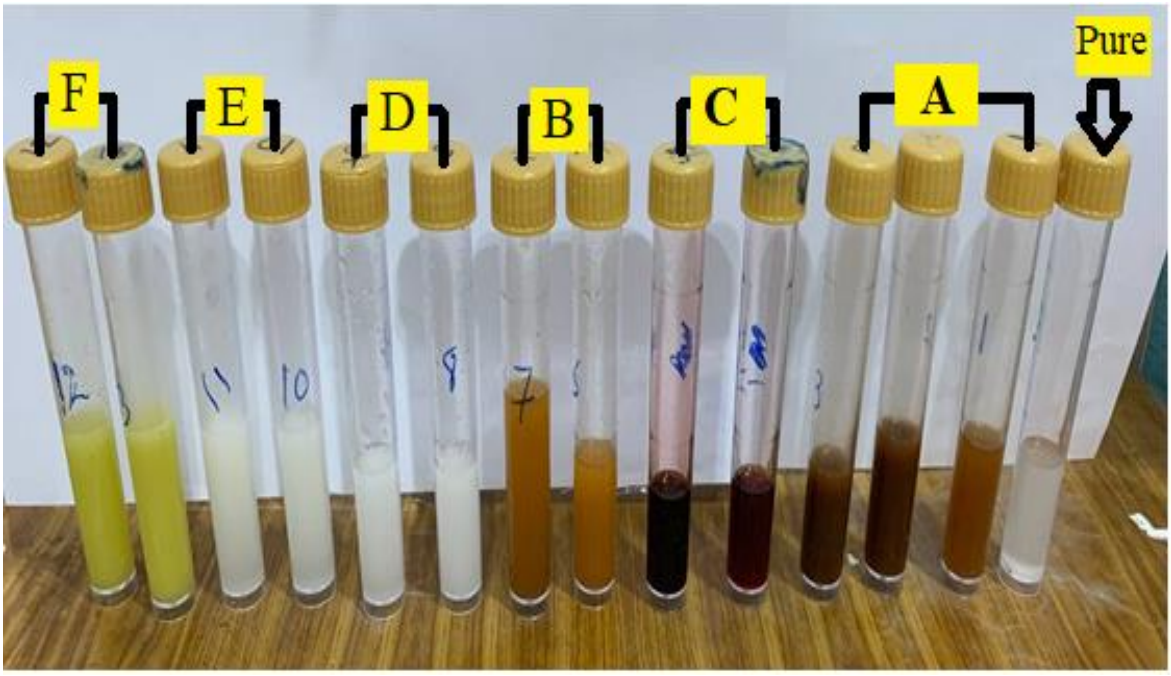

Fig.3.7:The prepared solutions.

3.4 Electrospinning process

After preparing solutions, an electrospinning process occurred to the solution to get the nanofiber textiles. The device used, and its modeling is illustrated in figure (3.8). The process conditions used where the applied voltage was 19 kV, tip-collector distance was 20 cm, the temperature was (25-37)℃, rotation speed was 600 rpm, and the flow rate was 1ml/hr.

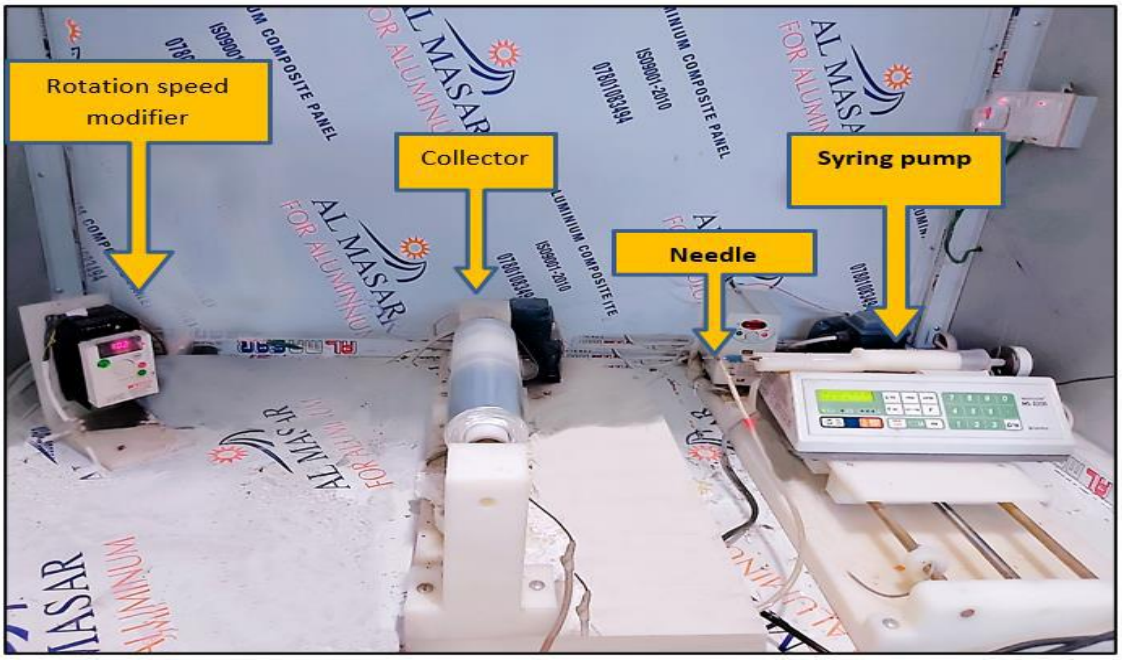

Fig.3.8: Electrospinning device.

3.5 Sampling

After using the electrospinning process, nano textiles are deposited on the aluminum foil, as shown in figure (3.9)

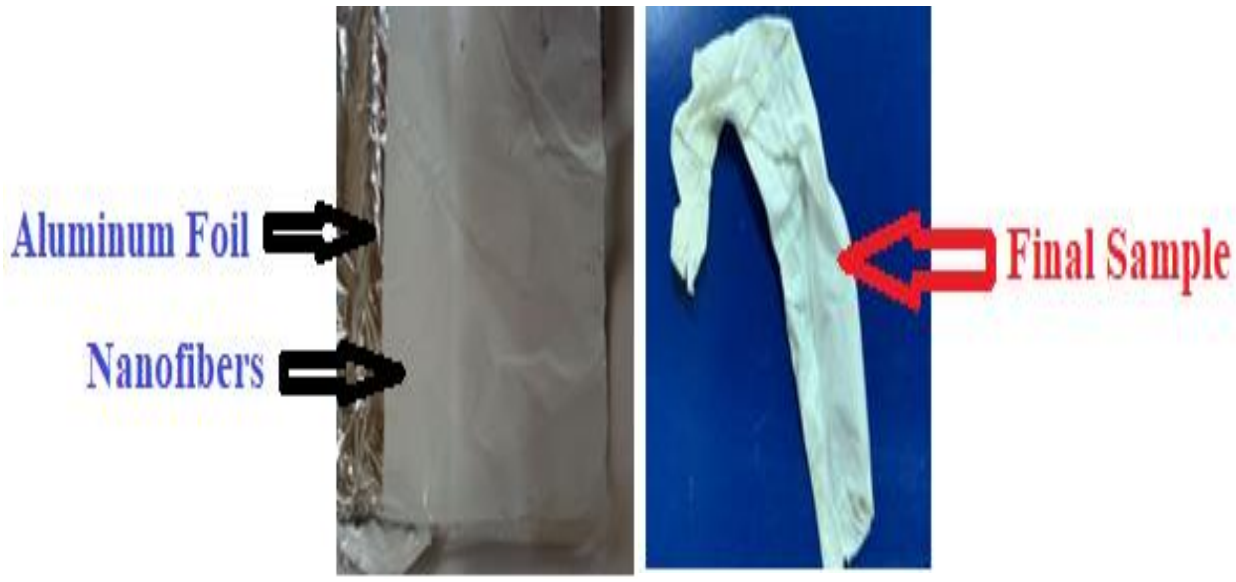

Fig.3.9: Nanofiber deposited on aluminum foil and final sample.

3.6 Testes

3.6.1 Solution tests

Solution tests as shown figure (3.10).

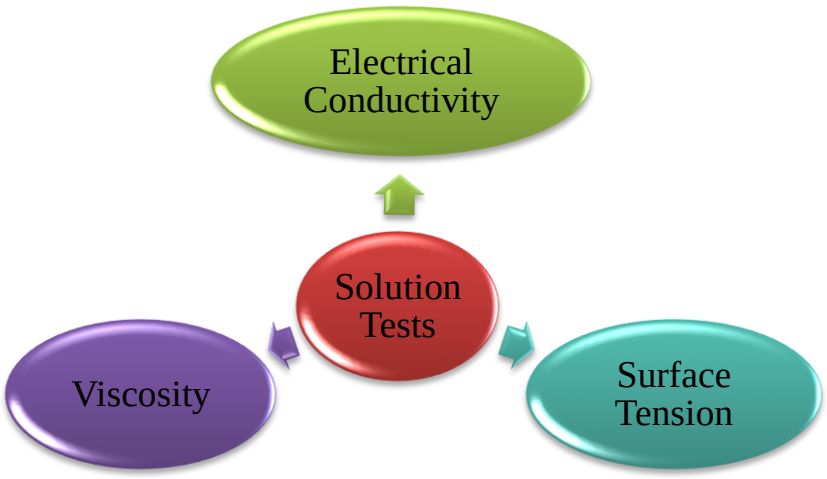

Fig.3.10: Solution tests.

3.6.1.1 Viscosity

The viscosity test was done using the "Brookfield DV-III Ultra Rheometer" to measure the viscosity of the prepared solutions in cP units.

3.6.1.2 Surface Tension

This test was carried out using Platinum Ring Method according to ISO:1995 by JZYW-200B Automatic Interface Tensiometer, Beijing United Test Co., Ltd. The measuring range of this device is 0-200 mN/m, and its resolution is 0.01mN/m. The average of three readings for each sample was adopted.

3.6.1.3 Electrical conductivity

This test was performed by an electrical conductivity device (model HANNA instruments - EC 214 conductivity Meter.

3.6.2 Nanofiber tests

The physical properties of produced nanofibers were tested according to the diagram was show in figure 3.11.

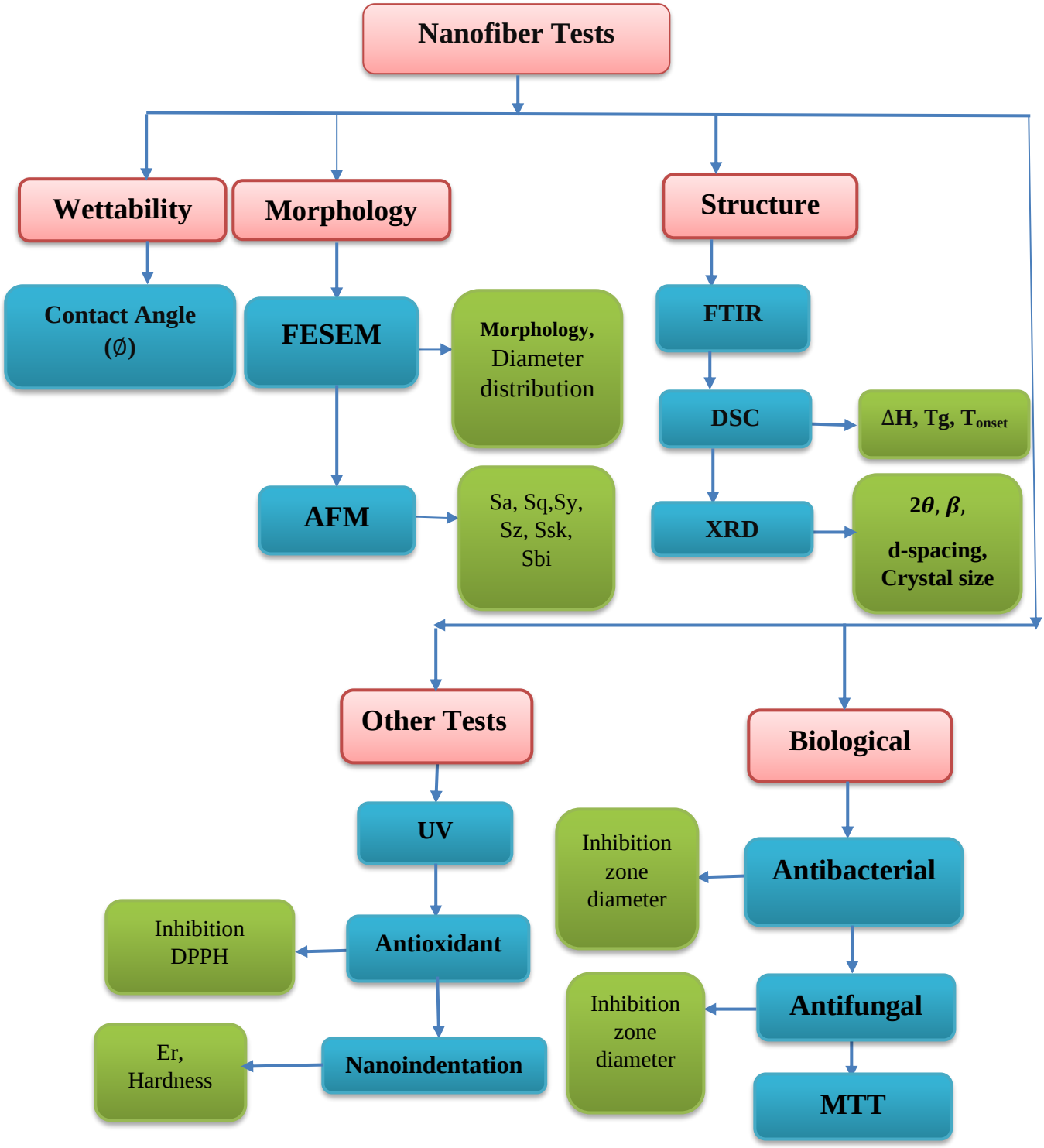

Fig.3.11: Procedure for testing the nanofiber textile.

3.6.2.1 Wettability

The used device is SL 200C - Optical Dynamic I Static Interfacial Tensiometer & Contact Angle Meter which is manufactured in KINO Industry Co., Ltd., the USA with a contact angle range from 0^o to 180^o (Figure 3.12).

Fig. 3.12: Contact Angle measurement device.

This device makes calculation and comparison of left and right contact angle as well as calculate their average value giving a Real-time data graph monitoring changes in contact angle with video recording.

3.6.2.2 Infrared Fourier transform spectrometer (FTIR)

Fourier transforms infrared technique used to characterize the prepared samples using instrument type (IR Affinity-1) made in (Kyoto Japan) located in Polymer and Petrochemicals Department. To measure a sample, calibrate the device using the KBr, and then prepare a powder of the sample to be examined, and mixed with KBr (mixing ratio 99% KBr). FTIR spectrum provides a diagram between the permeability or absorption and the number of waves that show the chemical composition of the material. This test was carried out according to ASTM E1252.

3.6.2.3 Field emission scanning electron microscopy (FESEM)

Field emission scanning electron microscopy and “energy dispersive x-ray (EDX) tests were carried to the prepared films to check the fiber’s diameter distribution, their smoothness and the chemical components of

them using the “FESEM (Zeiss Sigma 300- HV) GERMANY” instrument. figure (3.13).

Fig.3.13: FESEM with EDX instrument.

3.6.2.4 Atomic Force Microscopy (AFM)

AFM is a surface measurement technique that is based on the interaction of a tip with the surface of the sample. This technique allows the surface analysis of samples with Nanometric or even atomic resolution. For imaging, the reaction of the probe to the forces that the sample imposes on it can be used to form an image of the three-dimensional shape (topography) of a sample surface at a high resolution. This is achieved by raster scanning the position of the sample concerning the tip and recording the height of the probe that corresponds to constant probe-sample interaction. Device specifications are Nano Scope IIIA Multi Mode AFM instrument. The test proceeds in the air at ambient conditions using tapping mode probes with a constant amplitude of 200 mV. The rotated tapping mode etched silicone probe with a resonance frequency of 250 kHz was used. The height images were recorded at the resonance frequency of the cantilever with a scan rate of 1Hz.

3.6.2.5 X-Ray Diffraction (XRD)

It is a rapid analytical technique, primarily used for phase identification of crystalline materials, and can provide information on united cell dimensions. It is generated in a cathode ray tube by heating a filament to produce accelerated electrons toward the target by applying high voltage. Figure (3.14) shows the schematic of x-ray diffraction (XRD).

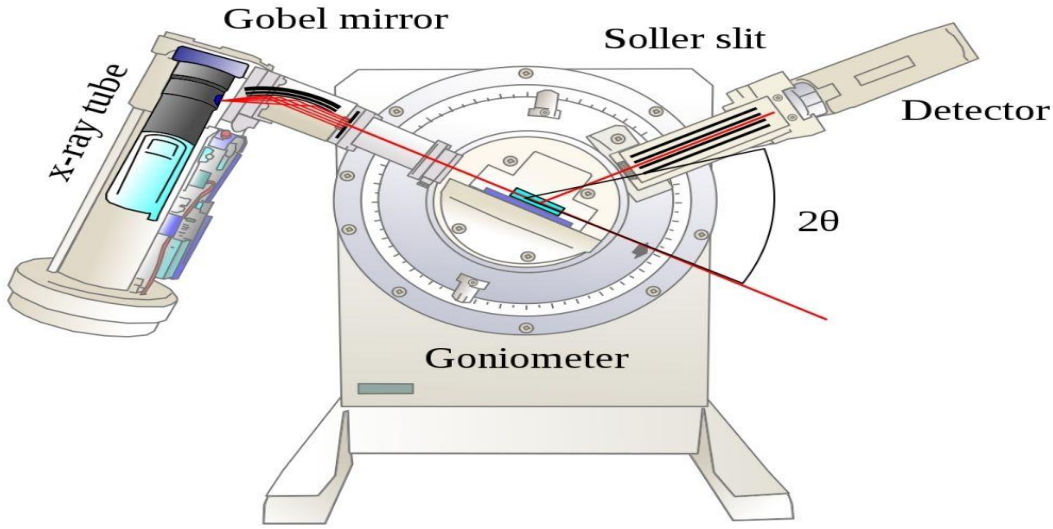

Fig.3.14: A schematic of X-ray diffraction (XRD) device.

3.6.2.6 Differential scanning calorimetry (DSC)

This device is used to measure thermal transitions, entropy, specific heat, and enthalpy. This test was done according to ASTM D3418-03 using the SH1MADZ-4 DSC-60 device. Samples of nanofibers were in the form of powder, then compress in a pan and placed in the device to conduct the examination. The specimen was tested under nitrogen gas and heating rate of 10 ˚C/min with a heating range from RT to 350 ˚C.

3.6.2.7Anti-bacterial

The Agar Well Diffusion Method achieved the antibacterial activity, where the Muller Hinton agar plates were prepared and inoculated with test organisms (Escherichia coli, Staphylococcus aureus) by spreading the inoculums on the surface of the media with the help of sterile swab. Wells

(9 mm in diameter) were punched in the agar using a sterile cork borer. The nanofibers were added to the well (100 microliters) shown in figure (3.15)

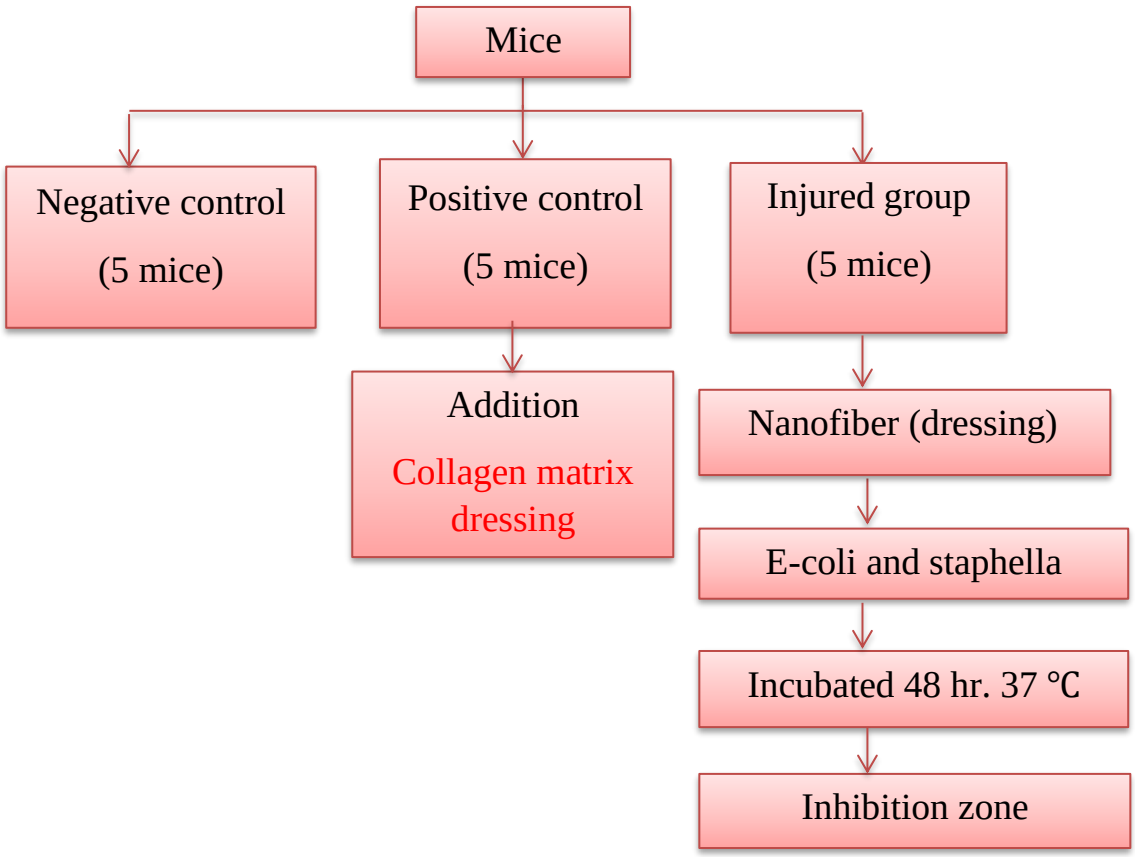

Fig.3.15: Procedure of the antibacterial action determination.

These mixtures were added to injured mice, while Collagen matrix dressing (TEBADERM) was added to the positive control mice, and the negative control remains without any treatment. The plates were incubated at 37°C for 48 hours. The antibacterial activity against E-Coli and Staphella microorganisms was assessed by measuring the diameter of the inhibition zone and recorded in mm [164]. Figure 3.15 shows the followed procedure to determine the antibacterial action.

The inhibition efficiency (IE) was calculated according to the following equation [7]:

$$IE = \frac{IZ\ at\ high\ concentration - IZ\ at\ low\ concentration}{IZ\ at\ low\ concentration} * 100\% \quad \text{..... (3.1)}$$

Where:

IZ: The inhibition zone diameter (mm).

3.6.2.8 Antifungal activity

The Antifungal potential of the prepared Samples was investigated against Candida strains using an agar well diffusion assay [2, 3]. About 20mL of Muller–Hinton (MH) agar was aseptically poured into sterile Petri dishes. The bacterial species were collected from their stock cultures using a sterile wire loop. After culturing the organisms, 6 mm-diameter wells were bored on the agar plates using of a sterile tip. Into the bored wells, different concentrations of the Samples were used. The cultured plates containing the Samples and the test organisms were incubated overnight at 37°C before measuring and recording the average zones of inhibition diameter [6].

Statistical analysis

Data were statically analyzed using the GraphPad prism program [169]. Data are represented as mean ± SD of three experiments. Indicate a statistically significant difference at $p<0.05$ [170].

3.6.2.9 Antioxidation

This test carried out using the Free radical scavenging activity (DPPH method), where DPPH represents 2,2-diphenyl-1-picrylhydrazyl.

The electron-donating ability of samples and standards - gallic acid and Vit-C were determined from bleaching of purple-colored ethanol solution of DPPH. This spectrophotometric assay uses the stable radical 2, 2-diphenyl-1-picrylhydrazyl as a reagent. DPPH was prepared at a concentration of 0.002%. Different concentrations of samples were taken in separate test tubes and volumes were made up to 2 mL using ethanol. Then 2 mL of DPPH solution (2.0 to 0.001 mg/mL) was added to each test tube and these solutions were kept in dark for thirty minutes. The same procedure was followed for Vit-C and gallic acid as well. All the samples were tested in triplicate. Later optical density was recorded at 517 nm using a spectrophotometer. Ethanol with DPPH was used as a control. The formula used for calculation is as below:

% Inhibition of DPPH activity = (A-B/A) X 100

Where A = Optical density of control

B = Optical density of sample [171].

3.6.2.10 MTT assay

Samples were placed in a UV light chamber for 2 h. Samples were cut into 1 cm^2 squares and placed in a 48-well polystyrene cell culture plate. Then, 250 μL cell culture media containing 12,500 Human dermal fibroblast (HDF) cells was added to each well and incubated at 37 C, 95% relative humidity, and 5% CO_2 for 1, 3, and 6 days. After completion of the time needed for cell culture, old media was discarded and 250 μL fresh media was added, followed by addition of 12 mM MTT dye. Samples were incubated for 3 h to let the dye react with cells and produce formazan precipitates. Finally, precipitated dye was dissolved in 200μLDMSO and absorbance was measured at 540 nm using ELISA reader.

3.6.2.11 Ultraviolet (UV)

UV-Visible: CECIL 2700 computerized spectrophotometer is used to determine the optical properties of samples. The sample is placed in a specific UV / VIS device position. The operating principle, where a double beam spectrophotometer utilizes two beams of light: a reference beam and a sampling beam that passes through the sample. Some double-beam spectrophotometers have two detectors that allow the two beams to be measured at one time.

3.6.2.12 Nano-indentation

Nanoindentation testing is a method to measure the mechanical properties of a material such as hardness and Young's modulus on the microscopic scale using Ultra Nano Hardness Tester (UNHT), manufactured by CSM Instruments (Switzerland), with a capacity of 30 μN to 100 mN having a load resolution of 5 μN (Figure 3.16).

Fig.3.16: Nanoindentation advice photograph.

Chapter Four

Results and Discussions

4.1 Introduction

This chapter includes the characterization of the used PVA, HAc, collagen, their binary, tertiary blends, solids, and essential oils (EOs). Additionally, the analysis of the results and the required calculations related to the solution tests, such as (viscosity, electrical conductivity, and surface tension) and nanofibers tests, such as (contact angle, FTIR, DSC, FESEM, Textile directionality results, such as the orientation, dispersion, goodness and so by using the Fiji software (Gaussian method) based on the FESEM images, AFM, UV-Vis spectroscopy, Anti-bacterial activity, Antioxidant activity, Antifungal activity, MTT assay and Nano-indentation) and their discussion as well as studying the effect of each addition on all properties of nanofibers used to wound dressings.

4.2 Solutions results

To obtain the desired properties of the final elctrospun nanofiber textiles, properties of the original solutions must be controlled. For examples, solution viscosity can play an important role in elongation of the solution, which change the average fiber diameters. Also, surface tension influenced the resultant fibers in which beads may occur. Therefore, it must develop sufficient charges in the polymeric solution in order to overcome the solution's surface tension.

4.2.1 Viscosity of polymeric blends

Figure 4.1 shows that the addition of both Coll. and HAc to PVA reduces the viscosity, especially HAc addition. This is because these additions increase the spacing among the PVA chains, which leads to weakening their interaction forces, resulting in reducing their friction forces and facilitating the sliding of these chains. HAc addition caused the greatest decrease in viscosity due to its known lubricating effect, which encouraged its medical use to reduce the pain of joint patients.

Results, also, showed that PVA solution and all its blends are of a non-Newtonian nature and generate the shear-thinning phenomenon, where their viscosities decreased as the shear rate increased. This stability in viscosity appears at higher ranges of shear rate for other solutions, especially PVA solution. Indeed, the PVA solution is composed of one type of chain; thus, there is no phase separation among their chains compared to the binary or tertiary blends.

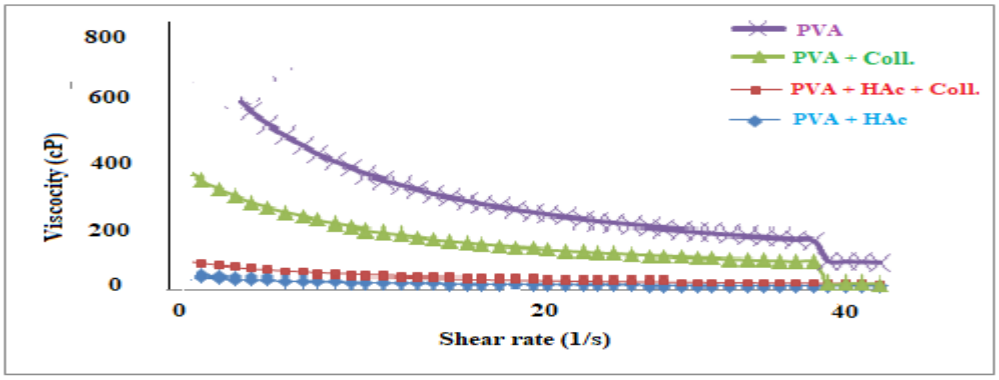

Fig. 4.1: Viscosity-shear rate relationship for the prepared polymeric blends.

4.2.2 Viscosity of blend with antibacterial & antioxidation

Figures 4.2-4.8 show the viscosity-shear rate relationships as a function of additive concetrations of Iodine (I_2), Rosemary oil, G. lucidum, Ocimum basilicum oil L.nobilis EO, and Capsicum annuum respectively. This relationship between viscosity and shear rate refers to what called Apparent, or shear viscosity. In Newtonian fluids, this value doesn't change, but with non-Newtonian fluids, apparent viscosity is directly affected by the shear rate.

The viscosity of a liquid is related to the ease with which the molecules can move with respect to one another. Thus, the viscosity of a liquid depends on the: strength of attractive forces between molecules, which depend on their composition, size, and shape. It is greater with larger than with smaller molecules, with elongated than with spherical molecules.

The shear rate is defined as the gradient in velocity, that is, the difference in velocity between the two surfaces containing the fluid, divided by the distance between them.

According to the figure 4.2, it is clear that the tertiary polymeric blend solution exhibits shear thinning phenomenon, where its viscosity decreases as the shear rate is increased. This refers to the rearrangements in the fluid microstructure in the plane of the applied shear. This is because that the teriary blend composed of low molecular weight polymers, as well as due to the low concentration of this blend. This means that, as the shear stress increased further, the fluid begins to deform more easily and shows to be less viscous.

In contrast, Iodine (I_2) additives caused the appearance of shear thickening at low shear rates (up to 10 s^{-1}), then the solutions return to show the shear thinning behavior. The reason for the appearance of shear thickening is the increase in the concentrations of the polymeric solutions in the presence of iodine (with different amounts), which leads to increase the viscosity with the shear rate. This means that at low shear rates, Iodine caused by a strong internal friction between the randomly coiled (swollen macromolecules) and the surrounding solvent molecules, which in turn increased the viscosity. At high shear rates, these friction forces do not withstand, but break down, causing a decrease in viscosity and the appearance of a new state of shear thinning. Indeed, shear thickening makes the non-Newtonian fluid beneficial in protective and impact resistance applications (found to improve the energy absorption under high-speed impact), which is desirable property in wound dressing applications. At higher shear rats, a reduction in molecular weight frequently occurs when polymers are subjected to the action of mechanical forces.

Shear thinning occurs due to the in-polymer systems such as polymer melts and solutions, shear thinning is caused by the disentanglement of polymer

chains during flow. At rest, high molecular weight polymers are entangled and randomly oriented.

The rapid growth of the viscosity with surfactant concentration is therefore attributed to the considerable cross links among micelles and polymers (transient network).

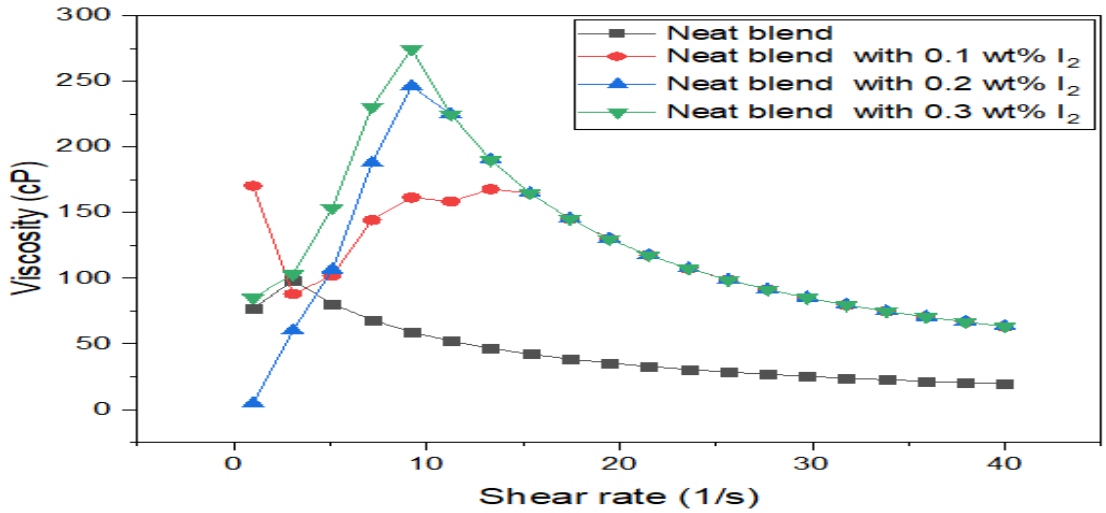

Fig.4.2: Relationship between viscosity and shear rate for the neat blend as a function of I_2 content

Same findings obtained with the Rosmarinus officinalis oil (Rosemary oil), where firstly shear thickening appeared and followed by shear thinning behavior at higher shear rates. This means that by increasing the shear stresses on the polymeric chains, the physical interaction, as well as hydrogen bonds (that had been established between the ternary mixture and Rosemary oil) will be broken. This disentanglement of polymer chains reduces their resistance to move, which facilities the flow of the polymeric solution (figure 4.3).

Compared with the Iodine effects, Rosemary oil raises the viscosities values due to the specific interactions with the neat blend.

It has a powerfully calming effect on the skin that can be useful in treating many conditions, including severe eczema [as well as psoriasis and dermatitis] and skin allergies.

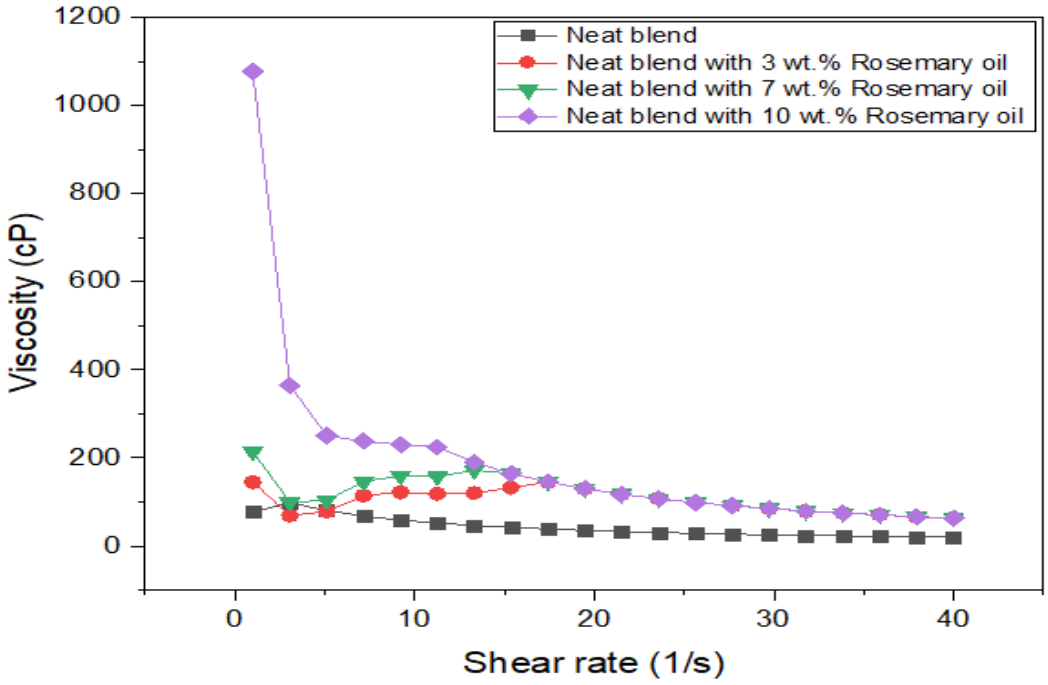

Fig.4.3: Relationship between viscosity and shear rate for the neat blend as a function of Rosmarinus officinalis oil content.

Figure 4.4 shows the effects of G. lucidum addition on the viscosity-shear rate relationships. It is clear that the viscosity of the neat solution (free from G. lucidum) is always less than solutions containing G. lucidum. As well as the viscosity increased as G. lucidum content increased. That means that, G. lucidum, generally caused drag reduction, which facilities the flow of the new solutions due to the reduction in the friction forces among solution layers. This new pattern flow encourages the fluid flow inside the needle, leading to formation of fine nano fibers easily by electrospinning technique.

Maximum viscosity obtained at about 15 (s^{-1}) shear rate and decreased for all solutions containing G. lucidum, which means that beyond this shear rate, the forces among fluid layers will be destroyed making these layers to be slip easily over each other.

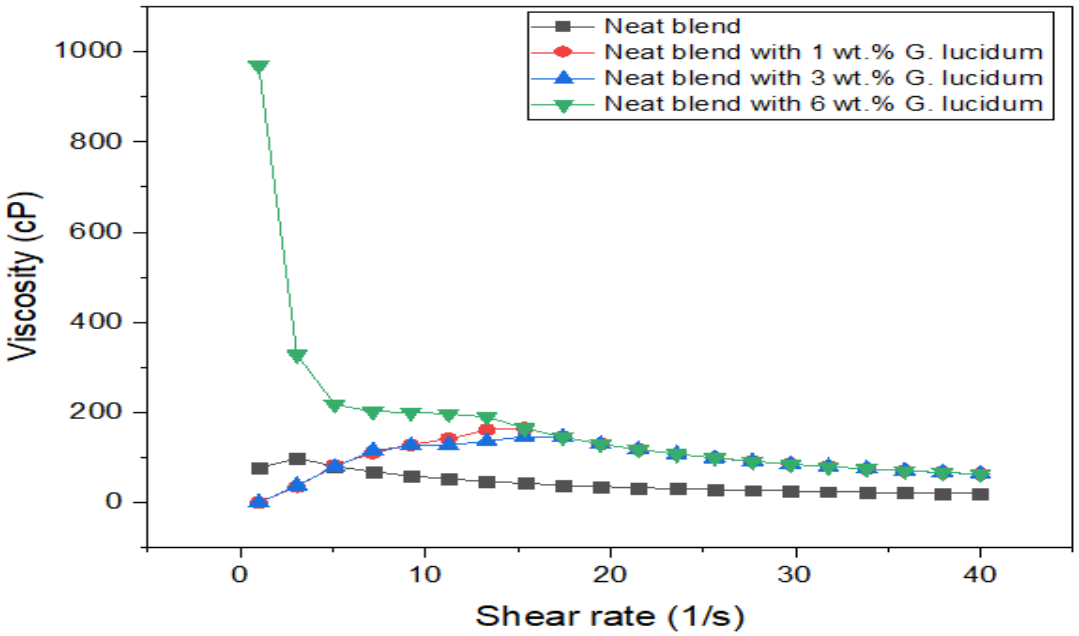

Fig.4.4: Relationship between viscosity and shear rate for the neat blend as a function of G. lucidum content.

The same behavior obtained with L.nobilis EO, Ocimum basilicum oil, Capsicum annuum and final solution shown in figures (4.5, 4.6, 4.7and 4.8) respectively.

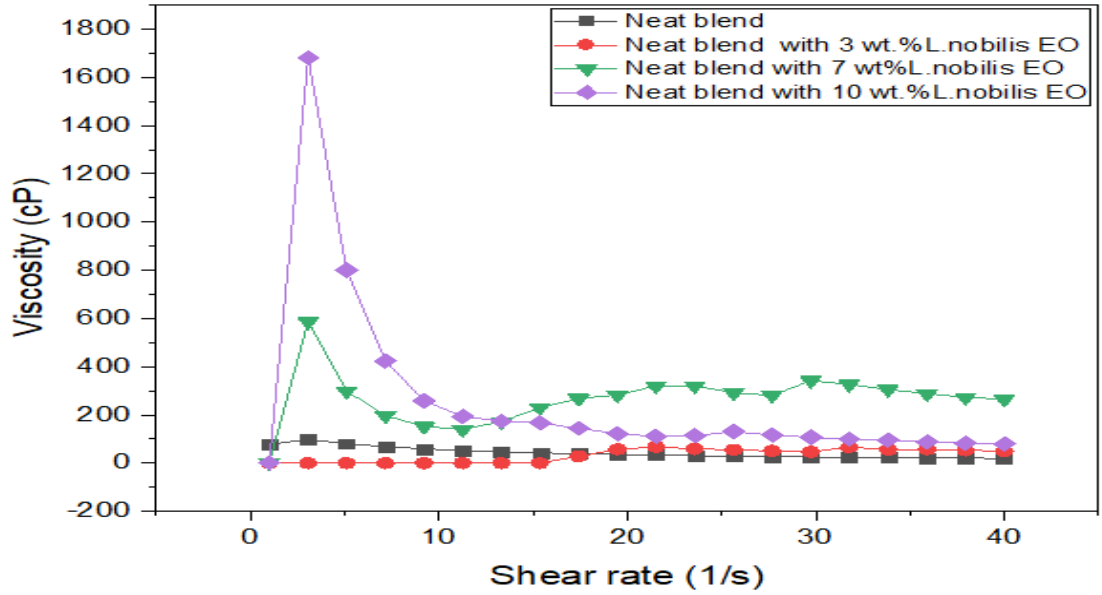

Fig.4.5 Relationship between viscosity and shear rate for the neat blend as a function of L.nobilis EO content.

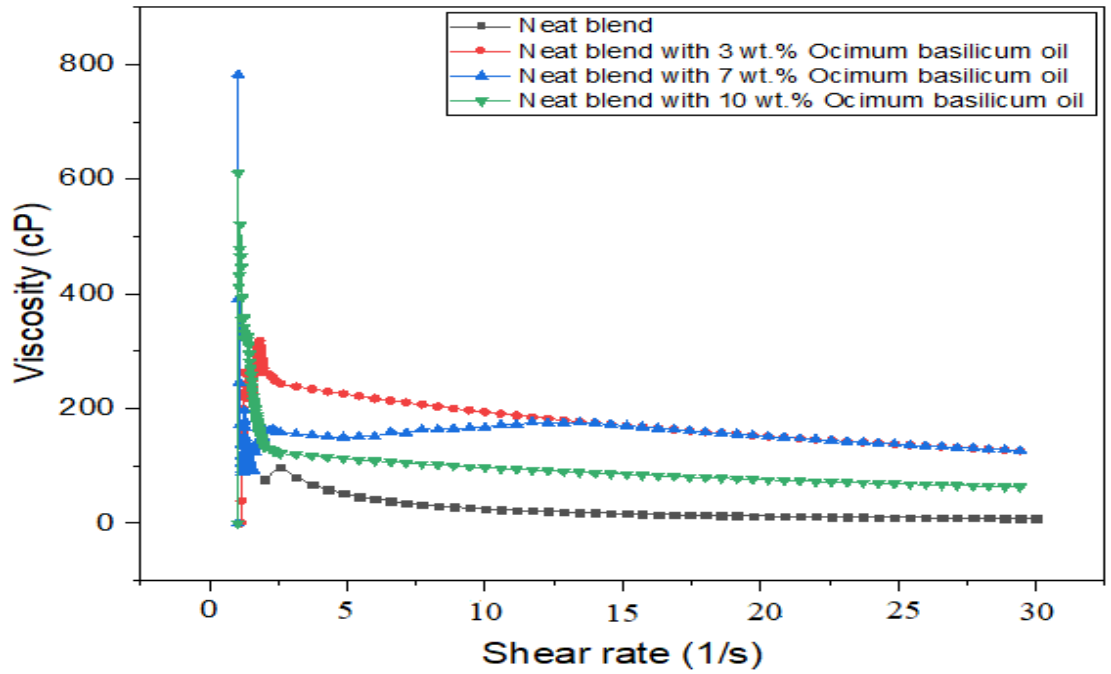

Fig.4.6: Relationship between viscosity and shear rate for the neat blend as a function of Ocimum basilicum oil content.

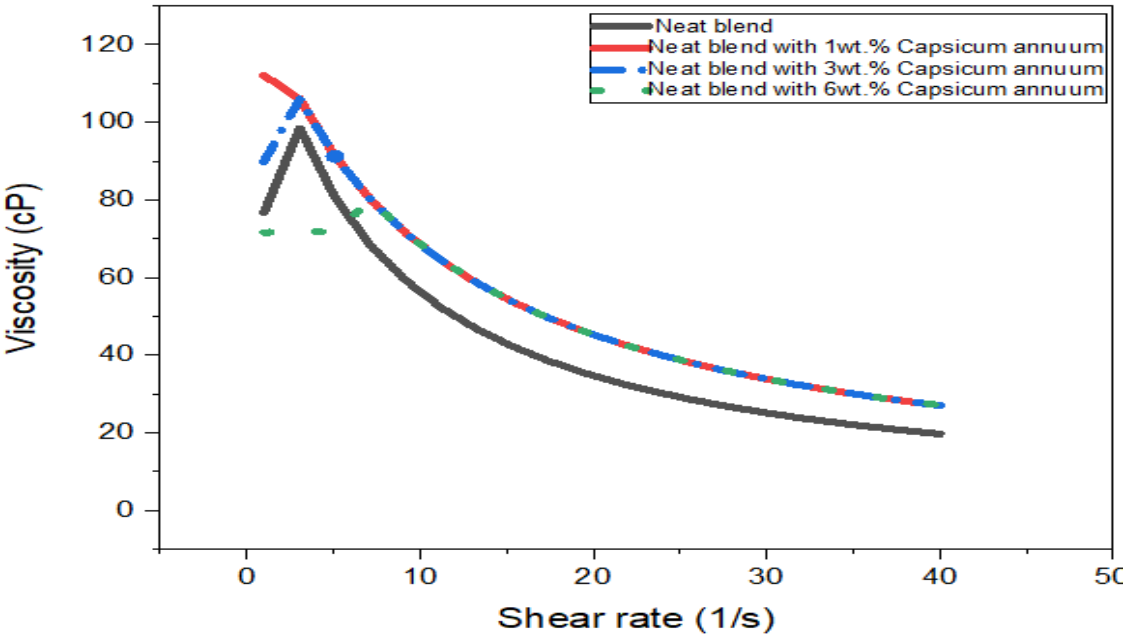

Fig.4.7: Relationship between viscosity and shear rate for the neat blend as a function of Capsicum annuum content.

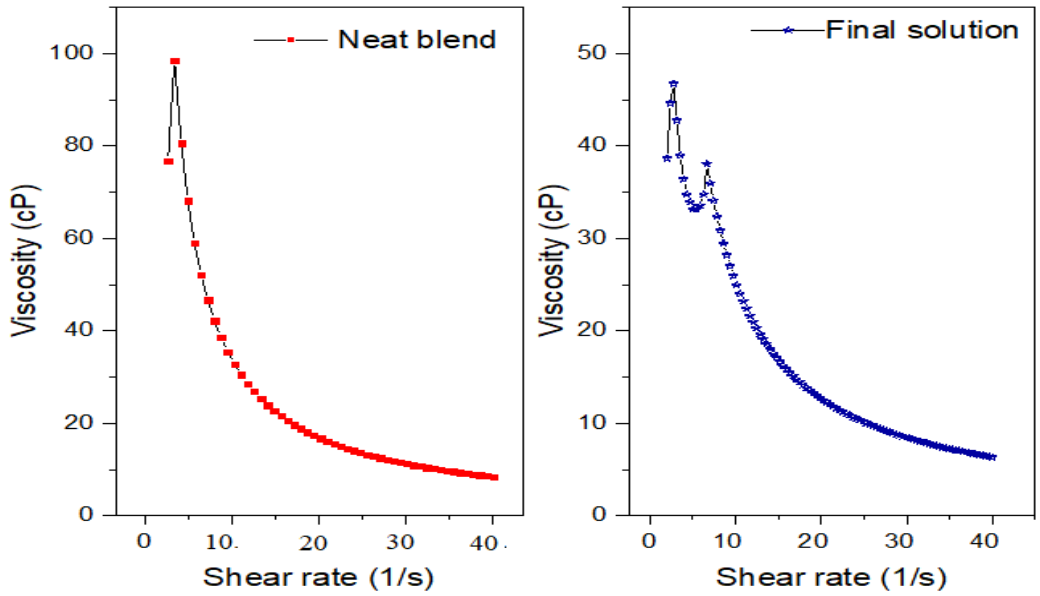

Fig.4.8: Relationship between viscosity and shear rate for the neat blend and final solution.

4.2.3 Surface tension of polymeric blends

Figure 4.9 shows that additions of Coll. and HAc increased the surface tension in the binary solutions, especially the HAc addition. This is due to the increments of the cohesive interactions among the polymeric chains within the solution. At the solution bulk, there is an equal pulling force in all directions. In contrast, at the surface, the upper forces disappeared, which encouraged surface molecules to shrink into the minimum possible surface area. In the tertiary solution, the cohesive energy among molecules was so high that the molecules be spherical in shape to resist the external forces; thus, their surface tension was raised.

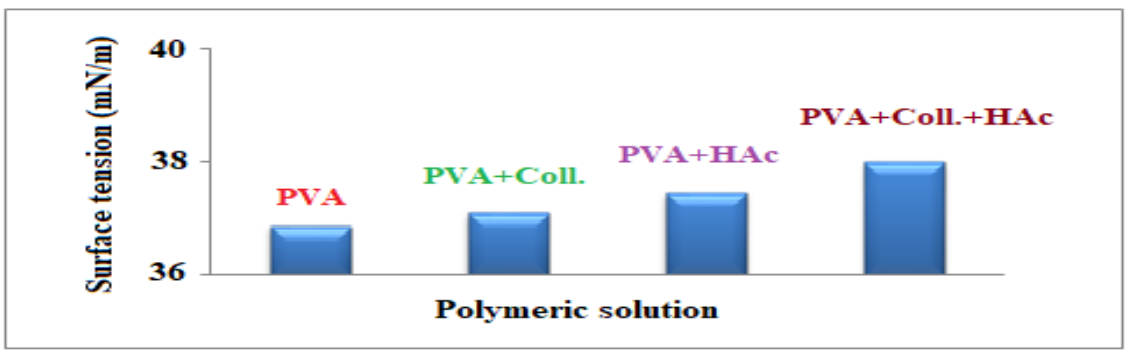

Fig. 4.9: Surface tension of the prepared polymeric solutions

4.2.4 Surface tension of blend with antibacterial & antioxidation

Most of the used additives increased the surface tension of the tertiary blend (Table 4.1), which is 34 mN/m except L.nobilis EO.

The increment order is Capsicum annuum > Rosemary oil > Ocimum basilicum G. luciudm = Iodine (I_2). These differences in their effects are due to the nature of the chemical compositions of the additives and the resulting interactions and cohesiveness with the tertiary polymeric chains.

Generally, as the content of any used additive increased, the surface tension increased due to the increment of the cohesiveness of the solution molecules, which leads finally to enlarge the dissimilarity and the phase separation among the solution components.

L.nobilis EO reduces the surface tension down to 31.32 mN/m with 10 wt.% addition, which indicates to its ability to reduce the surface area per unit mass of a solution by forming spheres. This finding facilitates the process of extruding the nano fibers (during the electrospinning process) or completing it by applied lower voltages. This means that, the charged solution can exit from the needle and easily overcome the "Taylor cone" and the electrostatic repulsions are high enough that a very fine stream of solution erupts from the needle.

The final solution, which contains all these additives (6 wt.% G. lucidum, 6 wt.% Capsicum annuum, 0.3 wt.% I_2, 10 wt.% basilicum oil, 10 wt.% Rosemary oil and 10 wt.% L. nobilis EO) have surface tension 36.7 mN/m, which is higher than the neat tertiary blend. Indeed, a decrease in the surface tension of the polymer solution induces instability to the jet and increases the breaking tendency of the extruded filament, with the formation of drops. Therefore, it is not necessarily a lower surface tension of the solution will always be suitable for electrospinning [172].

During flight, the solvent dries out and the charge moves to the surface of the forming fiber.

Table 4.1: Surface tension values of the prepared samples

Sample	Ratios %	Surface tension (mN/m)
Neat blend	10:5.5:7	34
G. lucidum	1	34.65
	3	34.96
	5	36.10
Capsicum annuum	1	37.11
	3	37.49
	5	37.83
I_2	0.1	34.65
	0.2	34.96
	0.3	36.10
Ocimum basilicum oil	3	35.24
	7	35.72
	10	35.55
Rosemary oil	3	36.73
	7	36.96
	10	37.29
Laurus nobilis oil	3	32.27
	7	33.19
	10	31.32
Final solution		36.7

4.2.5 Electrical conductivity of polymeric blends

Compared with the neat PVA solution, the electrical conductivity (Figure 4.10) of the remaining polymeric solutions was increased. This is because that HAc and Coll.

additions increase the free volumes among the polymer chains, which enhances the possibility of providing spaces for the free movement of charge

carriers in the solution. These carriers can transfer the free ions easily within the polymeric network; thus, increasing its conductivity.

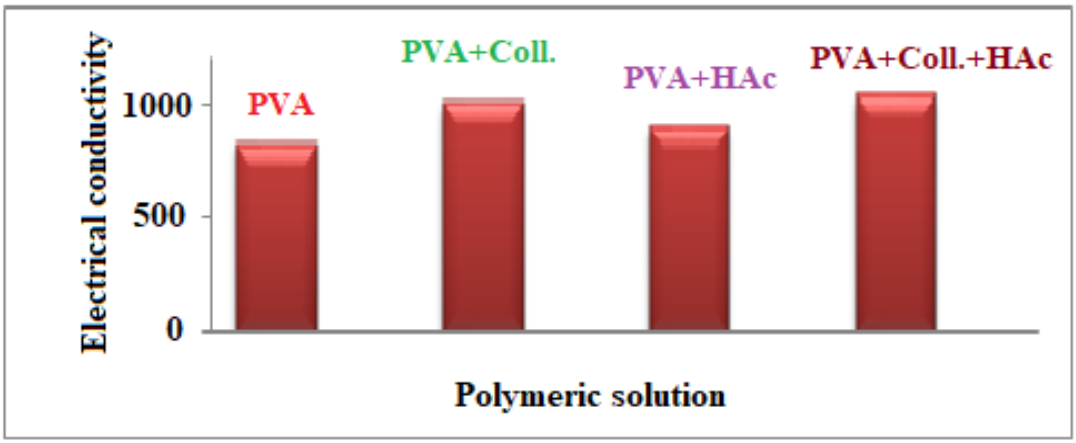

Fig.4.10: Electrical conductivity of the prepared polymeric solutions

4.2.6 Electrical conductivity of blend with antibacterial and antioxidation

Conductivity of the solution has a strong impact on the electrospinning process and fiber morphology. Also, increasing voltage will accelerate the electrospinning jet and this may result in greater volume of solution drawn from the tip of the needle.

Figure 4.11 shows the effects of the addition type (with different concentrations) on the electrical conductivity of solutions. Some of additives (Capsicum annuum, L.nobilis EO , and the final solution) increased it , while the remaining additives decreased it.

The conductivity of most additives increased with increasing its concentration except Rosemary oil, which give high values of surface tension (36.73-37.29 mN/m).

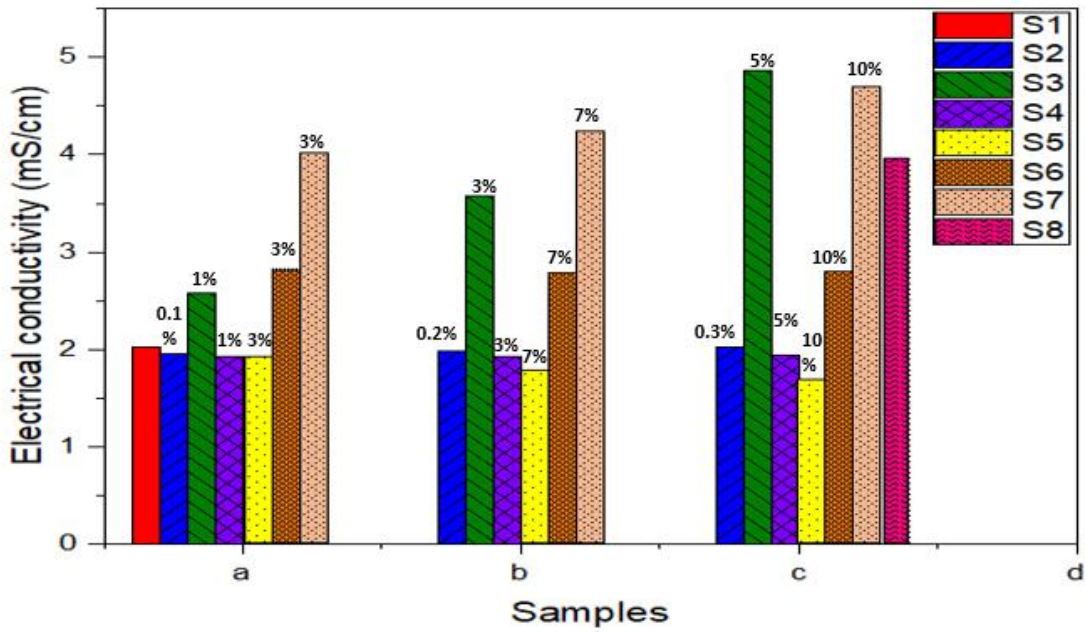

Fig.4.11: Electrical conductivity for (S1) blend polymeric, (S2) blend with I2, (S3) blend with Capsicum annuum, (S4) blend with G. lucidum, (S5) blend with Rosemary oil, (S6) blend with Ocimum basilicum oil, (S7) blend with L. nobilis EO, (S8) Final solution.

4.3 FTIR analysis

In order to specify the active chemical functional groups in the essential polymers (PVA, HAc and collagen) and their effects on the solutions and textiles behaviors, FTIR spectrum of these polymers as well as its tertiary blend were analyzed. Also, FTIR findings are employed to knowledge the bonding types among these polymers, if present.

Figure 4.12A shows the FTIR spectrum of PVA polymer. The hydroxyl group's stretching vibration causes the broad band at about 3402.43 cm-1 (-OH), while the band at 2939.52 cm^{-1} belongs to the stretching of the C–H alkyl group [173]. The band at 1728.22 cm^{-1} indicates the incompletely hydrolyzed acetate to polyvinyl alcohol (PVA). The band at 1651.07 cm^{-1} belongs to the C=C stretching. The peak corresponding to the C-O stretching occurs at 1095.57 cm^{-1}. The out-of-plane vibrations of O-H and C-H groups occur at 601.79 cm^{-1} and 848.68 cm^{-1} respectively [174].

Figure 4.12 B shows the FTIR spectrum of Collagen material, where the principal characteristics bands for Amide A, Amide I, Amide II, and Amide III exist. The strong band around 3425.58 cm^{-1} belongs to the N=H stretching vibration mode. The band at 2970 cm^{-1} refers to the asymmetrical vibration of CH_2 group. The stretching vibration of the carbonyl group (C=O) for Amide I appears at 1651.07 cm^{-1}. At the position 1543.05 cm^{-1}, the Amide II appears through the in-plane bending of the N-H group. The in-plane deformations of both CH_2 and CH_3 groups appear at 1458.18 cm^{-1} and 1410.18 cm^{-1}, respectively. The in-plane deformation vibration mode of N-H appears at 1242.16 cm_{-1}, which confirms the Amide III Collagen type. The presence of the carbohydrate motities was confirmed by the appearance of pulses at 1080.14 cm^{-1} and 1033.85 cm^{-1}, which refer to the out-of-plane deformations of CH_2-O-CH_2 and C-O, respectively. These results coincide with [3,4]. The observation peaks with types of bonds are listed in table 4.2.

Table 4.2: FTIR analysis peaks of collagen

Region type	Wave No. of Peaks cm^{-1}	Vibration Mode
Amide - A	3400 – 3600	-NH- starch with H-bond
Amide – B	2900 -2950 2400 -2500	-CH_2- asymmetrical stretch
Amide I	1650	C—O stretch/ hydrogen bond coupled & C—N stretch
Amid II	1550	-NH- bend coupled with CN stretch
	1450	CH_2 bend
Amide III	1250	NH- stretch bend
	1150	CO stretch (out of plan) deformation
	1000	COO (out of plane) deformation

The FTIR spectrum of hyaluronic acid (HA), was shown in figure 4.12C. The broadband from 3000 to 3700 cm^{-1} belongs to the combination of the O-H and N-H stretching. The band at 2931.80 cm^{-1} refers to the stretching

vibration of CH_2 group. The peak at 1620.21 cm^{-1} refers to the secondary Amide group (C=O group). The band at 1411.89 cm^{-1} corresponds to the C-OO group in combination with the C=O group. The band at 1147.57 cm^{-1} belongs to C-O-C. The C-OH stretching occurs at 1041.56 cm^{-1}. the resulted peaks and bonds were listed in table 4.3. The resulted peaks were matched with (Hongyue et al.) [177].

Table 4.3: FTIR analysis peaks of hyaluronic acid

Peaks Wave Numbers (cm^{-1})	**Vibration Mode**
3500	OH, and CH stretching
2900	CH_2 asymmetrical stretching
1200-1700	C=O, COO, C-O-C (symmetric C-O stretching vibrations)
900-1000	C—OH stretching (carbohydrates)
400-500	Aromatic group

Figure 4.12D. represents the FTIR analysis of (PVA: Coll.: HAc) blend, resulting from peaks listed in Table 4.4.

T**able 4.4 FTIR analysis peaks of (PVA: Coll.: HAc) tertiary blend**

Peaks Wave Numbers (cm^{-1})	**Vibration Mode**
3500 – 3600	OH stretching of PVA, HAc, collagen NH stretching of HAc, collagen
2900	CH_2 stretching of PVA, HAc, collagen
1700	Incomplete hydrolyzed of PVA
1600-1650	C==C from PVA, C==O from HA_c & Collagen
1000	C—O from PVA, C-O-C from HA_c & Collagen
900	C-C and C-H from PVA
400-600	Aromatic ring of HA_c

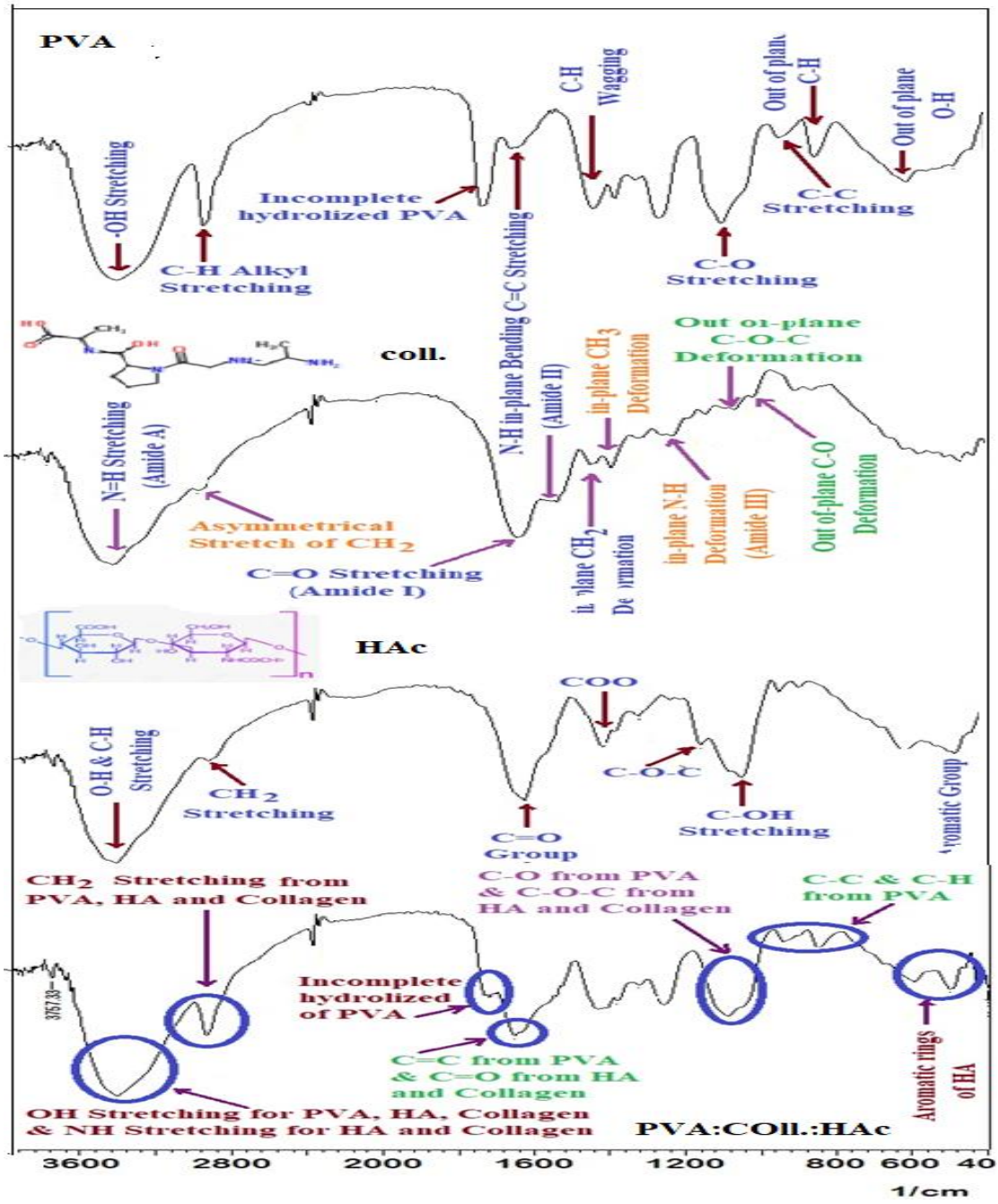

Fig.4.12: FTIR curves of the prepared nano fiber textiles.

All the pulses in the blend spectra are basically present in one or more of the three blend components, which means two things:

1- All three components (PVA, HAc, and Coll.) are present in the blend and there is no loss of any of them.

2- There is no chemical reaction between the three components and there is only physical interaction between the polymeric chains of the three components.

The pulses belonging to the chemical structure of PVA (-OH, CH_2, C=C, C-C, incomplete hydrolyzes of acetate, and C-H) are present in the blend spectrum with slight shifting. The same thing happened with the functional groups of HAc (-OH, -NH, C=O, and the aromatic rings) and Collagen (-OH, -NH, CH_2, C=C, and C-O-C).

Figure 4.13 shows the FTIR spectrum of G.lucidum (Boletus lucidus).Band at 3417.86 cm^{-1} is due to the R-CH_2-OH stretching vibration. Bands at 440-580 cm^{-1} belong to phosphor compound (P-Cl). Band at 1033.56 cm^{-1} is due to the Si-O-Si stretching in silicon compounds. Bands from 895-925.48 cm^{-1} is due to the P-O-P stretching. Amide I appear at 1635.64 cm^{-1}, while Amide II at 1234.44 cm^{-1}. Band at 1453.42 cm^{-1} is due to the scissoring bending of CH_2. Band at 1157.29 cm^{-1} C-O stretching in proteins and carbohydrates. The common backbone of –CH3 with C–H vibration was noted for the peak at 29321.8cm^{-1}.

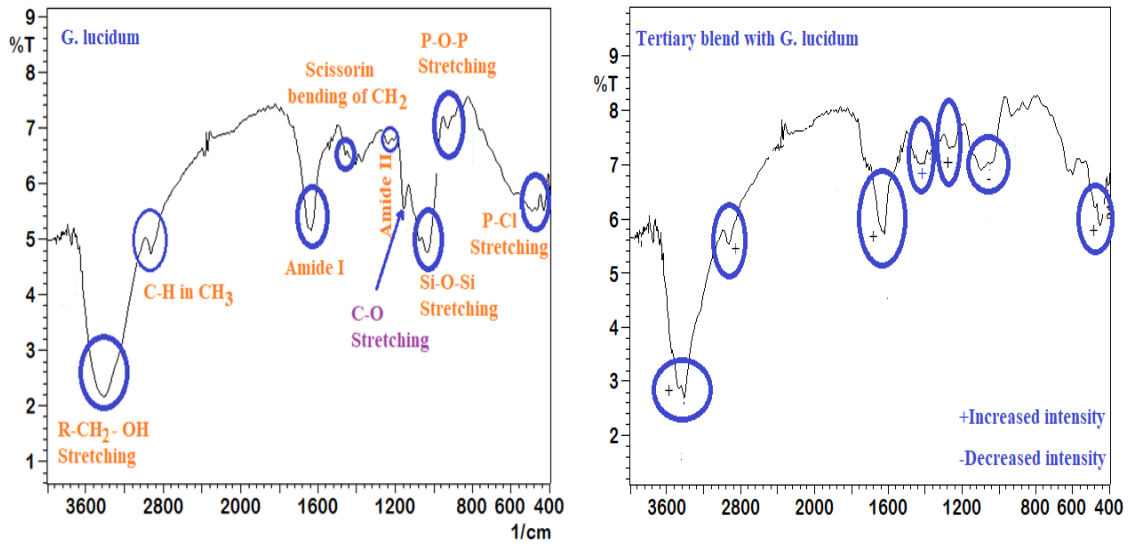

Fig.4.13: FTIR spectrum of G.lucidum and tertiary blend with G.lucidum.

Figure 4.14 shows the FTIR spectrum of capsicum. Absorption band around 3400 cm^{-1} is due to the presences of characteristic stretching vibrations of (N-H) in amino acids. Band at 2904.09 cm^{-1} belongs to the aliphatic C-H stretching, while the band at 1636.64 cm^{-1} is due carbonyl group (C=O) stretching. The stretching vibration of C-C bond in the aromatic ring appears

at 1404.18 cm^{-1} and the asymmetrical stretching of the C-O-C appears at 1242.16 cm^{-1}. Band at 1064,41 cm^{-1} belongs to the C-O asymmetrical stretching vibration.

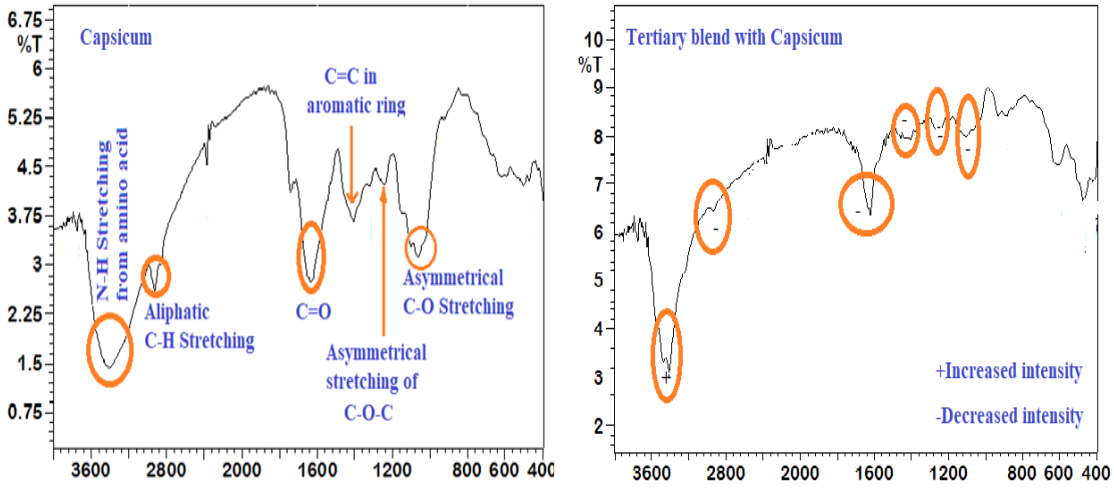

Fig.4.14: FTIR spectrum of capsicum and tertiary blend with capsicum.

Figure 4.15 shows the effects of iodine (1_2) on the tertiary polymeric blend, where all the characteristics bands of PVA, HA and Collagen present, as well as the bands of iodine, which appears at 500 cm-1 for C-I stretching vibration and at 650-720 cm-1 for C-I out of plane deformation [178].

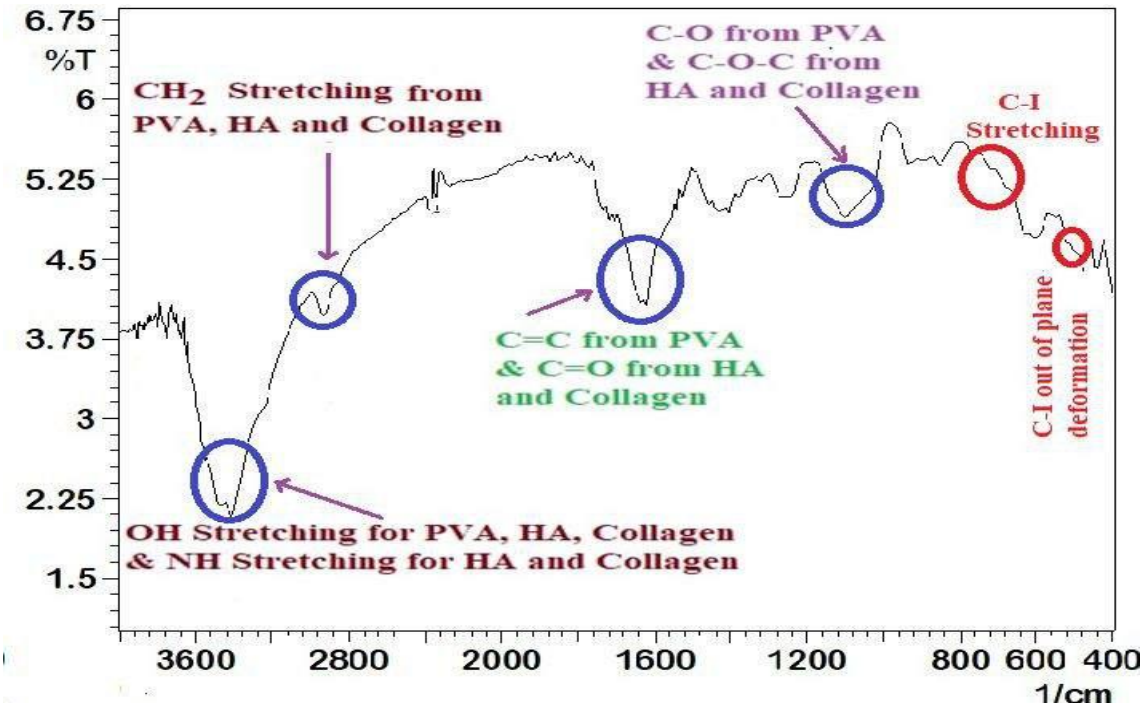

Fig.4.15: FTIR spectrum of tertiary blend with I_2

Figure 4.16 shows the FTIR spectrum of Ocimum basilicum oil. Bands from 3416.86 cm^{-1} to 3464.15 cm^{-1} due to the presence of bonded N-H/C-H/O-H

stretching of amines, amides, and alcohols. Band at 2924.09 cm^{-1} refers to the C-H stretching vibration of alkane. Band around 2854.65 cm^{-1} belongs to the stretching vibrations of O-CH_3 and C-H of methoxy and methoxy ether. Band at 2075.15 cm^{-1} indicates the vibration of (N=C=S) functional group of Isothiocyanate. The stretching vibration mode of carbonyl group (C=O) appears at 1743.44 cm^{-1}, (which refer to the presence of amino acids), while the band at 1458.18 cm^{-1} is due to the stretching vibration of C=C-C in the aromatic ring. Small band at 1234.44 cm^{-1} refers to the C-O-C vibration of protein.

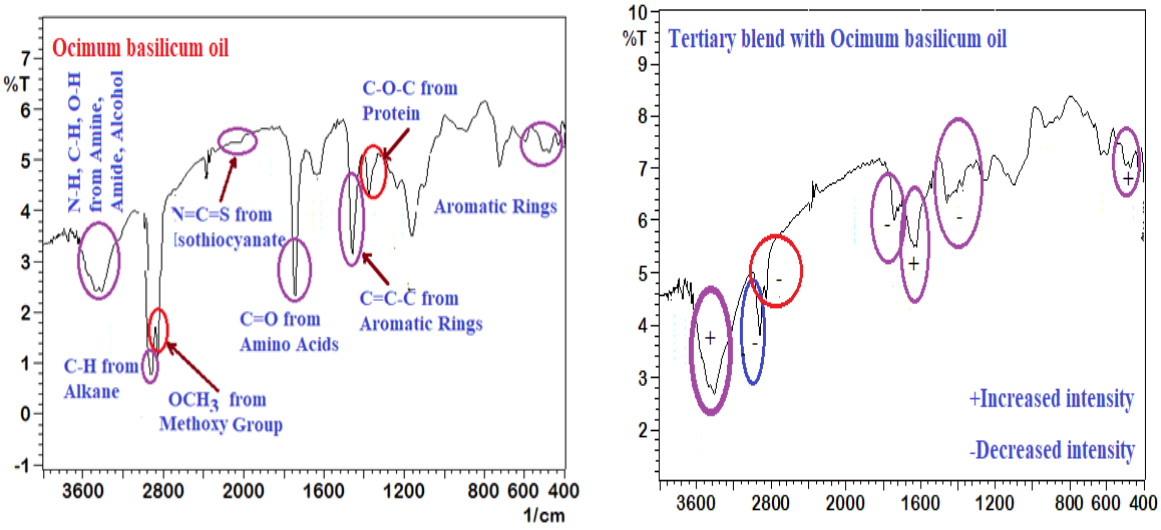

Fig.4.16: FTIR spectrum of Ocimum basilicum oil and tertiary blend with Ocimum basilicum oil.

It is clear from the above that, the chemical composition of Ocimum basilicum oil contains many ingredients, such as amines, amides, alcohols, amino acids and so on. These ingredients provide many activities, such as the Antimicrobial, Antibacterial, Anti-inflammatory, Antioxidant, Cancer-Preventive, Antispasmodic, Antiviral, insecticide, Antiviral and Acaricide [179].

Carboxylic acid present in the plants act as a main pharmaceutical agent in treatment of diseases like ulcers, jaundice, headache, stomatitis, fever, edema and rheumatic joint pains. Amine, amides, and amino acids are the main group of protein synthesis [180].

The active constituent present in Ocimum basilicum oil is Eugenol (about 0.27%). Its chemical structure is $C_{10}H_{12}O_2$ and named as 1- hydroxy-2-methoxy-4-allyl benzene [181].

Figure 4.17 shows the FTIR spectrum of Rosemary oil, where band at 1651.07 cm^{-1} (stretching vibrations of the C = O group, while bands from 1103.29 cm^{-1} to 1242.16 cm^{-1} are due to the C-O-C vibrations from 1,8-cineole. Broad band around 3450 cm^{-1} corresponding to stretching vibrations of the O-H. Bands from 2854.58 cm^{-1} to 2925.86 cm^{-1} are due to the C-H stretching of CH_2 and CH_3 groups [182].

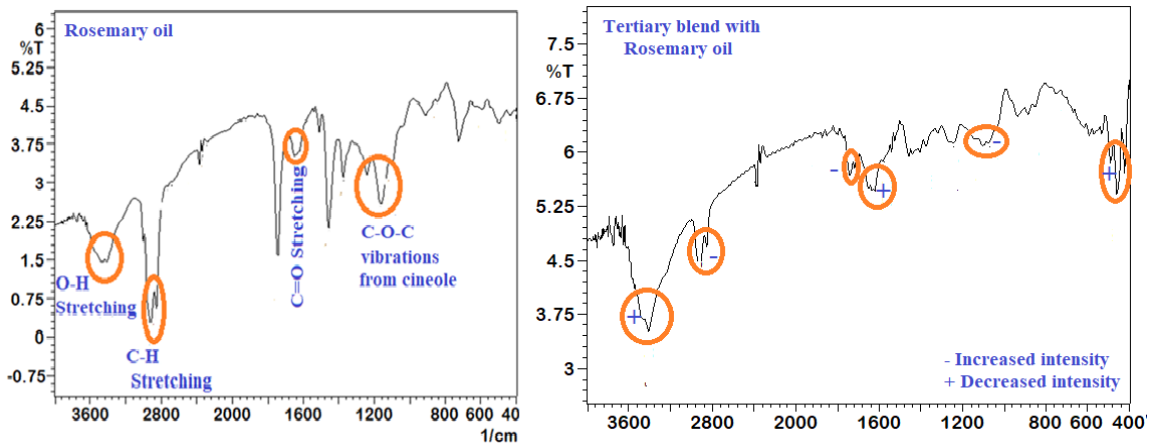

Fig.4.17: FTIR spectrum of Rosemary oil and tertiary blend with Rosemary oil.

Figure 4.18 shows the FTIR spectrum of L. nobilis EO. Band from 3417.86 cm^{-1} to 3471.86 cm^{-1} belong to the OH stretching from linalool, terpinene-4-ol- and α- terpineol. Bands from 2854.65 cm^{-1} to 2924.09 cm^{-1} refer to stretching vibrations of methylene group (CH_2) from sabinene, linalool, β-pinene and 1,8-cineole. Band at 1743.65 cm^{-1} is due to the stretching vibration of the carbonyl group (C=O) from α-terpinyl, bornyl and linalyl acetates. Band at 1620.21 cm^{-1} is of C=C stretching from terpene compounds, such as β-caryophllene, linallol, α- and β-pinene, sabinene and myrcene [137]. Band at 1458.18 cm^{-1} is due the vibration of the aromatic rings' methyl eugenol. Band at 1373.23 cm^{-1} due to the stretching vibration of (CH_3-C=O) group from 1,8-cineole, α- terpinyl acetates. Band at 1167.29 cm-1 belongs to symmetrical stretching of (C-O-C) group in the aromatic

rings of methyleugenol and eugenol acetate esters [183]. Band at 1080.14 cm^{-1} belongs to C-O-C stretching of 1.8- cineole. Bands at 887.26 cm-1 and 848.68 cm-1 belong out of plane deformation of $=CH_2$ group from limonene and wagging vibration of C-H group from ρ-cymene, Band at 725.23 cm^{-1} is due to in plane deformation (sp^2 C-H).

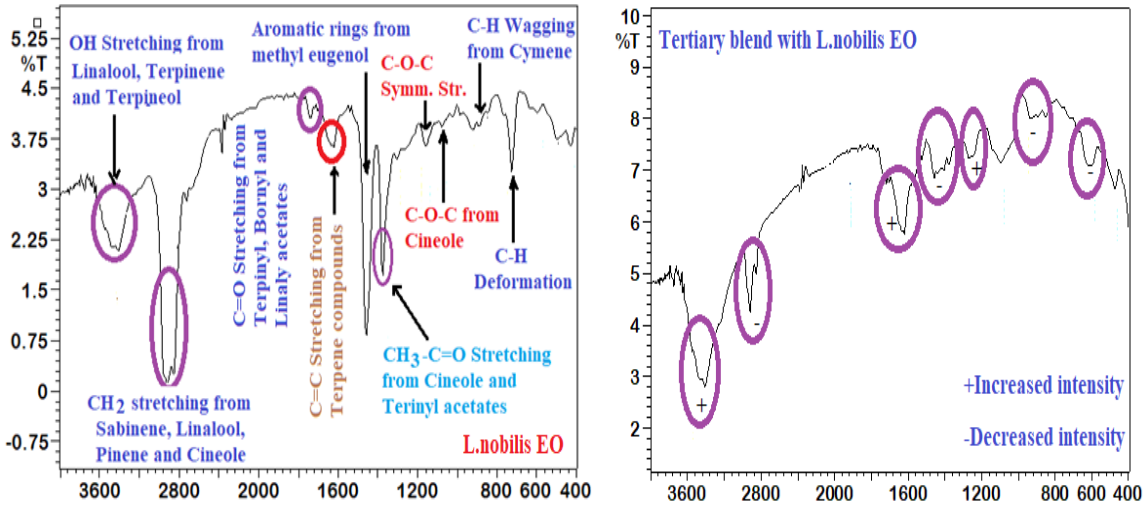

Fig.4.18: FTIR spectrum of L.nobilis EO and tertiary blend with L.nobilis EO.

Figure 4.19. represents the FTIR analysis of Final textile, resulting from peaks listed in Table 4.5. Band from 3417.86 cm^{-1} to 3471.86 cm^{-1} belong to OH stretching of PVA, HAc, collagen, linalool, terpinene, terpineol, Rosemary oil, NH stretching of HAc, collagen, R-CH_2-OH stretching from G.lucidum, N-H, C-H,O-H from Amine, Amide, Amide Alcohol from Ocimum. Bands from 2854.65 cm^{-1} to 2924.09 cm^{-1} refer to CH_2 stretching of PVA, HAc, collagen, CH-stretching Aliphatic from Capsicum. Band from 1200 cm^{-1} to 1700 cm^{-1} belong to C=C stretching from PVA and L.nobilis EO, C = O stretching from capsicum, Ocimum , Rosemary oil, HAc and Collagen, Amide I from G.lucidum, Aromatic rings from capsicum, Ocimum, Rosemary oil, L.nobilis EO ,C-O-C asymmetrical stretching from capsicum, Ocimum, Rosemary oil, L.nobilis EO, and Amide II from G.lucidum. Band at 1000 cm^{-1} belongs to C-O-C stretching from HA_c , Collagen and 1.8- cineole, C-O asymmetrical from PVA, and capsicum, Si-O-Si stretching from G.lucidum, C-H_2 deformation from Methoxy group.

Band at 500 cm-1 for C-I stretching vibration and at 650-720 cm-1 for C-I out of plane deformation.

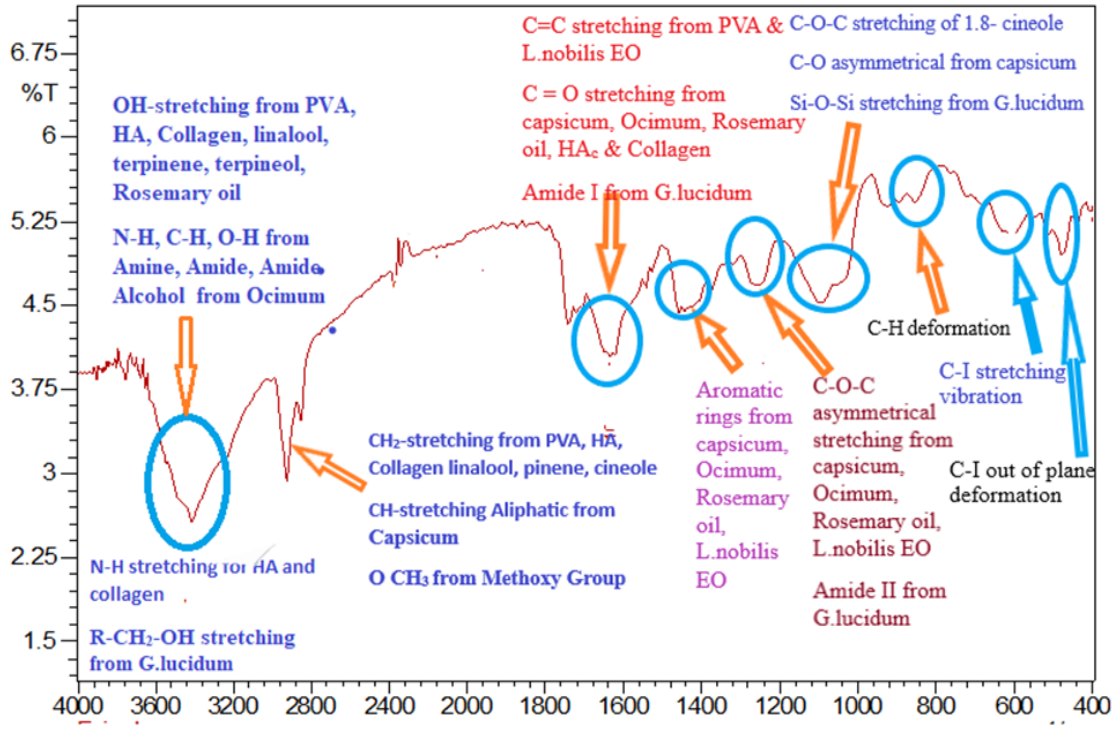

Fig.4.19: FTIR spectrum of (Final textile) nanofibers

Table 4.5 FTIR analysis peaks of Final textile.

Peaks Wave Numbers (cm^{-1})	**Vibration Mode**
3500 – 3600	OH stretching of PVA, HAc, collagen, linalool, terpinene, terpineol, Rosemary oil NH stretching of HAc, collagen R-CH_2-OH stretching from G.lucidum N-H, C-H, O-H from Amine, Amide, Amide Alcohol from Ocimum
2900	CH_2 stretching of PVA, HAc, collagen, CH-stretching Aliphatic from Capsicum
1200-1700	C=C stretching from PVA & L.nobilis EO C = O stretching from capsicum, Ocimum , Rosemary oil, HA_c & Collagen Amide I from G.lucidum Aromatic rings from capsicum, Ocimum, Rosemary oil, L.nobilis EO

	C-O-C asymmetrical stretching from capsicum, Ocimum, Rosemary oil, L.nobilis EO Amide II from G.lucidum
1000	C-O-C stretching from HA_c , Collagen, 1.8-cineole C-O asymmetrical from PVA, capsicum Si-O-Si stretching from G.lucidum C-H_2 deformation
650-720	C-I out of plane deformation
500	C-I stretching vibration

4.4 Wettability results

4.4.1 Wettability of blends polymeric

Contact angle results and adopting the wettability property as a basic criterion in choosing the optimum nano fiber textile (which possess the super hydrophilic behaviors) for wound dressings. These textiles will be studied and analyzed in some details in the remaining sections.

Wounds that have become infected are typically treated with antimicrobial substances like silver nano particles or bacterial cellulose. Several articles have been published as of late that show how hydrophobic surfaces can be used to remove bacteria from a wound dressing. There is evidence that hydrophilic surfaces have stronger adhesion to the skin than hydrophobic ones, while hydrophobic surfaces can make it such that the dressing doesn't stick to the skin at all [184]. Surface wettability is crucial in evaluating a wound dressing's effectiveness. Hydrophobic dressings are good for bacterial adsorption; nevertheless, most anchorage-dependent cell types require a hydrophilic surface for improved cell attachment. Additionally, the surface's hydrophobicity or hydrophilicity can be employed to guide cellular activities such cell initial attachment, adhesion, and migration during wound healing. Therefore, the dressing's usability is enhanced by surfaces that can change their surface wettability. The contact angle of the sample is affected

by the intensity of hydroxyl group (OH), it decreases with the increasing hydroxyl group number. The hydrophilicity and wettability increased as the contact angle decreased [185].

It is clear from table 4.6, that any addition to the PVA decreases its initial contact angle (CA), which is 70º. For example, Collagen additions by any ratio decrease CA to reach only 46.505º in sample with 7% Collagen and blending ratios of 55:45.

Table 4.6: Contact angles of the prepared samples.

Sample	Contents ratios (%)	Contact angle (degree)
10% PVA	100	70°
10% PVA: 3 % Coll.	75:25	54°
	65:35	60.437°
	55:45	59.538°
10% PVA: 5% Coll.	75:25	60°
	65:35	57°
	55:45	53.370°
10% PVA: 7% Coll.	75:25	69.581°
	65:35	56.368°
	55:45	46.505°
10% PVA: 3.5% HAc	75:25	67.568°
	65:35	53.022°
	55:45	57.646°
10% PVA: 5.5% HAc	75:25	62.518°
	65:35	52.7739°
	55:45	51.37°
10% PVA: 7% Coll.: 5.5 % HAc	55:30:15	61°
	55:15:30	49.944°
	55:22.5:22.5	41°

The same behavior occurs with HAc additions, where CA continued decreasing downward to 51.37º with the 5.5% HAc addition for the same blending ratios; 55:45. That means that, these additions increased the wettability, which is the desired character in wound dressing application. When combined with these two additions (7% Coll. and 5.5 % HAc) to the

10% PVA, the contact angle decreased downward to its lowest value of 41° with tertiary blending ratios of 55: 22.5: 22.5.

Since these three samples possess the lowest contact angles and experienced super hydrophilic behaviors, thus, these samples were selected as the optimum samples for wound healing application and will be furthered studied and analyzed.

4.4.2 Wettability of blends with antibacterial & antioxidation

An effective dressing is essential for wound healing. In fact, the wettability performance is one of the most important factors of a wound dressing. The fundamental functions of a wound dressing involve the absorption of excess exudates and maintenance of optimal moisture at the wound by controlling water evaporation [12, 22]

Table 4.7 showed that, some additions increased the wettability, such as some formulas of Capsicum annuum, Iodine and L.nobilis EO. This means that these dressings can degraded easily as well as release drug towards the injured skin quickly.

At standard processing conditions (19 kV applied voltage, 20 cm needle-to-collector distance, 600 rpm collector rotation speed, and the flow rate of 1ml/hr), the contact angle of the final solution is 52°, which is higher than it for the tertiary net blend (41°). This means that, the final solution is less wettability, therefore, the operating conditions were changed one by one (while keeping the remaining conditions constant) in order to obtain nano fiber textiles with high wettability, as shown in table 4.8.

Table 4.7: Contact angles for the prepared samples

Textile	Ratios %	Contact angle (°)
Neat blend	10:5.5:7	41
G. lucidum	1	48.76
	3	50
	6	54.766
Capsicum annuum	1	41.44
	3	23.862
	6	39
I_2	0.1	38.3
	0.2	45
	0.3	48
Ocimum basilicum oil	3	50
	7	49
	10	44
Rosemary oil	3	40.9
	7	56.8
	10	64
L. nobilis EO	3	53.482
	7	39.382
	10	35.148
Final Textile		52

It is clear that decreasing the needle-to-collector distance from 20 to 15 cm causes the highest increasing in the wettability, -42.3%. The smaller the distance between the needle-to-collector, the shorter the time for the solvent to evaporate from the nano fiber as it travels towards the collector.

Increasing the applied voltage by 25 kV, increases the wettability by 20%. The higher the voltage, the faster the fibers ejected from the needle, the less time it takes to reach the needle, and the less chance of evaporation of the solvent.

Increasing the collector speed from 600 up to 780 rpm, have no effect on the wettability, while reducing the flow rate in half caused an improvement in wettability by about 27%.

Table 4.8: Influence of processing parameters on contact angle

Variable processing parameter	New variable value	Contact angle (°)	Change (%)
No variable (standard conditions)	-	52	-
Applied voltage	25kV	41.6	- 20
Needle-to-collector distance	15 cm	30	-42.3
Collector speed	780 rpm	52	0
Flow rate	0.5ml/h	38	-26.9

4.5 Field- Emission Scanning Electron Microscopy (FESEM) images and EDX analysis

4.5.1 FESEM of blend polymeric nanofibers

Figures 4.20-4.23 show the FESEM morphological images and some relating findings, such as EDX elemental analysis and diameter distribution of the obtained electrospun nano fibers. It is clear from figure 4.20, that the electrospun nano fibers, obtained from the neat PVA solution are individual, smooth, with 214–447.35 nm diameter, aligned with random directions, and consist of 81.6 % C and 18.4% O.

Collagen addition to the neat PVA solution (Figure 4.21) causes a reduction of the nano-fiber diameter to be 70.011-350.05 nm and their elemental analysis changed to be 82.4 % C and 17.6 % O. The diameter reduction is due to the decreasing of viscosity [187] of the new solution compared with the high viscosity of the neat PVA solution, as shown earlier in figure 4.1. Although smooth fiber was obtained here, some fused and branched non-fibers appeared with random overall orientation. The smooth degree refluxes the good stability of the electrospinning process and the suitability of its conditions

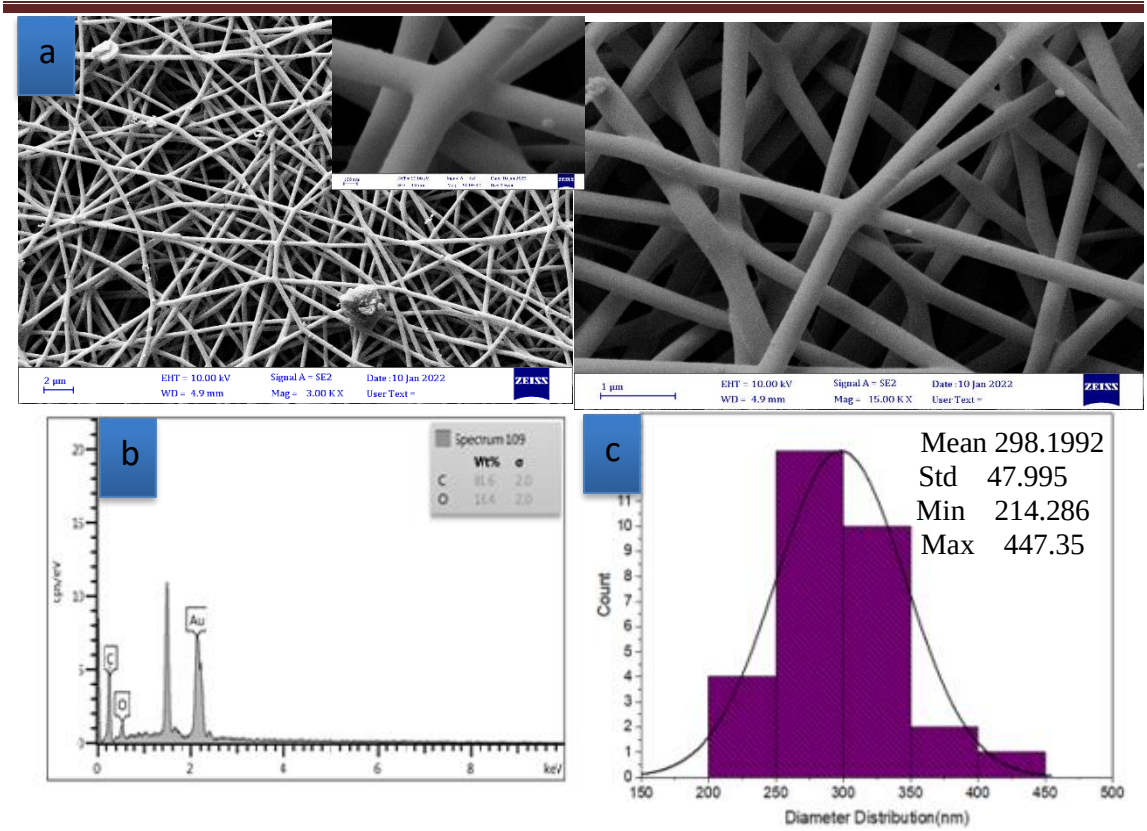

Fig.4.20: (a) FESEM images with 3000 and 15000 magnification powers respectively, (b) EDX analysis, (c) diameter distribution of PVA nano fibers.

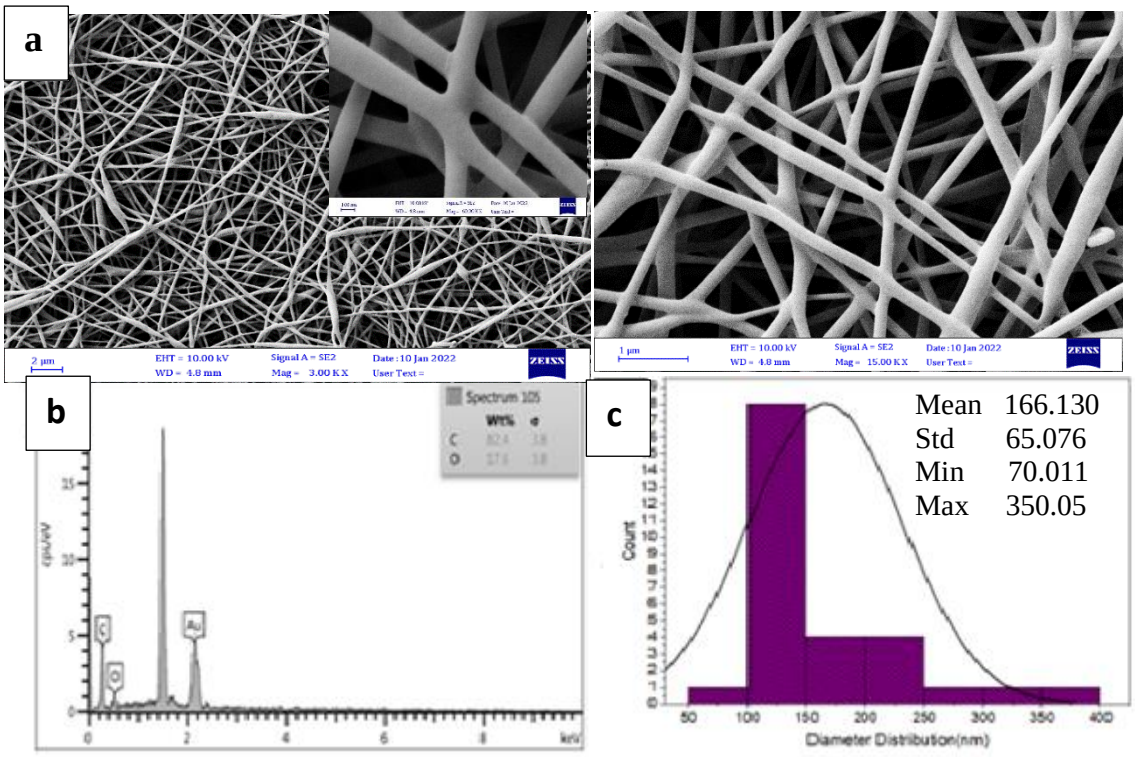

Fig.4.21: (a) FESEM images with 3000 and 15000 magnification powers respectively, (b) EDX analysis, (d) diameter distribution of PVA/ Coll. nano fibers.

HAc addition (Figure 4.22) gives a smooth nanofiber with 50-250 nm diameter and its EDX elemental analysis is 82 % C and 18 % O. The high reduction in the fiber diameter coincides with the high decrease in its viscosity [188] as shown in Figure 4.1 and with its high surface tension (Figure 4.3). The orientation was still randomly, and some beads appeared.

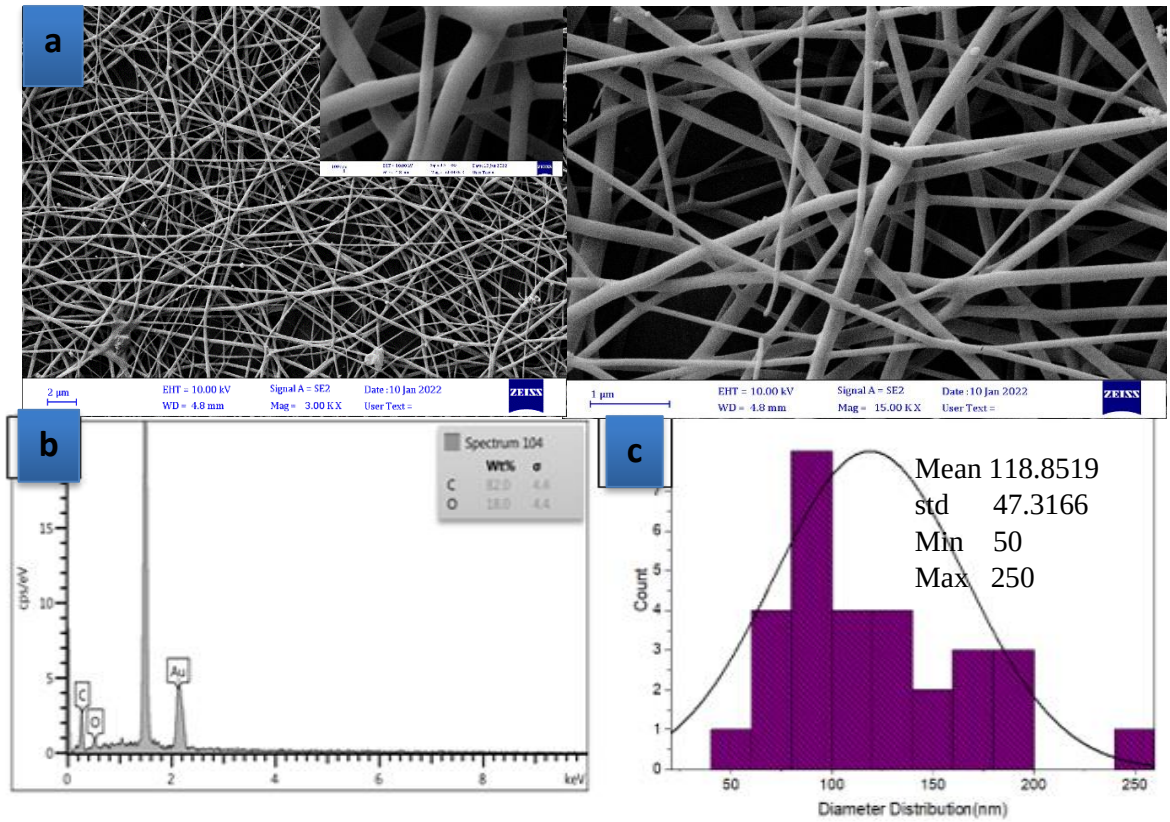

Fig.4.22: (a) FESEM images with 3000 and 15000 magnification powers respectively, (b) EDX analysis, (c) diameter distribution of PVA/ HAc. nanofibers.

The combined addition of HAc and Coll. (Figure 4.23) causes the elemental analysis to be 82.6 % C and 17.4 % O, producing smooth nano fibers with 74.6263- 349.285 nm diameter distribution and with average diameter of 120.8 nm. In this tertiary neat blend, some beads and random, branched nano fibers formed within textile with medium porosity.

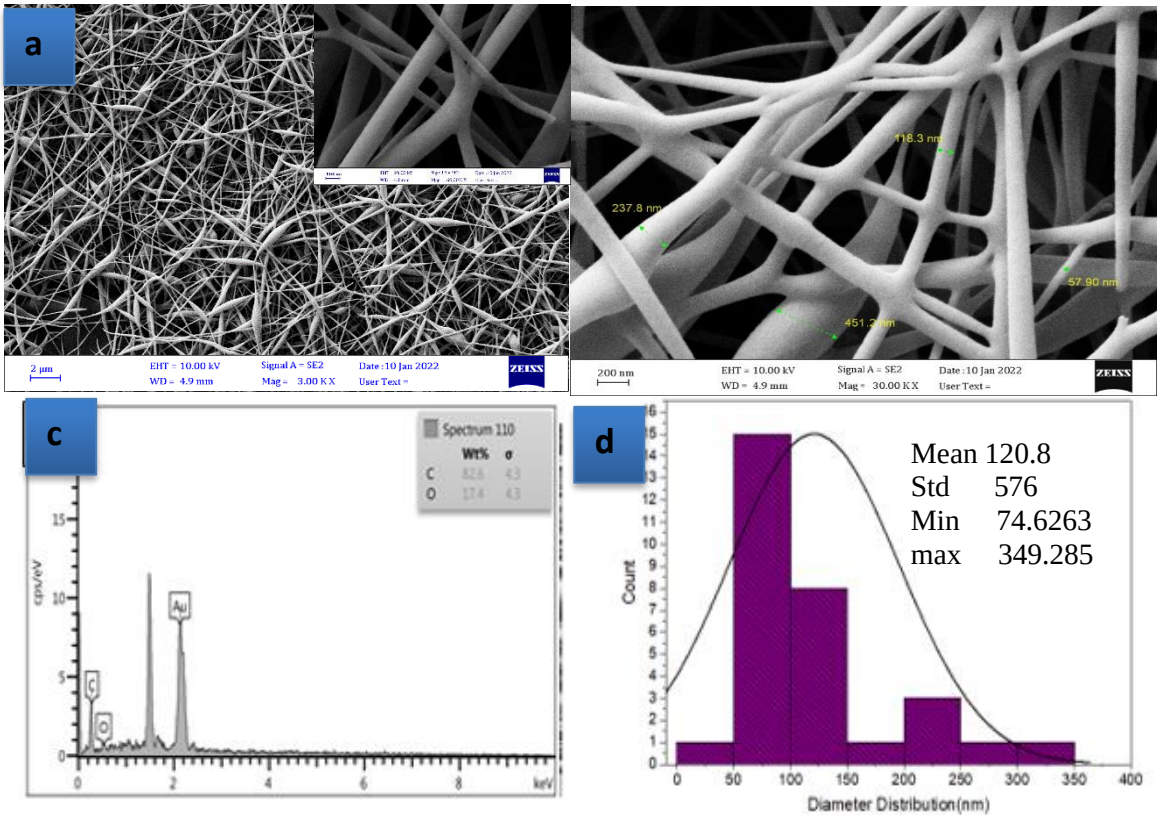

Fig.4.23:(a) FESEM images with 3000 and 15000 magnification powers respectively, (b) EDX analysis, (c) diameter distribution of tertiary neat blend nano fibers

4.5.2 FESEM and EDX of blend with antibacterial & antioxidation

Figures 4.24 and 4.25 show the FESEM images and the resulting fibers' diameter distribution, respectively. It is clear that as G. lucidum content increased, the fiber diameter increased as well as the number of beads. Compared with the morphology of the neat blend, high porous textile obtained with honeycomb, branched, fused fibers formed with no beads.

The mean diameter increased with G. lucidum addition from 67.1241nm to reach its maximum value (168.4079) at 3 wt.% addition; increased by 39.4%. This result coincides with the formation of big beads and fused fibers at 6 wt.% addition as shown in figure 4.24-D.

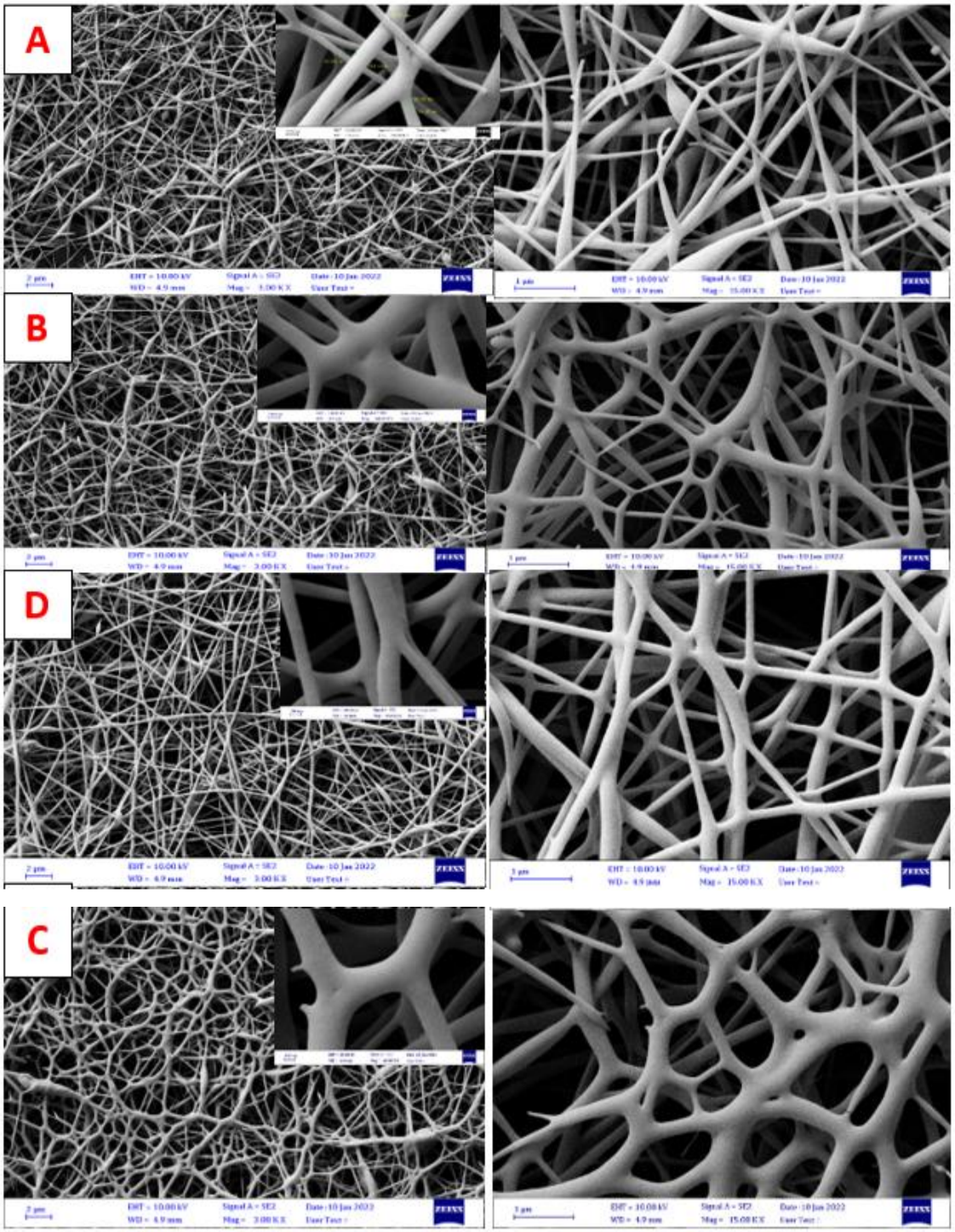

Fig.4.24: FESEM images with 3000 and 15000 magnification powers respectively, for (A) neat blend nanofiber (B) blend with l wt.% G. lucidum (C) blend with 3 wt.% G. lucidum (D) blend with 6 wt.% G. lucidum.

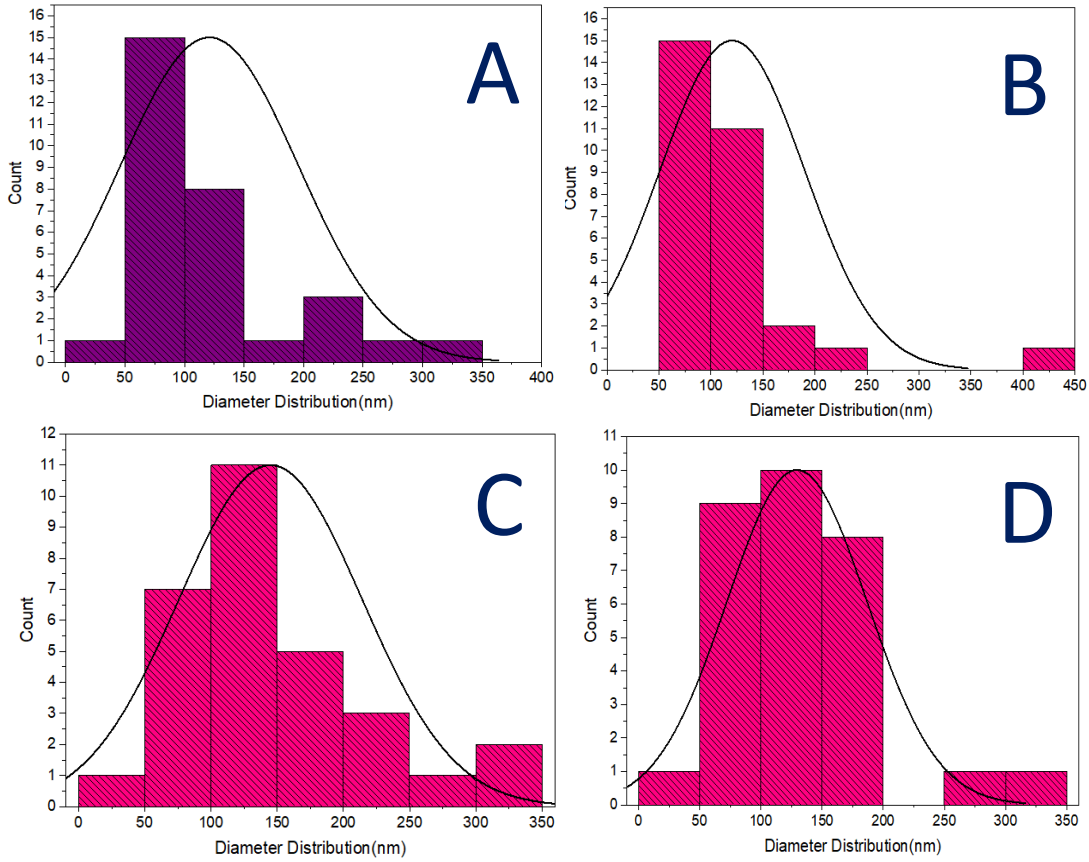

Fig.4.25: Diameter distribution of nanofiber (A) neat blend nanofiber (B) blend with l wt.% G. lucidum (C) blend with 3 wt.% G. lucidum (D) blend with 6 wt.% G. lucidum.

Capsicum annuum addition (Figures 4.26 and 4.27), increased the average diameter only by about 20% (up to 144.7402 nm). This can be attributed due to the interaction of Capsicum annuum with neat blend chains that resulted in increasing the spinning solution viscosity. Compared with the morphology of the neat blend, branched nano fiber obtained with medium porosity and decrease the number of beads.

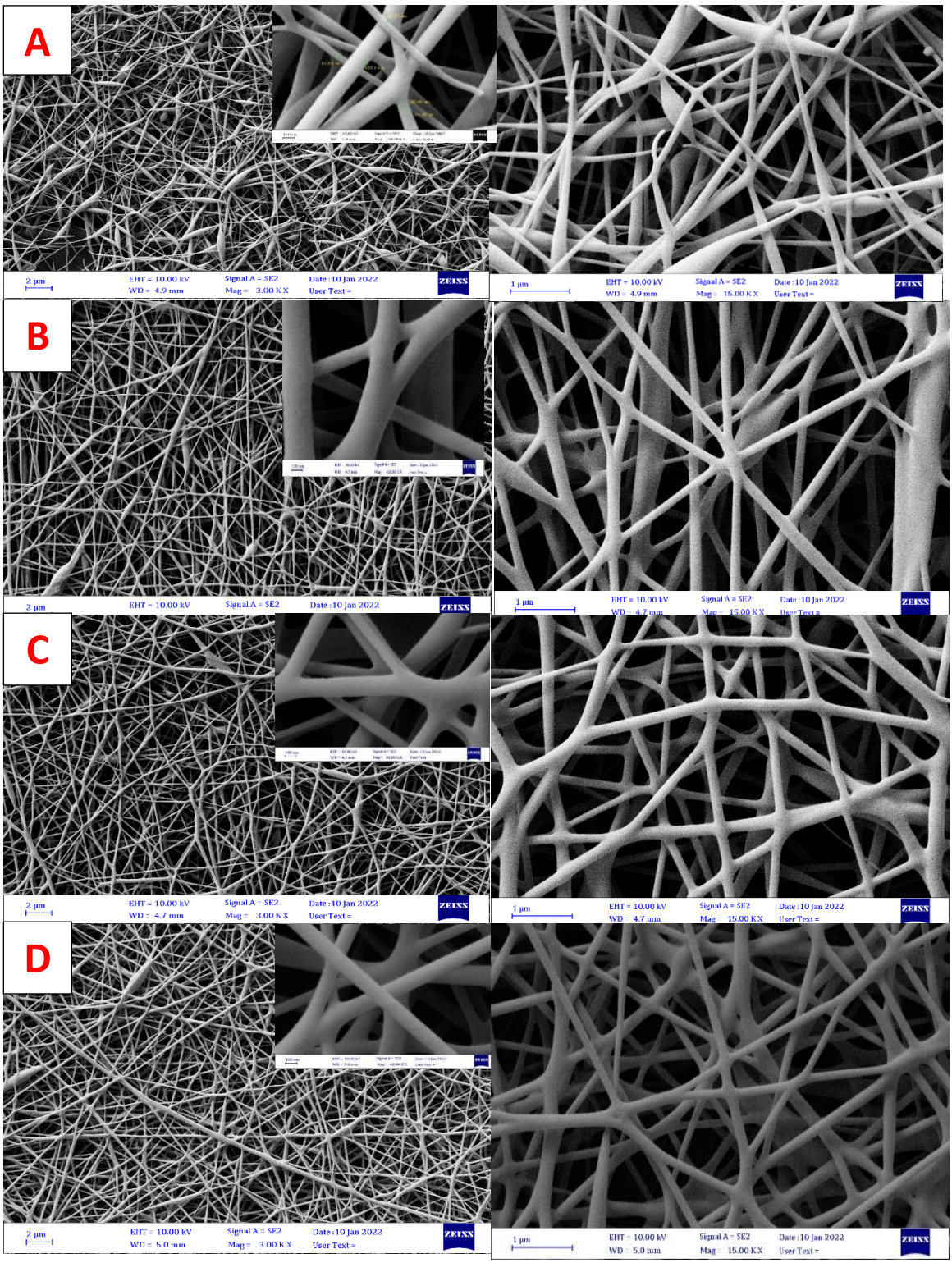

Fig.4.:26 FESEM images for (A) neat blend nanofiber (B) blend with 1 wt.% Capsicum annuum (C) blend with 3 wt.% Capsicum annum (D) blend with 6wt.% Capsicum annuum

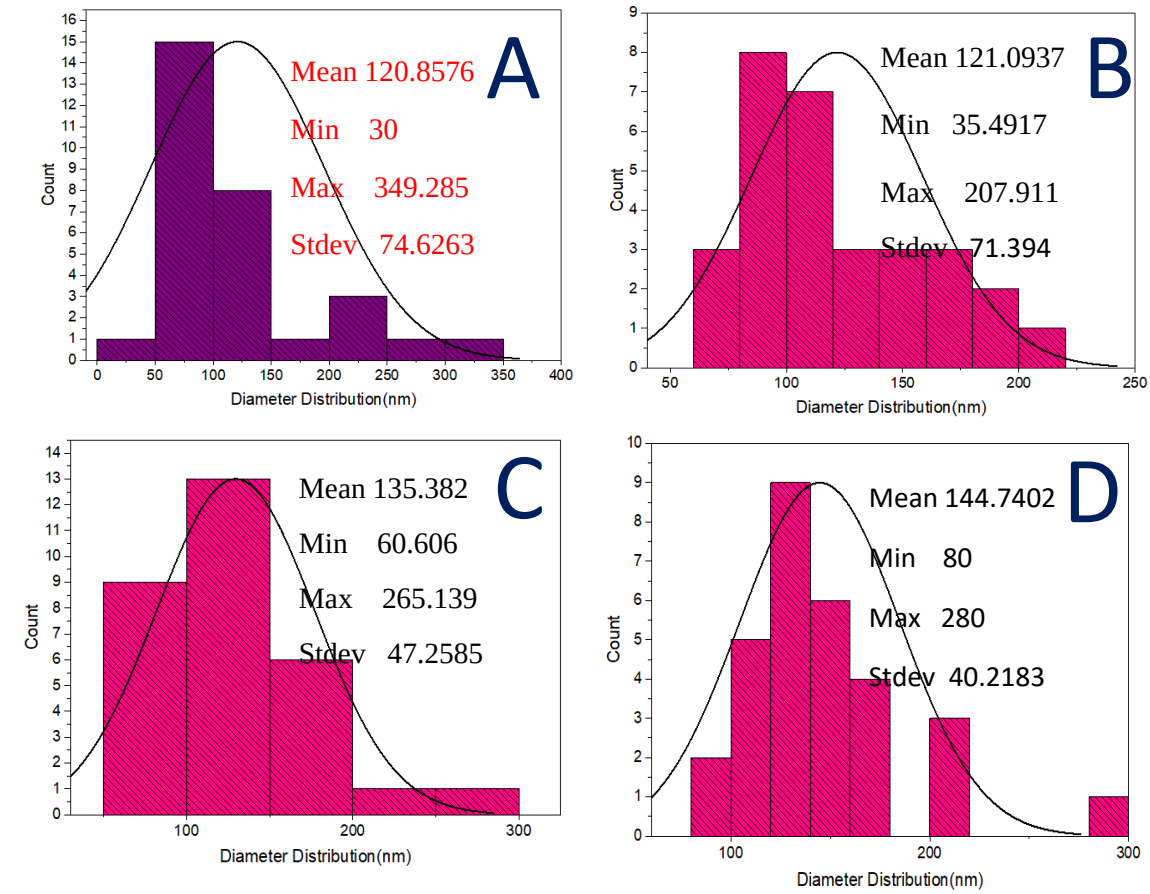

Fig.4.27: Diameter distribution of nanofiber (A) neat blend nanofiber (B) blend with 1 wt.% Capsicum annuum (C) blend with 3 wt.% Capsicum annum (D) blend with 6 wt.% Capsicum annuum.

Figures 4.28 and 4.29 show the FESEM images and fibers' diameter distribution of the nano fibers resulting from I_2 additions. Random nano fiber obtained, and the textile have uneven porosity distribution. As I_2 content increased up to with 0.3 wt.%, there was an increase in the diameter of the nano fiber by about 22% (from 120.8576 nm to 147.1937 nm and a change in the diameter range from (30-349 nm) to (82.902 - 306nm). Also, there is a decrease the number of beads. All these findings may be explained by the high solution viscosity of blend–iodine, as compared to that of pure blend and by the increase in the conductivity and, is explained by the higher charge density on the surface of the ejected jet during spinning, thus imposing higher elongation forces on the jet.

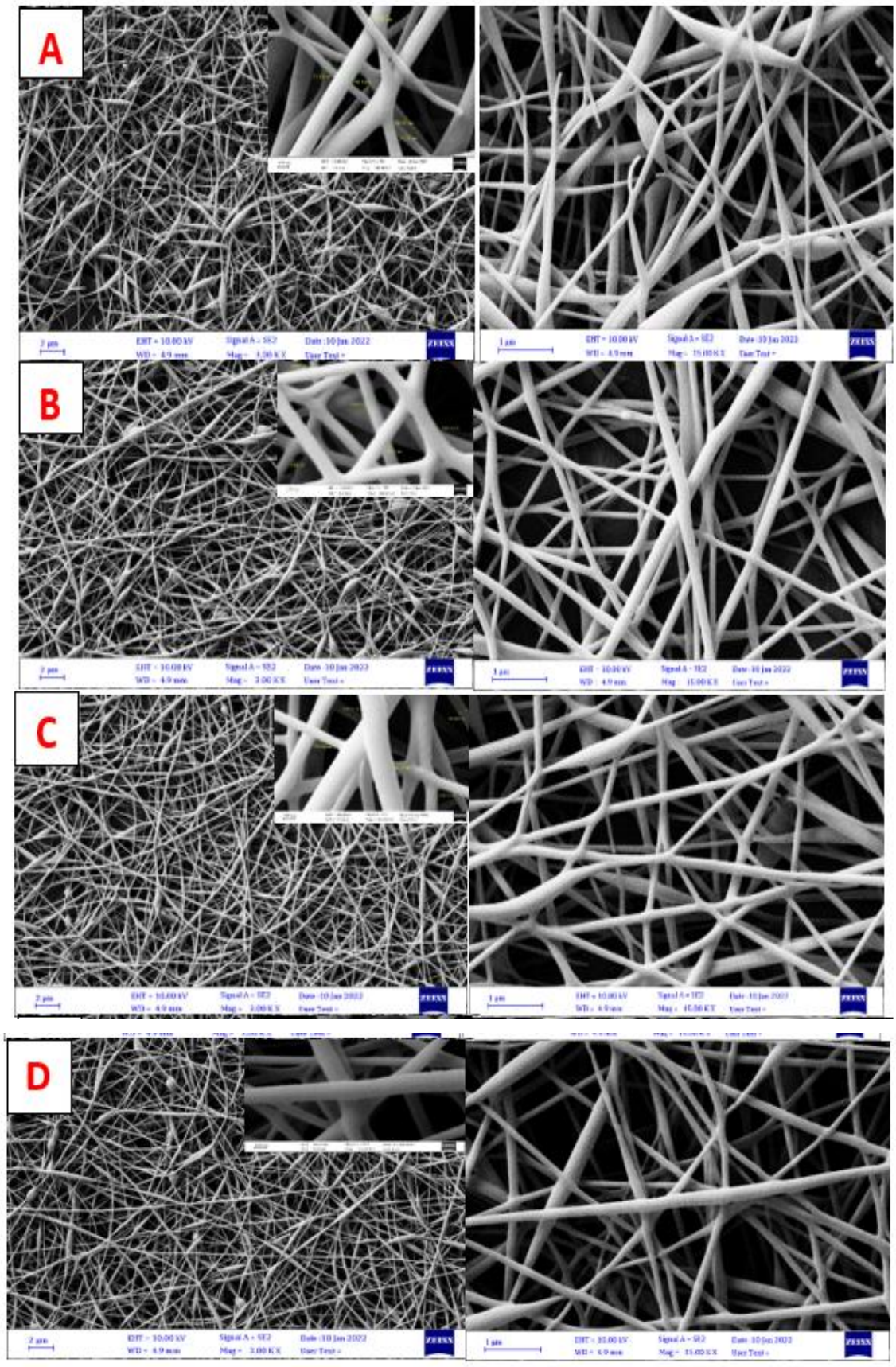

Fig.4.28: FESEM images with 3000 and 15000 magnification powers for (A) neat blend nanofiber (B) blend with 0.1 wt.% I_2 (C) blend with 0.2 wt.% I_2 (D) blend with 0.3 wt.% I_2

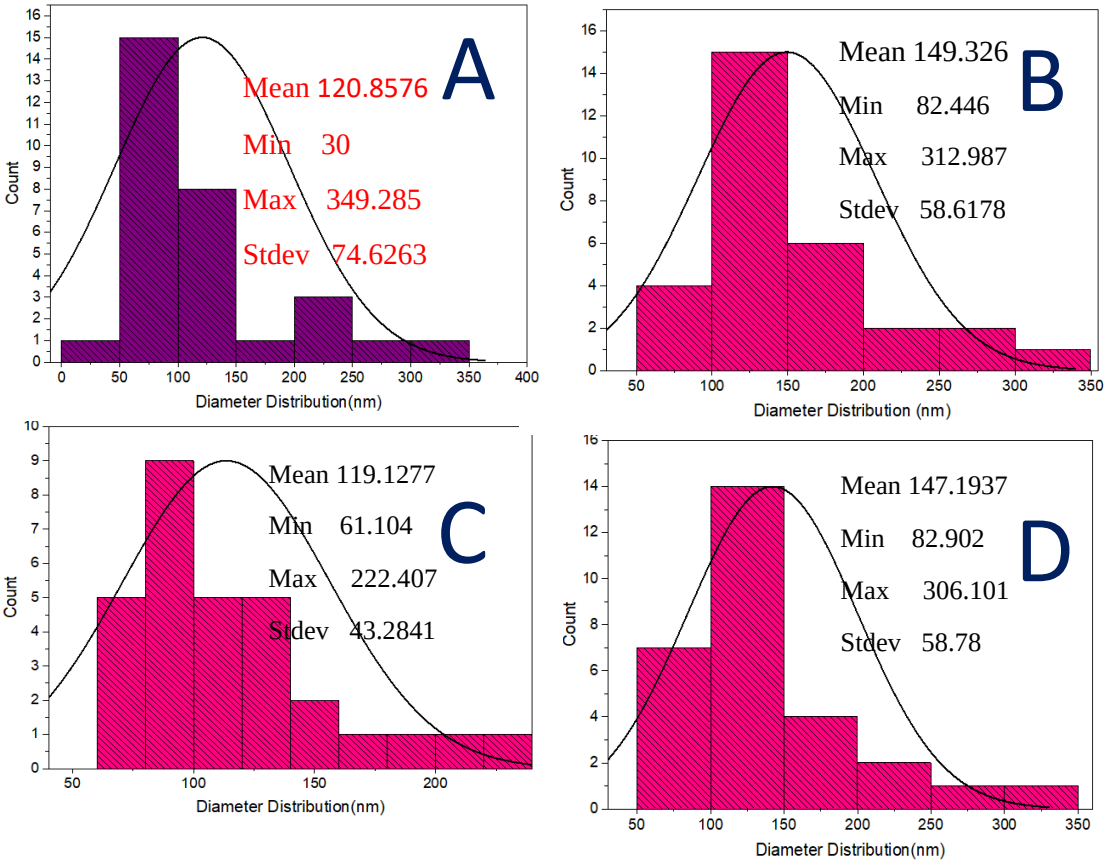

Fig.4.29: Diameter distribution of nanofiber (A) neat blend (B) blend with 0.1 wt.% I_2(C) blend with 0.2 wt.% I_2 (D) blend with 0.3 wt.% I_2.

Figures 4.30 and 31 show the FESEM images and the resulting fibers' diameter distribution of addition Ocimum bailicum oil. It is noticed the clear effect of Ocimum bailicum oil on the fiber form, and sizes of the formed beads. Fused, branched nano fiber obtained and the beads begin to be larger with the increase in the oil addition. Also, there was an increase in the fiber diameter by 76.81%, where it is increased up to 213.6887 nm and its range changed to be 79.038 -533.365 nm in the case of blend with 10 wt.% Ocimum basilicum oil. The obtained textile is high porous.

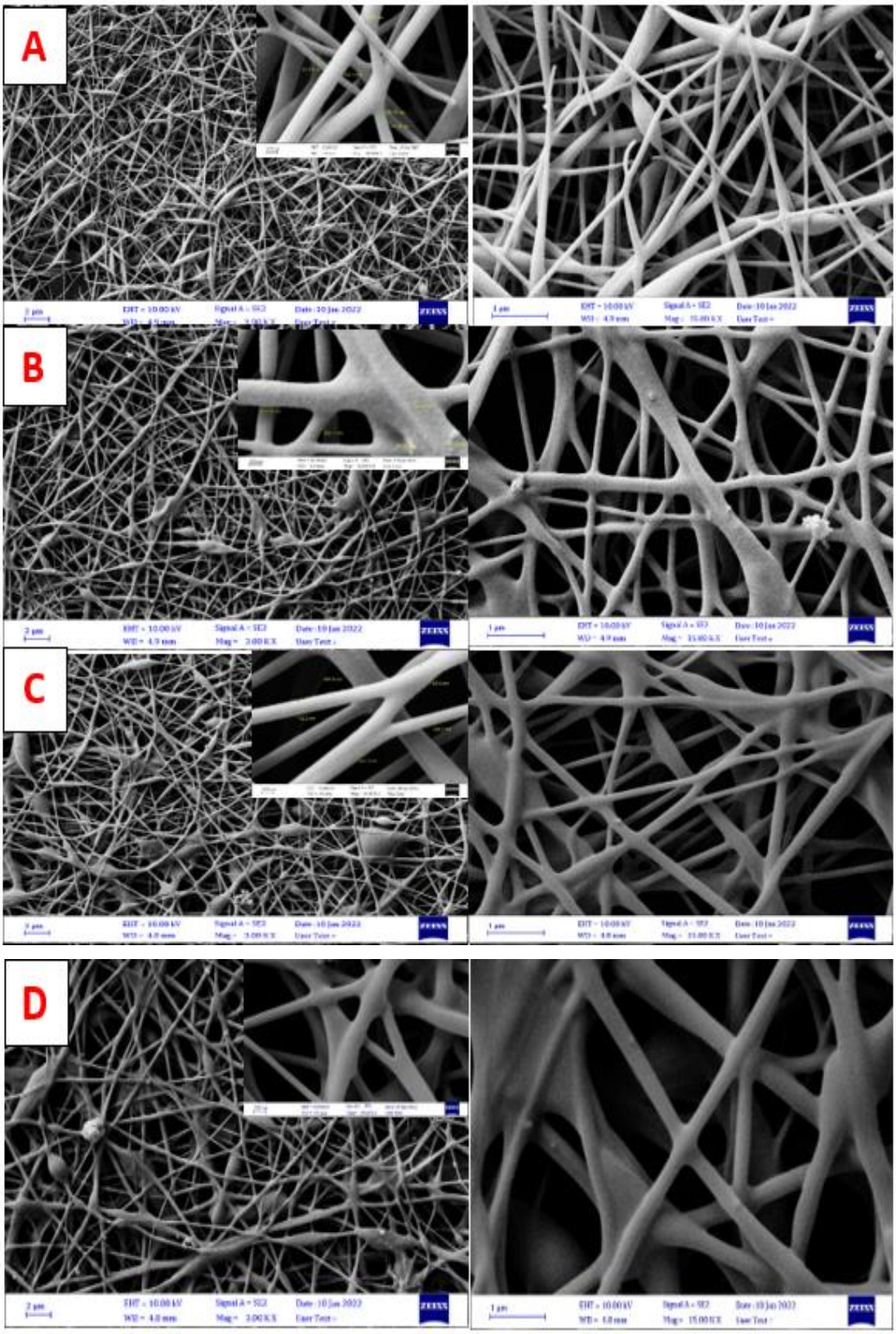

Fig.4.30: FESEM images with 3000 and 15000 magnification powers for (A) neat blend nanofiber (B) blend with 3 wt.% Ocimum basilicum oil (C) blend with 7 wt.% Ocimum basilicum oil (D) blend with 10 wt.% Ocimum basilicum oil.

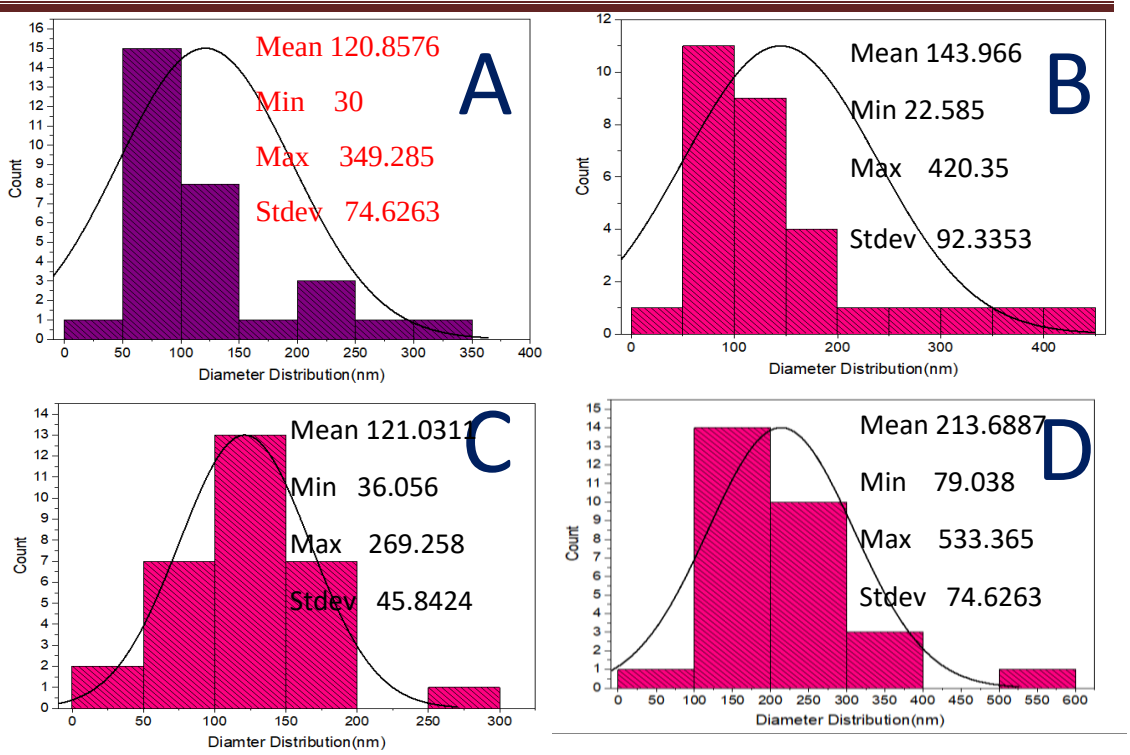

Fig.4.31: Diameter distribution of nanofiber(A) neat blend nanofiber (B) blend with 3 wt.% O. Basilicum oil (C) blend with 7 wt.% Ocimum basilicum oil (D) blend with 10 wt.% Ocimum basilicum oil

Figures 4.32 and 4.33 show the FESEM images and the resulting fibers' diameter distribution of Rosemary oil addition, respectively. The diameter increased by 67.78% (up to 202.7867nm) and the diameter range changed to be 58.899 - 594.674 nm in the case of blend with 10 wt.% Rosemary oil. The reason behind the increment of the diameter is due to the increased viscosity of the blend. Branched nano fiber obtained with increased number of beads in high porosity textile.

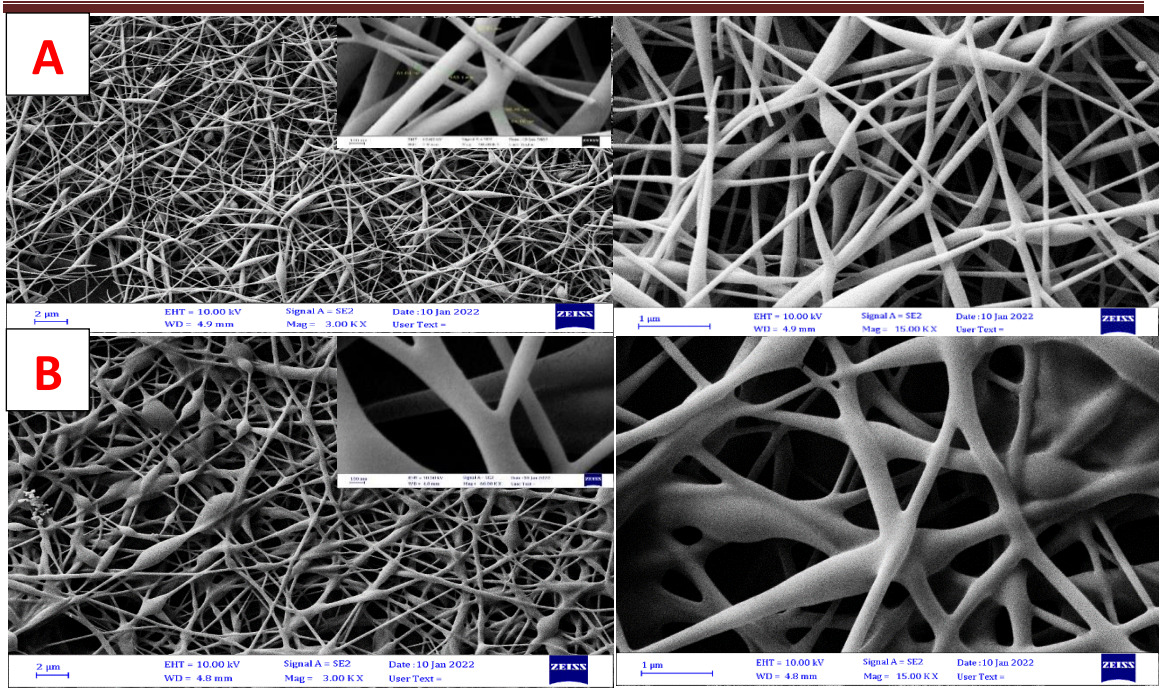

Fig.4.32: FESEM images with 3000 and 15000 magnification powers for (A) neat blend nanofiber (B) blend with 10 wt.% Rosemary oil.

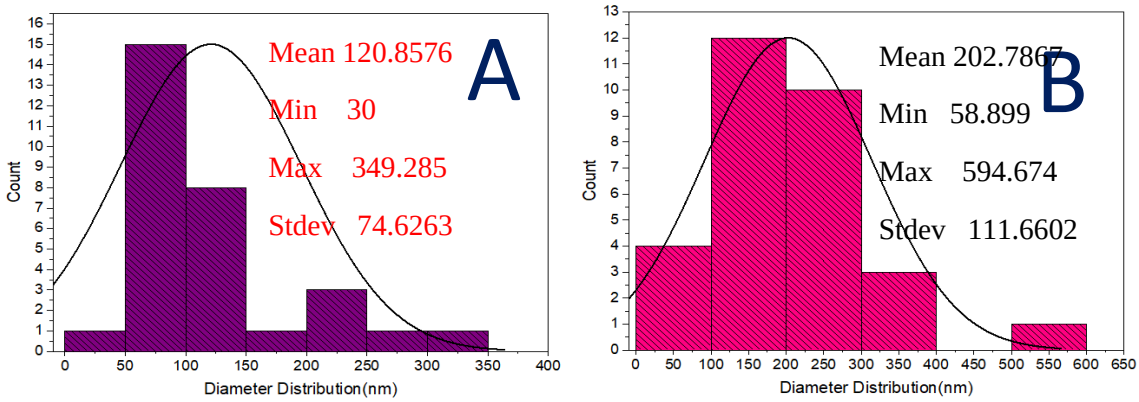

Fig.4.33: Diameter distribution of nanofiber(A) neat blend nanofiber (B) blend with 10 wt.% Rosemary oil.

Due to the oil's stickiness and high concentration, Ocimum basilicum contributes to a bimodal diameter distribution of the nanofibers, as does Rosemary oil. Moreover, cluster formation at the fibers' branching points was observed [19]. The observed branching is likely attributable to the spinning of a highly concentrated solution [189] utilizing a high voltage, in addition to the sticky character of such a solution. Spinning highly concentrated solutions creates a jet with a relatively large diameter, which may result in the development of branches [190]. Because of this, the resulting nanofibrous mat had bigger inter-fiber gaps, which were found to

be more beneficial for cell-related applications like wound healing and tissue engineering [191].

Figures 4.34 and 4.35 show the FESEM images and the resulting fibers' diameter distribution of addition Laurus nobilis oil, respectively. As Laurus nobilis oil content increased, there was an increase in the nano fiber diameter by about 50% (up to 181.2631nm) and its diameter range changed to be 62-271nm Also, there is increment in the number of beads (due to decrease in electrical conductivity) but with small sizes. The textile has high porosity.

Although beadless fibers are usually preferred to improve the uniformity of the electrospun nanofibers, bead-on-string nanofibers, with suitable control of the bead diameter, shape, and surface morphology, have provided efficient encapsulation of biomolecules and controlled release suitable for tissue engineering and wound dressing applications.

In vitro release studies have demonstrated that bead-on-string morphology has resulted in a more sustainable release profile with less initial burst release compared to uniform fibers [27, 28].

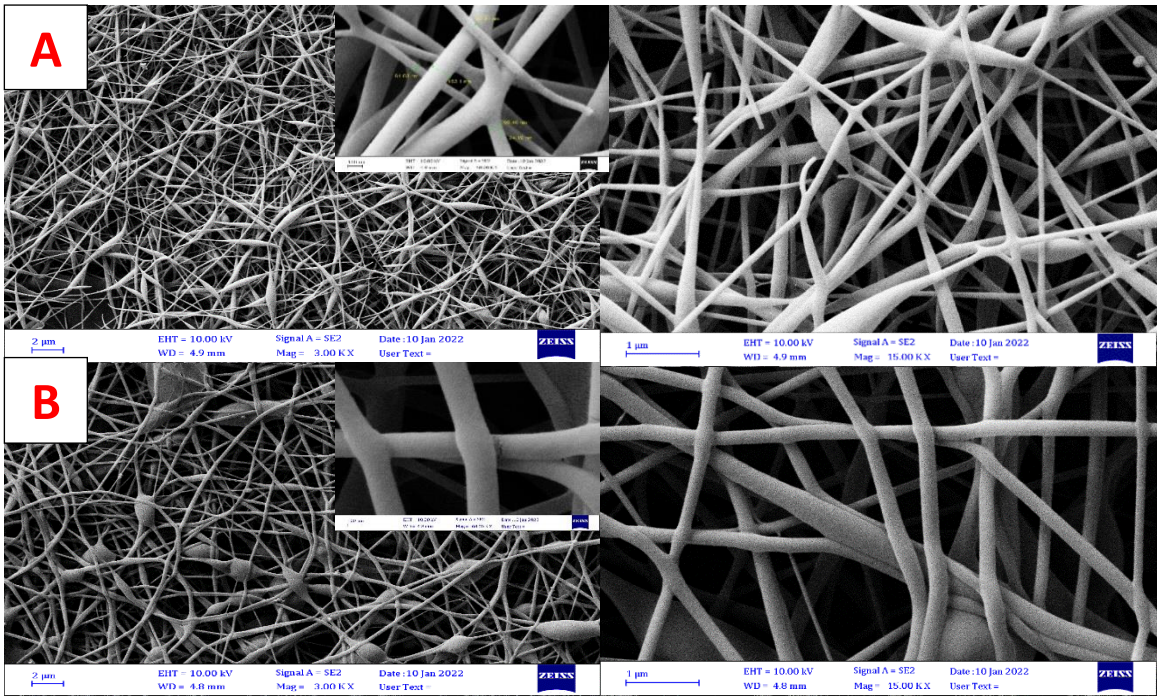

Fig.4.34: FESEM images with 3000 and 15000 magnification powers for (A) neat blend nanofiber (B) blend with 10 wt.% L.nobilis EO.

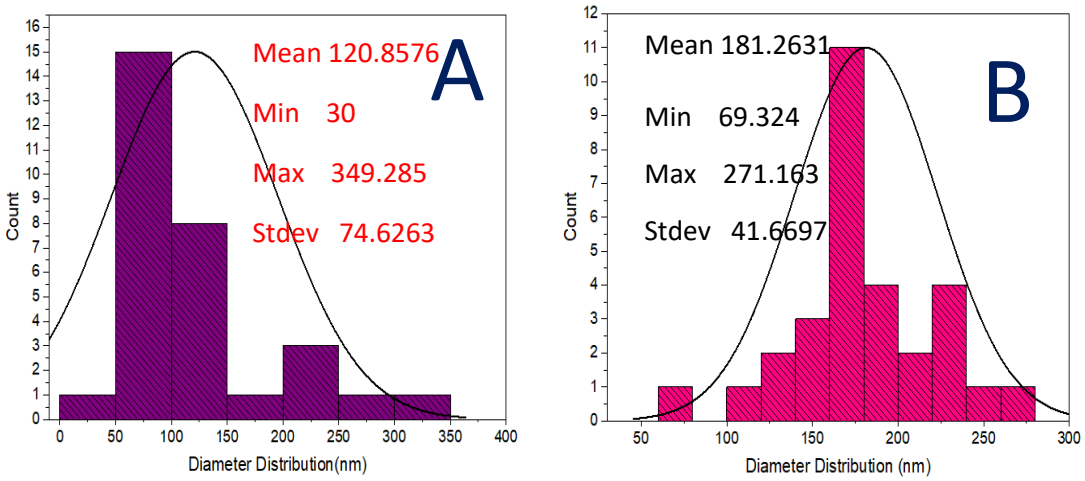

Fig.4.35: Diameter distribution of nanofiber (A) neat blend nanofiber (B) blend with 10 wt.% L.nobilis EO.

Table 4.9: Summery of additions effects on the textile morphology

Addition type	Average diameter (nm)	Diam. Increment (%)	Morphological features		
			Fiber morphology	Beads	Porosity
Without	120.8576	-	Branched fibers	some beads	Medium porosity
5 wt.% G. lucidum	168.4099	39.4	honeycomb, branched, fused fibers	No beads	High porous textile
5 wt.% Capsicum annuum	144.7402	20	Branched fiber	Less number of beads	Medium porosity
0.3 wt.% I_2	147.1937	22	Random fibers	decrease the number of beads	Uneven porosity distribution
10 wt.% Ocimum basilicum oil	213.6887	76.81	Fused & branched fibers	Be larger with addition	High porous textile
10 wt.% Rosemary oil	202.7867	67.78	Branched fibers	increased number of beads	High porous textile

10 wt.% Laurus nobilis oil	181.2631	50	Twisted fibers	increment in the number of beads with small sizes	High porous textile

EDX was then utilized to determine the composition of the charged particles from the SEM image. Figure 4.36 shows the elemental analysis of the textiles containing the above additions. The presence of gold is confirmed by the peak at 2.14 keV in the EDX spectra due to the nanofibers being sputter-coated with Au for conductivity enhancement before FESEM-EDX examination. The presence of the Aluminum peak is not alarming because the meshes are mounted on an aluminum surface.

It is clear that, the chemical compositions changed from one additive to another due to the variations in the compositions of these additives themselves. Generally, and except for Ocimum basilicum oil, the carbon content increased, while the oxygen content decreased.

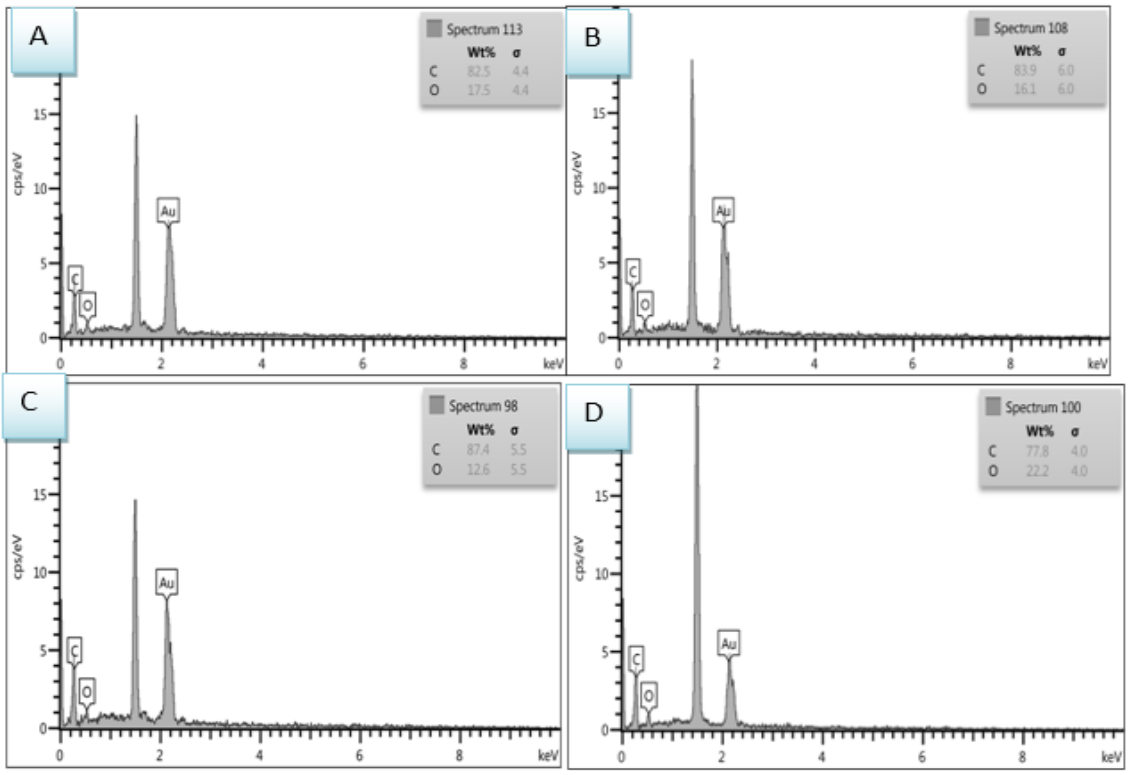

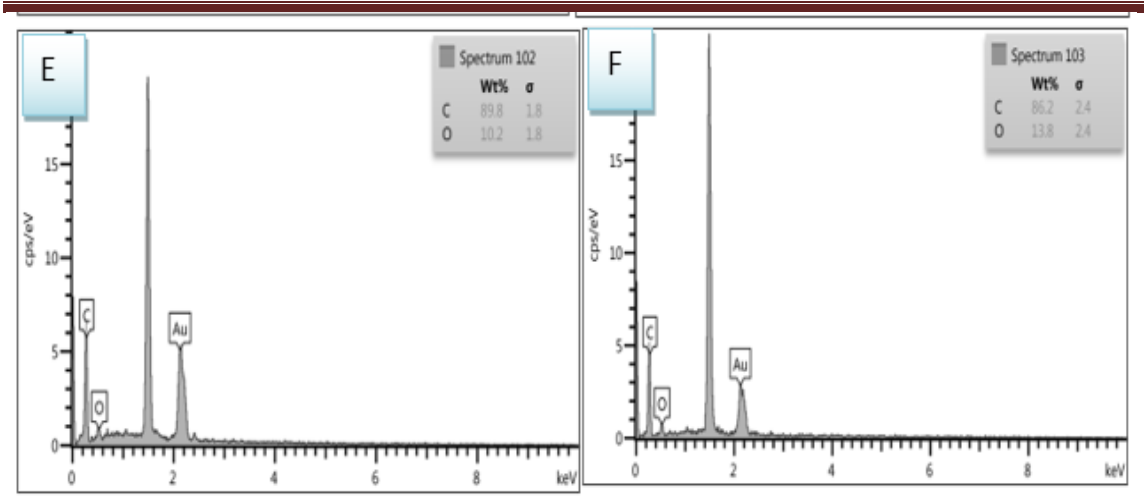

Fig.4.36: EDX analysis for (A) neat blend / G. lucidum (B) neat blend/ Capsicum annuum C) neat blend / I_2 (D) neat blend / Ocimum basilicum oil (E) neat blend / Rosemary oil (F) neat blend / L. nobilis EO.

4.5.3 FESEM and EDX of the final textile

The avearage diameter for the final textile, increased by 118.5% (be 264.0971 nm) and its distribution changed over wider range (59.524-724.725 nm) than any of the individual additive. The resultant morphology is crosslinked, fused nano fibers with some beads and the texile have medium porosity. The chemical composition changed also and the oxygen reached to its minmum content; 9.29%, as shown in figure 4.37.

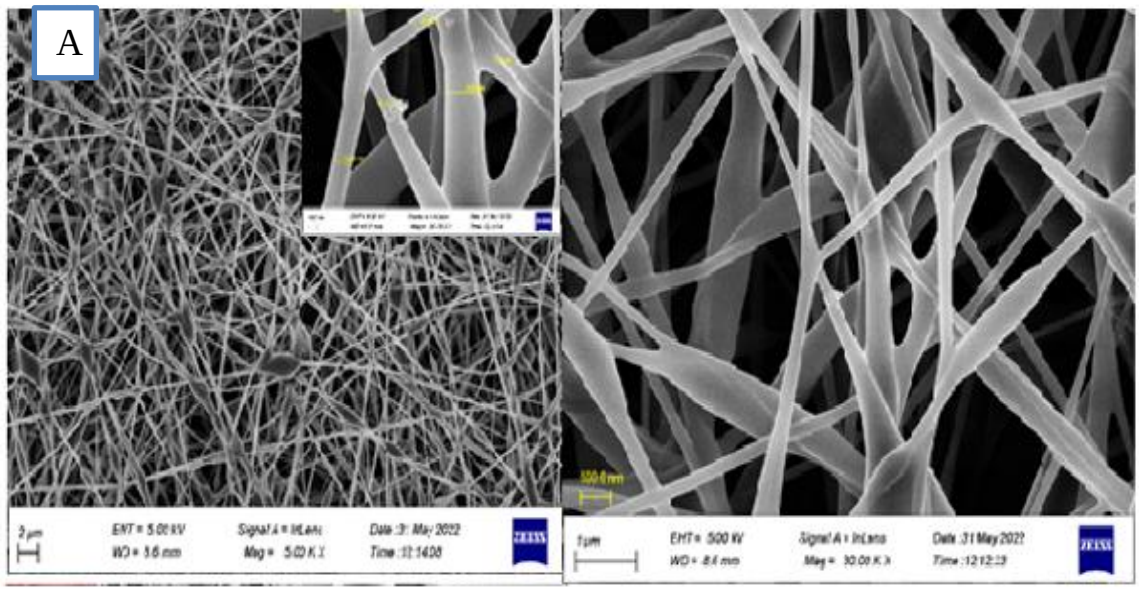

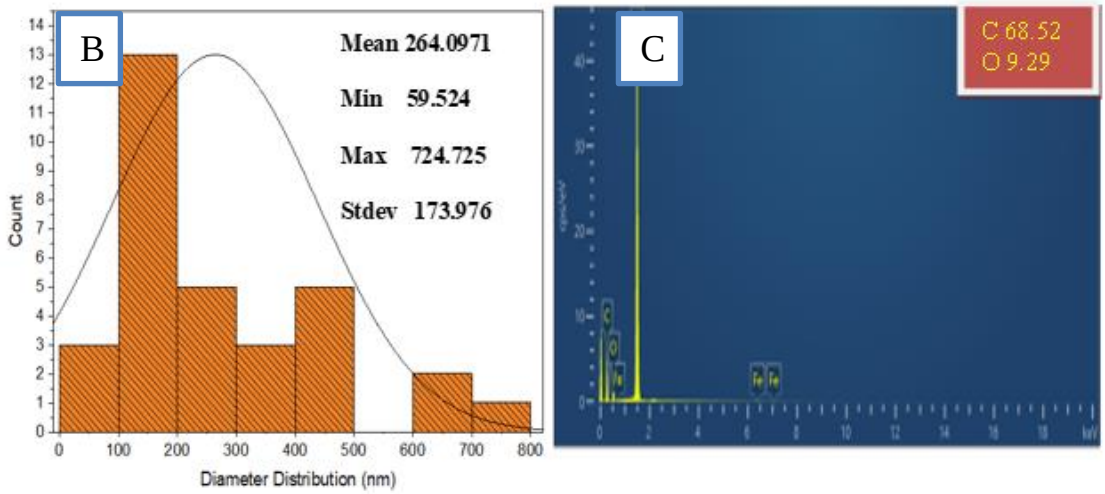

Fig4.37: FESEM images with 3000 and 15000 magnification powers respectively, (b) EDX analysis, (d) diameter distribution for the final nano fiber textile

To improve the performance of the final nano fiber textile, some processing parameters, the following parameters were changed, such as the applied voltage, flow rate, Needle-to-collector distance, and rotation speed (Figures 4.38, 4.39,4.40 and 4.41). Also, the effect of temperature was studied here, where this textile exposed to 70^{o}C for three hours (Figure 4.42).

Changing the applied voltage (figure 4.38) from 20 to 25kV, resulted in changing the diameter range to be from 44.721 to 420.476 nm and the average diameter decreased by about 24% (decreased down to 200.9842 nm).

Since the electrical force stretches the solution jet more as the voltage increases, the fibers' diameter decreases. For applied voltages above 20 KV, however, beads formed along the fibers due to the jet's tendency to hop, shortening the amount of time required to stretch and vaporize the entangled polymer chains in the solution (Ramakrishna et al., 2005). Conversely, when the voltage was decreased, the amount of stretching was reduced, resulting in an increase in fiber diameter. These findings suggest that 20 kV is the ideal voltage for achieving the highest quality nano fibers.

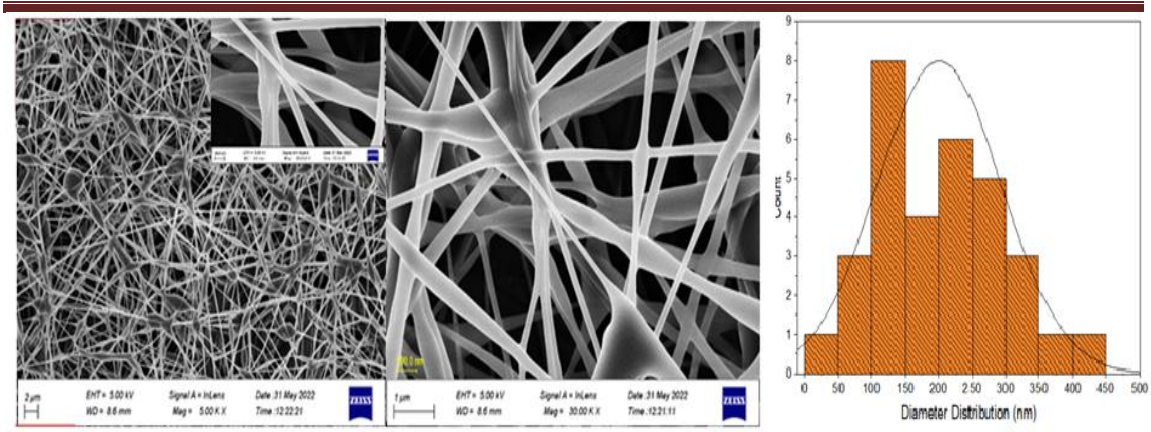

Fig. 4.38: Effects of applied voltage variable

Decreasing the needle-to-collector distance down to 15 cm (Figure 4.39), changed the diameter distribution range to 67.315 - 938.832 nm and the mean diameter increased by 8% (up to 285.463 nm). This was because the distance was short and if there was not enough time for evaporating merge the solvent before deposition of the fibers on the collector, the fibers Merge and the stretching force was increased with the decrease of the diameter and vice versa [194].

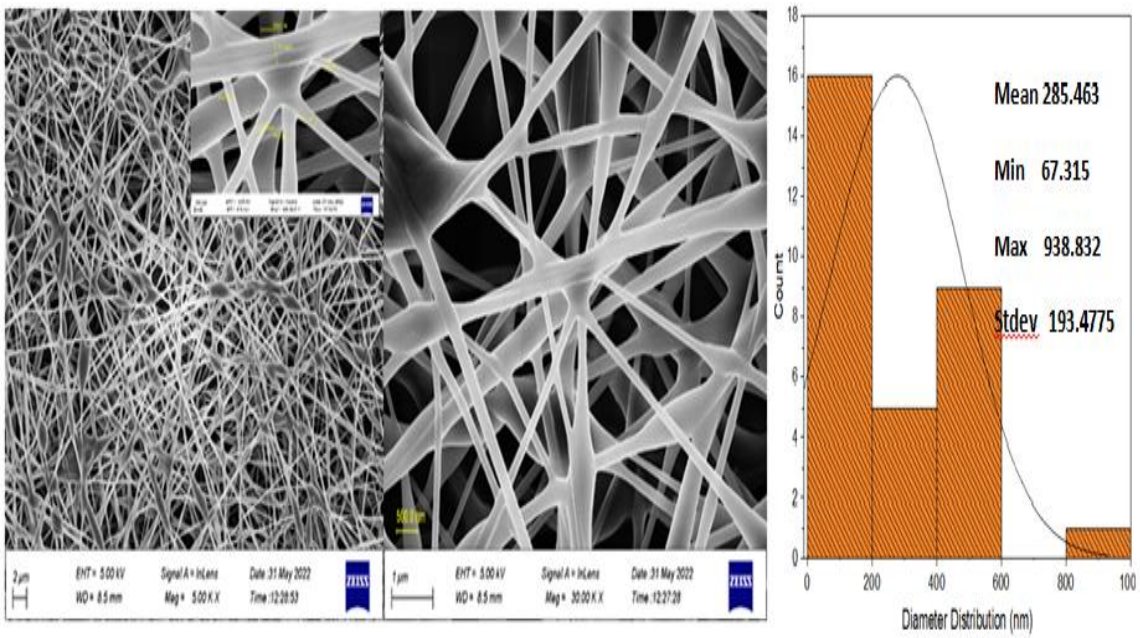

Fig. 4.39: Effect of needle-to-collector distance variable.

Increasing the rotation speed from 600 to 750 rpm, decreases the fiber diameter by 23% (decreased down to 203.3366 nm) and the diameter

distribution varied between 25 and 550.568. The increase in collector rotation resulted in more uniform and thinner fibers, potentially due to the higher stretching level imposed on them [195]. Random and porous textile obtained (Figure 4.40). These random orientations of most fibers can be attributed to repulsion forces during their movement towards the collector and to the atmosphere formed around the cylindrical collector. This causes some movement disturbances and forces the fibers to deviate from their path that is not perpendicular to the collecting axis.

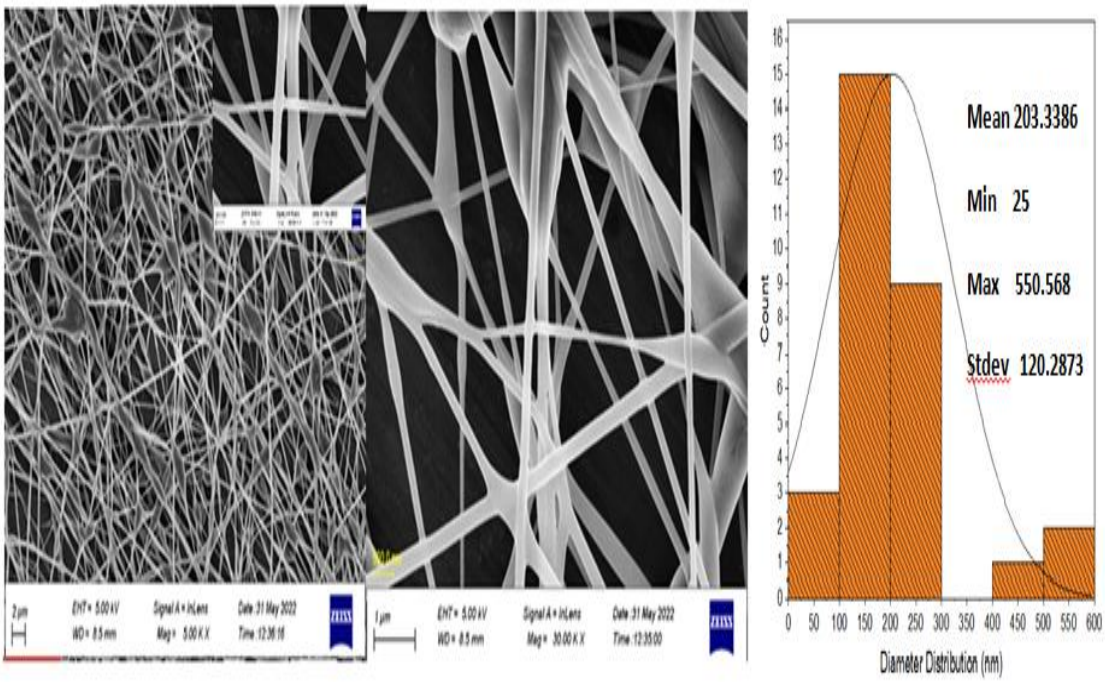

Fig. 4.40: Effect of rotation speed variable

To get the best and most consistent fibers, the electrospinning flow rate was also fine-tuned. In this optimization, only the flow rates of 0.5 and 1 ml/h were modified, while all other process parameters were held constant. An increased flow rate was demonstrated to increase fiber diameter. Using a flow rate of 0.5 ml/h, consistent and smooth nanofibers were formed. Beads began to form as the rate of solution flow increased. Higher flow rates resulted in less-than-perfect elongation of the polymer chain due to an increase in the volume of the droplets at the needle's tip. Further, because of the huge volume of the jet, the solvent is not completely evaporated even

after the flow rate was increased. Which is why the fibers that were collected are still damp [31].

The fiber diameters varied between 51.74 and 545.064 nm and its average decreased by 4.6 %: (be 251.7379 nm) (Figure 4.41). The obtained textile crossliked, branched and thin fibers with very little beads and with medium porosity.

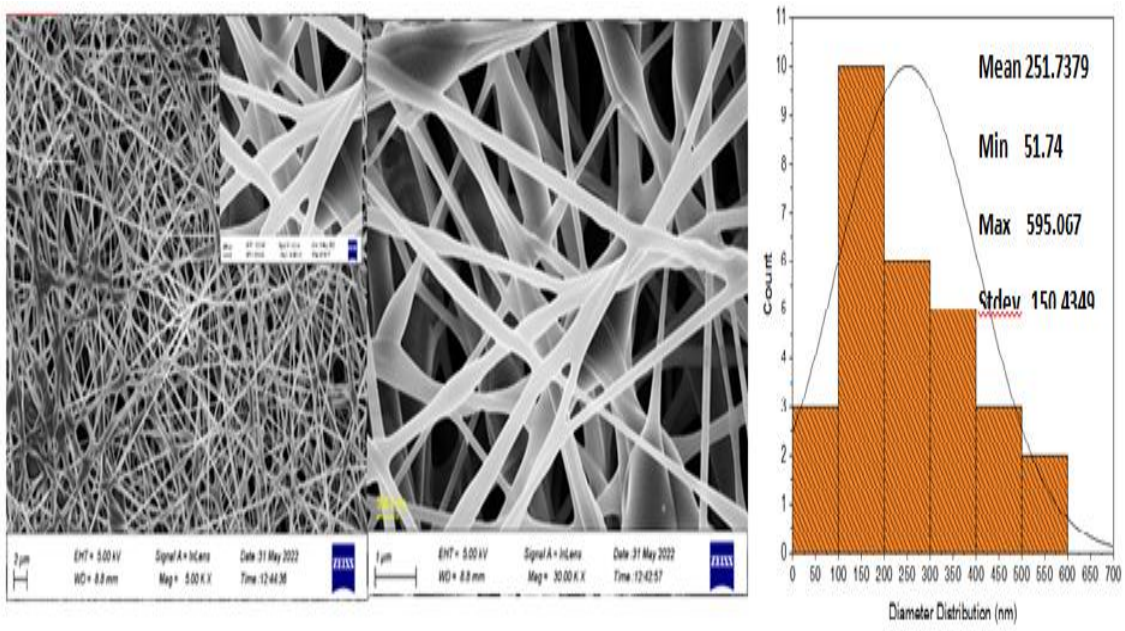

Fig. 4.41: Effect of flow rate variable.

Temperature also affected the fiber morphology, where exposing the textile to 70ºC for three hours, decreases the average diameter by 23% (decreased down to 203.3386 nm) (figure 4.42) and changing the distribution to be from 78.081 to 256.897 nm. The resultant textile is sticky and composed of fused, branched and thick fibers with low porosity. High temperatures melt the thin fibers, which facilitates the fusion action with other fibers. The sticky nature of the textile made it difficult to handle it. The oxygen content increased by 38.85% (from 9.29% to 12.9%), which indicates the oxidation process at high temperatures.

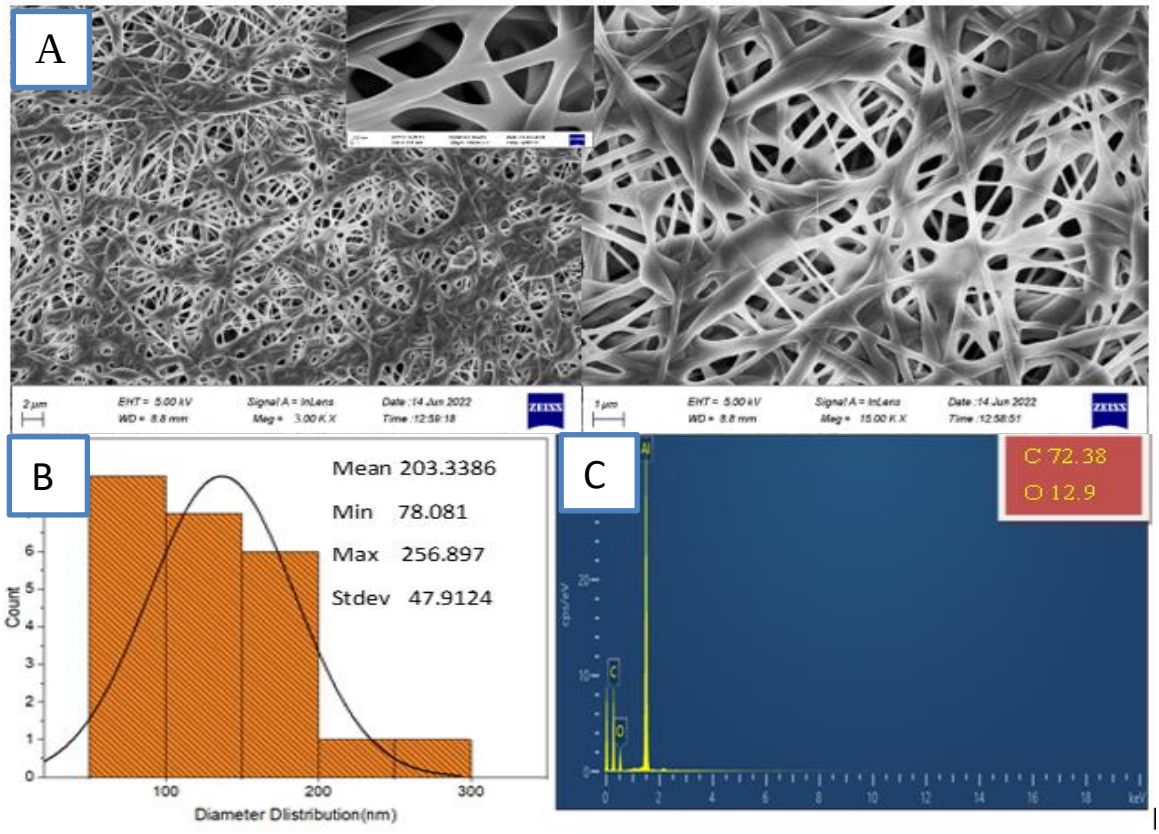

Fig.4.42: A) FESEM images with 3000 and 15000 magnification powers respectively, (b) EDX analysis, (d) diameter distribution for The final sample was exposed to a temperature at 70℃ of three hours

From the wound dressing viewpoint, the expected performance of this wormed textile is affected by the following parameters:

1- Because of its sticky nature, bacterial colonies will accumulate, which reduces the efficiency of the nano fiber textile in resisting bacteria.
2- Its oxidation tendency increases the active sites (oxygen atoms), which can promote hydrogen bonding with the wet environment, which enhances its wettability.
3- The state of melting the fibers and merging them with each other increased their diameters thickness at the expense of the free volumes among these fibers, which reduces their absorption of liquids.

Therefore, their performance as wound dressings will be the result of these contradictory factors.

As overall effects on the average diameter, the following order is occurred:

Applied voltage > Collector speed = Heat > Needle-to-collector distance > Flow rate.

Table 4.10: Summery of parameters effects on the textile morphology

Parameter	Average diameter (nm)	Diam. Increment (%)	Morphological features		
			Fiber morphology	Beads	Porosity
Without	264.0971	-	crosslink & fused fibers	some beads	Medium porosity
voltage	200.9842	24	branched& fused fibers	high beads	High porosity
Needle-to-collector distance	285.463	8	Merge fibers	Less number of beads	Medium porosity
Collector speed	203.3386	23	Random fibers	decrease the number of beads	Medium porosity
Flow rate	251.7379	4.6	crosslinked, branched &thin fibers	very little beads	Medium porosity
Heat	213.6887	23	fused, branched & thick fibers	Without beads	low porosity

4.6 Atomic force microscopy (AFM) results

4.6.1 AFM for blend polymeric

The surface roughness is considered as the key factor for the wettability, where high surface roughness induces hydrophobic surfaces. Surface roughness reduces surface energy and might consequently reduce the wettability of molecular liquids [184].

Figure 4.43 and table 4.11 monitored the surface roughness of the prepared fibers. Generally, the roughness parameters (S_a, S_q, S_y, S_z) of the neat PVA

fibers decreased with HAc or Collagen additives. The effect of collagen was more than HAc and this reduction reached its maximum values when these two fillers (HAc and collagen) were added together to form the tertiary blend. All these roughness parameters decreased by a third of its original values; about 33.3% in the tertiary blend form.

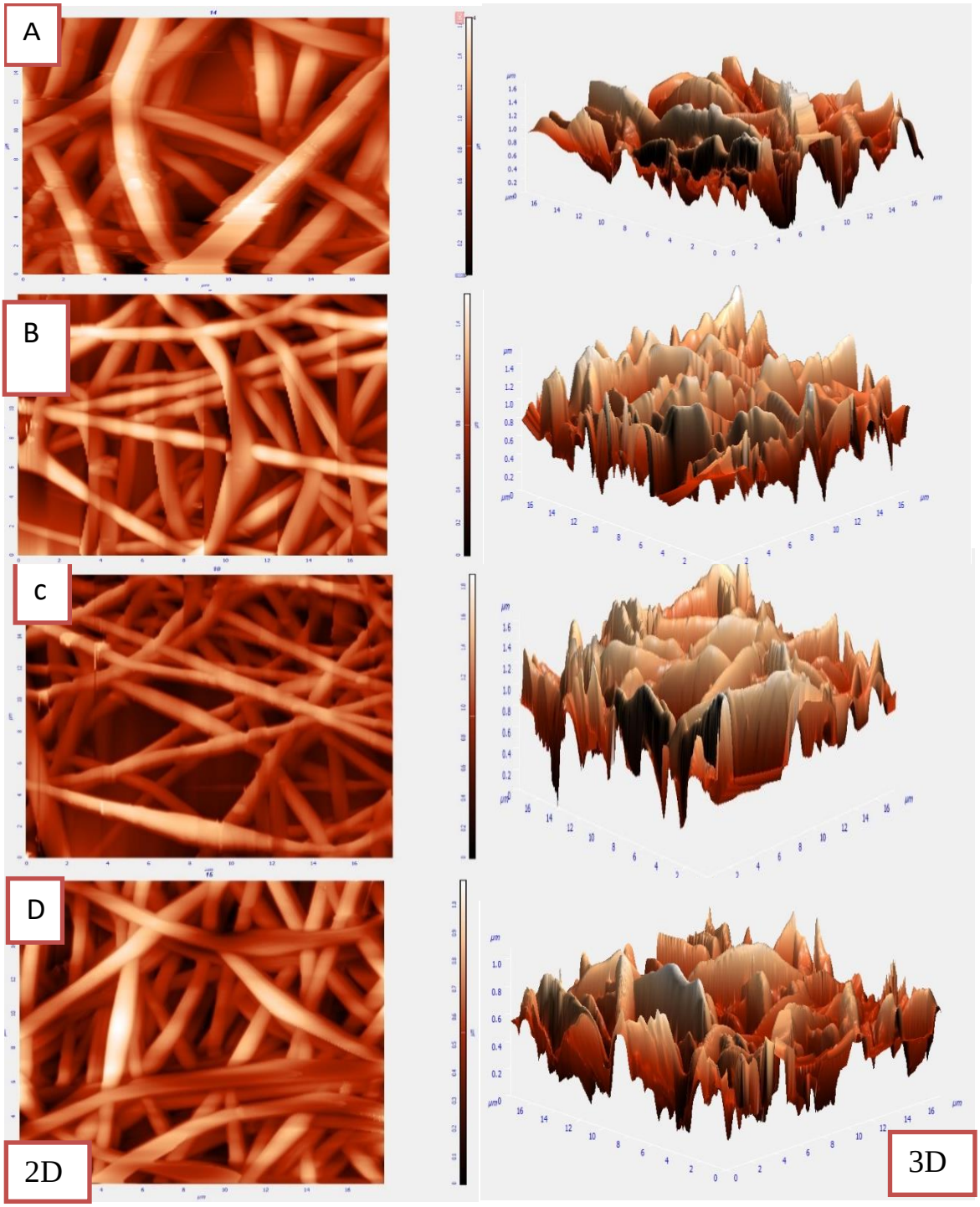

Fig. 4.43: 2D and 3D- micrographs AFM images for nanofibers of (A) PVA (B) PVA:5.5% HAc (C) PVA:7% Coll. (D) PVA: Coll.: HAc.

Table 4.11: Surface roughness of the prepared fibers

Roughness parameter	10% PVA	10 % PVA: 5.5 % HAc	10% PVA: 7% Coll.	10% PVA: 7% Coll.: 5.5% HAc	Property Change (%)
Average Roughness, S_a (nm)	221.29	189.56	147.916	145.019	- 34.46
Root Mean Square, S_q (nm)	277.755	241.401	185.148	183.626	- 33.88
Peak-to-peak, S_y (nm)	1642.49	1921.41	1413.28	1083.48	-.34.00
Ten-point height, S_z (nm)	822.746	948.449	692.158	543.762	- 33.90
Surface skewness, S_{sk}	0.0263149	-0.00271954	0.324149	0.00383049	- 85.44

Values of the average pore size (Figure 4.44) give another indicator on the influence of the additives on the neat PVA textile, where this property decreased from 6.5±0.008 μm^3 to 2.836 ± 0.007 μm^3 with 7% Collagen addition, to 1.159 ± 0.005 μm^3 with 5.5% HAc addition and down to 1.482 ± 0.006 μm^3 when both additions were combined. These findings proved that additions occupy the voids among PVA molecules or entangled with it.

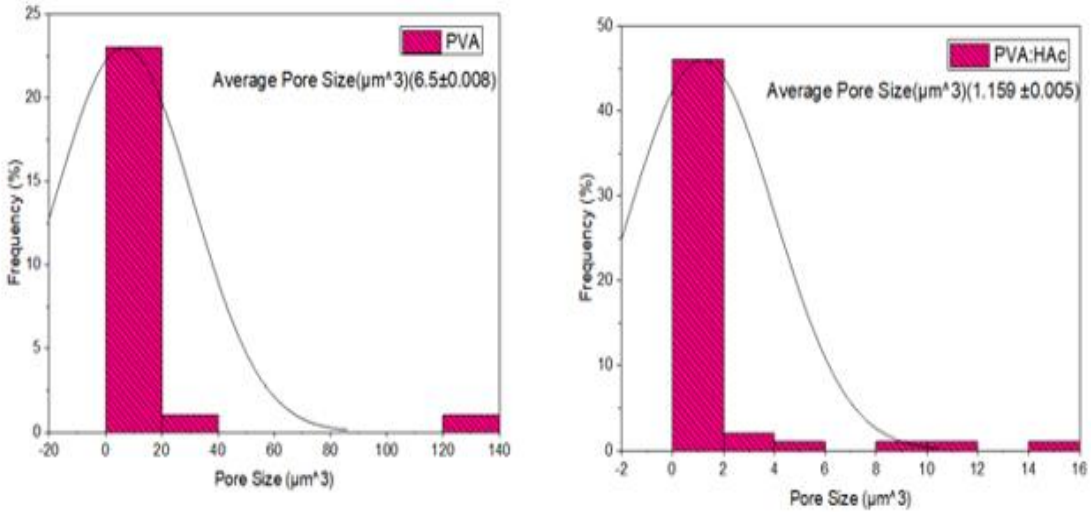

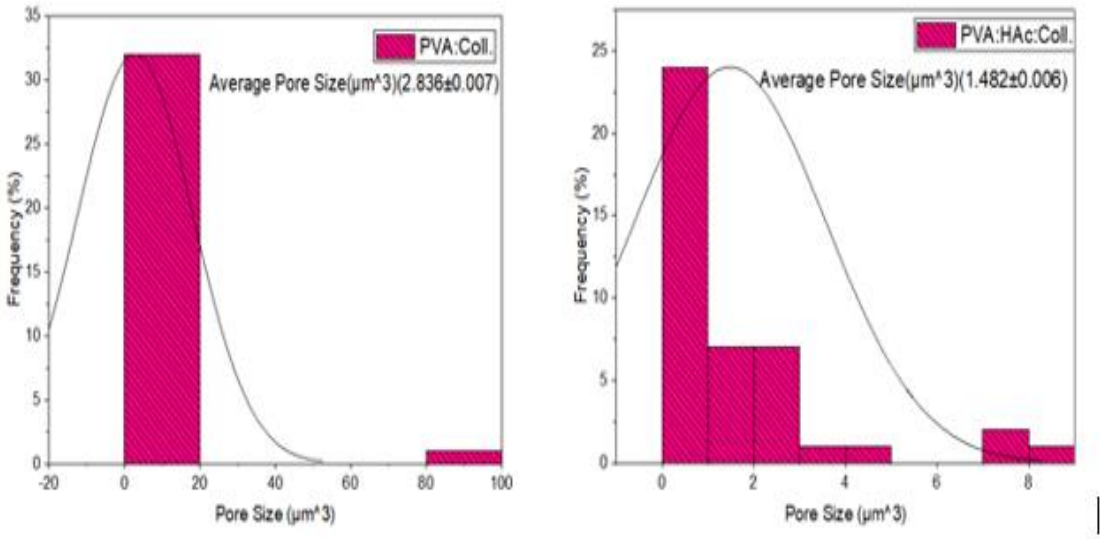

Fig.4.44: The average pore size of PVA and optimum textiles

4.6.2 AFM of blend with antibacterial & antioxidation

Surface properties play a key role in how biomaterials interact with the environment [196]**.** Cell adhesion to the tissue surface depends on its chemical properties such as material composition and hydrophilicity, and physical parameters such as porosity and roughness. The roughness of the tissue' surface also influences cell proliferation. Some investigators have related this to the influence of surface roughness and wettability. However, it should be noted that although the surface roughness of fibers enhanced the cell attachment and proliferation [197]**.** AFM result is clear from table 4.12 and figure 4.45, that iodine additions increased all the roughness parameters of the neat blend.

Table 4.12: Effects of iodine additions on the roughness parameters

Roughness parameter	Neat blend	Blend with 0.1 wt.% I_2	Blend with 0.2 wt.% I_2	Blend with 0.3 wt.% I_2	Property Change* (%)
Average Roughness, S_a (nm)	145.019	218.333	276.835	262.735	+ 81
Root Mean Square, S_q (nm)	183.626	265.304	327.51	317.513	+72

Peak-to-peak, S_y (nm)	1083.48	1155.07	1308.04	1366.26	+26
Ten-point height, S_z (nm)	543.762	573.198	653.554	683.061	+26

- Determined between the final wt.% of addition and the neat blend

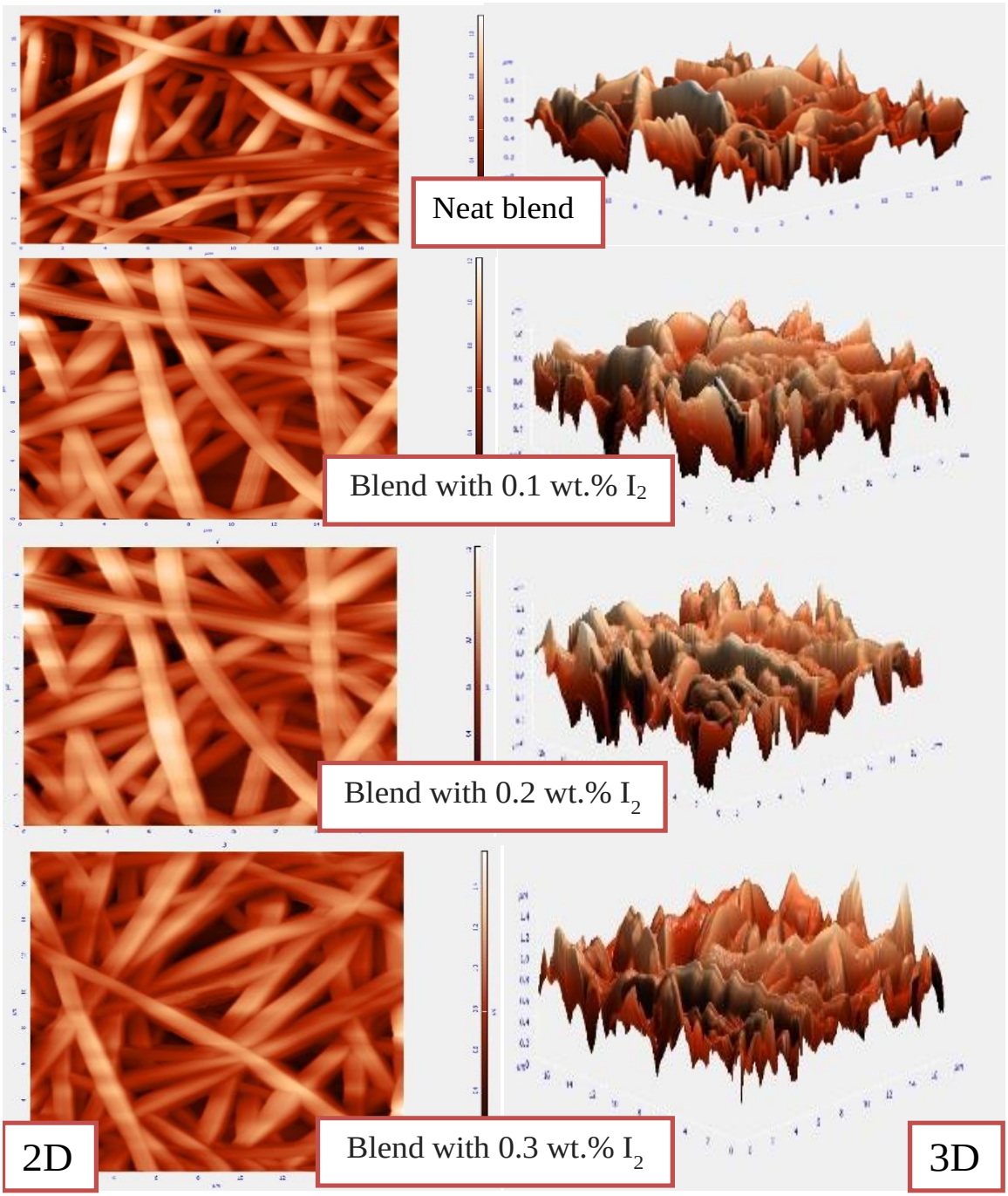

Fig.4.45: 2D and 3D- micrographs AFM images for neat blend nanofiber and iodine additions.

In contrast, Ocimum basil oil additions (Figure 4.46 and table 4.13), This addition increased all parameters means that rough fibers do adhere bacteria.

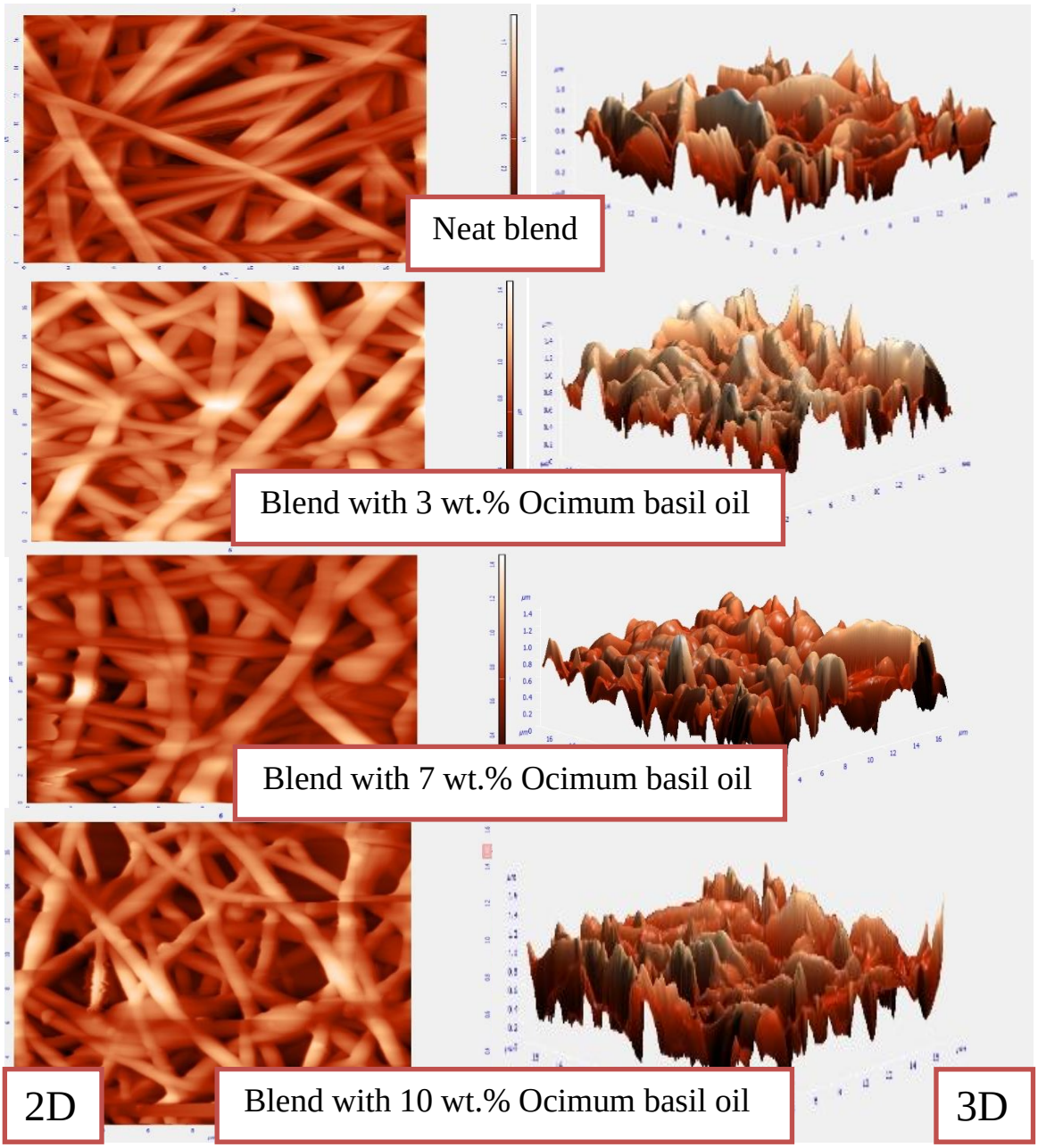

Fig.4.46: 2D and 3D- micrographs AFM images for neat blend nanofiber and Ocimum basil oil additions.

Table 4.13: Effects of Ocimum basil oil additions on the roughness parameters.

Roughness parameter	Neat blend	Blend with 3 wt.% Ocimum basil oil	Blend with 7 wt.% Ocimum basil oil	Blend with 10 wt.% Ocimum basil oil	Property Change* (%)
Average Roughness, S_a (nm)	145.019	230.627	236.334	207.836	+43.31639
Root Mean Square, S_q (nm)	183.626	285.115	286.208	255.489	+39.14
Peak-to-peak, S_y (nm)	1083.48	1366.43	1112.08	1320.53	+21.878
Ten-point height, S_z (nm)	543.762	683.202	555.336	957.359	+76.06

- Determined between the final wt.% of addition and the neat blend.

Also, Rosemary oil addition led to increase parameters, as shown in figure 4.47 and table 4.14.

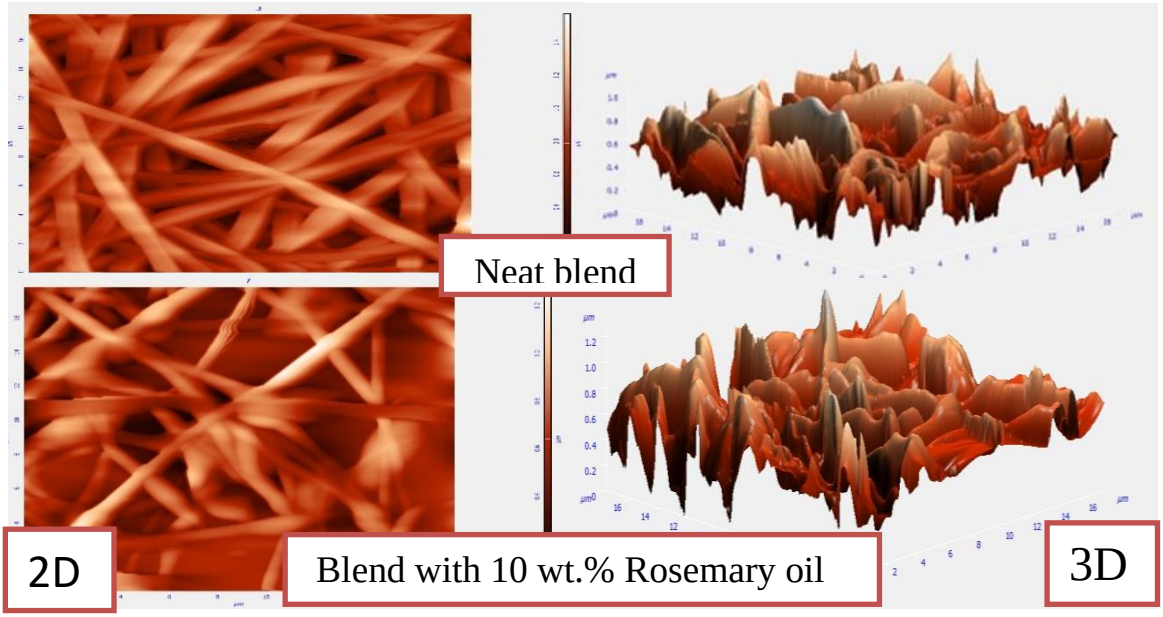

Fig.4.47: 2D and 3D- micrographs AFM images for neat blend nanofiber and Rosemary oil additions.

Table 4.14: Effects of Rosemary oil additions on the roughness parameters.

Roughness parameter	Neat blend	Neat blend with Rosemary oil	Property Change (%)*
Average Roughness, S_a (nm)	145.019	180.913	+ 24.75
Root Mean Square, S_q (nm)	183.626	228.319	+24.33
Peak-to-peak, S_y (nm)	1083.48	1886.34	+74.1
Ten-point height, S_z (nm)	543.762	882.95	+62.378

- Determined between the final wt% of addition and the neat blend

Addition L.nobilis EO led to increase all parameters, as shown in figure 4.48 and table 4.15.

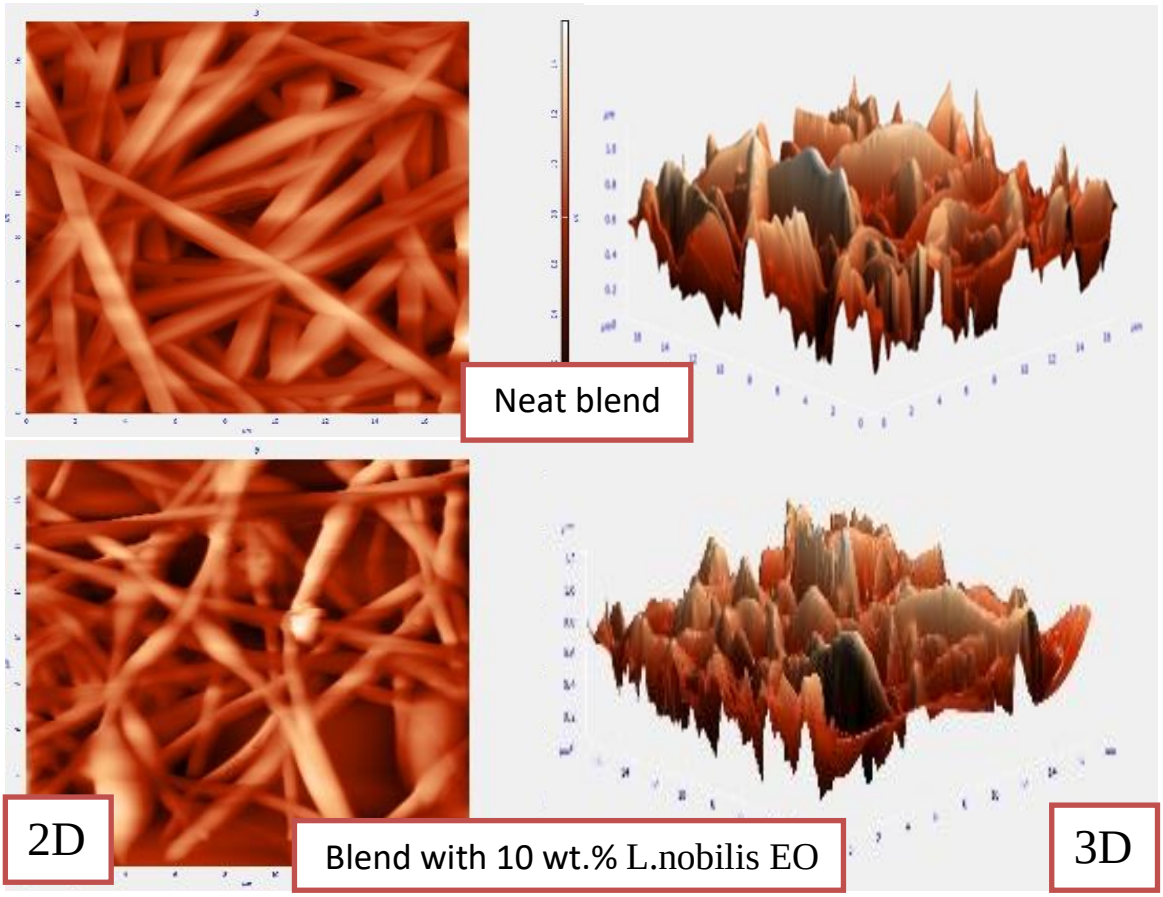

Fig.4.48: 2D and 3D- micrographs AFM images for neat blend nanofiber and L.nobilis EO addition.

Table 4.15: Effects of L.nobilis EO additions on the roughness parameters.

Roughness parameter	Neat blend	Neat blend with 10 wt.% L.nobilis EO	Property Change (%)*
Average Roughness, S_a (nm)	145.019	178.143	+22.8
Root Mean Square, S_q (nm)	183.626	229.834	+25
Peak-to-peak, S_y (nm)	1083.48	1737.98	+60
Ten-point height, S_z (nm)	543.762	850.115	+56

- Determined between the final wt% of addition and the neat blend.

This addition decreased some parameters as shown in figure 4.49 and table 4.16.

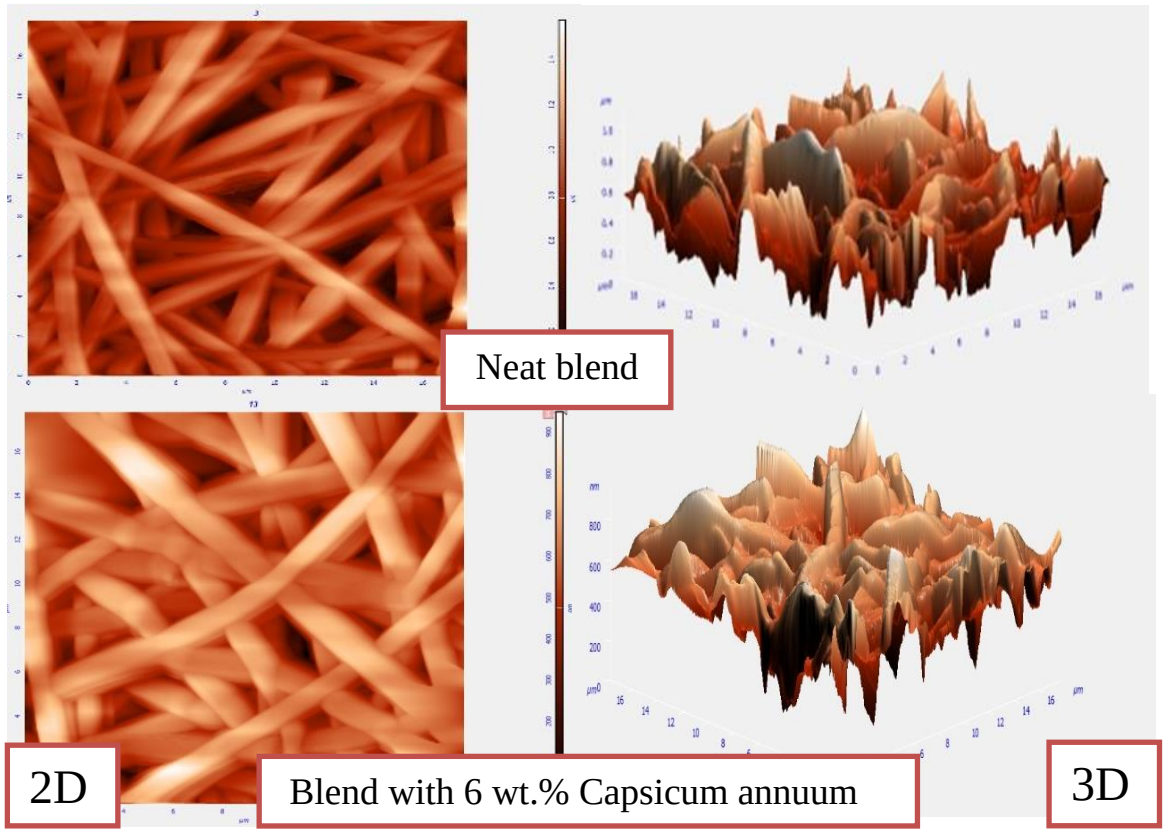

Fig.4.49: 2D and 3D- micrographs AFM images for neat blend nanofiber and Capsicum annuum addition.

Table 4.16: Effects of Capsicum annuum additions on the roughness parameters.

Roughness parameter	Neat blend	blend with Capsicum annuum	Property Change (%)*
Average Roughness, S_a (nm)	145.019	210.144	+44.9
Root Mean Square, S_q (nm)	183.626	268.606	+46.28
Peak-to-peak, S_y (nm)	1083.48	1686.81	+55.68
Ten-point height, S_z (nm)	543.762	798.207	+46.79

- Determined between the final wt% of addition and the neat blend.

The 2D and 3D AFM images (figure 4.50) gave additional evidence about the increase of porosity and fiber diameter upon G. lucidum addition. This addition, also, increased the surface roughness of the layer of the electrospun fibers as evidenced by all the roughness parameters in table 4.17. For example, the average roughness increased by 63.7%, the root mean square by 57%, and so on.

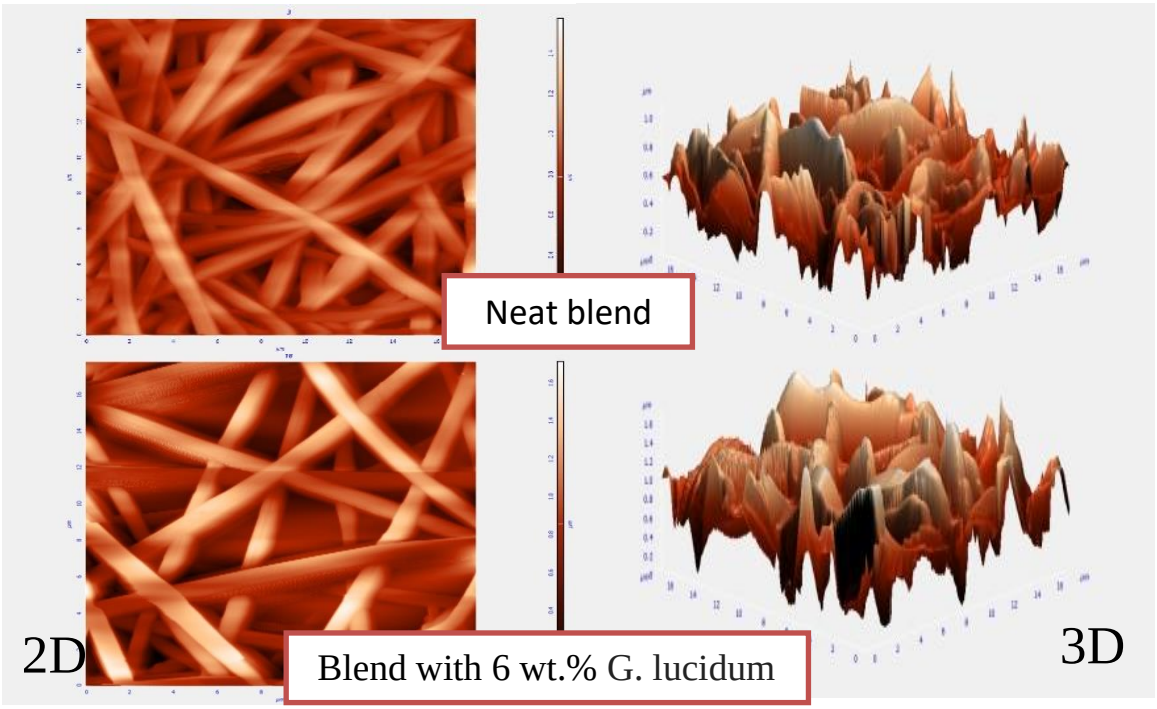

Fig.4.50: 2D and 3D- micrographs AFM images for neat blend nanofiber and G. lucidum addition

Table 4.17: Effects of G. lucidum additions on the roughness parameters.

Roughness parameter	Neat blend	Blend with 6 wt.% G. lucidum	Property Change (%)*
Average Roughness, S_a (nm)	145.019	237.391	+ 63.7
Root Mean Square, S_q (nm)	183.626	288.307	+ 57
Peak-to-peak, S_y (nm)	1083.48	1705.61	+ 57.4
Ten-point height, S_z (nm)	543.762	850.484	+ 56.4

- Determined between the final wt.% of addition and the neat blend.

The final nano fiber textile as shown in figure 4.51 and table 4.18 showed increase in parameters. The increase in the roughness due to the increase in the diameter of the fibers, which is in agreement with this present study (Bianco et al. 2009) [198] and this is consistent with the examination of FESEM which means that these rough textiles resist the bacterial collection. Roughness is known and here confirmed that fiber diameter dictates other surface properties, as the pore size and the surface roughness increase with increasing constituting fiber diameter [199]. A rougher surface is important as it can control the adhesion of osteoblast cells [200].

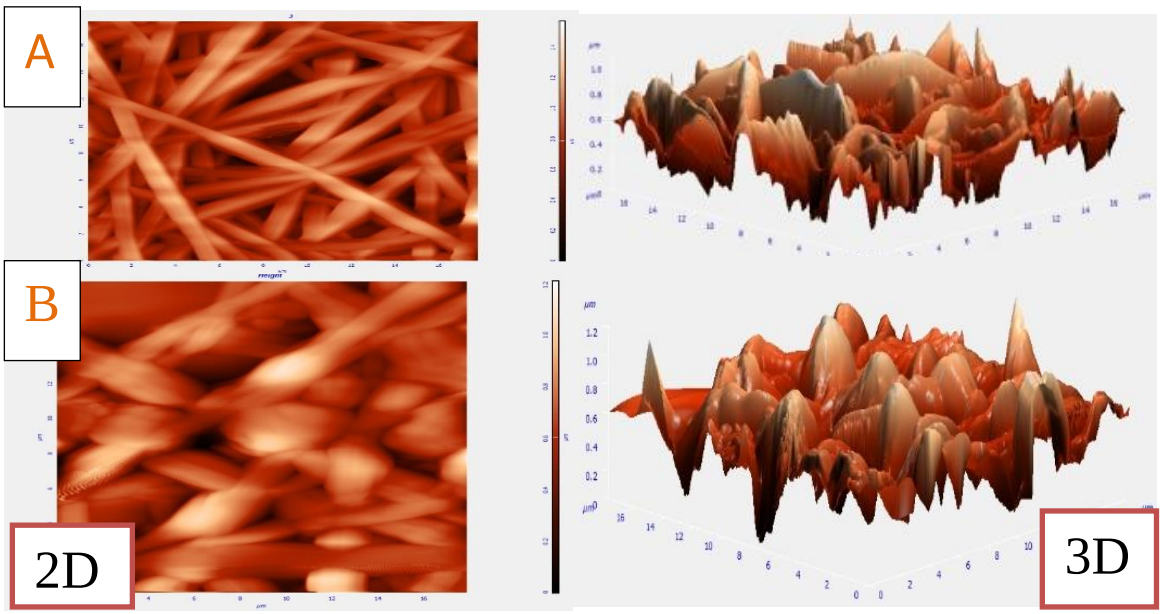

Fig.4.51: 2D and 3D- micrographs AFM images for (A) neat blend nanofiber (B) Final textile

Table 4.18: Roughness parameters for (A) neat blend nanofiber (B) final textile

Roughness parameter	Neat blend	Final nanofiber	Property Change (%)*
Average Roughness, S_a (nm)	145.019	232.529	+ 60
Root Mean Square, S_q (nm)	183.626	288.516	+57.121
Peak-to-peak, S_y (nm)	1083.48	1366.22	+26.09
Ten-point height, S_z (nm)	543.762	683.094	+25.6

- Determined between the final wt% of addition and the neat blend

Values of the average pore size (Figure 4.52) give another indicator on the influence of the additives on the final textile, where this property increase from 1.482 ± 0.006 μm^3 with (PVA: 7%Coll.: 5.5% HAc) figure (4.13) to 1.709 ± 0.008 μm^3 with 6% G. lucidum addition, to 5 ± 0.006 μm^3 with 6% Capsicum addition, 1.9 ± 0.009μm^3 with 0.3 % I_2, 1.71 ± 0.009 μm^3 with 10% Ocimum basil oil, 1.677± 0.009 μm^3 with 10 % L.nobilis EO addition, 2.844 ± 0.009 μm^3 with 10% Rosemary oil addition. In the case of the final textile (figure 4.53) that contains all the above-mentioned additives, we notice an increase in the average pore size to 2.531± 0.008 µm

The Surface porosity of fibers and increased hydrophilicity (verified by lowered contact angle values and improved wettability), due to the drug release together with the improved intrusion of an aqueous medium into the scaffold structure, improved the attachment of cells on the scaffolds [201].

Besides, the porous, nanofibrous membranes electrospun from biopolymers create favorable properties as wound dressings due to their high porosity and high surface area to volume ratio, inhibition of exogenous microorganism invasion due to their ultra-fine pores, excellent air permeability, controlled evaporative water loss and promotion of fluid drainage. Therefore most of the recent studies on wound dressing are focused on electrospinning and evaluating of biopolymers as wound healing dresses, among which we can refer to numerous studies on collagen which is a very suitable biopolymer for skin tissue regeneration [209, 210].

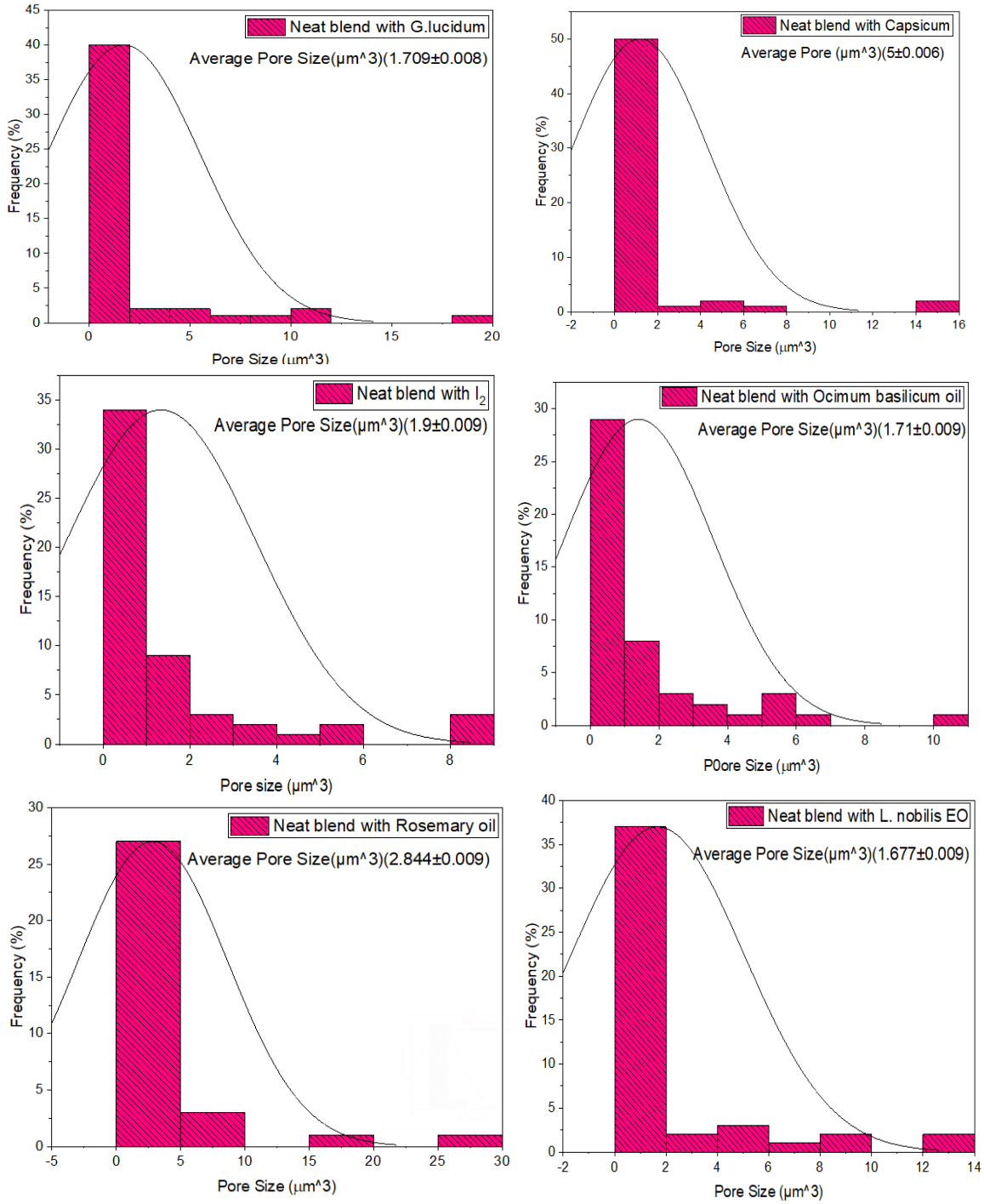

Fig.4.52: The average pore size of neat blend with additions.

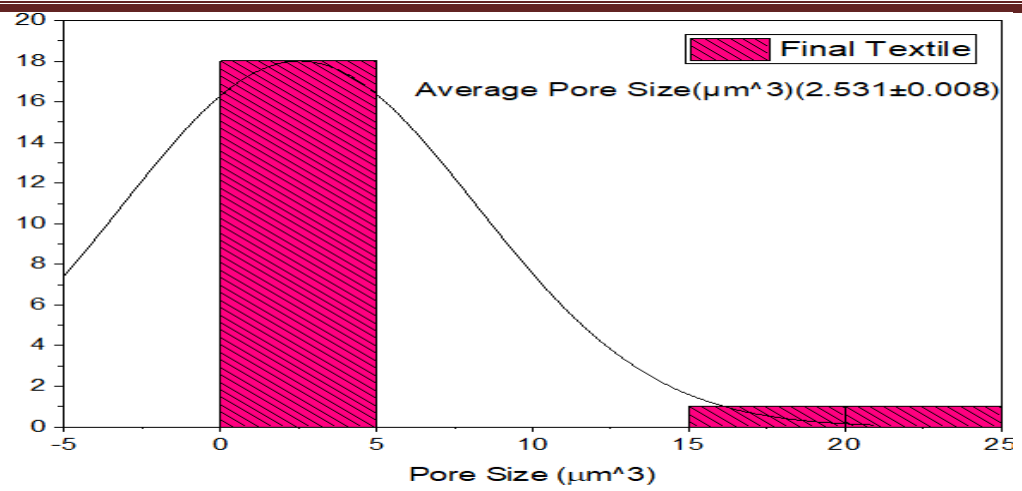

Fig.4.53: The average pore size of Final Textile.

4.7 Texture directionality

4.7.1 Directionality of blend polymeric

Orientation of the prepared nano fibers was measured by using the Fiji software (Gaussian method) based on the FESEM images. This technique is used to infer the preferred orientation of structures present in the input image. It computes a histogram indicating the amount of structures in a given direction.

The histogram consists of 90 bins and covered 180^{o} (for example, from -90^{o} to + 90^{o}). Images with completely isotropic content are expected to give a flat histogram, whereas images in which there is a preferred orientation are expected to give a histogram with a peak at that orientation. On top of the histogram, the plugin tries to generate statistics on the highest peak found.

The 'Direction (°)' column reports the center of the gaussian, while the 'Dispersion (°)' column reports the standard deviation of the gaussian. The 'Goodness' column reports the goodness of the fit; 1 is good, 0 is bad. The 'Amount' value as calculated here underestimates the real proportion of structures with the preferred orientation.

The plugin offers the possibility to generate an orientation map, where the image is colored according to its local directionality, or location orientation.

Orientation results showed in figure 4.54 and summarized in table 4.19.

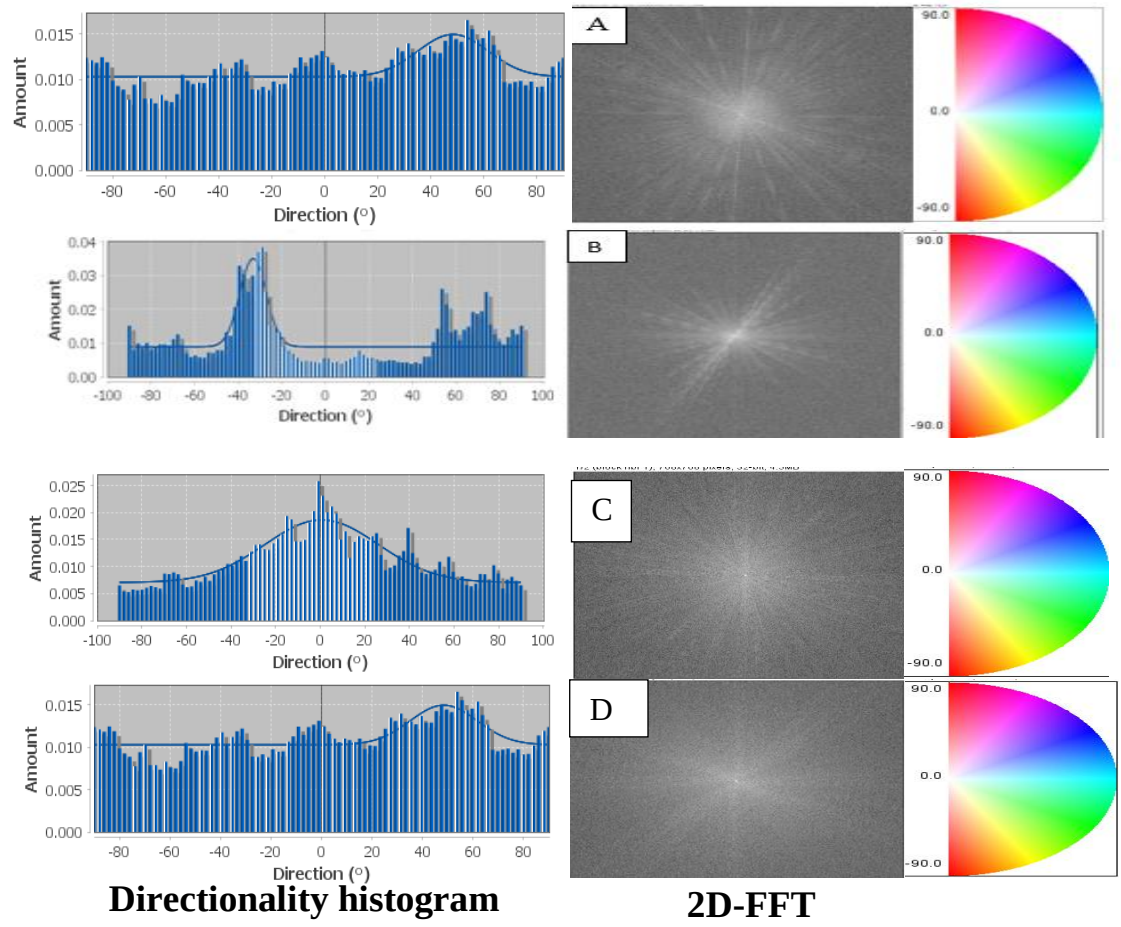

Fig 4.54: Directionality Histogram, and 2D-FFT For nano fibers of (A) Pure PVA, (B) PVA+7% Collagen, (C) PVA+5.5% HAc, and (D) PVA+7% Coll. +5.5% HAc.

Table 4.19: Directionality analysis for the prepared nano fiber textiles.

Sample of nano fibers	Direction (˚)	Dispersion (°)	Amount	Goodness
10% PVA	-23.93	15.84	0.41	0.23
10%PVA + 7% Coll.	-33.26	6.06	0. 29	0.57
10%PVA + 5.5% HAc	0.63	25.46	0.70	0.81
10%PVA + 7% Coll.+ 5.5% HAc	48.36	0.34	0.34	0.49

It is clear that in all the obtained textures, the nano fibers are located on the collector without a preferred direction (announced variations in the directionality histograms), except the sample contains 5.5 wt% HAc. About

41% of neat PVA fibers were located on the collector with the preferred -23.93º direction, and when 7% Coll. was added the number of directed fibers decreased to 29% (on -33.26º preferred direction). With HAc, more than two-thirds (70 %) of the fibers aligned in one direction (0.63º). Thus, this sample has a high dispersion value (25.46) and high goodness (81%). These behaviors reflected the effects of additives (HAc or Coll.) properties on the collecting fibers step. When the two additions were combined, one-third (0.34) of the fibers were in the new preferred direction (48.36º).

4.7.2 Directionality of blend with antibacterial & antioxidation

Orientation parameters of the obtained nano fibers was extracted from FESEM images by using the Fiji software. Effects of Iodine additions on the directionality is shown in figure 4.55 and table 4.20 where the neat blend give histogram with peak, which reflects its anisotropic properties. In contrast, 0.1 wt.% Iodine converts the properties to be isotropic (flat histogram), while with other additions, the properties became anisotropic again.

Images with completely isotropic content are expected to give a flat histogram, whereas images in which there is a preferred orientation are expected to give a histogram with a peak at that orientation.

Table 4.20: Directionality analysis for iodine additions.

Samples of Nanofibers	Direction (˚)	Dispersion (°)	Amount	Goodness
Neat blend	48.36	13.29	0.34	0.49
0.1 wt.% I_2	61.97	4.89	0.13	0.24
0.2 wt.% I_2	13.88	13.13	0.43	0.64
0.3 wt.% I_2	16.94	52.32	0.98	0.34

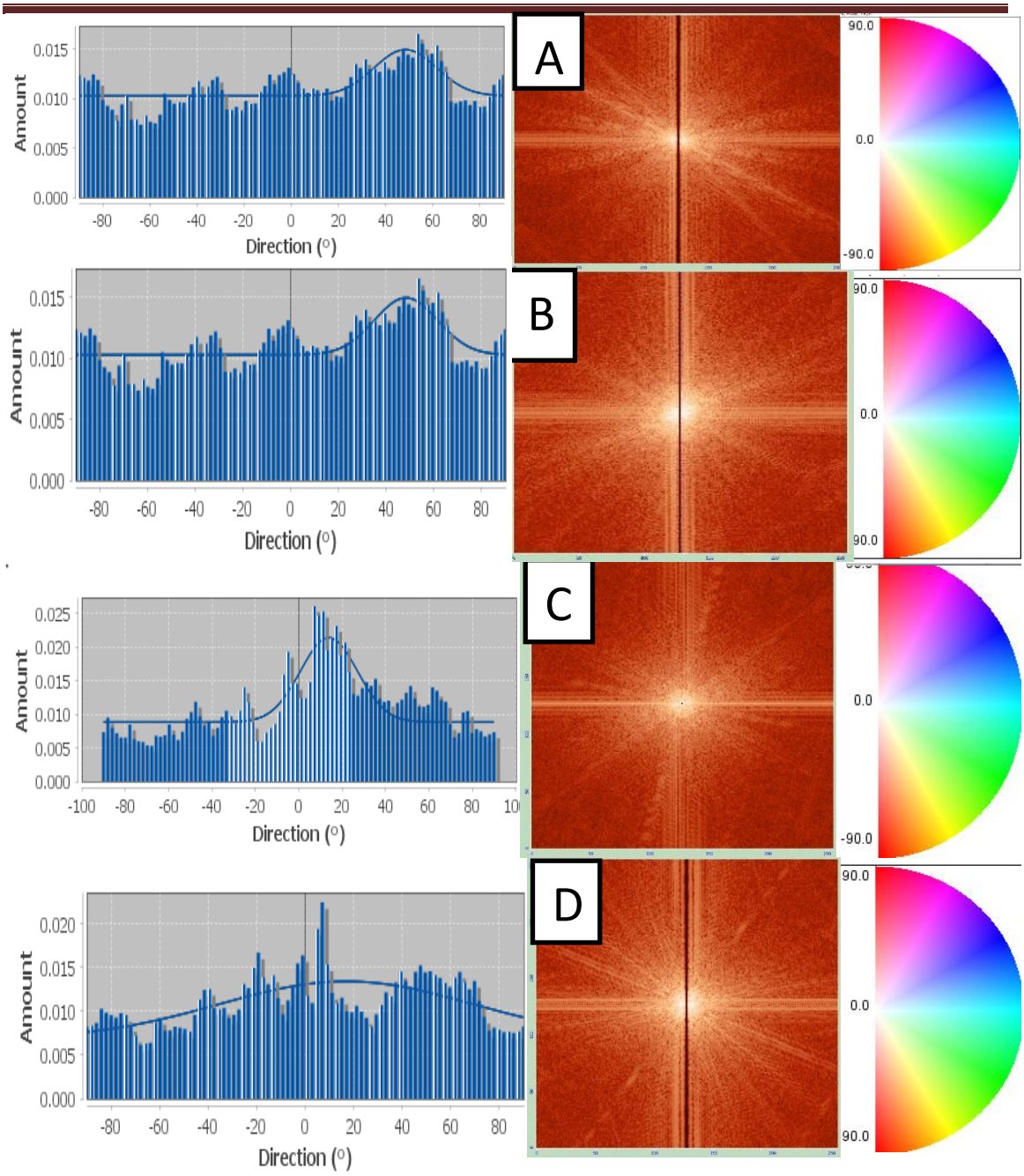

Fig 4.55: Directionality Histogram and 2D-FFT For (A) neat blend nano fiber (B) blend with 0.1 wt.% I_2 (C) blend with 0.2 wt.% I_2 (D) blend with 0.3 wt.% I_2.

Ocimum basil oil addition increased the directionality of the nano fibers from 0.49 up to 0.93 (as shown in figure 5.56 and table 4.21), which means that the properties are anisotropic.

Table 4.21: Directionality analysis for Ocimum basil oil additions.

Samples of Nanofibers	Direction (˚)	Dispersion (°)	Amount	Goodness
Neat blend	48.36	13.29	0.34	0.49
3 wt.% Ocimum basil oil	187.82	101.19	0.65	0.37
7 wt.% Ocimum basil oil	26.69	36.74	0.80	0.48
10 wt.% Ocimum basil oil	15.69	46.60	0.93	0.30

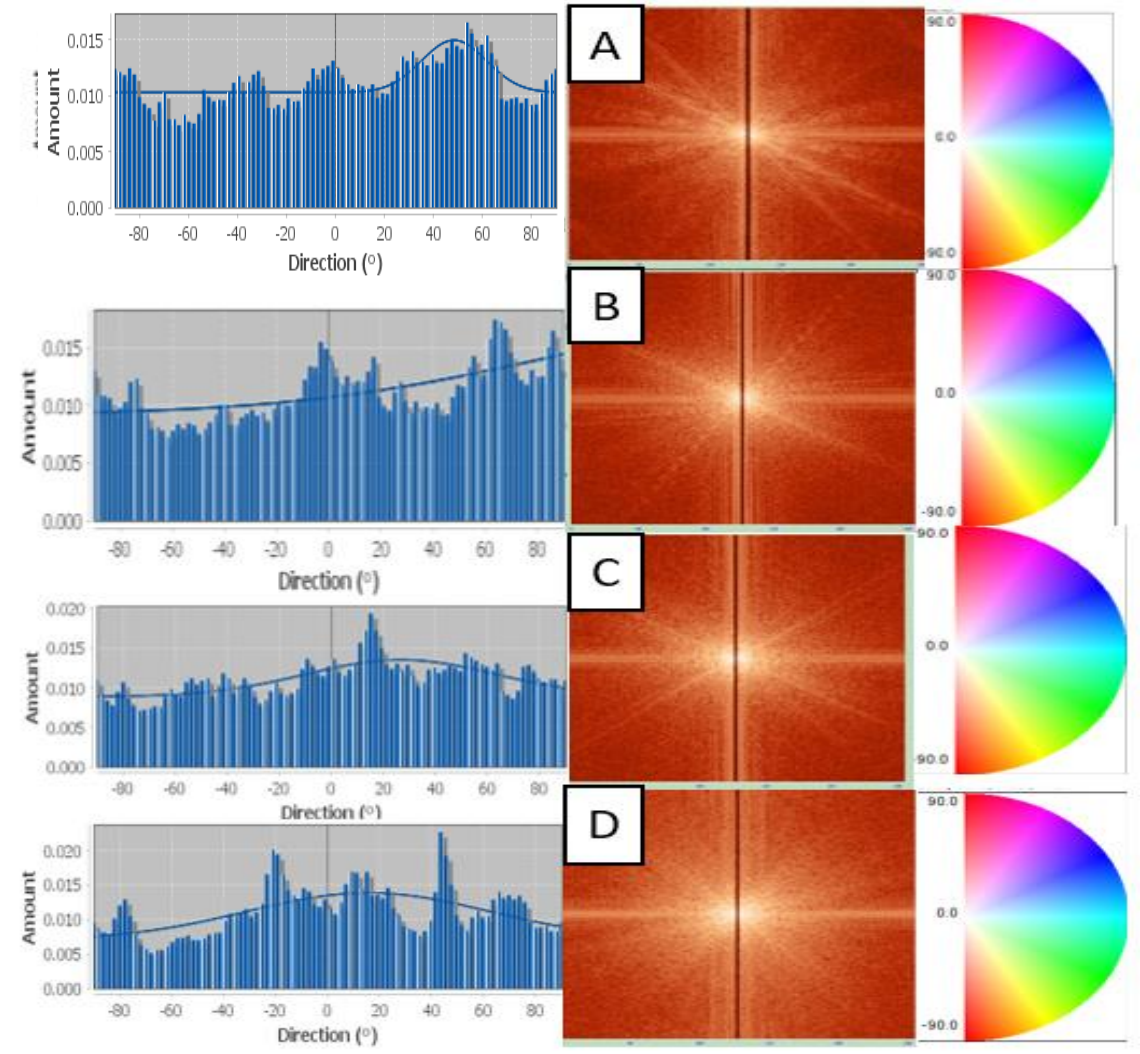

Fig 4.56. Directionality Histogram and 2D-FFT For (A) blend with 3 wt Ocimum basilicum oil (C) blend with 7 wt.% Ocimum basilicum oil (D) blend with 10 wt.% Ocimum basilicum oil.

10 wt.% of Rosemary oil causes more than half of fibers to be oriented in same direction (as shown in figure 4.57 and table 4.22), which reflects the anisotropic character of the textile.

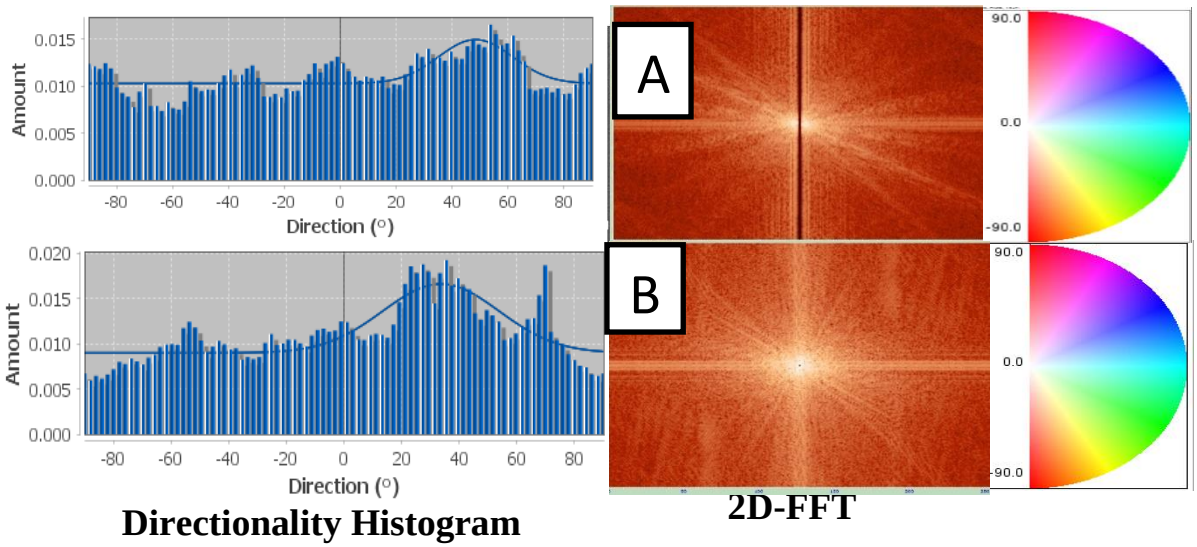

Fig.4.57: Directionality Histogram and 2D-FFT For (A) neat blend nano fiber (B) blend with 10 wt.% Rosemary oil.

Table 4.22: Directionality analysis for Rosemary oil addition.

Samples of Nanofibers	Direction (˚)	Dispersion (°)	Amount	Goodness
Neat blend	48.36	13.29	0.34	0.49
10 wt.%	33.62	20.19	0.55	0.64

10 wt.% Laurus nobilis oil addition causes only 15% of the fibers to be oriented in same direction (as shown in figure 4.58 and table 4.23).

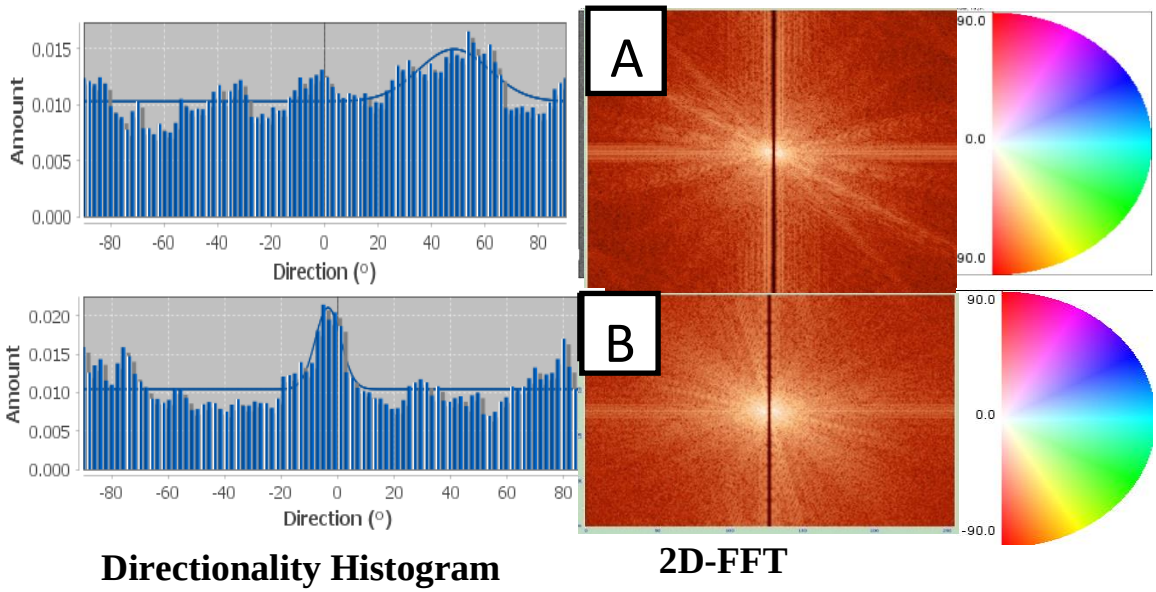

Fig.4.58. Directionality Histogram and 2D-FFT For (A) neat blend nano fiber (B) blend with 10 wt.% L. nobilis EO.

Table 4.23: Directionality analysis for L.nobilis EO.

Samples of Nanofibers	Direction (˚)	Dispersion (°)	Amount	Goodness
Neat blend	48.36	13.29	0.34	0.49
10 wt.% L.nobilis EO	-3.43	4.55	0.15	0.47

Only 9% of the fibers oriented in the same direction with the 5 wt.% Capsicum annuum (as shown in figure 4.59 and table 4.24).

Table 4.24: Directionality analysis for Capsicum annuum addition.

Samples of Nanofibers	Direction (˚)	Dispersion (°)	Amount	Goodness
Neat blend	48.36	13.29	0.34	0.49
6 wt.% Capsicum annuum	36.40	2.08	0.09	0.64

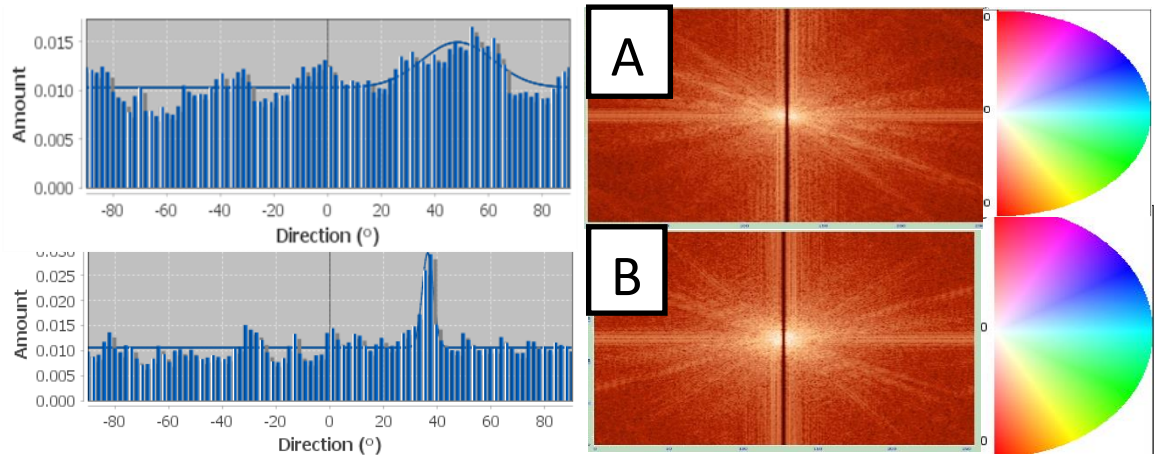

Directionality Histogram **2D-FFT**

Fig.4.59: Directionality Histogram And 2D-FFT For (A) neat blend nanofiber (B) blend with 6 wt.% Capsicum annuum.

Upon the G. lucidum addition, the preferred direction of the oriented nanofibers shifted from 48.36 ° to 53.84 ° as shown with the Gaussian profile, where more than two thirds of fibers oriented in same direction. This profile showed that in both cases, the fibers oriented in random directions. Also, there is an increment in the goodness of orientation nanofibers (as shown in figure 4.60 and table 4.25).

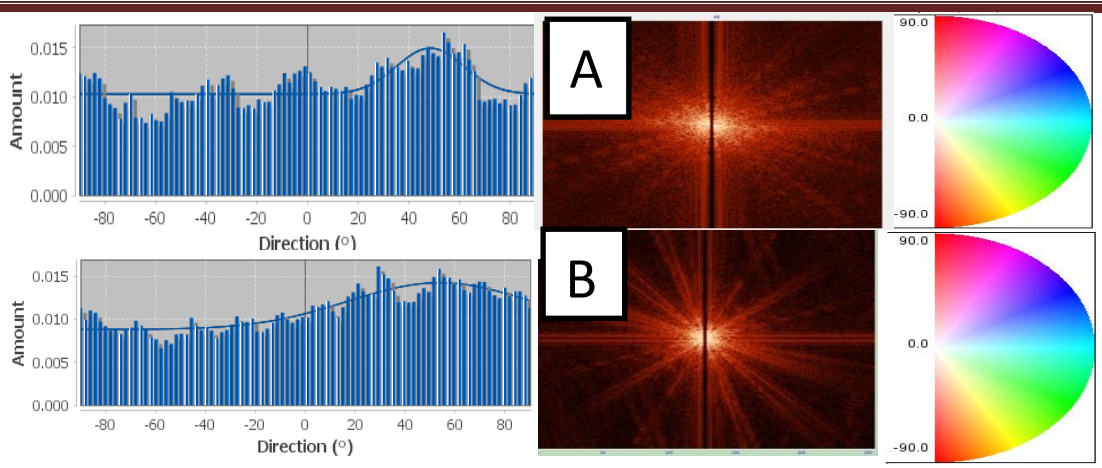

Directionality Histogram **2D-FFT**

Fig.4.60: Directionality Histogram and 2D-FFT For (A) neat blend nanofiber (B) blend with 6 wt.% G. lucid.

Table 4.25: Directionality analysis for the prepared nan fiber textiles

Nanofibers Sample	Direction (º)	Dispersion (°)	Amount	Goodness
Neat blend	48.36	013.29	0.34	0.49
Blend with 6 wt.% G. lucidum	53.84	36.61	0.69	0.80

The final textile have its own histogram and directionality (as shown in figure 4.61 and table 4.26), where only 5% of fibers oriented in the same direction.The processing variables, also, affected the diretionalty, where needle-to-collector distance and the flow rate parameters causes the more efects.

As overall effects on the fiber directionality, the following order is occurred, which is opposite to that of average diameter:

Needle-to-collector distance = Flow rate > Collector speed > Applied voltage > Heat.

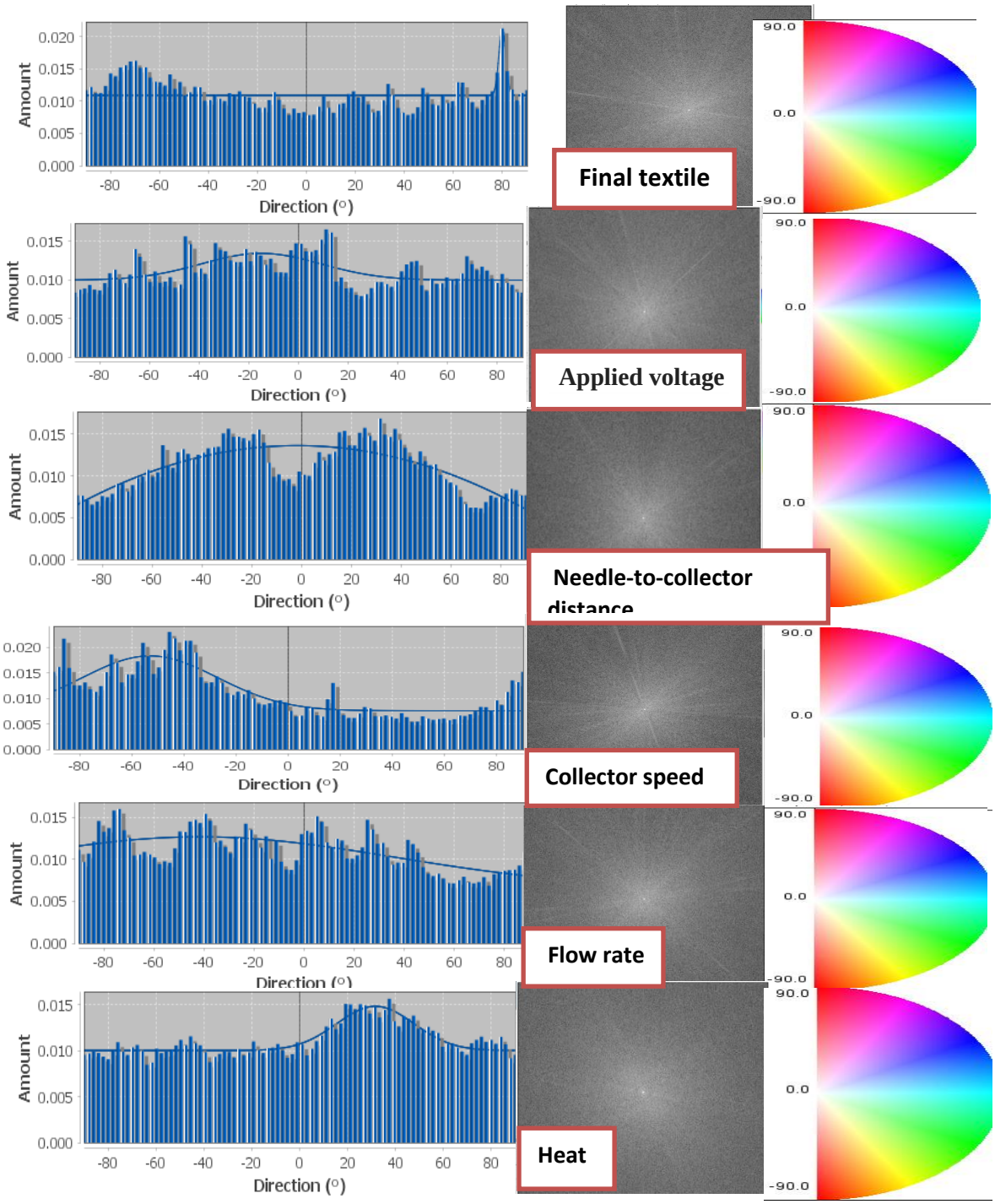

Fig.4.61: Directionality Histogram and 2D-FFT For the final textile at processing variable.

Table 4.26: Directionality analysis for the final textile at processing variable.

Processing variable	Direction (º)	Dispersion (°)	Amount	Goodness
No variable	79.92	1.42	0.05	0.24
Applied voltage. (at 25kV)	-15.05	24.11	0.56	0.32
Needle-to-collector distance (at D=15cm)	-1.81	8226.37	1.00	0.58
Collector speed (at 780 rpm)	-52.97	25.82	0.65	0.69
Flow rate (at 0.5 ml/h)	-41.52	77.36	1.00	0.39
Heat (3 hr at 70 ^{o}C)	31.58	16.15	0.41	0.82

4.8 Thermal transition analysis

4.8.1 DSC of blend polymeric

Figure 4.62 shows the DSC curves for the prepared nano fiber textiles, which monitor the thermal transitions and provide important findings, such as the glass transition temperature (T_g), transition enthalpy, melting transition and so on. Slight increment occurred with the T_g, were it increased from 88.80 ^{o}C for the neat PVA fibers to 88.92 with 7% Collagen addition, and to 88.99 ^{o}C with 5.5% HAc addition. This is because that both Collagen and hyaluronic acid increase the elasticity of the textile and this slight increment is due to the effects of nucleating cites, which promote the crystallization tendency.

The enthalpy associated to the glass transition can be used as an indicator of the crystallinity degree. The enthalpy increased from 142.8 J/g (for neat PVA) to 388.9 J/g for PVA with 7% Collagen and to 453.9 J/g for PVA with 5.5% HAc. That means that both additions causechains entanglement, which required additional heat to detangling these chains.

In contrast, the combined addition of HAc and Collagen, causes slight increment in Tg (from 88.80 ^{o}C to 92.37 ^{o}C) and large increment in the

enthalpy (from 142.88 J/g to 1065 J/g). This is because that, the presence of polar groups increases the intermolecular forces; inter chain attraction and cohesion, which needs an additional heat.

The overall conclusion of this test is that there is some improvement in the thermal stability of the formed textiles, which also predicts an improvement in their mechanical properties, which positively affects the safety of their handling and the length of their storage periods.

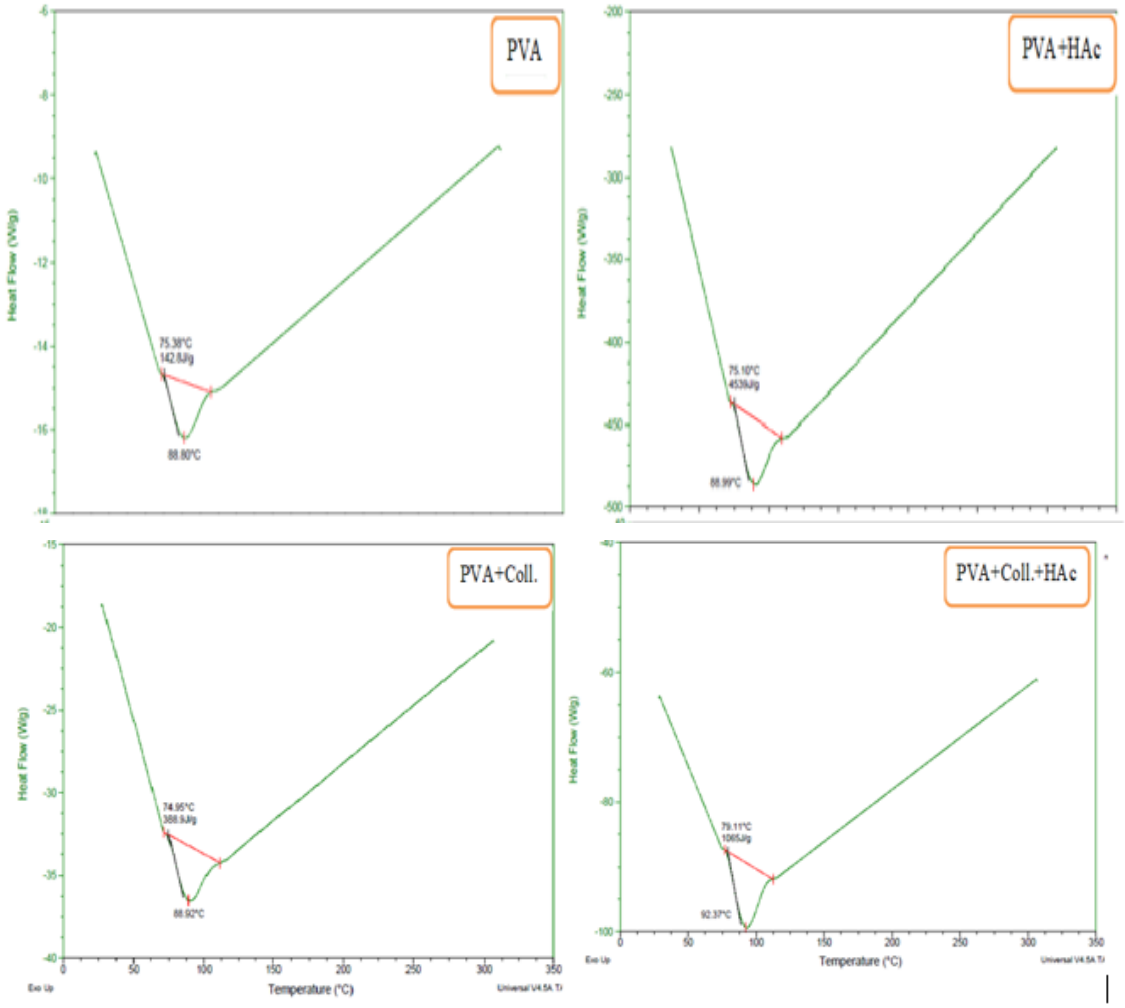

Fig.4.62: DSC curves of the prepared nano fiber textiles.

4.8.2 DSC of blend with antibacterial & antioxidation

DSC results (Figure 4.63 and table 4.27) showed, that compared to the single thermal transition for the neat blend, two transitions occurred upon additions of G. lucidum, Capsicum annuum, I_2, Ocimum basilicum oil,

Rosemary oil, and Laurus nobilis oil. These two adjacent transitions happened on wider temperature range and consumed lower enthalpy.

For neat blend, the transition occurred from 79.11ºC to about 110 ºC (its T_g is 92.37ºC) and needs 1065 J/g, while the G. lucidum addition facilitates the transition to occur at relatively lower temperature 75. 64^0C and extends to about 136ºC (with two T_g's; 90.23 and 121.28 ºC) and needs total enthalpy of 241.71 J/g.

Presence of two T_g's, emphases that this mushroom creating immiscible blend due to the phase separation within their structure. This separation is desirable from the viewpoint of wound dressing because it facilitates the drug releasing toward the injured skin from uncompacting dressings. This mushroom contains some acids (Ganoderic and Lucidenic acids), which in turn contains active carboxylic groups (COOH). These groups can arise many hydrogen bonds with the humid environment, which enlarges the scope of the thermal transition up to 137ºC.

Capsicum annuum (Pepper) addition caused transitions to be started at lower temperature; at 65.81 ºC and extends up to 132ºC and needs 3463J/g. This addition causes two opposite actions; decreased the onset temperature and increased the enthalpy compared with G. lucidum addition, which means that Pepper facilitates slipping of the polymer chains, as well as creating specific hydrogen bonds. Therefore, the two T_g's values decreased down to 80 and 111.95 ºC. These two opposite actions is due to that Pepper contains compounds with various chemical natures, where some of these compounds lubricates the polymeric chains and others crosslinking these chains, such as phenolic acid. When the chains cross-linked tightly or when the crosslinking density is high, it is needs high energy (enthalpy) to be disentangle.

It can be noted that, with both G. lucidum and Capsicum annuum additions, there is a phase separation, which reflected, as seen earlier, by increasing the

porosity among fibers, and reducing the crystallinity. As the porosity increases, the heat required for transition is less.

I_2 addition increased the onset (84.69 ^oC), endset (144 ^oC) temperatures as well as the two T_g's (97.26 and 129 ^oC), but needs only 180.26 J/g. This is because that Iodine particles occupy voids among the polymeric chains and have no lubricant ability. The shifting of thermal transitions to a higher temperatures, indicates that the thermal stability of the resulting nano fiber textile is high [204].

With the addition of Ocimum basilicum oil, the thermal transition started at relatively high temperature (77.79 ^oC), extends up to about 137 ^oC and needs high energy (1308.16 J/g). Their two T_g's are also high; 92.87 and 121.33^oC. This is because of the many aromatic and cyclic rings within its compounds, such as Anethole, Methyl chavicol, Cineole and so on. These rings contain strong bonds, such as the double bonds, which required higher energies to be broken. These compounds increase the thermal stability of the wound dressings, which enhances their performances during sterilizing process under high temperatures.

With Rosemary oil addition, the transition begins from 80.55^oC to about 143^oC, needs high energy; 1363J/g with high two T_g's; 94.03 and 124 ^oC. These high enthalpy and temperatures are due to the polar, aromatic and cyclic components, where Rosemary oil contains polar compound (such as Borneol), aromatic compound (such as δ-Cadinene, and Humiene) and cyclic compounds (such as β-Pinene and α-Capacne). These compounds give the wound dressings an additional thermal stability and enhances their mechanical properties.

In the final textile, the first thermal transition occurred early at 48.48 ^oC, while the second transition ended at a high temperature (194.19^oC). This is because that the final textile contains compounds with the lubricant tendency as well as compounds with the cross-linking tendency. These two

contradictory natures of the components of this textile caused the occurrence of glass transitions over a wider range of temperatures; from 69.01 °C to 182.25 °C and needs less energies; 57.37 J/g and 21.77 J/g.

Compared with neat blend, the T_g extent of the final textile be doubled, and needs less energy, which means that this textile have more flexibility or be soft over wider temperatures. These results indicate that the final textile has high mechanical properties and can withstand sever conditions, whether in storage, handling, or during application to wounds.

Table 4. 27: Thermal transition outputs as a function of addition type

Sample	**Temperature span**		**Enthalpy $(J/g)(\Delta H)$**		**Tg** ℃	
	T_{onset} of 1^{st} transition (℃)	T_{endset} of 2^{nd} transition (℃)	ΔH_1	ΔH_2	T_{g1}	T_{g2}
G. lucidum	75.84	136	209.7	32.01	90.23	121.28
Capsicum annuum	65.81	132	2675	788	80	111.95
I_2	84.69	144	283	82.89	97.26	129
Ocimum basilicum oil	77.79	137	1262	46.16	92.87	121.33
Rosemary oil	80.55	143	1099	264	94.03	124
Final textile	48.48	194.19	57.37	21.77	69.01	182.25

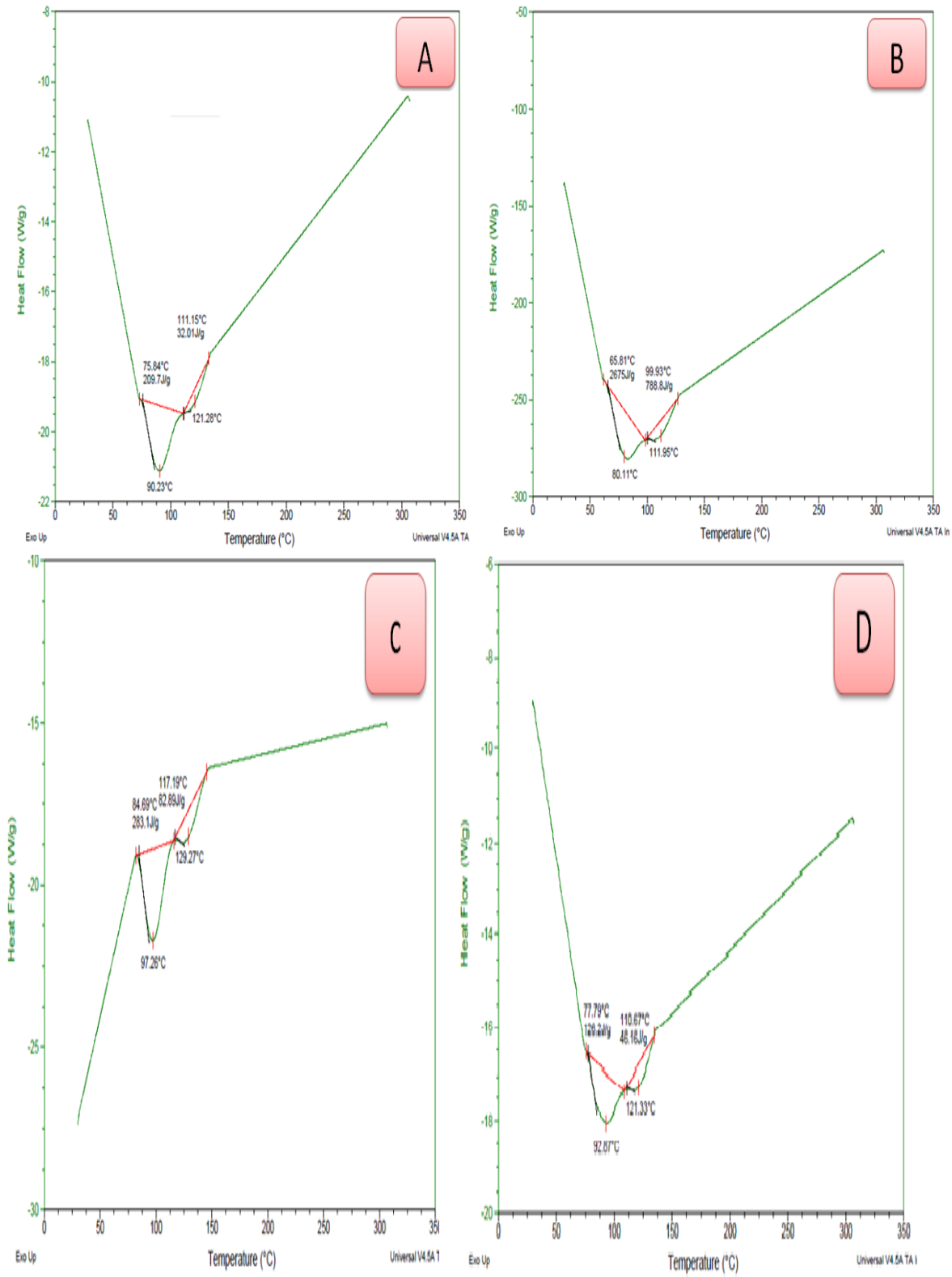
A
Heat Flow (W/g)
Temperature (°C)
Exo Up
Universal V4.5A TA
111.15°C
32.01J/g
75.84°C
209.7J/g
121.28°C
90.23°C
B
Heat Flow (W/g)
Temperature (°C)
Exo Up
Universal V4.5A TA In
65.81°C
2675J/g
99.93°C
788.8J/g
111.95°C
80.11°C
C
Heat Flow (W/g)
Temperature (°C)
Exo Up
117.19°C
84.69°C 82.89J/g
283.1J/g
129.27°C
97.26°C
D
Heat Flow (W/g)
Temperature (°C)
Exo Up
77.79°C
110.67°C
46.16J/g
121.33°C
92.87°C

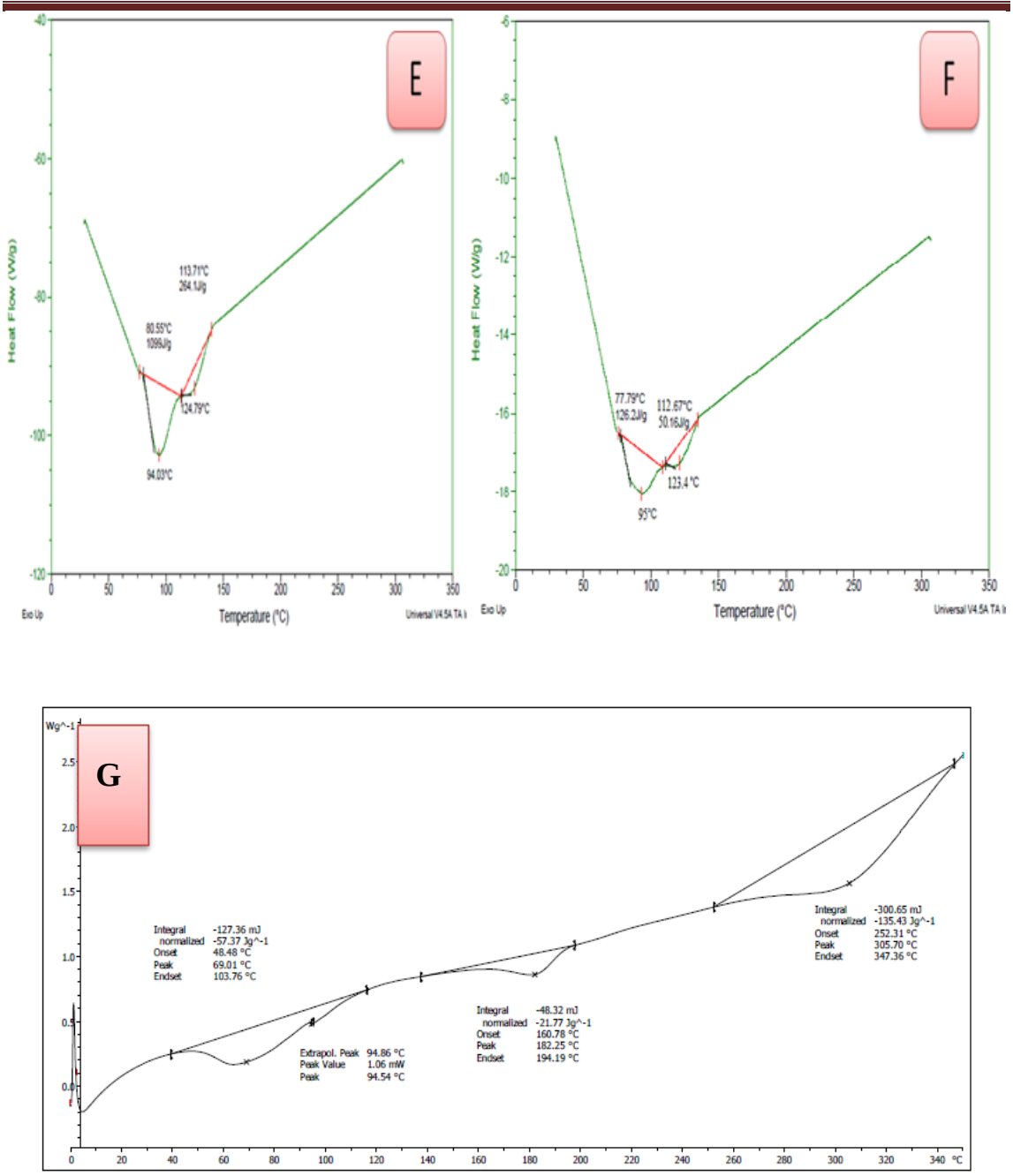

Fig.4.63: DSC Curves of Neat blend with (A) G. lucidum (B) Capsicum annuum (C) I_2 (D) Ocimum basilicum oil (E) Rosemary oil (F) Laurus nobilis oil and (G) Final textile.

4.9 UV absorbance

4.9.1 UV absorbance of blend polymeric

Ultraviolet (UV) light refers to the region of the electromagnetic spectrum between visible light and X-rays, with a wavelength falling between 10 and 400 nanometers. This electromagnetic radiation is not visible to the human eye, because it has a shorter wavelength and higher frequency than the light

our brain perceives as images. UV radiation is a form of non-ionizing radiation that is emitted mostly by the sun. While it has some benefits for people, including the creation of Vitamin D, it also can cause health risks. UV radiation is divided into the following regions:

1- Extreme Ultraviolet (EUV) light (10-100 nm), which can only travel through a vacuum, and it is completely absorbed in Earth's atmosphere.

2- Far Ultraviolet (FUV) light (100-200 nm), which has the most energy and highest frequency of all UV radiation.

3- Middle Ultraviolet (MUV) light (200-300nm)

4- Near Ultraviolet (NUV) light (300-400nm)

Figure 4.64 shows the absorption of the prepared textiles starting from 190 nm; starting from MUV region. It is clear from this figure, that the neat PVA textile absorbs UV radiation in the MUV region only and there is no absorption in the NUV region. In contrast, additives of Collagen, HAc and their combined extended the absorption to the NUV and visible regions, especially HAc addition.

The absorbance order is: tertiary blend > PVA: 5.5% HAc > PVA: 7% Collagen > PVA, which means that the blended nano fiber textiles have the ability to absorb an additional radiations and dissipate their energies as a slight heat. This little heat do not affect the physical form of the wound dressing textile due to the high thermal stability, as seen earlier from DSC results, where T_g is approximately constant.

This means that, while HAc and Collagen additives enhance the mechanical properties of the dressings, they do not stop the creation of vitamin D through the skin, but rather enhance its production due to the increased absorption of rays. Also, the heat generated within the skin tissue kills bacteria there, which speeds up wound healing process; enhances its antibacterial performance.

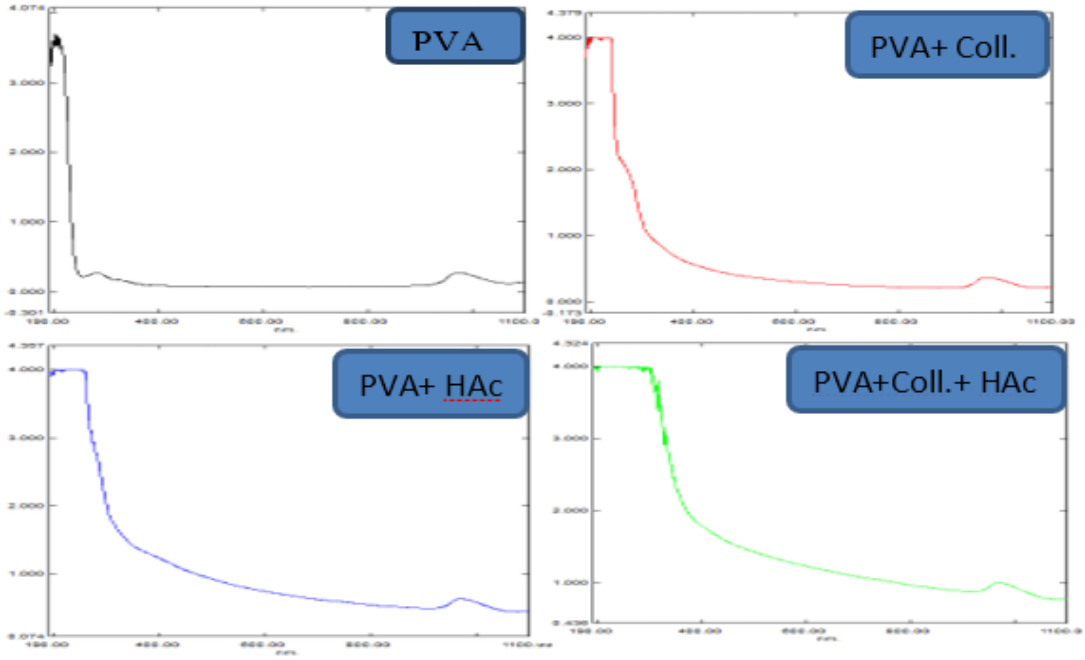

Fig.4.64: UV absorbance of the prepared nano fiber textile.

4.9.2 UV-Visible absorbance of blend with antibacterial & antioxidation

Figure 4.65 shows the effects of the mention additives on the UV-Visible absorbance of the prepared nano fiber textiles. It is clear that all additives (especially the final textile) increased the light absorbance in the three regions: UV region (190-380 nm), Visible region (380-780) and IR region (above of 780 nm). This means that, these additives enhance the antibacterial activity, as well as the production of vitamin D within the skin layers, which considered as a benefit for the wound dressing's performance.

As light penetrates the complex, an electron is promoted from a bonding or non-bonding orbital into an empty anti-bonding orbital, thereby releasing energy trapped in the bond. As a result, there could be some electron leaps (figure 4.65). In each possible case, an electron is excited from a full orbital into an empty anti-bonding orbital. Each jump takes energy from the light, and a big jump obviously needs more energy than a small one. Each wavelength of light has a particular energy associated with it. If that particular amount of energy is just right for making one of these energy

jumps, then that wavelength will be absorbed - its energy will have been used in promoting an electron.

The antibonding orbitals are normally empty, while the nonbonding orbital contains lone electron pairs, and the bonding orbitals contain normal bonding pairs of electrons.

The **σ to σ*** transition requires an absorption of a photon with a wavelength which does not fall in the UV-Visible range. Therefore, only **π to π*** and **n to π*** transitions occur in the UV-Visible region are observed (figure 4.69). The "**n**" electrons (or the nonbonding electrons) are the ones located on the oxygen of the carbonyl group. Thus, the **n to π*** transition corresponds to the excitation of an electron from one of the unshared pair to the **π*** orbital.

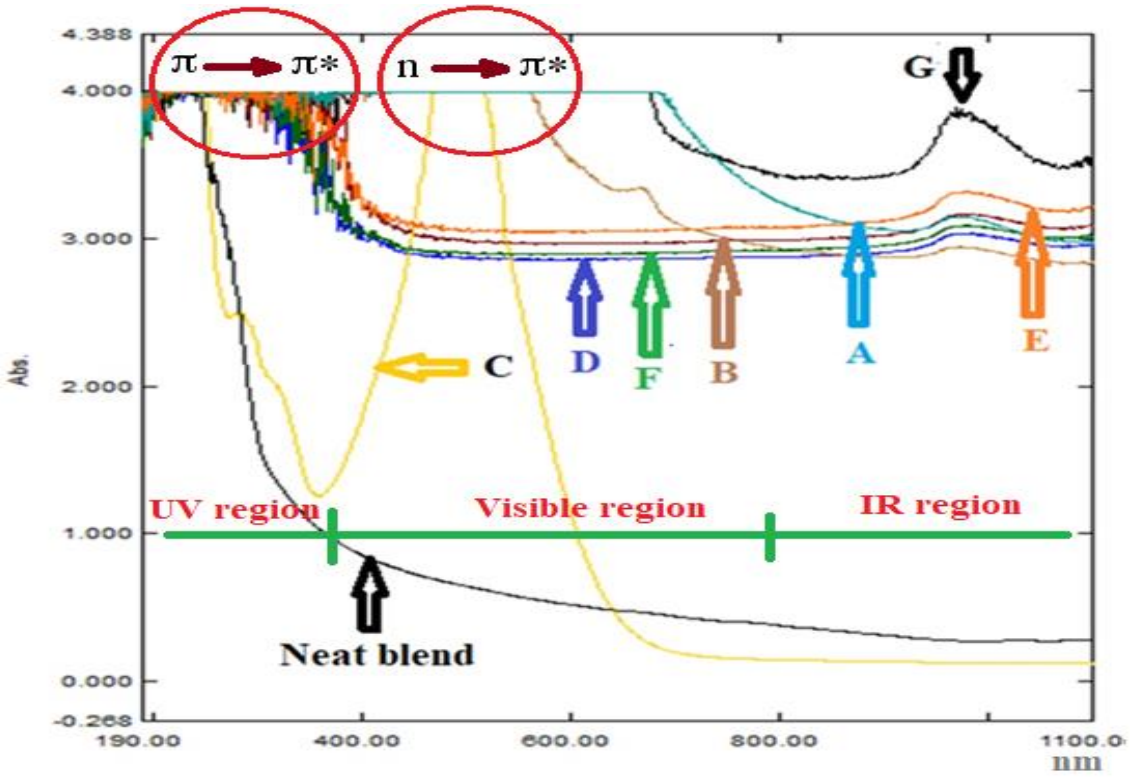

Fig 4.65: UV-Visible absorbance of (A) neat blend with G. lucidum (B) neat blend with Capsicum annuum (C) neat blend with I_2 D) neat blend with Ocimum basilicum oil (E) neat blend with Rosemary oil (F) neat blend with Laurus nobilis oil (G) Final sample.

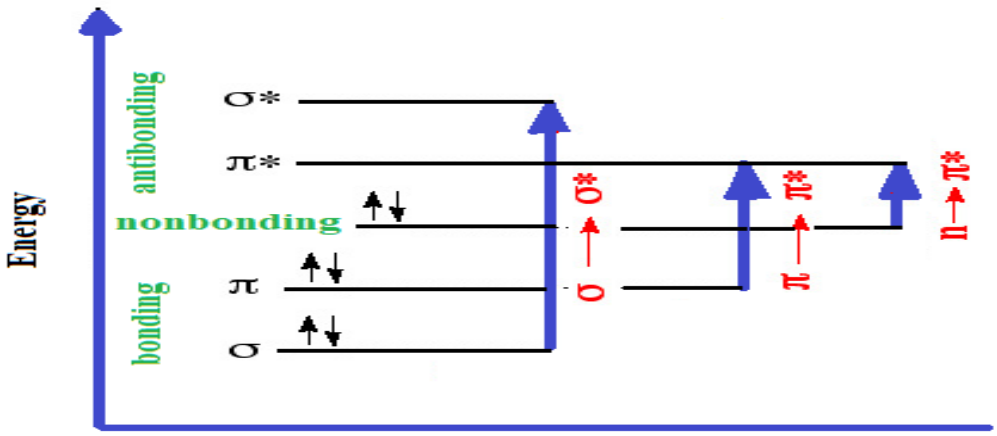

Fig.4.66: The typical energy diagram of the electronic transitions

All additives are known to cause **π to π*** and **n to π*** transitions (figure 4.66), as their molecules contain either pi bonds (inside the double bonds) or atoms with non-bonding orbitals, such as a lone pair on oxygen, nitrogen, or a halogen.

Since the energy of the non-bonding orbital is greater than that of the bonding orbital, less energy is required for an oxygen lone pair to hop from the non-bonding level to the anti-bonding orbital. That implies it takes in longer-wavelength, lower-frequency light. Accordingly, these modern textiles absorb light at two distinct wavelengths (two absorbent beaks appeared).

4.10 XRD analysis

Figure 4.67 and table 4.28 display XRD results of the neat blend and final textile. Results showed that the mentioned additives (G. lucidum, Capsicum annuum, I_2, Ocimum basilicum oil, Rosmarinus officinalis oil, and Laurus nobilis oil) affected the lattice parameters and create a modified crystalline structure. For example, the crystalline peak shifted from $2\theta = 24°$ to $2\theta = 22°$, the d-spacing increased from 3.772 to 3.9943 A^o, the crystallite size increased from 0.34 to 0.378nm and the peak be narrower. This means that some components of these additives act as enucleating agents, which

accelerated the crystalline rate. Also, the polarity nature of these additives and their extra hydrogen bonds, encourage the interaction among the polymeric chains, which in turn increased their lineup.

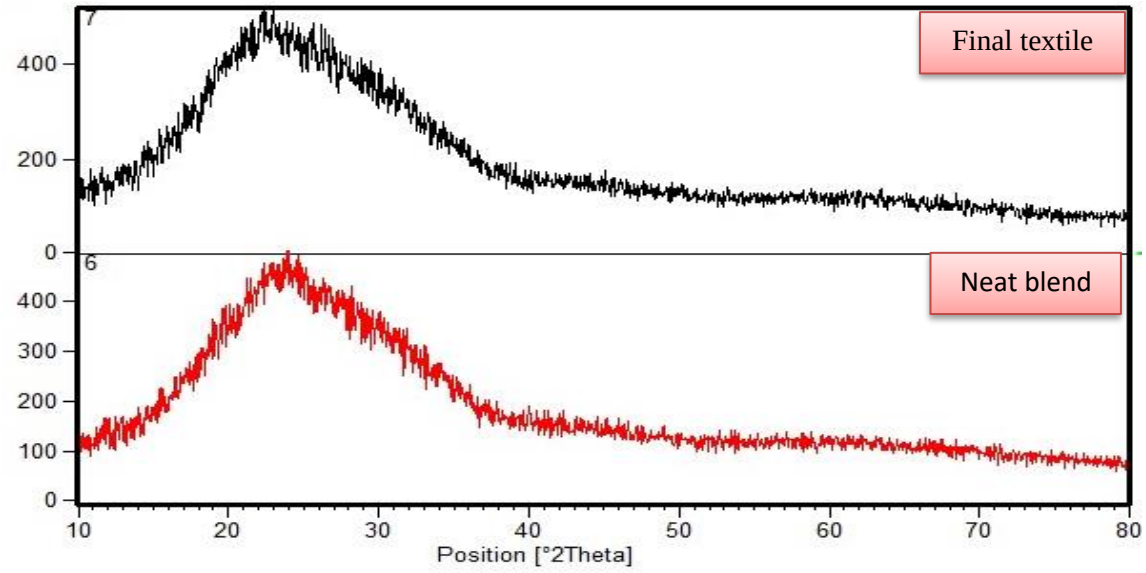

Fig.4.67.: XRD spectrum of (A) The neat blend, (B) Final textile

Table 4.28: Parameters extracted from XRD spectra of the neat blend, and Final.

Samlpe	2θ(°)	β(°)	d-spacing (A°)	Crystal size (nm)
Neat blend	24	23	3.722	0.34
Final	22	26	3.9943	0.378

4.11 Nanoindentation hardness

The nanoindentation test is a useful technique for characterizing various mechanical properties (e.g., hardness, elastic modulus, and viscoelasticity) of materials ranging from hard alloys to soft biomaterials. As the load is applied, the depth of penetration is measured.

The contact depth (h_c) is defined as the depth of indenter in contact with the sample under load. The depth measured during the indentation (h) includes the depression of the sample around the indentation, in addition to the contact depth.

The slope of the curve, (dp/dh), upon unloading is indicative of the stiffness (S) of the contact. This value generally includes a contribution from both the material being tested and the response of the test device itself. The stiffness of the contact can be used to calculate the reduced Young's modulus.

To analyze the reinforcement effect of additives, modulus of the electrospun fiber has been measured using a nanoindenter. The neat blend and final sample fibers were fabricated on a glass substrate.

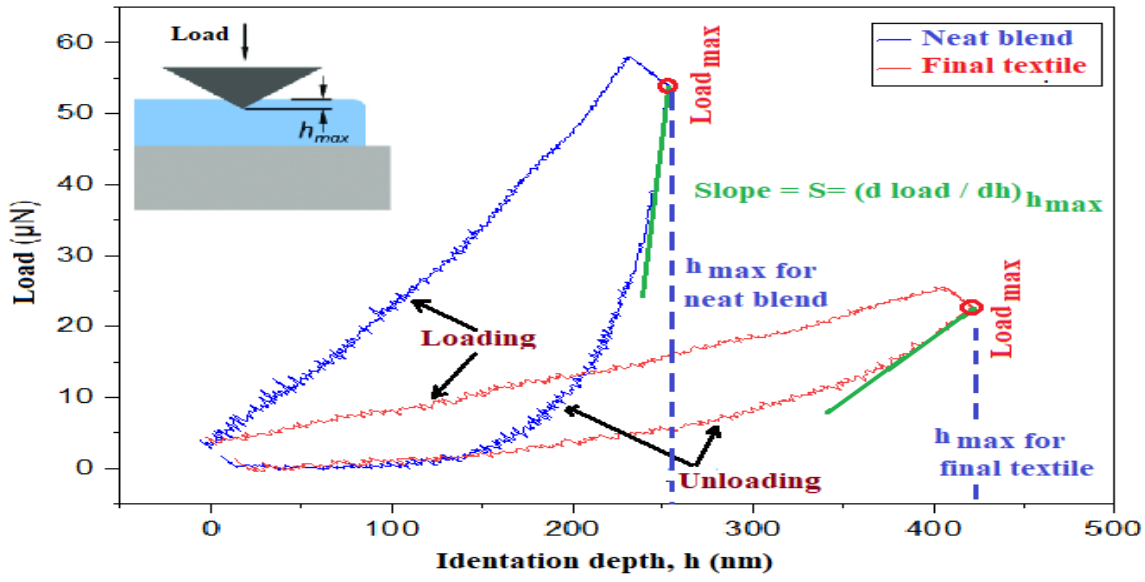

Fig.4.68: Relation between the load and indendation depth for neat blend and final textile.

The Young's modulus (E) is a property of the material that tells us how easily it can stretch and deform and is defined as the ratio of tensile stress (σ) to tensile strain (ε). The reduced Young's modulus (Er) is related to the Young's modulus (E) with the simple equation $Er = E/(1-v^2)$, where v is the sample's Poisson's ratio.

Results showed that the final textile (figure 4.68) have very low Er (0.08 Gpa), which means that this dressing is floppy and stretch a lot when they are pulled (squash down a lot when pushed).

Elastic modulus measures the resistance of the material to elastic—or "springy"—deformation.

Table 4.29: Properties of nanoindentation for neat blend and final textile.

Property	Neat blend nanofibers	Final textile	Proprty change (%)
Reduced elastic modulus, Er (Gpa)	1.58	0.08	- 94.93
Hardness (Gpa)	0.054	0.012	- 77.77
Contact Depth (nm)	228.28	301.2	+ 31.95
Contact Stiffness ($\mu N/nm$)	1.68	0.14	- 91.66
Max Force	50.44	22.88	- 54.63
Depth Max(nm)	253.3	424.96	+ 67.76
h.f	132.478	40.984	- 69.06

Hardness is the ability of a material to resist deformation. It is dependent on many properties, such as viscoelasticity, and viscosity, ductility, elastic stiffness, plasticity, strain, strength, toughness. Measuring hardness levels can help predict the ability of the material to recover after being indented through force. Also, it enables it to withstand plastic deformation, penetration, scratching, and indentation; hence, hardness is significant for determining specific material's applications.

The hardness of final textile decreased from 0.054 to 0.012 Gpa, which means that the new dressing will be much more flexible in its response to the applied load. These ductile dressings have low strength, low brittleness, low wear resistance and degraded easily.

The contact depth (h_c) (figure 4.69) increased by 31.95%, which means an increase in the area of adhesion between the polymeric nano fiber textile and the indantor, and this reflects the soft state of the new dressing.

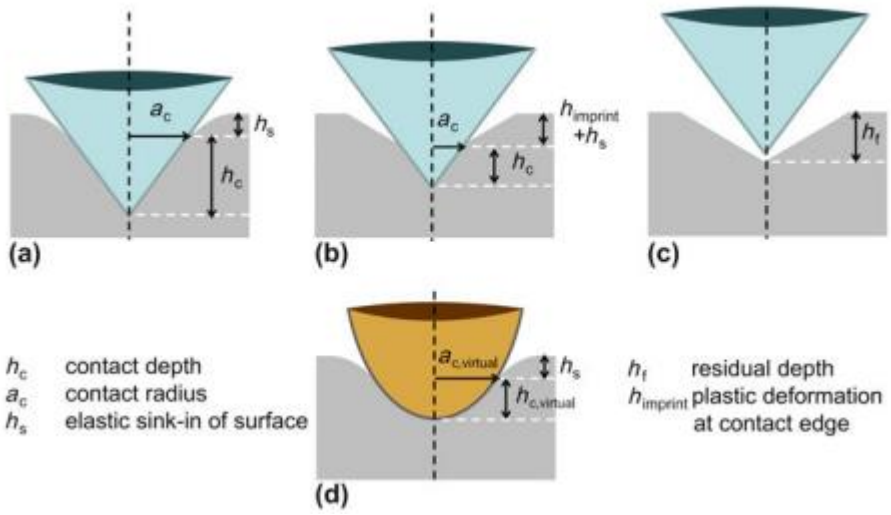

Fig.4.69: Schematic of the indenter (a) at maximum load (b) during unloading, (c) after unloading, and (d) corresponding effective indenter [218].

Modulus of elasticity is a measure of stiffness, with higher-modulus materials exhibiting less deformation under load compared to low-modulus materials.

4.12 Antioxidation

As the FTIR spectrum study has already established, the neat mix and the final sample both contain polyphenols from (HAc, Capsicum annuum, Ocimum basilicum oil, Rosemary oil, and Laurus nobilis oi), which are well-known for their antioxidant qualities. It is believed that the chemical structure's ability to bind and neutralize free radicals in lipids is due in large part to the presence of hydroxyl groups and aromatic rings. The free radical DPPH is converted into a stable molecule by receiving electrons from antioxidant or hydrogen radicals present in the (neat blend and final sample). Although the DPPH solution started off purple, the presence of an antioxidant causes the hue to shift to a mustard (near yellow) and the absorbance value to drop [205]. This visual color change confirms the DPPH free radical scavenging by the antioxidant molecule.

Different concentrations (40, 50, 60, 70, 80, 90 µg/ml) of neat blend and final sample were subjected to this investigation and showed the % inhibition at the same concentration in Figure 4.70 and table 4.30.

Table 4.30: DPPH of inhibition of neat blend and final sample

Concentration (µg/ml)	Inhibition of neat blend (%)	Inhibition of final textile (%)	Inhibition change (%)
40	22.019	33.367	+ 51.53
50	25.081	37.665	+ 50.17
60	30.689	34.726	+ 13.15
70	33.552	36.571	+ 8.99
80	35.889	34.547	- 3.74
90	38.277	43.493	+ 13.64

These results showed that the antioxidant activity of neat blend and final sample increased with the concentration (except the 80 µg/ml for the final textile). Results also showed that high inhibition change % obtained with the low concentrations, when comparing with the neat blend.

Since oxidative stress is implicated in pathophysiology, it stands to reason that antioxidant qualities play a vital role in certain of the biological actions of Essential Oils (EOs). Some of their components, especially phenols, have the inherent ability to inhibit or slow the aerobic oxidation of organic matter, which is responsible for these properties. However, because many of these compounds are nonvolatile, the distillation process used to extract the oil from the raw material limits the content of phenolics in the final matrix, which negates some of these benefits. Antioxidant behavior can be shown by EOs that don't include phenol, though.

As free radicals impede the normal and natural recovery of tissues, proper infected and non-infected wound care and healing can be enhanced by the action of antioxidant compounds that act as free radical scavenging agents, promoting tissue recovery and reducing healing times [42 , 43].

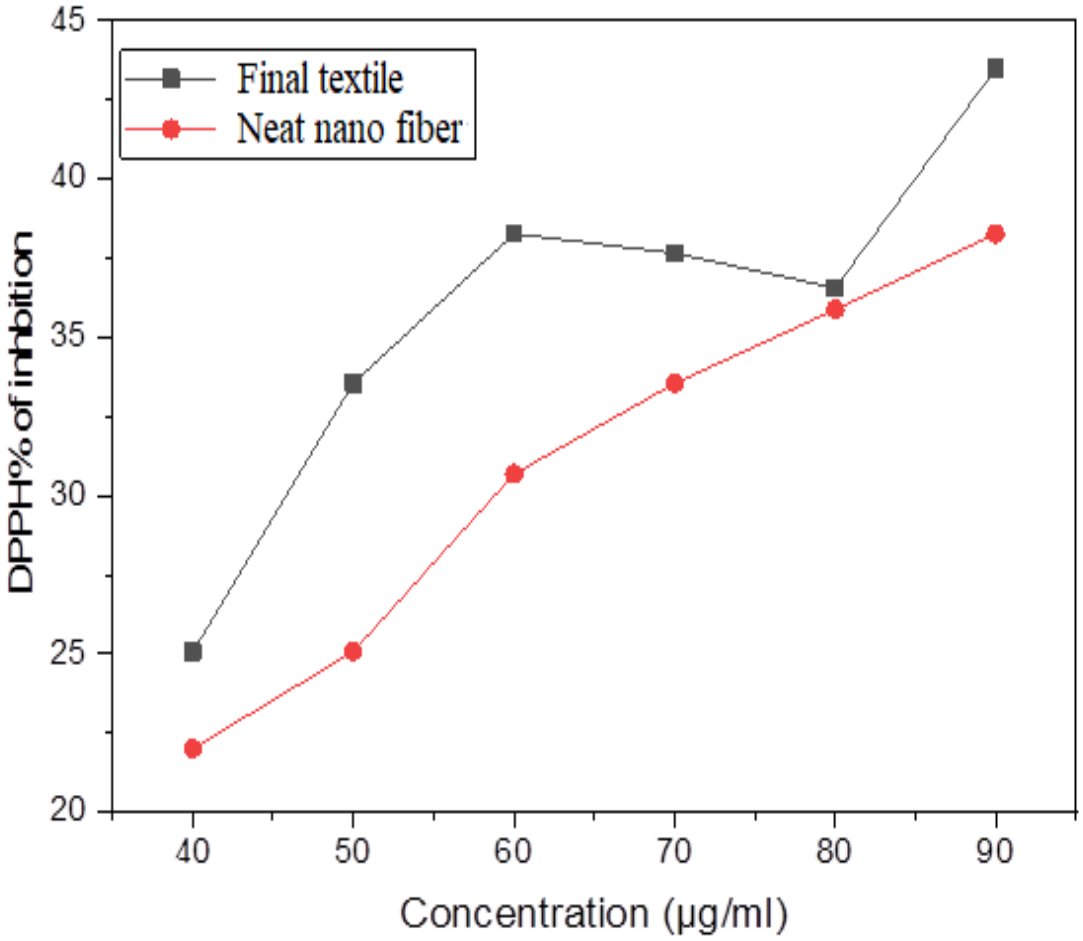

Fig.4.70: DPPH free radical scavenging activity of neat nanofiber and final Textile.

4.13 Antibacterial activity

Antibacterial activity of nano fiber was determined by measuring the inhibition zone diameter (IZ) after 48 h, in comparison with control sample. Results showed that, IZ for (neat blend /G. lucidum, neat blend/Capsicum annuum, neat blend / I_2, neat blend /Ocimum basilicum oil, neat blend /Rosemary oil, and neat blend /Laurus nobilis oil), increased with increasing the concentration of any of the used additives as show in Figure 4.71 and table 2.31.

This conclusion is evaluated in terms of the IZ of nano fibers at two concentrations, and neat blend used as control sample against E. coli and S. aureus microorganisms.

Table 2.31: Inhibition zone diameter for Textile with additives

Textile with	IZ (mm)		IE (%)	
	E-coli	S. aureus	E-coli	S. aureus
3% G. lucidum	18	15	38	33
6% G. lucidum	25	20		
3% Capsicum annuum	13	13	33	15
6% Capsicum annuum	15	14.5		
0.2% I_2	14	11	53.8	27.2
0.3% I_2	20	13		
7% Ocimum basil oil	17	15	17	33
10 % Ocimum basil oil	20	20		
7% Rosemary oil	15	13	33	38
10 % Rosemary oil	20	18		
7% L. nobilis EO	15	6	30	33
10 % L. nobilis EO	18	10		

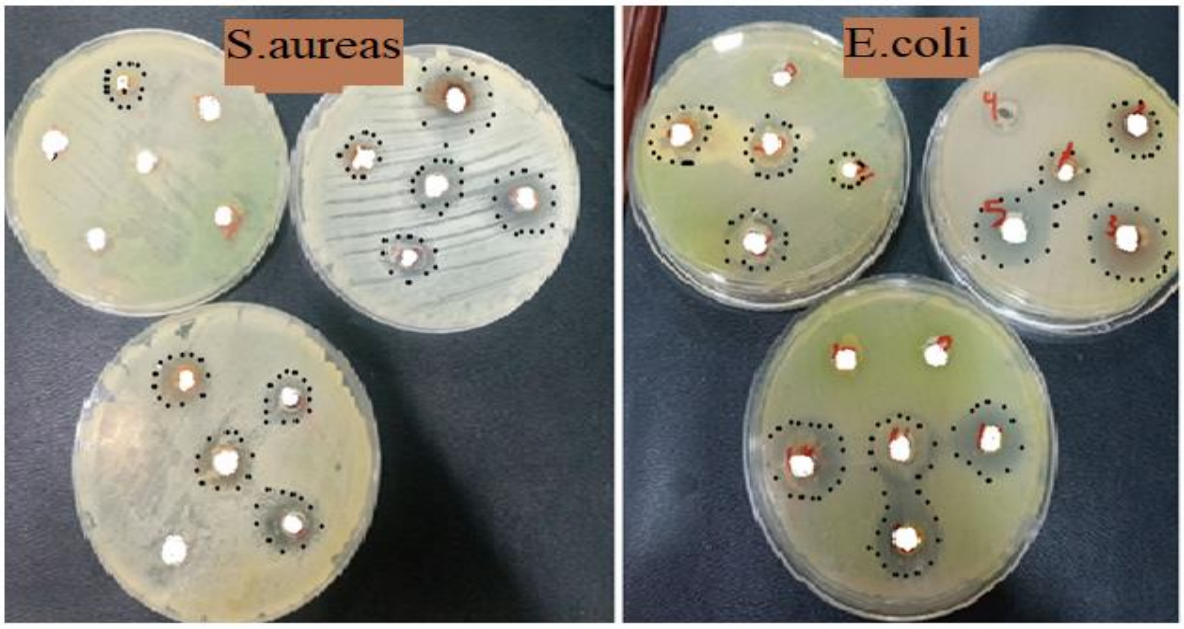

Fig.4.71: Inhibition zone diameter for nano fibers.

Figure 4.72 shows that when compared to the findings obtained with 3 wt.% G. lucidum, the IE (equeation: 3.1) achieved with 6 wt.% G. lucidum against E. coli and S. aureus was 38% and 33% higher, respectively. Further, the antibacterial activity of the neat blend containing G. lucidum is at its highest against E. coli and S.aureus at a concentration of G. lucidum of 6 weight percent (25mm and 20mm, respectively), while it is at its lowest at a concentration of 3 weight percent (20mm and 15mm, respectively). Conclusions drawn from our study are consistent with those drawn from (Sadaf Quereshi. et al)[208].

From Figure 4.72, we can see that the concentration of Capsicum annuum (6 wt.%) provides the greatest antibacterial activity against E. coli and S. aureus (15 and 14.5 mm, respectively), while the concentration of Capsicum annuum (3 wt.%) provides the least activity against these pathogens (13 and 13 mm, respectively). The results showed that compared to 3wt% Capsicum annuum, the IE of 9 wt.% Capsicum annuum against E. coli and S. aureus increased by 33% and 15%, respectively. The outcomes obtained here are comparable to those of (Sharafaldin Al-Musawi.et al)[4].

For neat blend / I_2 (Figure 4.72), the result showed that the maximum antibacterial activities at concentration of I_2 (3 wt.%) against bacteria E. coli and S. aureus are (20, 14mm) respectively and minimum of antibacterial activity at concentration of I_2 (1 wt %) against bacteria E. coli and S. aureus are (13, 11mm) respectively. The results showed that the (IE) of 3 wt.% I_2 against E. coli and S.a ureus increased by 53.8 % and 27.2% respectively compared with 1wt.% I_2.

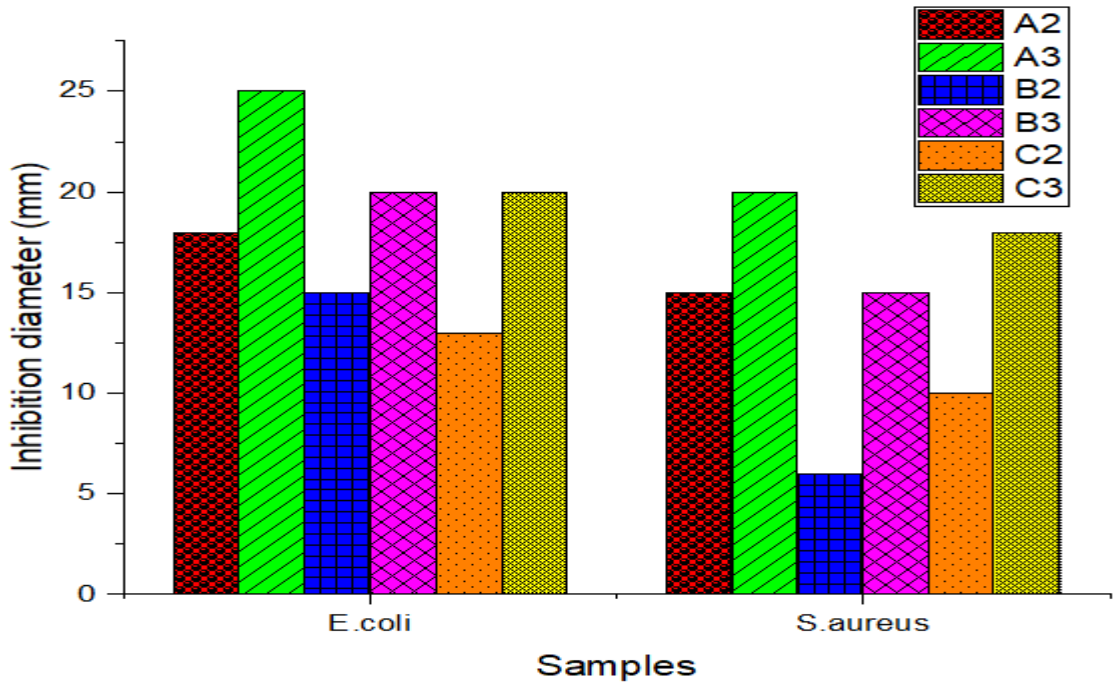

Fig.4.72: Antibacterial activity for (A2, A3) neat blend /G. lucidum, (B2, B3) neat blend/Capsicum annuum, (C2, C3) neat blend / I_2 .

For neat blend /Ocimum basilicum oil, (Figure 4.73), the result showed that the maximum antibacterial activities at concentration of Ocimum basilicum oil (10 wt. %) against bacteria E. coli and S. aureus are (20, 20 mm) respectively and minimum of antibacterial activity at concentration of Ocimum basilicum oil (7 wt.%) against bacteria E.coli and S.aureus are (17, 15mm) respectively. The results showed that the (IE) of 10 wt.% Ocimum basilicum oil against E. coli and S. aureus increased by 17 % and 33% respectively compared with 7 wt.% Ocimum basilicum oil. Our results are close to results of (Uzma Nazir. et al.) [209].

For neat blend /Rosemary oil, (Figure 4.73), the result showed that the maximum antibacterial activities at concentration of Rosmary oil (10 wt .%) against bacteria E. coli and S. aureus are (20, 18 mm) respectively and minimum of antibacterial activity at concentration of Rosemary oil (7 wt.%) against bacteria E. coli and S.aureus are (15, 13mm) respectively. The results showed that the (IE) of 10 wt.% Rosemary oil against E. coli and S. aureus

increased by 33 % and 38% respectively compared with 7 wt% Rosemary oil. Our results are close to results of (Abdullah Ijaz Hussain. et al.) [210].

For neat blend /L.nobilis EO, (Figure 4.73), the result showed that the maximum antibacterial activities at concentration of Laurus nobilis oil (10 wt.%) against bacteria E. coli and S. aureus are (13, 8 mm) respectively and minimum of antibacterial activity at concentration of L.nobilis EO (7 wt.%) against bacteria E. coli and S. aureus are (10, 6 mm) respectively. The results showed that the (IE) of 10 wt.% Laurus nobilis oil against E. coli and S. aureus increased by 30 % and 33% respectively compared with 7 wt.% Laurus nobilis oil. Our results are close to results of (Elhoussine Derwich. et al.) [211].

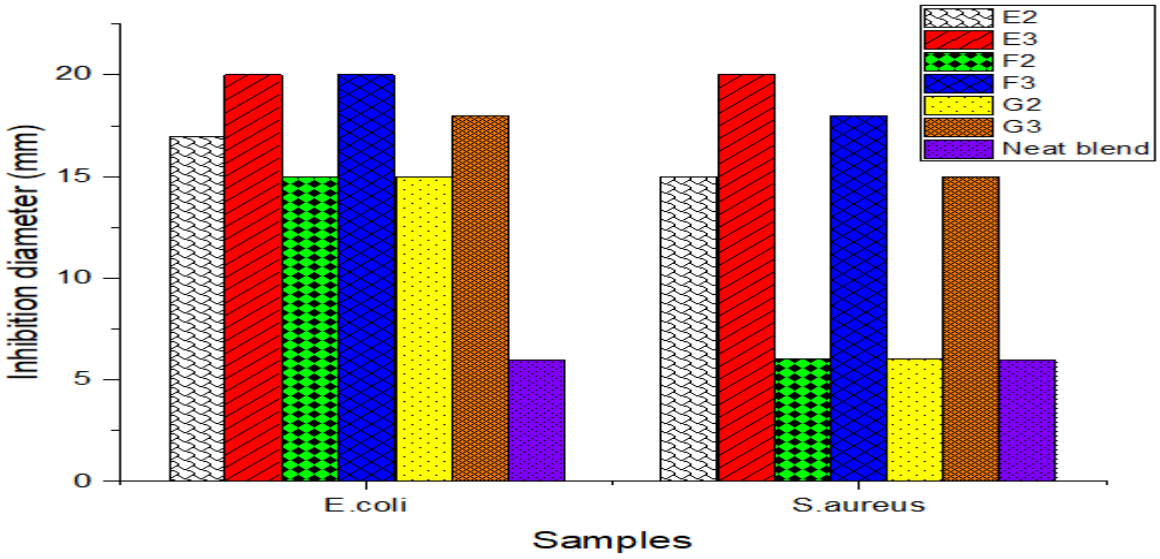

Fig.4.73: Antibacterial activity for (E2, E3) neat blend /Ocimum basilicum oil, (F2 ,F3) neat blend /Rosemary oil, and (G2 ,G3) neat blend /L. nobilis EO.

For final sample (neat blend, G. lucidum, Capsicum annuum, I_2, Ocimum basilicum oil, Rosemary oil, and Laurus nobilis oil) (Figures 4.74 and 4.75), the result showed that the maximum antibacterial activities at concentration of Final sample (500 wt. %) against bacteria E. coli and S. aureus are (30, 34 mm) respectively and minimum of antibacterial activity at concentration of final sample (62.5 wt %) against bacteria E. coli and S. aureus are (15, 25

mm) respectively. The results showed that the (IE) of 500 wt.% final sample against E. coli and S. aureus increased by 40% and 100 % respectively compared with 62. 5 wt.% final sample.

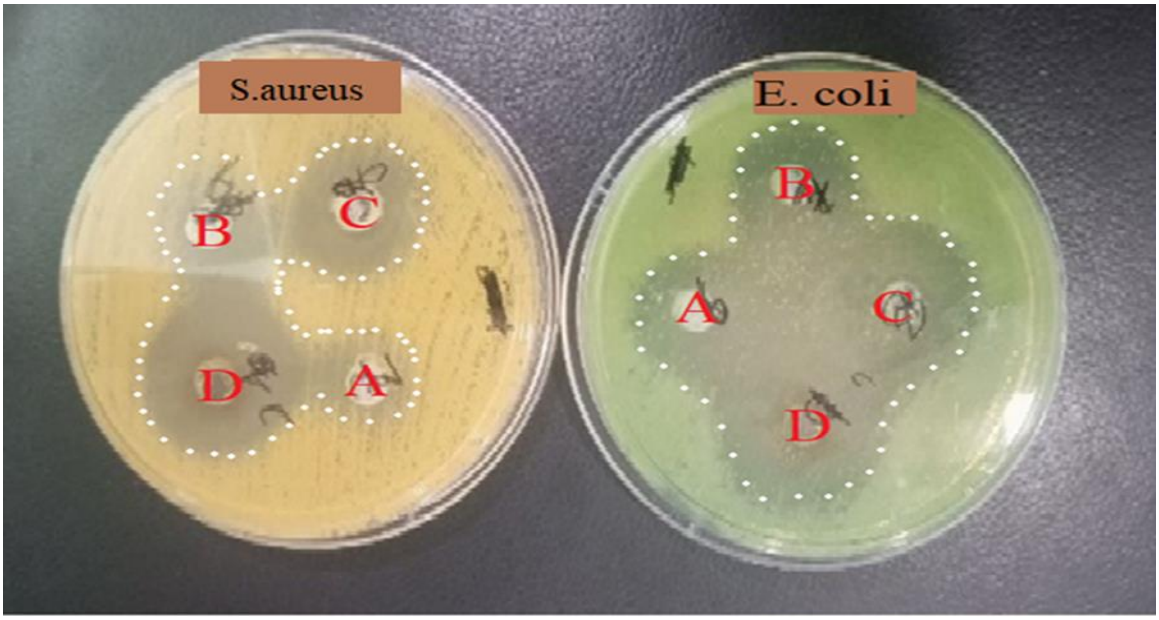

Fig.4.74: Inhibition zone diameter for final sample of A, 62.5 %. B, 125 %. C, 250 %. D, 500 %.

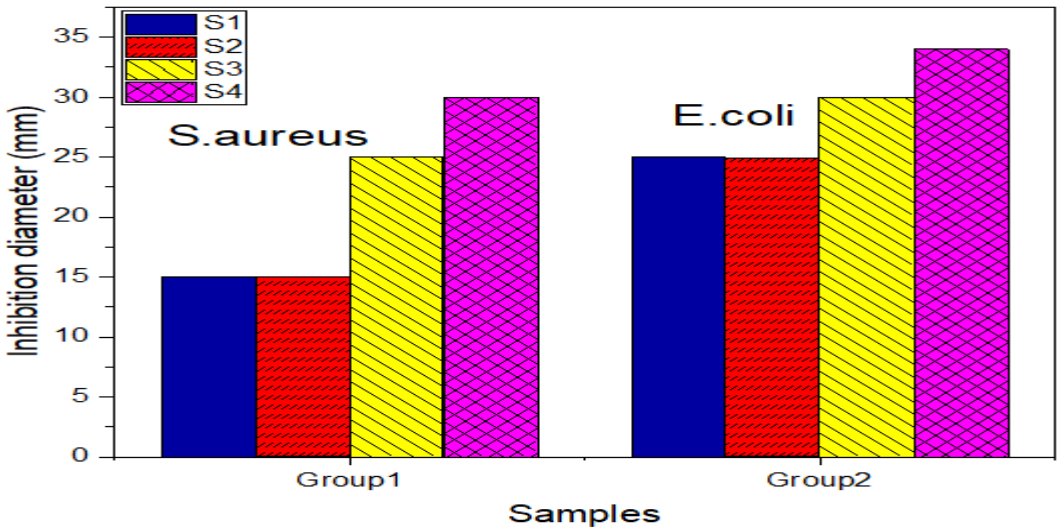

Fig.4.75: Inhibition zone diameter for final textile with different concentrations; 62.5 % (S1), 125 % (S2), 250 % (S3) and 500 %. (S4)

4.14 Antifungal activity

The antifungal potential of the prepared nano fibers textiles (neat blend /G. lucidum (A), neat blend/Capsicum annuum (B), neat blend / I_2 (C), neat blend / Ocimum basilicum oil, neat blend / Rosemary oil, and neat blend / Laurus nobilis oil) was investigated against Candida strains using agar well diffusion assay. All prepared nano fibers were diluted to four concentrations in Phosphate Buffer solution (PBS) (25, 50, 75 and 100) wt.%.

Result showed that inhibition zone (IZ) for these textiles, increased with increasing the concentration of any of the used additives, as show in table (4.32).

G. lucidum addition increased the inhibition of Candida growth as its concentration increased (Figure 4.76), where the inhibition zones are 7, 8, 11, and 15 mm respectively (Table 4.32). Compared with 25 wt.% G. lucidum, the inhibition efficiency (IE) of 100 wt.% G. lucidum against Candida is 114 % [212].

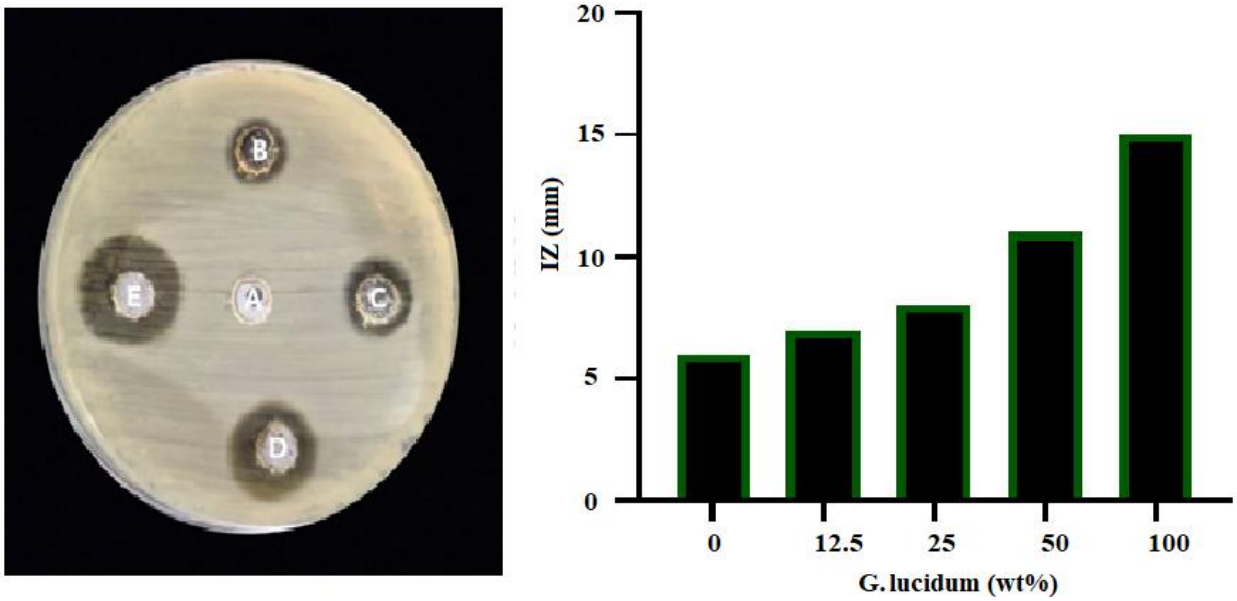

Fig.4.76: Antifungal activity against Candida as a function of G. lucidum content.

Capsicum annum addition causes less inhibition ability (Figure 4.77), where the inhibition zone span extends from 7 mm to 10 mm only and the IE reached to 42% (compared with 25 wt.% Capsicum annum

concentration). Our results are close to results of (Alan Chrisleyr Maracahipes.et al.) [213]. Same results exactly obtained with Ocimum basilicum oil (Figure 4.78). The obtained results are close to results of (Neveen Helmy Abou El-Soud.et al.) [214].

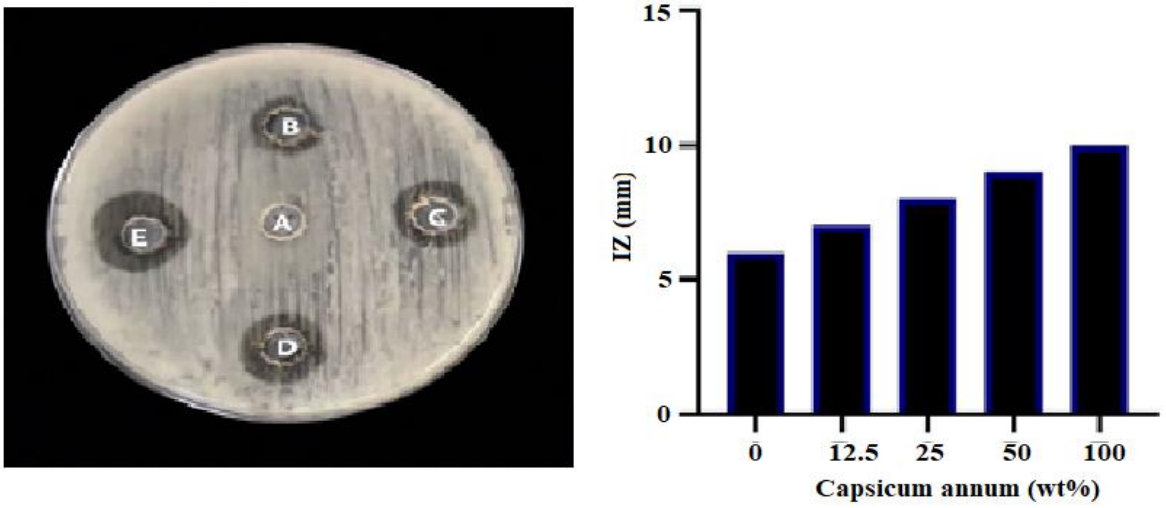

Fig.4.78: Antifungal activity against Candida as a function of Capsicum annum content.

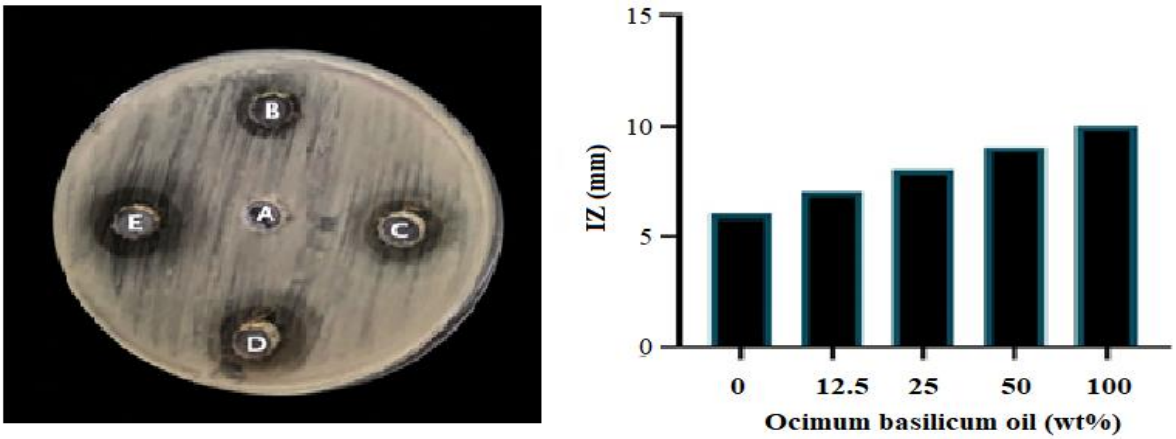

Fig.4.79: Antifungal activity against Candida as a function of Ocimum basilicum oil content.

Anti-Candida activity I_2 addition enlarged the inhibition zone up to 16 mm (Figure 4.80) and the IE reached to 100%. Our results are similar to results of (Sergio Cuellar-Rufino.et al.) [215].

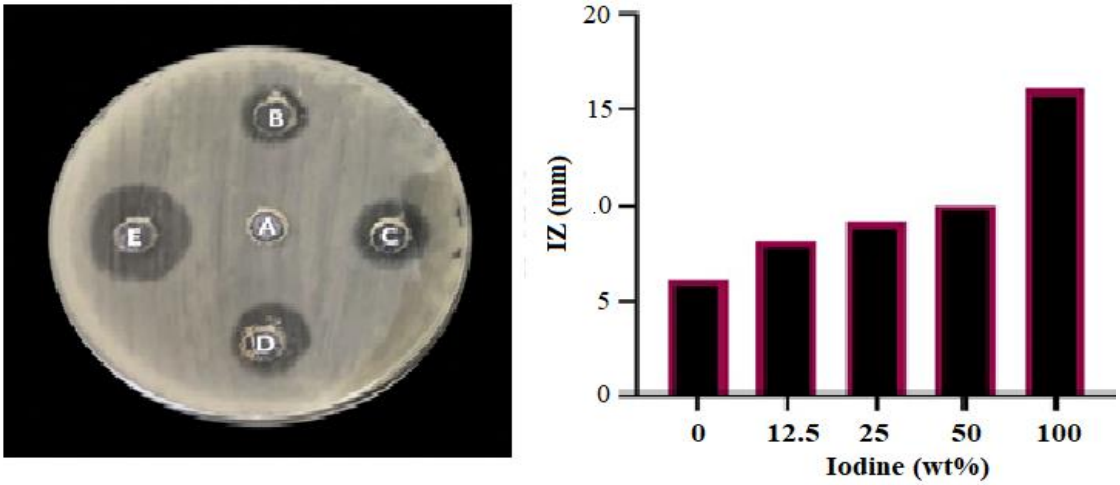

Fig.4.81: Antifungal activity against candida. As a function of Iodine content.

Rosemary oil addition enlarged the antifungal span up to 17 mm (Figure 4.82) and the IE reached to 142.8%. These results are close to the results of (Bernadya Yogatri Anjuwita Saputri.et al) [216].

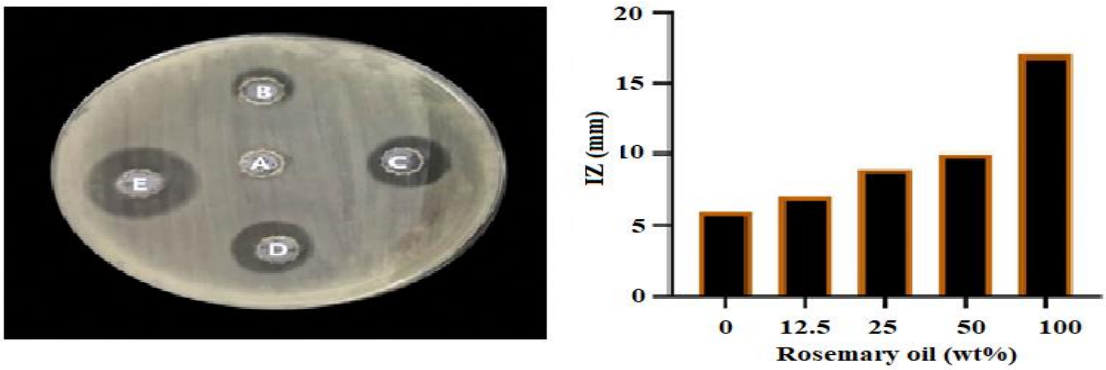

Fig.4.82: Antifungal activity against Candida as a function of Resomary oil content.

Laurus nobilis oil addition increased the inhibition zone up to 14 mm (Figure 4.83) and the IE reached 75%. L. nobilis EO has antifungal activity probably due to the presence of the major monoterpenes and sesquiterpenes identified, likely acts interfering with the cell wall biosynthesis and ionic permeability of the membrane and has deleterious effects on Candida albicans biofilm adhesion and formation. As this EO is free to use, safe and with negligible toxicity according to the Food and Drug Administration (FDA), it could be considered a promising target for drug development [217].

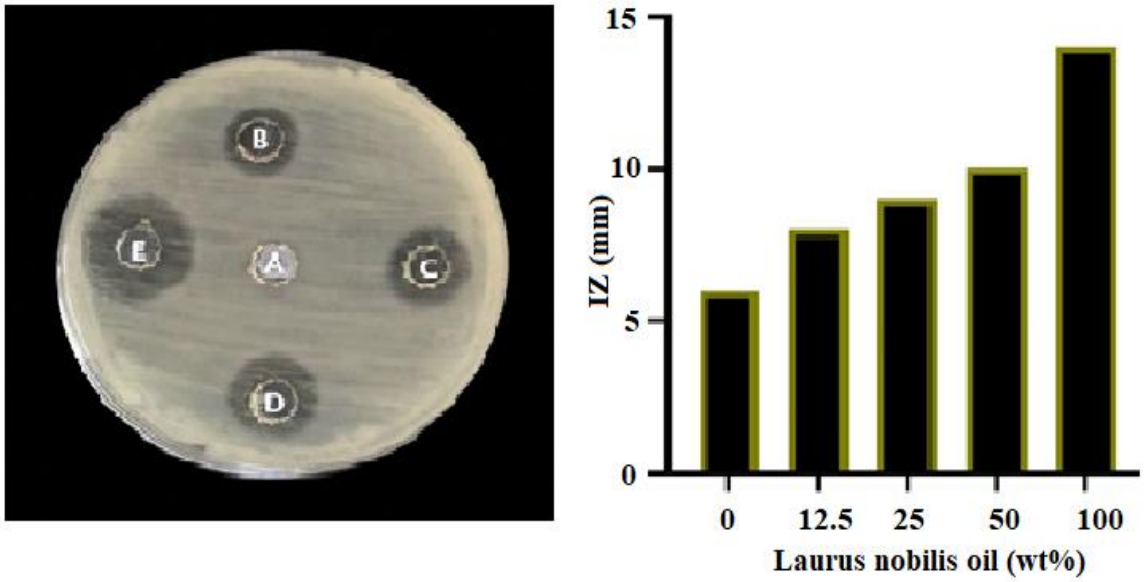

Fig4.84: Antifungal activity against Candida as a function of Laurus nobilis oil content.

The final textile shows more activity against Candida than other textiles (Figure 4.85), where the inhibition zone enlarged up to 20mm and the IE reached to 122.22%.

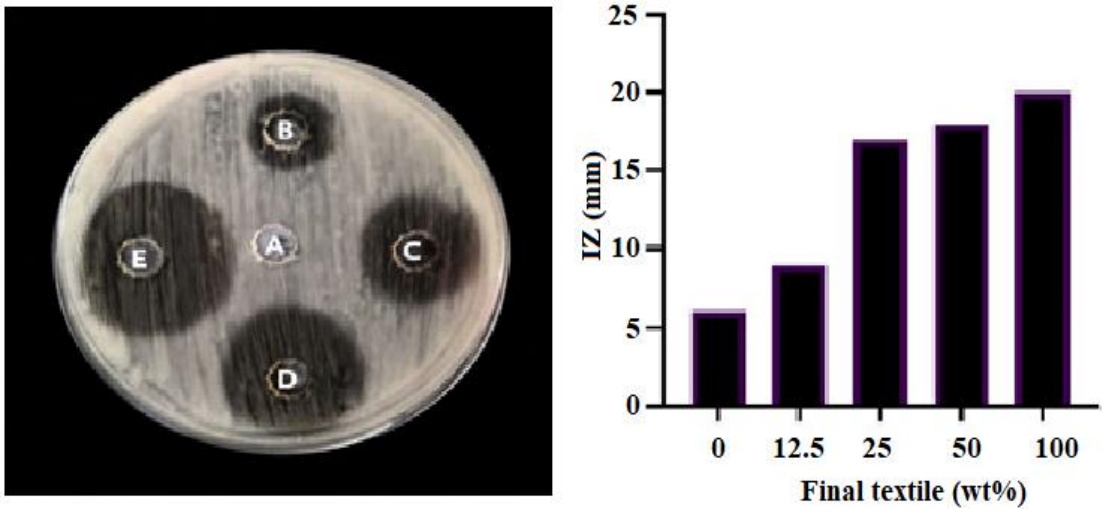

Fig.4.85: Antifungal activity of (final sample) against Candida.

Many researchers reported that essential oil of plants was able to inhibit both growth and/or mycotoxin production. The anti-aflatoxigenic actions of essential oil may be related to inhibition of the ternary steps of aflatoxin biosynthesis involving lipid peroxidation and oxygenation. In addition, essential oils protect the cells from harmful impact of aflatoxins through two

possible mechanisms firstly by reducing DNA binding formation of aflatoxins, secondly by reacting with reactive oxygen species (ROS) increased by aflatoxins [214].

Table (4.32): Antifungal activities of the prepared nano fiber textiles against Candida

Con. (%)	**Inhibition Zone Diameter (IZ) for textile with:**						
	G. lucidum	Capsicum annuum	I_2	Ocimum basilicum oil	Rosemary oil	Laurus nobilis oil	Final textile
25	7	7	8	7	7	8	9
50	8	8	9	8	9	9	17
75	11	9	10	9	10	10	18
100	15	10	16	10	17	14	20

4.15 Cell Viability

Figure 4.86 shows the MTT results obtained for 7 days of culture. The biological response of the scaffolds was examined by MTT analysis. The increase in absorbance value is directly related to the number of viable cells, which increase for the textile selected during the culture period. Our results indicate that Human dermal fibroblast (HDF) cell line attached to the samples. The attachment was significantly high for all the mention periods. Results indicate no major cytotoxic secretion for all samples.

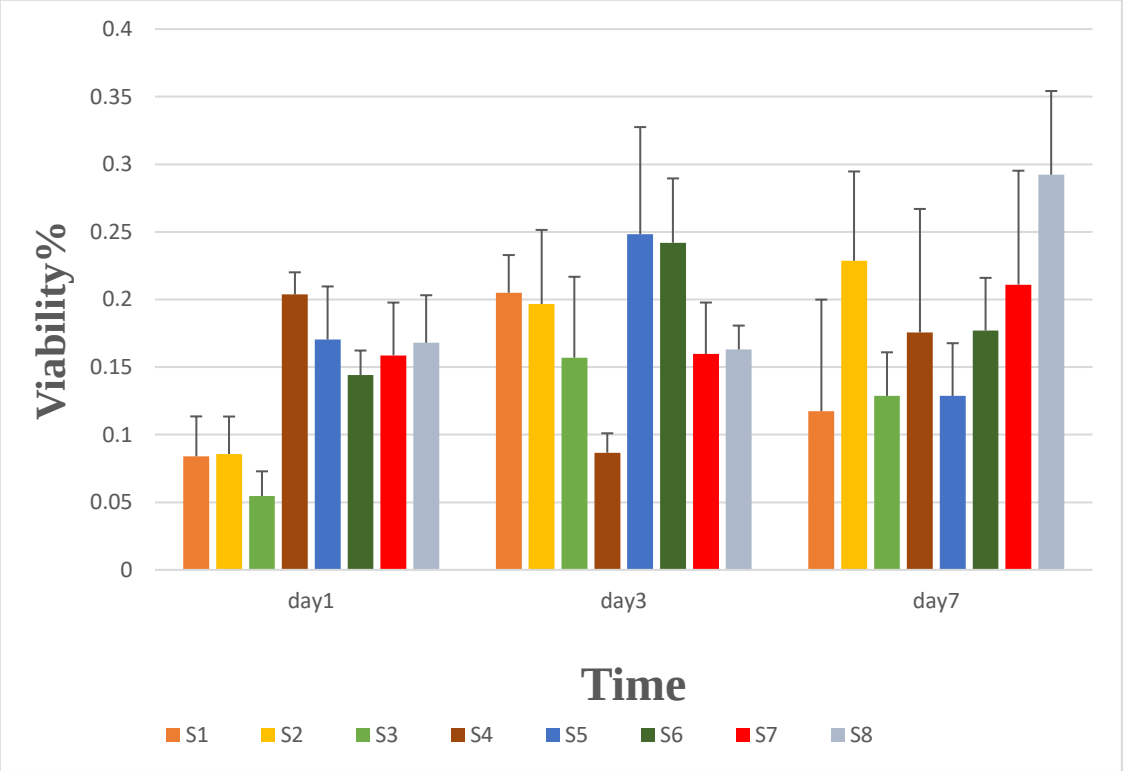

Fig.4.86: The Viability of Human dermal fibroblast Cell Seeded on textiles (S1: neat blend, S2: neat blend / Capsicum annuum, S3: neat blend/ G. lucidum, S4: neat blend / I_2, S5: neat blend /Ocimum basilicum oil, S6: neat blend /Rosemary oil, S7: neat blend /Laurus nobilis oil and S8: final textile) After 7 Days.

4.16 Monitoring the healing rate of injured mice by final textile

Because of that the final textile shows the highest antibacterial and antifungal activities, this textile was applied on the injured mice to follow its effect upon the healing rates (Figure 4.87).

Mice with the same sex (male) and of the same age were divided into three groups (each group with five mice) to monitor this effect. The first group (a) considered as negative control (without treatment), the second group (b) as a positive control with TEBADERM (Collagen matrix dressing), while the third group (c) represents the injured mice whom treated with the final textile nano fibers. The healing tendency for all samples was monitored daily by taking photos. It is clear, that after five days, the mice treated with the nano

fiber textile were completely healed while the other wounds remained wet, redness and there is some coagulation. That means that the final electrospun nano fiber is better than the traditional TEBADERM dressings due to the many active ingredients in the current dressing.

Days	A	B	C
1			
3	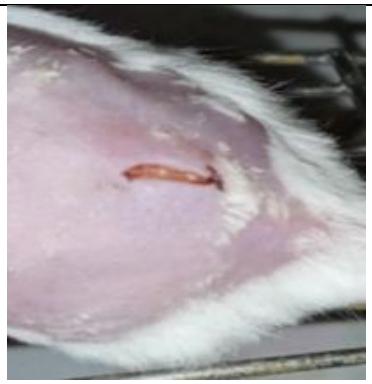		
5			

Fig.4.87: Photos monitoring the healing rate of injured mice (a) control negative (b) control positive (c) treated with electrospum nanofibers.

Chapter Five

Conclusions and Recommendations

5.1Conclusions: -

The following conclusions can be summarized from the results and the following conclusions can be included:

1. Polymeric solution studies show that viscosity, surface tension, and electrical conductivity all significantly affect the behavior of electrospun fibers. When Coll. and HAc are added to PVA, the viscosity drops significantly. PVA solution and all its Coll. and HAc bio blends showed a non-Newtonian behavior and the shear thinning phenomenon. The surface tension of binary solutions was raised when Coll. and HAc were added to solutions, and their electrical conductivity was enhanced as well.
2. The addition of oils and solids to neat blend (PVA:7%Coll.:5.5HAc) increased viscosity. The following is the order of viscosity: G. lucidum > L.nobilis EO > Rosemary oil > I_2 > Ocimum basilicum oil > Capsicum annuum > neat bend. But combining these additives into a neat blend led to a decrease in viscosity. Most of the used additives increased the surface tension of the tertiary blend except L.nobilis EO. The conductivity of most additives increased with increasing their concentration except Rosemary oil.
3. FTIR analysis shows that the only interaction between the polymeric chains of the (PVA: Coll.: HAc) is physical and that there is no chemical reaction between them. The addition of oils and solids to neat blend proved no losses of any net blend component and no chemical reaction among them.
4. Coll. or HAc additions increase the wettability so some textiles possess the super hydrophilic character, which is desired in wound healing applications.

5. Some formulations of capsicum annuum, iodine, and L. nobilis essential oil increased wettability. This implies the medicine can be released rapidly toward the wounded skin as the dressings deteriorate.
6. The final solution has a greater contact angle than the tertiary net blend (41^o vs. 52^o). Because of this, we needed to find a way to increase the wettability of the nanofiber fabrics we produced by gradually altering the operating parameters.
7. It was found through morphological testing of nanofibers that their smoothness and diameter reduction occurred after the addition of Coll. and HAc. As a result, the surface's roughness and porosity were decreased.
8. The average diameter for the final textile, increased compared with the neat blend, and The resultant morphology is crosslinked, fused nanofibers with some beads and the textile has medium porosity.
9. The increase in the roughness of the final textile due to the increase in the diameter of the fibers means that these rough textiles resist bacterial collection. And led to an increase in The Surface porosity of fibers and increased hydrophilicity.
10. Tg increased after Coll. and HAc were added to PVA, and this led to an increase in enthalpy and an improvement in the thermal stability of the formed textiles, which predicts an improvement in their mechanical properties, which positively affects the safety of their handling and the length of their storage periods.
11. The findings from the UV-Vis spectra, the following is the order of absorbance: tertiary blend > PVA: 5.5 % HAc > PVA: 7% Collagen > PVA. This shows that HAc and Collagen additions to dressings improve mechanical qualities without inhibiting vitamin D synthesis in the skin; rather, the increased absorption of rays from sunlight enhances vitamin D synthesis. Also, the heat generated within the skin

tissue kills bacteria there, which speeds up the wound healing process; enhances its antibacterial performance.

12. Also, the addition of any of the additives to the neat blend resulted in greater absorption of light across all three wavelength ranges (UV, Visible, and Infrared). When this occurs, the wound dressing functions more effectively.
13. The antioxidant activity results, noticed the inhibition of DPPH activity increased for the final sample which was proven in the FTIR curve.
14. From biological test results, the antibacterial inhibition increased for the final textile because of the incorporation of all additives in the neat blend. In addition, the antifungal properties increment by increasing the inhibition zone diameter against candida.
15. The healing action for injured mice with the prepared films is better than for TEBADERM treatment, and complete healing is achieved within five days.
16. The hardness of the final textile decreased, which means that the new dressing will be much more flexible in its response to the applied load. These ductile dressings have low strength, low brittleness, low wear resistance and degraded easily.

5.2 Suggestions and Recommendations for Further Studies

1- Preparation of dressing for Tissue Engineering by using another technique such as Coaxial Electrospinning.

2- Altering the pumping settings to achieve the optimal morphology of the resultant fibers, such as altering the solution concentrations, the target being employed, or the needle diameter.

3- Finding another natural substance that has antibacterial activity and using alginate instead of PVA.

Reference

[1] J. Sunthornvarabhas, P. Chatakanonda, K. Piyachomkwan, G. G. Chase, H. J. Kim, and K. Sriroth, "Physical structure behavior to wettability of electrospun poly(lactic acid)/polysaccharide composite nanofibers," *Adv. Compos. Mater.*, vol. 22, no. 6, pp. 401–409, 2013, doi: 10.1080/09243046.2013.843815.

[2] K. S. Rho *Rho, Kyong Su ,Jeong, Lim, Lee, Gene Seo, Byoung Moo Park, Yoon Jeong Hong, Seong Doo Roh, Sangho Cho, Jae Jin Park, Won HoMin, Byung Moo.*, "Electrospinning of collagen nanofibers: Effects on the behavior of normal human keratinocytes and early-stage wound healing," *Biomaterials*, vol. 27, no. 8, pp. 1452–1461, 2006, doi: 10.1016/j.biomaterials.2005.08.004.

[3] X. Q. Dou, D. Zhang, and C. L. Feng, "Wettability of supramolecular nanofibers for controlled cell adhesion and proliferation," *Langmuir*, vol. 29, no. 49, pp. 15359–15366, 2013, doi: 10.1021/la4040276.

[4] S. Al-musawi, S. Albukhaty, and H. Al-karagoly, "molecules Antibacterial Activity of Honey / Chitosan Nanofibers," *molecules Article*, vol. 25. p. 4770, 2020. Available: www.mdpi.com/journal/molecules

[5] B.Azimi, H. Maleki, L.Zavagna, J.de la Ossa, S.Linari, A.Lazzeri, S.Danti, "Bio-based electrospun fibers for wound healing," *J. Funct. Biomater.*, vol. 11, no. 3, 2020, doi: 10.3390/JFB11030067.

[6] J. K. Ahmed, A. J. Braihi, and D. Kadham, "(Polyvinyl Alcohol-Iodine) Bio-Composites and Their Applications," vol. 321185223, no. October, 2017.

[7] A. J. Braihi, J. K. Ahmed, and R. S. Jabbar, "Prevent Intravenous Therapy (IV) Contamination by Addition of Magnesium Oxide Nanoparticles to Silicone Rubber," *J. Univ. Babylon Eng. Sci.*, vol. 27, no. 1, pp. 409–417, 2019, doi: 10.29196/jubes.v27i1.2195.

[8] Y. Kong Kong, Y.Zhao, X.Chen, K.Yao, L,Zhang, Q.Han, Zhang, Luzhong Ling, Jue Wang, Yongjun Yang, Yumin "Degradable tough chitosan dressing for skin wound recovery," *Nanotechnol. Rev.*, vol. 9, no. 1, pp. 1576–1585, 2020, doi: 10.1515/ntrev-2020-0105.

[9] H. S. Sofi, T. Akram, A. H. Tamboli, A. Majeed, N. Shabir, and F. A. Sheikh, "Novel lavender oil and silver nanoparticles simultaneously loaded onto polyurethane nanofibers for wound-healing applications," *Int. J. Pharm.*, vol. 569, no. April, 2019, doi: 10.1016/j.ijpharm.2019.118590.

[10] J. P. Chen, G. Y. Chang, and J. K. Chen, "Electrospun collagen/chitosan nanofibrous membrane as wound dressing," *Colloids Surfaces A Physicochem. Eng. Asp.*, vol. 313–314, pp. 183–188, 2008, doi: 10.1016/j.colsurfa.2007.04.129.

[11] E. J. Mulholland, "Electrospun Biomaterials in the Treatment and Prevention of Scars in Skin Wound Healing," *Front. Bioeng. Biotechnol.*, vol. 8, no. June 2020, pp. 1–15, 2020, doi: 10.3389/fbioe.2020.00481.

[12] S. J. Liu, Y. C. Kau, C. Y. Chou, J. K. Chen, R. C. Wu, and W. L. Yeh, "Electrospun PLGA/collagen nanofibrous membrane as early-stage wound dressing," *J. Memb. Sci.*, vol. 355, no. 1–2, pp. 53–59, 2010, doi: 10.1016/j.memsci.2010.03.012.

[13] M. Gizaw, J. Thompson, A. Faglie, S. Y. Lee, P. Neuenschwander, and S. F. Chou, "Electrospun fibers as a dressing material for drug and biological agent delivery in wound healing applications," *Bioengineering*, vol. 5, no. 1, pp. 1–28, 2018, doi: 10.3390/bioengineering5010009.

[14] K. C. Gupta, A. Haider, Y. R. Choi, and I. K. Kang, "Nanofibrous scaffolds in biomedical applications," *Biomater. Res.*, vol. 18, no. 1, pp. 1–11, 2014, doi: 10.1186/2055-7124-18-5.

[15] I. Last, Y. Levy, and J. Jortner, "Beyond the Rayleigh instability limit for multicharged finite systems: From fission to Coulomb explosion,"

Proc. Natl. Acad. Sci. U. S. A., vol. 99, no. 14, pp. 9107–9112, 2002, doi: 10.1073/pnas.142253999.

[16] H. Wu, W. Pan, D. Lin, and H. Li, "Electrospinning of ceramic nanofibers: Fabrication, assembly and applications," *J. Adv. Ceram.*, vol. 1, no. 1, pp. 2–23, 2012, doi: 10.1007/s40145-012-0002-4.

[17] R. Ranjith, S. Balraj, J. Ganesh, and M. C. John Milton, "Therapeutic agents loaded chitosan-based nanofibrous mats as potential wound dressings: A review," *Mater. Today Chem.*, vol. 12, pp. 386–395, 2019, doi: 10.1016/j.mtchem.2019.03.008.

[18] M. Liu, X. P. Duan, Y. M. Li, D. P. Yang, and Y. Z. Long, "Electrospun nanofibers for wound healing," *Mater. Sci. Eng. C*, vol. 76, pp. 1413–1423, 2017, doi: 10.1016/j.msec.2017.03.034.

[19] B. Wang, C. Xu, F. Xu, and T. Lu, "Electrospinning of poly(ethylene-co-vinyl alcohol) nanofibres encapsulated with Ag nanoparticles for skin wound healing," *J. Nanomater.*, vol. 2011, 2011, doi: 10.1155/2011/201834.

[20] J. M. Morais, F. Papadimitrakopoulos, and D. J. Burgess, "Biomaterials/tissue interactions: Possible solutions to overcome foreign body response," *AAPS J.*, vol. 12, no. 2, pp. 188–196, 2010, doi: 10.1208/s12248-010-9175-3.

[21] M. Niinomi, "Recent research and development in metallic materials for biomedical, dental and healthcare products applications," *Mater. Sci. Forum*, vol. 539–543, no. PART 1, pp. 193–200, 2007, doi: 10.4028/0-87849-428-6.193.

[22] M. Mehdizadeh and J. Yang, "Design Strategies and Applications of Tissue Bioadhesives," *Macromol. Biosci.*, vol. 13, no. 3, pp. 271–288, 2013, doi: 10.1002/mabi.201200332.

[23] R. Nayak, R. Padhye, I. L. Kyratzis, Y. B. Truong, and L. Arnold, "Recent advances in nanofibre fabrication techniques," *Text. Res. J.*, vol. 82, no. 2, pp. 129–147, 2012, doi: 10.1177/0040517511424524.

[24] P. Kumar, “Effect of Collector on Electrospinning To Fabricate Aligned Nanofiber Effect of Collector on Electrospinning To Fabricate Aligned Nanofiber,” *Natl. Inst. Technol.*, pp. 1–40, 2012, [Online]. Available: http://ethesis.nitrkl.ac.in/3825/1/108BM019_PankajKumar.pdf

[25] E. Stojanovska *et al.*, “A review on non-electro nanofibre spinning techniques,” *RSC Adv.*, vol. 6, no. 87, pp. 83783–83801, 2016, doi: 10.1039/c6ra16986d.

[26] J. Wang and A. S. Nain, “Suspended micro/nanofiber hierarchical biological scaffolds fabricated using non-electrospinning STEP technique,” *Langmuir*, vol. 30, no. 45, pp. 13641–13649, 2014, doi: 10.1021/la503011u.

[27] X. Zhang and Y. Lu, “Centrifugal spinning: An alternative approach to fabricate nanofibers at high speed and low cost,” *Polym. Rev.*, vol. 54, no. 4, pp. 677–701, 2014, doi: 10.1080/15583724.2014.935858.

[28] V. Beachley and X. Wen, “Polymer nanofibrous structures: Fabrication, biofunctionalization, and cell interactions,” *Prog. Polym. Sci.*, vol. 35, no. 7, pp. 868–892, 2010, doi: 10.1016/j.progpolymsci.2010.03.003.

[29] W.-J. Li, R. M. Shanti, and R. S. Tuan, *Electrospinning Technology for Nanofibrous Scaffolds in Tissue Engineering*, vol. 9. 2007. doi: 10.1002/9783527610419.ntls0097.

[30] T. Lu, Y. Li, and T. Chen, “Techniques for fabrication and construction of three-dimensional scaffolds for tissue engineering,” *Int. J. Nanomedicine*, vol. 8, pp. 337–350, 2013, doi: 10.2147/IJN.S38635.

[31] S. Ramakrishna, K. Fujihara, W. E. Teo, T. C. Lim, and Z. Ma, *An introduction to electrospinning and nanofibers*. 2005. doi: 10.1142/5894.

[32] N. G. Rim, C. S. Shin, and H. Shin, “Current approaches to electrospun nanofibers for tissue engineering,” *Biomed. Mater.*, vol. 8, no. 1, 2013,

doi: 10.1088/1748-6041/8/1/014102.

[33] Z. Kurban and E. Doctorate, “Electrospun nanostructured composite fibres for hydrogen storage applications Zeynep Kurban,” *J. Polym. Sci. Part B Polym. Phys.*, vol. 47, no. March, pp. 261–275, 2011.

[34] C. J. Buchko, L. C. Chen, Y. Shen, and D. C. Martin, “Processing and microstructural characterization of porous biocompatible protein polymer thin films,” *Polymer (Guildf).*, vol. 40, no. 26, pp. 7397–7407, 1999, doi: 10.1016/S0032-3861(98)00866-0.

[35] J. Kameoka Kameoka, Orth, Reid Yang, Yanou Czaplewski, David Mathers, RoberT Coates, Geoffrey W. Craighead, H. G. , “A scanning tip electrospinning source for deposition of oriented nanofibres,” *Nanotechnology*, vol. 14, no. 10, pp. 1124–1129, 2003, doi: 10.1088/0957-4484/14/10/310.

[36] X. Zong, K. Kim, D. Fang, S. Ran, B. S. Hsiao, and B. Chu, “Structure and process relationship of electrospun bioabsorbable nanofiber membranes,” *Polymer (Guildf).*, vol. 43, no. 16, pp. 4403–4412, 2002, doi: 10.1016/S0032-3861(02)00275-6.

[37] P. Schümmer and K. H. Tebel, “A new elongational rheometer for polymer solutions,” *J. Nonnewton. Fluid Mech.*, vol. 12, no. 3, pp. 331–347, 1983, doi: 10.1016/0377-0257(83)85006-X.

[38] W. K. Son, J. H. Youk, T. S. Lee, and W. H. Park, “Electrospinning of ultrafine cellulose acetate fibers: Studies of a new solvent system and deacetylation of ultrafine cellulose acetate fibers,” *J. Polym. Sci. Part B Polym. Phys.*, vol. 42, no. 1, pp. 5–11, 2004, doi: 10.1002/polb.10668.

[39] K. H. Lee, H. Y. Kim, M. S. Khil, Y. M. Ra, and D. R. Lee, “Characterization of nano-structured poly(ε-caprolactone) nonwoven mats via electrospinning,” *Polymer (Guildf).*, vol. 44, no. 4, pp. 1287–1294, 2003, doi: 10.1016/S0032-3861(02)00820-0.

[40] C. M. Hsu and S. Shivkumar, “N,N-dimethylformamide additions to the solution for the electrospinning of poly(ε-caprolactone)

nanofibers," *Macromol. Mater. Eng.*, vol. 289, no. 4, pp. 334–340, 2004, doi: 10.1002/mame.200300224.

[41] S. Megelski, J. S. Stephens, D. Bruce Chase, and J. F. Rabolt, "Micro- and nanostructured surface morphology on electrospun polymer fibers," *Macromolecules*, vol. 35, no. 22, pp. 8456–8466, 2002, doi: 10.1021/ma020444a.

[42] J. Y. Park and I. H. Lee, "Relative humidity effect on the preparation of porous electrospun polystyrene fibers," *J. Nanosci. Nanotechnol.*, vol. 10, no. 5, pp. 3473–3477, 2010, doi: 10.1166/jnn.2010.2349.

[43] M. Halabi *et al.*, "Electrospun anion-conducting ionomer fibers-effect of humidity on final properties," *Polymers (Basel).*, vol. 12, no. 5, pp. 1–12, 2020, doi: 10.3390/POLYM12051020.

[44] P. K. Baumgarten, "Electrostatic spinning of acrylic microfibers," *J. Colloid Interface Sci.*, vol. 36, no. 1, pp. 71–79, 1971, doi: 10.1016/0021-9797(71)90241-4.

[45] M. M. Demir, I. Yilgor, E. Yilgor, and B. Erman, "Electrospinning of polyurethane fibers," *Polymer (Guildf).*, vol. 43, no. 11, pp. 3303–3309, 2002, doi: 10.1016/S0032-3861(02)00136-2.

[46] C. Mit-Uppatham, M. Nithitanakul, and P. Supaphol, "Ultrafine electrospun polyamide-6 fibers: Effect of solution conditions on morphology and average fiber diameter," *Macromol. Chem. Phys.*, vol. 205, no. 17, pp. 2327–2338, 2004, doi: 10.1002/macp.200400225.

[47] B. Sundaray, V. Subramanian, T. S. Natarajan, R. Z. Xiang, C. C. Chang, and W. S. Fann, "Electrospinning of continuous aligned polymer fibers," *Appl. Phys. Lett.*, vol. 84, no. 7, pp. 1222–1224, 2004, doi: 10.1063/1.1647685.

[48] Q. P. Pham, U. Sharma, and A. G. Mikos, "Electrospinning of polymeric nanofibers for tissue engineering applications: A review," *Tissue Eng.*, vol. 12, no. 5, pp. 1197–1211, 2006, doi: 10.1089/ten.2006.12.1197.

[49] K. Singh, A. Ohlan, P. Saini, and S. K. Dhawan, “composite – super paramagnetic behavior and variable range hopping 1D conduction mechanism – synthesis and characterization,” *Polym. Adv. Technol.*, no. November 2007, pp. 229–236, 2008, doi: 10.1002/pat.

[50] C. Yang, Z. Jia, J. Liu, Z. Xu, Z. Guan, and L. Wang, “Guiding effect of surface electric field of collector on deposited electrospinning fibers,” *IEEE Trans. Dielectr. Electr. Insul.*, vol. 16, no. 3, pp. 785–792, 2009, doi: 10.1109/TDEI.2009.5128519.

[51] N. M. Neves, R. Campos, A. Pedro, J. Cunha, F. Macedo, and R. L. Reis, “Patterning of polymer nanofiber meshes by electrospinning for biomedical applications,” *Int. J. Nanomedicine*, vol. 2, no. 3, pp. 433–448, 2007.

[52] A. Krishnan K and S. Thomas, “Recent advances on herb-derived constituents-incorporated wound-dressing materials: A review,” *Polymers for Advanced Technologies*, vol. 30, no. 4. pp. 823–838, 2019. doi: 10.1002/pat.4540.

[53] V. Vivcharenko and A. Przekora, “Modifications of wound dressings with bioactive agents to achieve improved pro-healing properties,” *Appl. Sci.*, vol. 11, no. 9, 2021, doi: 10.3390/app11094114.

[54] K. Nuutila and E. Eriksson, “Moist Wound Healing with Commonly Available Dressings,” *Adv. Wound Care*, vol. 10, no. 12, pp. 685–698, 2021, doi: 10.1089/wound.2020.1232.

[55] A. M. Hajialyani M, Tewari D, Sobarzo-Sánchez E, Nabavi SM, Farzaei MH, *Int. J. Nanomedicine*, vol. 2018, no. 13, p. 5023—5043, 2018, doi: 10.2147/IJN.S174072.

[56] M. Palencia, T. A. Lerma, V. Garcés, M. A. Mora, J. M. Martínez, and S. L. Palencia, “Biopolymers and bioplastics,” *Eco-friendly Funct. Polym.*, pp. 23–34, 2021, doi: 10.1016/b978-0-12-821842-6.00028-2.

[57] G. Bachir and B. Abouni, “Escherichia coli and Staphylococcus aureus most common source of infection,” *Battle Against Microb. Pathog.*

Basic Sci., vol. 2, no. January 2015, pp. 637–48, 2015.

[58] R. C. Anderson and P. L. Yu, "Factors affecting the antimicrobial activity of ovine-derived cathelicidins against E. coli 0157:H7," *Int. J. Antimicrob. Agents*, vol. 25, no. 3, pp. 205–210, 2005, doi: 10.1016/j.ijantimicag.2004.10.010.

[59] M. Rezaei, M. Komijani, and S. Morteza, "Bacteriostatic Agents," *A Search Antibact. Agents*, no. September, 2012, doi: 10.5772/45652.

[60] S. Alven, S. Peter, Z. Mbese, and B. A. Aderibigbe, "Polymer-Based Wound Dressing Materials Loaded with Bioactive Agents: Potential Materials for the Treatment of Diabetic Wounds," *Polymers (Basel).*, vol. 14, no. 4, 2022, doi: 10.3390/polym14040724.

[61] F. Scialò, D. J. Fernández-Ayala, and A. Sanz, "Role of mitochondrial reverse electron transport in ROS signaling: Potential roles in health and disease," *Front. Physiol.*, vol. 8, no. JUN, pp. 1–7, 2017, doi: 10.3389/fphys.2017.00428.

[62] R. Z. Zhao, S. Jiang, L. Zhang, and Z. Bin Yu, "Mitochondrial electron transport chain, ROS generation and uncoupling (Review)," *Int. J. Mol. Med.*, vol. 44, no. 1, pp. 3–15, 2019, doi: 10.3892/ijmm.2019.4188.

[63] I. M. Comino-Sanz, M. D. López-Franco, B. Castro, and P. L. Pancorbo-Hidalgo, "The role of antioxidants on wound healing: A review of the current evidence," *J. Clin. Med.*, vol. 10, no. 16, 2021, doi: 10.3390/jcm10163558.

[64] M. C. Sanchez, S. Lancel, E. Boulanger, and R. Neviere, "Targeting oxidative stress and mitochondrial dysfunction in the treatment of impaired wound healing: A systematic review," *Antioxidants*, vol. 7, no. 8, pp. 1–14, 2018, doi: 10.3390/antiox7080098.

[65] C. Dunnill Dunnill, Patton, ThomasBrennan, James Barrett, John Dryden, Matthew Cooke, Jonathan Leaper, David Georgopoulos, Nikolaos "Reactive oxygen species (ROS) and wound healing: the functional role of ROS and emerging ROS-modulating technologies for

augmentation of the healing process," *Int. Wound J.*, vol. 14, no. 1, pp. 89–96, 2017, doi: 10.1111/iwj.12557.

[66] S. D. Fitzmaurice, R. K. Sivamani, and R. R. Isseroff, "Antioxidant therapies for wound healing: A clinical guide to currently commercially available products," *Skin Pharmacol. Physiol.*, vol. 24, no. 3, pp. 113–126, 2011, doi: 10.1159/000322643.

[67] R. Xu Xu, Xia, Hesheng He, Weifeng Li, Zhichao Zhao, Jian Liu, Bo Wang, Yuzhen Lei, Qiang Kong, Yi Bai, Yang Yao, ZhihuiYan, Rongshuai Li, Haisheng Zhan, Rixing Yang, Sisi Luo, Gaoxing Wu, Jun., "Controlled water vapor transmission rate promotes wound-healing via wound re-epithelialization and contraction enhancement," *Sci. Rep.*, vol. 6, no. April, pp. 1–12, 2016, doi: 10.1038/srep24596.

[68] F. M. Andreopoulos and I. Persaud, "Delivery of basic fibroblast growth factor (bFGF) from photoresponsive hydrogel scaffolds," *Biomaterials*, vol. 27, no. 11, pp. 2468–2476, 2006, doi: 10.1016/j.biomaterials.2005.11.019.

[69] Z. Ujang, A. H. A. Rashid, S. K. Suboh, A. S. Halim, and C. K. Lim, "Physical properties and biocompatibility of oligochitosan membrane film as wound dressing," *J. Appl. Biomater. Funct. Mater.*, vol. 12, no. 3, pp. 155–162, 2014, doi: 10.5301/jabfm.5000190.

[70] D. C. Aduba and H. Yang, "Polysaccharide fabrication platforms and biocompatibility assessment as candidate wound dressing materials," *Bioengineering*, vol. 4, no. 1, pp. 1–16, 2017, doi: 10.3390/bioengineering4010001.

[71] A. A. Dongargaonkar, G. L. Bowlin, and H. Yang, "Electrospun blends of gelatin and gelatin-dendrimer conjugates as a wound-dressing and drug-delivery platform," *Biomacromolecules*, vol. 14, no. 11, pp. 4038–4045, 2013, doi: 10.1021/bm401143p.

[72] S. Tavakoli and A. S. Klar, "Advanced hydrogels as wound dressings," *Biomolecules*, vol. 10, no. 8, pp. 1–20, 2020, doi: 10.3390/biom10081169.

[73] M. Rippon, P. Davies, and R. White, "Taking the trauma out of wound

care: The importance of undisturbed healing," *J. Wound Care*, vol. 21, no. 8, pp. 359–368, 2012, doi: 10.12968/jowc.2012.21.8.359.

[74] J. C. Fernandez-Toledano, T. D. Blake, P. Lambert, and J. De Coninck, "On the cohesion of fluids and their adhesion to solids: Young's equation at the atomic scale," *Adv. Colloid Interface Sci.*, vol. 245, no. 2016, pp. 102–107, 2017, doi: 10.1016/j.cis.2017.03.006.

[75] C. W. Extrand and Y. Kumagai, "An Experimental Study of Contact Angle Hysteresis," vol. 383, no. 191, pp. 378–383, 1997.

[76] G. Zhao, Schwartz, Z. Wieland, M. Rupp, F. Geis-Gerstorfer, J. Cochran, D. L.
Boyan, B. D. "High surface energy enhances cell response to titanium substrate microstructure," *J. Biomed. Mater. Res. - Part A*, vol. 74, no. 1, pp. 49–58, 2005, doi: 10.1002/jbm.a.30320.

[77] D. Tian, Y. Song, and L. Jiang, "Patterning of controllable surface wettability for printing techniques," *Chem. Soc. Rev.*, vol. 42, no. 12, pp. 5184–5209, 2013, doi: 10.1039/c3cs35501b.

[78] J. T. Korhonen, M. Kettunen, R. H. A. Ras, and O. Ikkala, "Hydrophobic nanocellulose aerogels as floating, sustainable, reusable, and recyclable oil absorbents," *ACS Appl. Mater. Interfaces*, vol. 3, no. 6, pp. 1813–1816, 2011, doi: 10.1021/am200475b.

[79] C. M. Magin, S. P. Cooper, and A. B. Brennan, "Non-toxic antifouling strategies," *Mater. Today*, vol. 13, no. 4, pp. 36–44, 2010, doi: 10.1016/S1369-7021(10)70058-4.

[80] J. I. Rosales-Leal Rodríguez-Valverde, M. A. Mazzaglia, G.Ramón-Torregrosa, P. J.Díaz-Rodríguez, L.García-Martínez, O.Vallecillo-Capilla, M.Ruiz, C. Cabrerizo-Vílchez, M. A., "Effect of roughness, wettability and morphology of engineered titanium surfaces on osteoblast-like cell adhesion," *Colloids Surfaces A Physicochem. Eng. Asp.*, vol. 365, no. 1–3, pp. 222–229, 2010, doi: 10.1016/j.colsurfa.2009.12.017.

[81] R. N. Wenzel, "Resistance of solid surfaces to wetting by water," *Ind. Eng. Chem.*, vol. 28, no. 8, pp. 988–994, 1936, doi:

10.1021/ie50320a024.

[82] Biolin Scientific, “Effect of Wettability in Biomedical Applications”, [Online]. Available: https://www.biolinchina.com/wp-content/uploads/2020/06/7a3f31f7b72d8c505673ea79c464c57a.pdf

[83] K. Liu, M. Cao, A. Fujishima, and L. Jiang, “Bio-inspired titanium dioxide materials with special wettability and their applications,” *Chem. Rev.*, vol. 114, no. 19, pp. 10044–10094, 2014, doi: 10.1021/cr4006796.

[84] G. P. Chate Kale, Narendra R. Khobragade, Vrushali Rahane, Chinmay Calderón, Marcelo Banerjee, Shashwat S. Khandare, Jayant J., “Selective Cell Isolation by Transferrin Functionalized Silane–Carbon Soot Mediated Superhydrophobic Micropatterns,” *Adv. Mater. Interfaces*, vol. 5, no. 7, pp. 1–6, 2018, doi: 10.1002/admi.201701581.

[85] P. Beyazkilic, U. Tuvshindorj, A. Yildirim, C. Elbuken, and M. Bayindir, “Robust superhydrophilic patterning of superhydrophobic ormosil surfaces for high-throughput on-chip screening applications,” *RSC Adv.*, vol. 6, no. 83, pp. 80049–80054, 2016, doi: 10.1039/c6ra19669a.

[86] L. Sun Sun, Lingyu Guo, Jiahu Chen, Hanxu Zhang, Dagan Shang, Luoran Zhang, Bing Zhao, Yuanjin., “Tailoring Materials with Specific Wettability in Biomedical Engineering,” *Adv. Sci.*, vol. 8, no. 19, pp. 1–34, 2021, doi: 10.1002/advs.202100126.

[87] S. J. Haller and A. T. Dudley, “Mechanotransduction by Membrane Proteins Extracellular mechanotransduction,” *J. Gen. Physiol.*, vol. 154, no. 3, pp. 1–5, 2022.

[88] Y. Zhang, T. L. Chwee, S. Ramakrishna, and Z. M. Huang, “Recent development of polymer nanofibers for biomedical and biotechnological applications,” *J. Mater. Sci. Mater. Med.*, vol. 16, no. 10, pp. 933–946, 2005, doi: 10.1007/s10856-005-4428-x.

[89] Y. Pilehvar-Soltanahmadi, M. Dadashpour, A. Mohajeri, A. Fattahi, R. Sheervalilou, and N. Zarghami, “An Overview on Application of Natural Substances Incorporated with Electrospun Nanofibrous

Scaffolds to Development of Innovative Wound Dressings," *Mini-Reviews Med. Chem.*, vol. 18, no. 5, pp. 414–427, 2017, doi: 10.2174/1389557517666170308112147.

[90] L. Sun Sun, Luyao Gao, Wendong Fu, Xiaoling Shi, Miao Xie, Weihan Zhang, Wen Zhao, Fujian Chen, Xiaofeng, "Enhanced wound healing in diabetic rats by nanofibrous scaffolds mimicking the basketweave pattern of collagen fibrils in native skin," *Biomater. Sci.*, vol. 6, no. 2, pp. 340–349, 2018, doi: 10.1039/c7bm00545h.

[91] A. D. Juncos Bombin, N. J. Dunne, and H. O. McCarthy, "Electrospinning of natural polymers for the production of nanofibres for wound healing applications," *Materials Science and Engineering C*, vol. 114. 2020. doi: 10.1016/j.msec.2020.110994.

[92] E. M. Jones, C. A. Cochrane, and S. L. Percival, "The Effect of pH on the Extracellular Matrix and Biofilms," *Adv. Wound Care*, vol. 4, no. 7, pp. 431–439, 2015, doi: 10.1089/wound.2014.0538.

[93] A. J. Braihi, K. Ahmed, and D. Abbass Kadham, "Preparing Medical (Polyvinyl Alcohol-Iodine) As A Pressure Sensor and Investigating Its Physical Properties," *Int. J. Pharm. Phytopharm. Res.*, vol. 7, no. 1, pp. 34–41, 2017, [Online]. Available: www.eijppr.com

[94] J. Kareem, A. Auda, J. Braihi, and D. Abbass Kadham, "Copolymer Production From Poly(Vinyl Alcohol)," *Engineering Sciences*, no. 26. p. 2018.

[95] G. Rivera-Hernández, M. Antunes-Ricardo, P. Martínez-Morales, and M. L. Sánchez, "Polyvinyl alcohol based-drug delivery systems for cancer treatment," *Int. J. Pharm.*, vol. 600, no. February, 2021, doi: 10.1016/j.ijpharm.2021.120478.

[96] Z. Yang, H. Peng, W. Wang, and T. Liu, "Crystallization behavior of poly(ε-caprolactone)/layered double hydroxide nanocomposites," *J. Appl. Polym. Sci.*, vol. 116, no. 5, pp. 2658–2667, 2010, doi: 10.1002/app.

[97] S. I. Song and B. C. Kim, "Characteristic rheological features of PVA

solutions in water-containing solvents with different hydration states," *Polymer (Guildf).*, vol. 45, no. 7, pp. 2381–2386, 2004, doi: 10.1016/j.polymer.2004.01.057.

[98] R. Lagoa, J. Silva, J. R. Rodrigues, and A. Bishayee, "Advances in phytochemical delivery systems for improved anticancer activity," *Biotechnol. Adv.*, vol. 38, no. April, pp. 1–22, 2020, doi: 10.1016/j.biotechadv.2019.04.004.

[99] W. R. Rolim Rolim, Pieretti, Joana C.Renó, Débora L.S. Lima, Bruna A. Nascimento, Mônica H.M. Ambrosio, Felipe N.Lombello, Christiane B. Brocchi, Marcelo De Souza, Ana Carolina S. Seabra, Amedea ., "Antimicrobial Activity and Cytotoxicity to Tumor Cells of Nitric Oxide Donor and Silver Nanoparticles Containing PVA/PEG Films for Topical Applications," *ACS Appl. Mater. Interfaces*, 2019, doi: 10.1021/acsami.8b19021.

[100] U. K. Fatema, M. M. Rahman, M. R. Islam, M. Y. A. Mollah, and M. A. B. H. Susan, "Silver/poly(vinyl alcohol) nanocomposite film prepared using water in oil microemulsion for antibacterial applications," *J. Colloid Interface Sci.*, vol. 514, pp. 648–655, 2018, doi: 10.1016/j.jcis.2017.12.084.

[101] S. King, "Catrix: an easy-to-use collagen treatment for wound healing.," *Br. J. Community Nurs.*, vol. 10, no. 9, pp. 31–34, 2005, doi: 10.12968/bjcn.2005.10.sup3.19697.

[102] Y. Ji Ji, Yuan Ghosh, Kaustabh Shu, Xiao Zheng Li, BingquanSokolov, Jonathan C. Prestwich, Glenn D. Clark, Richard A.F. Rafailovich, Miriam H, "Electrospun three-dimensional hyaluronic acid nanofibrous scaffolds," *Biomaterials*, vol. 27, no. 20, pp. 3782–3792, 2006, doi: 10.1016/j.biomaterials.2006.02.037.

[103] F. Y. Hsu, Y. S. Hung, H. M. Liou, and C. H. Shen, "Electrospun hyaluronate-collagen nanofibrous matrix and the effects of varying the concentration of hyaluronate on the characteristics of foreskin fibroblast cells," *Acta Biomater.*, vol. 6, no. 6, pp. 2140–2147, 2010, doi: 10.1016/j.actbio.2009.12.023.

[104] M. M. Hohman, M. Shin, G. Rutledge, and M. P. Brenner,

"Electrospinning and electrically forced jets. II. Applications," *Phys. Fluids*, vol. 13, no. 8, pp. 2221–2236, 2001, doi: 10.1063/1.1384013.

[105] S. P. Zhong, D. Campoccia, P. J. Doherty, R. L. Williams, L. Benedetti, and D. F. Williams, "Biodegradation of hyaluronic acid derivatives by hyaluronidase," *Biomaterials*, vol. 15, no. 5, pp. 359–365, 1994, doi: 10.1016/0142-9612(94)90248-8.

[106] J. Necas, L. Bartosikova, P. Brauner, and J. Kolar, "Hyaluronic acid (hyaluronan): A review," *Vet. Med. (Praha).*, vol. 53, no. 8, pp. 397–411, 2008, doi: 10.17221/1930-VETMED.

[107] S. Su Su, Sena Bedir, Tuba Kalkandelen, Cevriye Ozan Başar, Ahmet Turkoğlu Şaşmazel, Hilal Bulent Ustundag, Cem Sengor, Mustafa Gunduz, Oguzhan "Coaxial and emulsion electrospinning of extracted hyaluronic acid and keratin based nanofibers for wound healing applications," *Eur. Polym. J.*, vol. 142, p. 110158, 2021, doi: 10.1016/j.eurpolymj.2020.110158.

[108] A. Chanda Chanda, Amit Adhikari, Jaideep Ghosh, AritriChowdhury, Sougata Roy Thomas, SabuDatta, Pallab Saha, Prosenjit , "Electrospun chitosan/polycaprolactone-hyaluronic acid bilayered scaffold for potential wound healing applications," *Int. J. Biol. Macromol.*, vol. 116, no. 2017, pp. 774–785, 2018, doi: 10.1016/j.ijbiomac.2018.05.099.

[109] M. G. Neuman, R. M. Nanau, L. Oruña-Sanchez, and G. Coto, "Hyaluronic acid and wound healing," *J. Pharm. Pharm. Sci.*, vol. 18, no. 1, pp. 53–60, 2015, doi: 10.18433/j3k89d.

[110] M. Séon-Lutz, A. C. Couffin, S. Vignoud, G. Schlatter, and A. Hébraud, "Electrospinning in water and in situ crosslinking of hyaluronic acid / cyclodextrin nanofibers: Towards wound dressing with controlled drug release," *Carbohydr. Polym.*, vol. 207, no. October 2018, pp. 276–287, 2019, doi: 10.1016/j.carbpol.2018.11.085.

[111] R. Stern, "Hyaluronan catabolism: A new metabolic pathway," *Eur. J. Cell Biol.*, vol. 83, no. 7, pp. 317–325, 2004, doi: 10.1078/0171-9335-00392.

[112] X. Zhou, J. Lin, Y. Yin, J. Zhao, X. Sun, and K. Tang, "Ganodermataceae: Natural products and their related

pharmacological functions," *Am. J. Chin. Med.*, vol. 35, no. 4, pp. 559–574, 2007, doi: 10.1142/S0192415X07005065.

[113] X. Wang, X. Chen, Z. Qi, X. Liu, W. Li, and S. Wang, "A study of Ganoderma lucidum spores by FTIR microspectroscopy," *Spectrochimica Acta - Part A: Molecular and Biomolecular Spectroscopy*, vol. 91. pp. 285–289, 2012. doi: 10.1016/j.saa.2012.02.004.

[114] P. G. Cheng, C. W. Phan, V. Sabaratnam, N. Abdullah, M. A. Abdulla, and U. R. Kuppusamy, "Polysaccharides-rich extract of Ganoderma lucidum (M.A. Curtis:Fr.) P. Karst accelerates wound healing in streptozotocin-induced diabetic rats," *Evidence-based Complement. Altern. Med.*, vol. 2013, 2013, doi: 10.1155/2013/671252.

[115] M. F. Ahmad, "Ganoderma lucidum: A rational pharmacological approach to surmount cancer," *J. Ethnopharmacol.*, vol. 260, no. June, p. 113047, 2020, doi: 10.1016/j.jep.2020.113047.

[116] Y. Zhang Chanda, Amit Adhikari, Jaideep Ghosh, Aritri Chowdhury, Sougata Roy Thomas, SabuDatta, Pallab Saha, Prosenjit, "Ganoderma lucidum spore oil (GLSO), a novel antioxidant, extends the average life span in Drosophila melanogaster," *Food Sci. Hum. Wellness*, vol. 10, no. 1, pp. 38–44, 2021, doi: 10.1016/j.fshw.2020.05.011.

[117] M. F. Ahmad *et al.*, "Ganoderma lucidum: A potential source to surmount viral infections through β-glucans immunomodulatory and triterpenoids antiviral properties," *Int. J. Biol. Macromol.*, vol. 187, no. June, pp. 769–779, 2021, doi: 10.1016/j.ijbiomac.2021.06.122.

[118] M. A. Rahman, S. Hossain, N. Abdullah, and N. Aminudin, "Ganoderma lucidum Ameliorates Spatial Memory and Memory-Related Protein Markers in Hypercholesterolemic and Alzheimer's Disease Model Rats," *Arch. Neurol. Neurol. Disord.*, vol. 3, no. 2, 2020, [Online]. Available: www.yumedtext.com

[119] S. Savin Chanda, Amit Adhikari, Jaideep Ghosh, Aritri Chowdhury, Sougata Roy Thomas, Sabu Datta, Pallab Saha, Prosenjit , “Antioxidant, Cytotoxic and Antimicrobial Activity of Chitosan Preparations Extracted from Ganoderma Lucidum Mushroom,” *Chem. Biodivers.*, vol. 17, no. 7, 2020, doi: 10.1002/cbdv.202000175.

[120] I. A. Isoglu and N. Koc, “Centella Asiatica Extract Containing Bilayered Electrospun Wound Dressing,” *Fibers Polym.*, vol. 21, no. 7, pp. 1453–1465, 2020, doi: 10.1007/s12221-020-9956-y.

[121] T. Nishitoba, S. Shirasu, and G. Recently, “Ganoderiol A and B ? NewTriterpenoids from the Fungus Ganoderma lucidum (Reishi) The neutral fraction was separated repeatedly Ganoderiol at C-3jS from the chemical shift and multi-,” vol. 50, no. ll, pp. 2887–2890, 1986.

[122] S. E. kom, J. D. D. Tamokou, and V. Kuete, “Antibacterial and Therapeutic Potentials of the Capsicum annuum Extract against Infected Wound in a Rat Model with Its Mechanisms of Antibacterial Action,” *Biomed Res. Int.*, vol. 2021, 2021, doi: 10.1155/2021/4303902.

[123] M. K. Meghvansi *et al.*, “Naga chilli: A potential source of capsaicinoids with broad-spectrum ethnopharmacological applications,” *J. Ethnopharmacol.*, vol. 132, no. 1, pp. 1–14, 2010, doi: 10.1016/j.jep.2010.08.034.

[124] J. S. Park, J. H. Chyun, Y. K. Kim, L. L. Line, and B. P. Chew, “Astaxanthin decreased oxidative stress and inflammation and enhanced immune response in humans,” *Nutr. Metab.*, vol. 7, pp. 1–10, 2010, doi: 10.1186/1743-7075-7-18.

[125] and H. N.-M. Marcela Hern´andez-Ortega, Alicia Ortiz-Moreno, Mar´ıa Dolores Hern´andez-Navarro, Germ´an Chamorro-Cevallos, Lidia Dorantes-Alvarez and 1Departamento, “Antioxidant, Antinociceptive, and Anti-Inflammatory Effects ofCarotenoids Extracted from DriedPepper(Capsicumannuum L.) Marcela,” vol. ID 524019, pp. 1–10, 2012.

[126] Y. Wahyuni, A. R. Ballester, E. Sudarmonowati, R. J. Bino, and A. G. Bovy, "Secondary metabolites of Capsicum species and their importance in the human diet," *J. Nat. Prod.*, vol. 76, no. 4, pp. 783–793, 2013, doi: 10.1021/np300898z.

[127] R. Sibbald, D. Leaper, and D. Queen, "Iodine made easy," *Wounds Int.*, vol. 2, no. 2, pp. 1–6, 2011.

[128] T. T. Zava and D. T. Zava, "Assessment of Japanese iodine intake based on seaweed consumption in Japan: A literature-based analysis," *Thyroid Res.*, vol. 4, no. 1, pp. 1–7, 2011, doi: 10.1186/1756-6614-4-14.

[129] A. Kompelly, S. Kompelly, B. Vasudha, and B. Narender, "Rosmarinus officinalis L.: an update review of its phytochemistry and biological activity," *J. Drug Deliv. Ther.*, vol. 9, no. 1, pp. 323–330, 2019, doi: 10.22270/jddt.v9i1.2218.

[130] M. J. Jordán, V. Lax, M. C. Rota, S. Lorán, and J. A. Sotomayor, "Effect of bioclimatic area on the essential oil composition and antibacterial activity of rosmarinus officinalis L," *Food Control*, vol. 30, no. 2, pp. 463–468, 2013, doi: 10.1016/j.foodcont.2012.07.029.

[131] M. Oluwatuyi, G. W. Kaatz, and S. Gibbons, "Antibacterial and resistance modifying activity of Rosmarinus officinalis," *Phytochemistry*, vol. 65, no. 24, pp. 3249–3254, 2004, doi: 10.1016/j.phytochem.2004.10.009.

[132] R. H, "Rosmarinus officinalis (Rosemary): A Novel Therapeutic Agent for Antioxidant, Antimicrobial, Anticancer, Antidiabetic, Antidepressant, Neuroprotective, Anti-Inflammatory and Anti-Obesity Treatment," *Herb. Med. Open Access*, vol. 03, no. 02, pp. 1–6, 2017, doi: 10.21767/2472-0151.100028.

[133] S. K. Tavassoli, S. M. Mousavi, Z. Emam-Djomeh, and S. H. Razavi, "Chemical composition and evaluation of antimicrobial properties of Rosmarinus officinalis L. essential oil," *African J. Biotechnol.*, vol. 10,

no. 63, pp. 13895–13899, 2011, doi: 10.5897/ajb11.788.

[134] C. Chifiriuc, V. Grumezescu, A. M. Grumezescu, C. Saviuc, V. Lazăr, and E. Andronescu, "Hybrid magnetite nanoparticles/rosmarinus officinalis essential oil nanobiosystem with antibiofilm activity," *Nanoscale Res. Lett.*, vol. 7, pp. 1–7, 2012, doi: 10.1186/1556-276X-7-209.

[135] A. Mutlu-Ingok, D. Devecioglu, D. N. Dikmetas, F. Karbancioglu-Guler, and E. Capanoglu, "Antibacterial, antifungal, antimycotoxigenic, and antioxidant activities of essential oils: an updated review," *Molecules*, vol. 25, no. 20, 2020, doi: 10.3390/molecules25204711.

[136] S. Selmi, K. Rtibi, D. Grami, H. Sebai, and L. Marzouki, "Rosemary (Rosmarinus officinalis) essential oil components exhibit anti-hyperglycemic, anti-hyperlipidemic and antioxidant effects in experimental diabetes," *Pathophysiology*, vol. 24, no. 4, pp. 297–303, 2017, doi: 10.1016/j.pathophys.2017.08.002.

[137] N. J. Fernández Damiani, Natalia Podaza, Enrique Artur Martucci, Josefa Fabiana Fasce, Diana Quiroz, Federico Meretta, Pablo Ezequiel Quintana, Silvina Eguaras, Martín Javier Gende, Liesel Brenda "Laurus nobilis L. Extracts against Paenibacillus larvae: Antimicrobial activity, antioxidant capacity, hygienic behavior and colony strength," *Saudi J. Biol. Sci.*, vol. 26, no. 5, pp. 906–912, 2019, doi: 10.1016/j.sjbs.2018.04.008.

[138] E. Dobroslavić, M. Repajić, V. Dragović-Uzelac, and I. E. Garofulić, "Isolation of Laurus nobilis Leaf Polyphenols: A Review on Current Techniques and Future Perspectives," *Foods*, vol. 11, no. 2, 2022, doi: 10.3390/foods11020235.

[139] V. R. Pai and S. Hegde, "Research Article Preliminary Phytochemical Screening of Members of Lamiaceae Family:," *Int. J. Pharm. Sci. Rev. Res.*, vol. 21, no. 1, pp. 131–137, 2013.

[140] L. Vlase *et al.*, "Evaluation of antioxidant and antimicrobial activities and phenolic profile for Hyssopus officinalis, Ocimum basilicum and

Teucrium chamaedrys," *Molecules*, vol. 19, no. 5, pp. 5490–5507, 2014, doi: 10.3390/molecules19055490.

[141] P. Kawsud, J. Puripattanavong, and R. Teanpaisan, "Screening for anticandidal and antibiofilm activity of some herbs in Thailand," *Trop. J. Pharm. Res.*, vol. 13, no. 9, pp. 1495–1501, 2014, doi: 10.4314/tjpr.v13i9.16.

[142] K. R. Nagulendran, S. Velavan, R. Mahesh, and V. Hazeena Begum, "In vitro antioxidant activity and total polyphenolic content of Cyperus rotundus rhizomes," *E-Journal Chem.*, vol. 4, no. 3, pp. 440–449, 2007, doi: 10.1155/2007/903496.

[143] T. Dasgupta, A. R. Rao, and P. K. Yadava, "Chemomodulatory efficacy of Basil leaf (Ocimum basilicum) on drug metabolizing and antioxidant enzymes, and on carcinogen-induced skin and forestomach papillomagenesis," *Phytomedicine*, vol. 11, no. 2–3, pp. 139–151, 2004, doi: 10.1078/0944-7113-00289.

[144] A. K. Pandey, P. Singh, and N. N. Tripathi, "Chemistry and bioactivities of essential oils of some Ocimum species: An overview," *Asian Pac. J. Trop. Biomed.*, vol. 4, no. 9, pp. 682–694, 2014, doi: 10.12980/APJTB.4.2014C77.

[145] M. Sadri, S. Arab-Sorkhi, H. Vatani, and A. Bagheri-Pebdeni, "New wound dressing polymeric nanofiber containing green tea extract prepared by electrospinning method," *Fibers Polym.*, vol. 16, no. 8, pp. 1742–1750, 2015, doi: 10.1007/s12221-015-5297-7.

[146] H. Hajiali *et al.*, "Alginate-lavender nanofibers with antibacterial and anti-inflammatory activity to effectively promote burn healing," *J. Mater. Chem. B*, vol. 4, no. 9, pp. 1686–1695, 2016, doi: 10.1039/c5tb02174j.

[147] F. Pourhojat, M. Sohrabi, S. Shariati, H. Mahdavi, and L. Asadpour, "Evaluation of poly ε-caprolactone electrospun nanofibers loaded with Hypericum perforatum extract as a wound dressing," *Res. Chem.*

Intermed., vol. 43, no. 1, pp. 297–320, 2017, doi: 10.1007/s11164-016-2623-7.

[148] J. Il Choi, M. S. Kim, G. Y. Chun, and H. S. Shin, "Spirulina extract-impregnated alginate-PCL nanofiber wound dressing for skin regeneration," *Biotechnol. Bioprocess Eng.*, vol. 22, no. 6, pp. 679–685, 2017, doi: 10.1007/s12257-017-0329-3.

[149] A. Shababdoust, M. Ehsani, P. Shokrollahi, and M. Zandi, "Fabrication of curcumin-loaded electrospun nanofiberous polyurethanes with anti-bacterial activity," *Prog. Biomater.*, vol. 7, no. 1, pp. 23–33, 2018, doi: 10.1007/s40204-017-0079-5.

[150] R. Ahmed *et al.*, "Novel electrospun chitosan/polyvinyl alcohol/zinc oxide nanofibrous mats with antibacterial and antioxidant properties for diabetic wound healing," *Int. J. Biol. Macromol.*, vol. 120, pp. 385–393, 2018, doi: 10.1016/j.ijbiomac.2018.08.057.

[151] M. S. Kim, H. J. Kim, J. Y. Jang, and H. S. Shin, "Development of coaxial alginate-PCL nanofibrous dressing for controlled release of Spirulina extract," *J. Biomater. Sci. Polym. Ed.*, vol. 29, no. 12, pp. 1389–1400, 2018, doi: 10.1080/09205063.2018.1462931.

[152] Q. Chen *et al.*, "Electrospun chitosan/PVA/bioglass Nanofibrous membrane with spatially designed structure for accelerating chronic wound healing," *Mater. Sci. Eng. C*, vol. 105, no. June, p. 110083, 2019, doi: 10.1016/j.msec.2019.110083.

[153] Ö. Eğri and N. Erdemir, "Production of Hypericum perforatum oil-loaded membranes for wound dressing material and in vitro tests," *Artif. Cells, Nanomedicine Biotechnol.*, vol. 47, no. 1, pp. 1404–1415, 2019, doi: 10.1080/21691401.2019.1596933.

[154] Y. Ge, J. Tang, H. Fu, Y. Fu, and Y. Wu, "Characteristics, Controlled-release and Antimicrobial Properties of Tea Tree Oil Liposomes-incorporated Chitosan-based Electrospun Nanofiber Mats," *Fibers Polym.*, vol. 20, no. 4, pp. 698–708, 2019, doi: 10.1007/s12221-019-

1092-1.

[155] I. Unalan, B. Slavik, A. Buettner, W. H. Goldmann, G. Frank, and A. R. Boccaccini, “Physical and Antibacterial Properties of Peppermint Essential Oil Loaded Poly (ε-caprolactone) (PCL) Electrospun Fiber Mats for Wound Healing,” *Front. Bioeng. Biotechnol.*, vol. 7, no. November, pp. 1–11, 2019, doi: 10.3389/fbioe.2019.00346.

[156] M. Salehi *et al.*, “Porous electrospun poly(ε-caprolactone)/gelatin nanofibrous mat containing cinnamon for wound healing application: in vitro and in vivo study,” *Biomed. Eng. Lett.*, vol. 10, no. 1, pp. 149–161, 2020, doi: 10.1007/s13534-019-00138-4.

[157] P. Snetkov, S. Morozkina, R. Olekhnovich, T. H. Nhung Vu, M. Tyanutova, and M. Uspenskaya, “Curcumin/usnic acid-loaded electrospun nanofibers based on hyaluronic acid,” *Materials (Basel).*, vol. 13, no. 16, 2020, doi: 10.3390/MA13163476.

[158] M. A. Shahid *et al.*, “Antibacterial wound dressing electrospun nanofibrous material from polyvinyl alcohol, honey and Curcumin longa extract,” *J. Ind. Text.*, vol. 51, no. 3, pp. 455–469, 2021, doi: 10.1177/1528083720904379.

[159] Y. Yue *et al.*, “In-situ electrospinning of thymol-loaded polyurethane fibrous membranes for waterproof, breathable, and antibacterial wound dressing application,” *J. Colloid Interface Sci.*, vol. 592, pp. 310–318, 2021, doi: 10.1016/j.jcis.2021.02.048.

[160] K. Chen, H. Pan, D. Ji, Y. Li, H. Duan, and W. Pan, “Curcumin-loaded sandwich-like nanofibrous membrane prepared by electrospinning technology as wound dressing for accelerate wound healing,” *Mater. Sci. Eng. C*, vol. 127, no. January, p. 112245, 2021, doi: 10.1016/j.msec.2021.112245.

[161] M. N. Sarwar *et al.*, “Electrospun PVA/CuONPs/Bitter Gourd Nanofibers with Improved Cytocompatibility and Antibacterial Properties: Application as Antibacterial Wound Dressing,” *Polymers*

(Basel)., vol. 14, no. 7, 2022, doi: 10.3390/polym14071361.

[162] M. Suliman Maashi, S. G. Felemban, H. A. Almasmoum, and M. Jarahian, "Nicaraven-loaded electrospun wound dressings promote diabetic wound healing via proangiogenic and immunomodulatory functions: a preclinical investigation," *Drug Deliv. Transl. Res.*, no. June, 2022, doi: 10.1007/s13346-022-01176-9.

[163] W. S. Aburayan *et al.*, "Melittin from Bee Venom Encapsulating Electrospun Fibers as a Potential Antimicrobial Wound Dressing Patches for Skin Infections," *Pharmaceutics*, vol. 14, no. 4, 2022, doi: 10.3390/pharmaceutics14040725.

[164] K. S. Khashan, B. A. Badr, G. M. Sulaiman, M. S. Jabir, and S. A. Hussain, "Antibacterial activity of Zinc Oxide nanostructured materials synthesis by laser ablation method," *J. Phys. Conf. Ser.*, vol. 1795, no. 1, 2021, doi: 10.1088/1742-6596/1795/1/012040.

[165] H. H. Bahjat, R. A. Ismail, G. M. Sulaiman, and M. S. Jabir, "Magnetic Field-Assisted Laser Ablation of Titanium Dioxide Nanoparticles in Water for Anti-Bacterial Applications," *J. Inorg. Organomet. Polym. Mater.*, vol. 31, no. 9, pp. 3649–3656, 2021, doi: 10.1007/s10904-021-01973-8.

[166] K. S. Khashan, F. A. Abdulameer, M. S. Jabir, A. A. Hadi, and G. M. Sulaiman, "Anticancer activity and toxicity of carbon nanoparticles produced by pulsed laser ablation of graphite in water," *Adv. Nat. Sci. Nanosci. Nanotechnol.*, vol. 11, no. 3, 2020, doi: 10.1088/2043-6254/aba1de.

[167] M. A. Jihad, F. T. M. Noori, M. S. Jabir, S. Albukhaty, F. A. Almalki, and A. A. Alyamani, "Polyethylene glycol functionalized graphene oxide nanoparticles loaded with nigella sativa extract: A smart antibacterial therapeutic drug delivery system," *Molecules*, vol. 26, no. 11, 2021, doi: 10.3390/molecules26113067.

[168] M. K. A. Mohammed, M. R. Mohammad, M. S. Jabir, and D. S.

Ahmed, “Functionalization, characterization, and antibacterial activity of single wall and multi wall carbon nanotubes,” *IOP Conf. Ser. Mater. Sci. Eng.*, vol. 757, no. 1, 2020, doi: 10.1088/1757-899X/757/1/012028.

[169] I. H. Ali, M. S. Jabir, H. S. A. Al-Shmgani, G. M. Sulaiman, and A. H. Sadoon, “Pathological and Immunological Study on Infection with Escherichia Coli in ale BALB/c mice,” *J. Phys. Conf. Ser.*, vol. 1003, no. 1, 2018, doi: 10.1088/1742-6596/1003/1/012009.

[170] M. S. Jabir *et al.*, “Inhibition of Staphylococcus aureus α-Hemolysin Production Using Nanocurcumin Capped Au@ZnO Nanocomposite,” *Bioinorg. Chem. Appl.*, vol. 2022, pp. 1–18, 2022, doi: 10.1155/2022/2663812.

[171] G. Marinova and V. Batchvarov, “EVALUATION OF THE METHODS FOR DETERMINATION OF THE FREE RADICAL SCAVENGING ACTIVITY BY DPPH,” *Bulg. J. Agric. Sci.*, vol. 17, no. 1, pp. 11–24, 2011.

[172] N. Amariei, L. R. Manea, A. P. Bertea, A. Bertea, and A. Popa, “The Influence of Polymer Solution on the Properties of Electrospun 3D Nanostructures,” *IOP Conf. Ser. Mater. Sci. Eng.*, vol. 209, no. 1, 2017, doi: 10.1088/1757-899X/209/1/012092.

[173] H. S. Mansur, R. L. Oréfice, and A. A. P. Mansur, “Characterization of poly(vinyl alcohol)/poly(ethylene glycol) hydrogels and PVA-derived hybrids by small-angle X-ray scattering and FTIR spectroscopy,” *Polymer (Guildf).*, vol. 45, no. 21, pp. 7193–7202, 2004, doi: 10.1016/j.polymer.2004.08.036.

[174] E. F. dos Reis ., “Synthesis and characterization of poly (vinyl alcohol) hydrogels and hybrids for rMPB70 protein adsorption,” *Materials Research*, vol. 9, no. 2. pp. 185–191, 2006. doi: 10.1590/s1516-14392006000200014.

[175] K. Belbachir, R. Noreen, G. Gouspillou, and C. Petibois, “Collagen

types analysis and differentiation by FTIR spectroscopy," *Anal. Bioanal. Chem.*, vol. 395, no. 3, pp. 829–837, 2009, doi: 10.1007/s00216-009-3019-y.

[176] T. Riaz., "FTIR analysis of natural and synthetic collagen," *Appl. Spectrosc. Rev.*, vol. 53, no. 9, pp. 703–746, 2018, doi: 10.1080/05704928.2018.1426595.

[177] H. Chen, J. Qin, and Y. Hu, "Efficient degradation of high-molecular-weight hyaluronic acid by a combination of ultrasound, hydrogen peroxide, and copper ion," *Molecules*, vol. 24, no. 3, 2019, doi: 10.3390/molecules24030617.

[178] D. Barinov, "Study of substances containing iodine adduct by IR spectroscopy," no. December, pp. 1–6, 2016.

[179] S. Kiruba Daniel, R. Kumar, V. Sathish, M. Sivakumar, S. Sunitha, and T. Anitha Sironmani, "Green Synthesis (Ocimum tenuiflorum) of Silver Nanoparticles and Toxicity Studies in Zebra Fish (Danio rerio) Model," *Int. J. Nanosci. Nanotechnol.*, vol. 2, no. 2, pp. 974–3081, 2011, [Online]. Available: http://www.irphouse.com

[180] L. D. Nair, S. K. Sar, and A. Arora, "Chemical Characterization of Ocimum Sanctum in Bhilai – Durg Region of Chhattisgarh," no. July 2001, 2016.

[181] P. Opanasopit, W. Sila-On, T. Rojanarata, and T. Ngawhirunpat, "Fabrication and properties of capsicum extract-loaded PVA and CA nanofiber patches," *Pharmaceutical Development and Technology*, vol. 18, no. 5. pp. 1140–1147, 2013. doi: 10.3109/10837450.2012.727004.

[182] P. P. a A. Dzimitrowicz, S. Berent, A. Motyka, Piotr Jamroz, Konrad Kurcbach, Wojciech Sledz, "Comparison of the characteristics of gold nanoparticles synthesized using aqueous plant extracts and natural plant essential oils of Eucalyptus globulus and Rosmarinus officinalis Annaftir," *Arab. J. Chem.*, vol. 12, pp. 4795–4805, 2019.

[183] S. A. Ordoudi, M. Papapostolou, S. Kokkini, and M. Z. Tsimidou, “Diagnostic Potential of FT-IR Fingerprinting in Botanical Origin Evaluation of Laurus nobilis L. Essential Oil is Supported by GC-FID-MS Data,” vol. 25, no. 583, pp. 1–16, 2020.

[184] W. C. Lin and N. A. M. Razali, “Temporary wettability tuning of PCL/PDMS micro pattern using the plasma treatments,” *Materials (Basel).*, vol. 12, no. 4, 2019, doi: 10.3390/ma12040644.

[185] R. Mohammed, H. Jawad, and A. Al-Zubiedy, “Blended PVA/PVP Electro spun nanofibers for Coating Application,” *J. Phys. Conf. Ser.*, vol. 2114, no. 1, 2021, doi: 10.1088/1742-6596/2114/1/012031.

[186] J. Liu ., “An asymmetric wettable chitosan-silk fibroin composite dressing with fixed silver nanoparticles for infected wound repair:: In vitro and in vivo evaluation,” *RSC Adv.*, vol. 7, no. 69, pp. 43909–43920, 2017, doi: 10.1039/c7ra07588j.

[187] W. Jia, M. Li, L. Kang, G. Gu, Z. Guo, and Z. Chen, “Fabrication and Comprehensive Characterization of Biomimetic Extracellular Matrix Electrospun Scaffold for Vascular Tissue Engineering Applications,” *J. Mater. Sci.*, vol. 54, no. 15, pp. 10871–10883, 2019, doi: 10.1007/s10853-019-03667-6.

[188] R. Nayak, R. Padhye, I. L. Kyratzis, Y. B. Truong, and L. Arnold, “Effect of viscosity and electrical conductivity on the morphology and fiber diameter in melt electrospinning of polypropylene,” *Text. Res. J.*, vol. 83, no. 6, pp. 606–617, 2013, doi: 10.1177/0040517512458347.

[189] D. H. Reneker and A. L. Yarin, “Electrospinning jets and polymer nanofibers,” *Polymer (Guildf).*, vol. 49, no. 10, pp. 2387–2425, 2008, doi: 10.1016/j.polymer.2008.02.002.

[190] A. L. Yarin, W. Kataphinan, and D. H. Reneker, “Branching in electrospinning of nanofibers,” *J. Appl. Phys.*, vol. 98, no. 6, 2005, doi: 10.1063/1.2060928.

[191] B. K. Gu, S. J. Park, M. S. Kim, C. M. Kang, J. Il Kim, and C. H. Kim,

"Fabrication of sonicated chitosan nanofiber mat with enlarged porosity for use as hemostatic materials," *Carbohydr. Polym.*, vol. 97, no. 1, pp. 65–73, 2013, doi: 10.1016/j.carbpol.2013.04.060.

[192] A. K. Gaharwar *et al.*, "Amphiphilic beads as depots for sustained drug release integrated into fibrillar scaffolds," *J. Control. Release*, vol. 187, pp. 66–73, 2014, doi: 10.1016/j.jconrel.2014.04.035.

[193] T. Li, X. Ding, L. Tian, J. Hu, X. Yang, and S. Ramakrishna, "The control of beads diameter of bead-on-string electrospun nanofibers and the corresponding release behaviors of embedded drugs," *Mater. Sci. Eng. C*, vol. 74, pp. 471–477, 2017, doi: 10.1016/j.msec.2016.12.050.

[194] N. Z. A. Al-Hazeem, "Effect of the Distance between the Needle Tip and the Collector on Nanofibers Morphology," *Nanomedicine Nanotechnol.*, vol. 5, no. 3, pp. 1–5, 2020, doi: 10.23880/nnoa-16000195.

[195] E. S. Medeiros *et al.*, "Electrospun nanofibers of poly(vinyl alcohol) reinforced with cellulose nanofibrils," *J. Biobased Mater. Bioenergy*, vol. 2, no. 3, pp. 231–242, 2008, doi: 10.1166/jbmb.2008.411.

[196] C. Jiang, K. Wang, X. Jiang, C. Zhang, and B. Wang, "Quantitative investigation of the process parameters of electrohydrodynamic direct-writing and their effects on fiber surface roughness and cell adhesion," *Polymers (Basel).*, vol. 12, no. 11, pp. 1–12, 2020, doi: 10.3390/polym12112475.

[197] F. Zamani, M. Amani-Tehran, M. Latifi, and M. A. Shokrgozar, "The influence of surface nanoroughness of electrospun PLGA nanofibrous scaffold on nerve cell adhesion and proliferation," *J. Mater. Sci. Mater. Med.*, vol. 24, no. 6, pp. 1551–1560, 2013, doi: 10.1007/s10856-013-4905-6.

[198] A. Bianco *et al.*, "Electrospun poly(ε-caprolactone)/Ca-deficient hydroxyapatite nanohybrids: Microstructure, mechanical properties and cell response by murine embryonic stem cells," *Mater. Sci. Eng.*

C, vol. 29, no. 6, pp. 2063–2071, 2009, doi: 10.1016/j.msec.2009.04.004.

[199] Z. O. Repository, “grafts on blood activation Influence of fiber diameter and surface roughness of electrospun vascular grafts on blood activation Laboratory for Urologic Tissue Engineering and Stem Cell Therapy , Department of,” vol. 8, pp. 4349–4356, 2012.

[200] M. I. Hassan and N. Sultana, “Characterization, drug loading and antibacterial activity of nanohydroxyapatite/polycaprolactone (nHA/PCL) electrospun membrane,” *3 Biotech*, vol. 7, no. 4, pp. 1–9, 2017, doi: 10.1007/s13205-017-0889-0.

[201] T. M. Farooque, C. H. Camp, C. K. Tison, G. Kumar, S. H. Parekh, and C. G. Simon, “Measuring stem cell dimensionality in tissue scaffolds,” *Biomaterials*, vol. 35, no. 9, pp. 2558–2567, 2014, doi: 10.1016/j.biomaterials.2013.12.092.

[202] A. J. B. J. K. Dalal Abbass Kadham, “Electro spun polymeric membranes for wound healing: A review,” *Int. J. Health Sci. (Qassim).*, vol. 6(S4), pp. 4491–4527, 2022.

[203] S. A. Ravandi, C. Gandhimathi, M. Valizadeh, and S. Ramakrishna, “Application of Electrospun Natural Biopolymer Nanofibers,” *Curr. Nanosci.*, vol. 9, no. 4, pp. 423–433, 2013, doi: 10.2174/1573413711309040002.

[204] A. Aytimur, S. Koçyiğit, and I. Uslu, “Synthesis and Characterization of Poly(vinyl alcohol)/Poly(vinyl pyrrolidone)-Iodine Nanofibers with Poloxamer 188 and Chitosan,” *Polym. - Plast. Technol. Eng.*, vol. 52, no. 7, pp. 661–666, 2013, doi: 10.1080/03602559.2012.762662.

[205] P. Pusporini, D. Edikresnha, I. Sriyanti, T. Suciati, M. M. Munir, and K. Khairurrijal, “Electrospun polyvinylpyrrolidone (PVP)/green tea extract composite nanofiber mats and their antioxidant activities,” *Mater. Res. Express*, vol. 5, no. 5, 2018, doi: 10.1088/2053-1591/aac1e6.

[206] A. Vilchez, F. Acevedo, M. Cea, M. Seeger, and R. Navia, "Applications of electrospun nanofibers with antioxidant properties: A review," *Nanomaterials*, vol. 10, no. 1, pp. 1–25, 2020, doi: 10.3390/nano10010175.

[207] R. Amorati, M. C. Foti, and L. Valgimigli, "Antioxidant activity of essential oils," *J. Agric. Food Chem.*, vol. 61, no. 46, pp. 10835–10847, 2013, doi: 10.1021/jf403496k.

[208] S. Quereshi, A. K. Pandey, and S. S. Sandhu, "Evaluation of antibacterial activity of different Ganoderma lucidum extracts," *People's J. Sci. Res.*, vol. 3, no. 1, pp. 9–13, 2010, [Online]. Available: https://www.pjsr.org/abstract-PDF/Dr. Sadaf Qureshi.pdf

[209] U. Nazir, "Biochemical potential and screening of bioactive components of Ocimum basilicum," *Pure Appl. Biol.*, vol. 10, no. 4, pp. 1004–1013, 2021, doi: 10.19045/bspab.2021.100105.

[210] A. I. Hussain, F. Anwar, S. A. S. Chatha, A. Jabbar, S. Mahboob, and P. S. Nigam, "Rosmarinus officinalis essential oil: Antiproliferative, antioxidant and antibacterial activities," *Brazilian J. Microbiol.*, vol. 41, no. 4, pp. 1070–1078, 2010, doi: 10.1590/S1517-83822010000400027.

[211] E. Derwich, Z. Benziane, and A. Boukir, "Chemical composition and antibacterial activity of Leaves essential oil of laurus nobilis from Morocco," *Aust. J. Basic Appl. Sci.*, vol. 3, no. 4, pp. 3818–3824, 2009.

[212] C. Naveen Kumar, G. Jayalakshmi, R. Chidambaram, and R. Srikumar, "In-vitro evaluation of antifungal activity of ganoderma lucidum against the biofilm producing candida species," *Indian J. Pharm. Educ. Res.*, vol. 51, no. 4, pp. S623–S630, 2017, doi: 10.5530/ijper.51.4s.91.

[213] Á. C. Maracahipes, "Characterization and antifungal activity of a plant peptide expressed in the interaction between Capsicum annuum fruits and the anthracnose fungus," *Biosci. Rep.*, vol. 39, no. 12, pp. 1–12, 2019, doi: 10.1042/BSR20192803.

[214] D. Neveen, Helmy Abou El-Soud Mohamed, L. A. El-Kassem, and M. Khalil, “Chemical composition and antifungal activity of Syzygium aromaticum L. essential oil,” *Iran. J. Med. Aromat. Plants*, vol. 33, no. 4, pp. 552–561, 2017.

[215] S. Cuellar-Rufino, O. Arroyo-Xochihua, A. Salazar-Luna, and O. Arroyo-Helguera, “Iodine induces toxicity against Candida albicans and Candida glabrata through oxidative stress,” *Iran. J. Microbiol.*, vol. 14, no. 2, pp. 260–267, 2022, doi: 10.18502/ijm.v14i2.9195.

[216] B. Y. Anjuwita, “Antifungal Activity of Rosmarinus Officinalis Essential Oil and Nystatin on Store Isolate of Candida species from HIV/AIDS Patients with Oral Candidiasis,” *Berk. Ilmu Kesehat. Kulit dan Kelamin*, vol. 32, no. 3, p. 167, 2020, doi: 10.20473/bikk.v32.3.2020.167-173.

[217] L. R. Peixoto, “Antifungal activity, mode of action and anti-biofilm effects of Laurus nobilis Linnaeus essential oil against Candida spp.,” *Arch. Oral Biol.*, vol. 73, pp. 179–185, 2017, doi: 10.1016/j.archoralbio.2016.10.013.

[218] B. Merle, V. Maier, M. Göken, and K. Durst, “Experimental determination of the effective indenter shape and ε-factor for nanoindentation by continuously measuring the unloading stiffness,” *J. Mater. Res.*, vol. 27, no. 1, pp. 214–221, 2012, doi: 10.1557/jmr.2011.245.

الخلاصة

تعاني ضمادات الجروح التقليدية من العديد من المشاكل، مثل قلة احتباس الرطوبة، قلة امتصاص الماء وضعف الفتها له، وعدم فاعليتها ضد الجراثيم ناهيك عن اختراق بعض مكوناتها للجلد واحداث اضرار لجسم الانسان. لذا بات من الضروري تصميم ضمادات جديدة للتغلب على مثل هذه العيوب.

تم في العمل الحالي، تصنيع ضمادات بوليمرية بالاعتماد على بوليمر بولي فينيل الكحول (PVA) باستخدام تقنية الغزل الكهربائي.

تم تصنيع المنسوجات المصنوعة من الألياف البوليمرية النانوية باستخدام بولي فينيل الكحول و هيالورنيك اسيد والكولاجين وخلطاتها الثنائية والثالثية. تم خلط الزيوت الأساسية والمواد الصلبة بكميات مختلفة لصنع أفضل الضمادات.الريحان و الاكليل الجبل و الغارهي زيوت الاساسيه ؛ يعتبر كل من الفطرالريشي والفلفل و اليود من الإضافات الصلبة . " النسيج النهائي" يحتوي على كل هذه المكونات. كانت هناك حاجة إلى العديد من الاختبارات لإنهاء العمل. بعض هذه الاختبارات مخصصة للمحلول (اللزوجة ، التوتر السطحي ، والتوصيل الكهربائي) ، في حين أن البعض الآخر مخصص لمنسوجات الألياف النانوية المغزولة كهربائيًا (قابلية البلل ، مطياف فورييه للأشعة تحت الحمراء (FTIR)، صور المجهر الإلكتروني لمسح الانبعاث الميداني (FESEM) ، الطاقة تحليل الأشعة السينية المشتتة (EDX) ، الفحص المجهري للقوة الذرية (AFM) ، اتجاهية النسيج ، التحولات الحرارية ، الامتصاص المرئي للأشعة فوق البنفسجية ، XRD، المسافة النانوية واتجاه النسيج .(تم استخدام النسيج النهائي و TEBADERM لتتبع شفاء الفئران المجروحة. محلول بولي فينيل الكحول وجميع خلطاته غير نيوتونية مع ظاهرة ترقق القص وإضافة الكولاجين أو الهيارونيك اسيد إلى بولي فنيل الكحول يقلل اللزوجة ويزيد التوتر السطحي ، خاصة الهيارونيك اسيد و زيادة التوصيل الكهربائي. أظهر FTIR أن المزيج الثالث يحتوي على بولي فنيل الكحول و هيالورنيك اسيد و الكولاجين بدون تفاعل كيميائي. المواد المضافة تسبب سماكة القص بمعدلات قص منخفضة. باستثناء زيت الغار ، فإن معظم المواد المضافة حسنت التوتر السطحي والتوصيل الكهربائي بشكل مختلف. أظهر FTIR جميع المكونات في النسيج النهائي أي عدم وجود أي تفاعل كيمائي.

بالاعتماد على نتائج قابلية الترطيب، تم اختيار ثلاث تركيبات على أنها الأمثل لضمادات الجروح ولذا تم التوسع بتحليلها. انخفضت زوايا تلامسها الخاصة بهم من 70 درجة لـ PVA النقي إلى 46.505 درجة و 51.37 درجة و 41 درجة لـ 55:45 (10٪ Coll 7٪ :PVA) و 55: 45: 5.5٪ HAc و 55: 22.5: 22.5 (10٪ PVA، 7٪ Coll ، 5.5٪ HAc). من المتوقع أن تمتص هذه الضمادات الإفرازات الزائدة وتحافظ على الرطوبة المثلى للجرح من خلال التحكم في تبخر الماء عملت مضافات الفلفل ،اليود و زيت الغارعلى تحسين قابلية الضمادة للتحلل واطلاق السريع المتوقع

للأدوية نحو الجلد المصاب. على العكس من ذلك ، فقد كان للنسيج النهائي قابلية أقل للترطيب ولمعالجة ذلك فقد تم تغيير ظروف التشغيل وأظهرت النتائج أن تقليل مسافة الإبرة إلى المجمع أو معدل التدفق يمكن أن يحسن قابلية الترطيب. أدت جميع المضافات (مساحيق وزيوت اساس) الى زيادة قطر الألياف (بنسبة 20٪ - 76.81٪) ، والى ظهور اشكال مورفولوجية جديدة (قرص العسل، ألياف المتفرعة ، الياف مدمجة ، الياف ملتوية) ، وظهور خرزً(Beads) وكذلك مستويات مسامية مختلفة. في المقابل، أزداد متوسط قطر النسيج النهائي بنسبة 118.5٪ ، وتغير توزيعه على نطاق أوسع، وتشكله بألياف نانوية متشابكة مدمجة مع وجود بعض الخرزات وكانت مسامية النسيج متوسطة. تسببت هذه المضافات كذلك بزيادة معاملات الخشونة وفي تغير اتجاهية الألياف كما تسببت باحداث الانفصال الطوري (ظهور درجتي انتقال زجاجي بدلا من واحدة فقط للخليط الاصلي)، مما أدى إلى الحصول على خليط بوليمري غير متجانس (Immiscible blend)، وتغيير المحتوى الحراري المطلوب، وتسهيل إطلاق الدواء نحو الجلد المصاب من الضمادات غير المضغوطة.

تسببت جميع المضافات بانتقالات الكترونية من نوعي π إلى π^* و n إلى π^* ، مما يشير الى امكانية هذه المنسوجات الحديثة الى امتصاص الضوء عند طولين موجيين متميزين .

أظهر اختبار مقاومة الأكسدة أن النسيج النهائي يمتلك نشاطاً أعلى مقارنةً بالخليط الاساسي في إزالة الجذور الحرة DPPH ، مما يعزز استعادة الأنسجة ويقلل من وقت الشفاء.

أظهر اليود أعلى فعالية في مقاومة بكتيريا E-coli، بينما أظهر زيت إكليل الجبل أعلى مقاومة ضد بكتيريا S. aureus. أظهر النسيج النهائي أعلى نشاط مقاومة لفطريات الكانديدا يليه زيت إكليل الجبل واليود على التوالي.

تمت دراسة النشاط المضاد للبكتيريا أيضًا من خلال مراقبة الحالة الصحية للفئران المصابة ومقارنتها بضمادات TEBADERM والتي أظهرت أنه بعد خمسة أيام ، التشافي الكامل للفئران التي عولجت بنسيج الألياف النانوية بينما ظلت جروح الفئران الأخرى رطبة ومحمرة وبوجود بعض التخثر.

أثبتت نتائج XRD أن المواد المضافة قد أثرت على طبيعة التراكيب البلورية وانها قد عملت كعوامل تنويه. أظهرت نتائج الصلادة النانوية للنسيج النهائي، انخفاض في الصلادة ومعامل المرونة، بينما زاد عمق التلامس

وزارة التعليم العالي والبحث العلمي
جامعـــــــــــة بابـــــــــــل
كليـــــــــة هنـــــــــــدسة المواد
قسم البوليمر والصناعات البتروكيمياوية

تصنيع ضمادات الجروح من أنسجة الالياف النانويه بطريقة الغزل الكهربائي

رسالة

مقدمه إلى قسم هندسة البوليمر والصناعات البتروكيمياوية في كلية هندسة المواد/ جامعة بابل

وهي جزء من متطلبات نيل درجة الدكتوراه فلسفة في هندسة المواد/البوليمر

مقدمة من قبل

دلال عباس كاظم سلمان

بإشراف

أ.د. عودة جبار البريهي **أ.د. هناء جواد كاظم**

م 1444 هـ **2023**